Advances in Clinical and Experimental Medicine

MONTHLY ISSN 1899-5276 (PRINT) ISSN 2451-2680 (ONLINE) advances.umw.edu.pl

2022, Vol. 31, No. 12 (December)

Impact Factor (IF) – 1.736
Ministry of Science and Higher Education – 70 pts
Index Copernicus (ICV) – 168.52 pts

Wroclaw Medical University

Advances
in Clinical and Experimental
Medicine

Advances
in Clinical and Experimental Medicine

ISSN 1899-5276 (PRINT) ISSN 2451-2680 (ONLINE) advances.umw.edu.pl

MONTHLY 2022
Vol. 31, No. 12
(December)

Advances in Clinical and Experimental Medicine (*Adv Clin Exp Med*) publishes high-quality original articles, research-in-progress, research letters and systematic reviews and meta-analyses of recognized scientists that deal with all clinical and experimental medicine.

Editorial Office
ul. Marcinkowskiego 2–6
50-368 Wrocław, Poland
Tel.: +48 71 784 12 05
E-mail: redakcja@umw.edu.pl

Publisher
Wroclaw Medical University
Wybrzeże L. Pasteura 1
50-367 Wrocław, Poland

Online edition is the original version of the journal

Editorial Policy

Advances in Clinical and Experimental Medicine (Adv Clin Exp Med) is an independent multidisciplinary forum for exchange of scientific and clinical information, publishing original research and news encompassing all aspects of medicine, including molecular biology, biochemistry, genetics, biotechnology and other areas. During the review process, the Editorial Board conforms to the "Uniform Requirements for Manuscripts Submitted to Biomedical Journals: Writing and Editing for Biomedical Publication" approved by the International Committee of Medical Journal Editors (www.ICMJE.org). The journal publishes (in English only) original papers and reviews. Short works considered original, novel and significant are given priority. Experimental studies must include a statement that the experimental protocol and informed consent procedure were in compliance with the Helsinki Convention and were approved by an ethics committee.

For all subscription-related queries please contact our Editorial Office:
redakcja@umw.edu.pl

For more information visit the journal's website:
advances.umw.edu.pl

Pursuant to the ordinance No. 134/XV R/2017 of the Rector of Wroclaw Medical University (as of December 28, 2017) from January 1, 2018 authors are required to pay a fee amounting to 700 euros for each manuscript accepted for publication in the journal Advances in Clinical and Experimental Medicine.

Indexed in: MEDLINE, Science Citation Index Expanded, Journal Citation Reports/Science Edition, Scopus, EMBASE/Excerpta Medica, Ulrich's™ International Periodicals Directory, Index Copernicus

Typographic design: Piotr Gil, Monika Kolęda
DTP: Wydawnictwo UMW
Cover: Monika Kolęda
Printing and binding: Drukarnia I-BiS Bierońscy Sp.k.

Advances
in Clinical and Experimental Medicine

MONTHLY 2022, Vol. 31, No. 12 (December)

ISSN 1899-5276 (PRINT)
ISSN 2451-2680 (ONLINE)
advances.umw.edu.pl

Contents

Acknowledgements

We would like to express our gratitude to all reviewers who devoted their time and expertise to evaluate manuscripts in Advances in Clinical and Experimental Medicine. We sincerely appreciate all your hard work and dedication. It is due to your contribution that we can achieve the standard of excellence.

Editors

Reviewers in 2022:

Mohamed Abdelrahim, Bogusz Aksak-Wąs, Yasser Albadrany, Özgür Albuz, Amr Al-Haidari, Nastaran Alinezhad, Mohammed Alradhi, Saif Alrasheed, Baoquan An, Vijaya Anand, Darko Antičević, Mabel Aoun, Cüneyt Arıkan, Tareq Aro, Loordhurani Asaikumar, Muhammad Sohaib Asghar, Erica Avila, Gulbin Aygencel, Maleeha Azam, Jan Azarov, Dagmara Baczyńska, Preeti Bagri, Xiaodong Bai, Christian Bailly, Banwari I. Bairwa, May Bakkar, Agata Bałdys-Waligórska, Marta Banach, Marta Banaszkiewicz, Julia Bar, Valentim Adelino Ricardo Barão, Marcin Barczyński, Satish Barnawal, Maria Magdalena Barreca, Grzegorz Bartosz, Paweł Basta, Simone Battaglia, Stanisława Bazan-Socha, Katarzyna Bąbol-Pokora, Ilona Bednarek, Monika Bekiesińska-Figatowska, Yuri Belenkov, Alexander E. Berezin, Sonu Bhaskar, Maciej Biały, Jan Biegus, Monika Bielecka, Iwona Bil-Lula, Carlo Biz, Anna Bizoń, Joanna Bladowska, Florin-Teodor Bobircă, Joanna Bogusławska, Andrzej Bohatyrewicz, Agnieszka Bojarska-Junak, Dimorvan Bordin, Dariusz Boroń, Rafael Boscolo-Berto, Özlem Bostan Gayret, Giuseppe Brisinda, Sergey Brodsky, Mariusz Bromke, Marlena Broncel, Anna Brzecka, Liang Bu, Grzegorz Bukato, Jessica Carlsson, Alessandra Cassoni, Nidia Castro, Piotr Celichowski, Maja Cemazar, Radosław Chaber, Mariusz Chabowski, Yubo Chai, Mohamed Chaouch, Andrzej Chciałowski, Chong Chen, Linyan Chen, Min Chen, Steven Chen, Ying Chen, Meer Chisthi, Iwona Chlebicka, Magdalena Chmielewska, Grzegorz Chodaczek, Justyna Chojdak-Łukasiewicz, Anna Choromanska, Rupshikha Choudhury, Sinhayana Choudhury, Jerzy Chudek, Agnieszka Chwiłkowska, Halina Cichoż-Lach, Olga Ciepiela, Joanna Cieślińska-Świder, Sofie Claerhout, Szczepan Cofta, Pellegrino Crafa, Jennifer Craig, Alessandro Crestani, Michał Czapla, Monika Czerwińska, Jacek Daroszewski, Manna Debrashri, Marek Dedecjus, Mehmet Demir, Andrzej Deptała, Engin Deveci, Dominika Dęborska-Materkowska, Chiara Di Fazio, Rosanna di Paola, Dorota Diakowska, Greg Dion, Ebubekir Dirican, Rafał Dobek, Marzena Dominiak, Adrian Doroszko, Szymon Dragan, Jarosław Drożdż, Katarzyna Drożdż, Monika Dudzisz, Dan Lucian Dumitrașcu, Mainak Dutta, Tolga Duzenli, Edyta Dziadkowiak, Dariusz Dziedzic, Katarzyna Dzierżanowsk-Fangrat, Piotr Dzięgiel, Eman Mohamad El Nashar, Muhammed Elayadeth-Meethal, Tarek Elhamaky, Feriha Ercan, Antonio Facciorusso, Ammad Farooqui, Julia Fedotova, Qiming Feng, Xuehua Feng, Yaling Feng, Farzaneh Fesahat, Luciene Figueiredo, Agata Filip, Martin Floer, Michael Fowler, Aleksandra Franczak, Marcin Frączek, Irena Frydecka, Shoichi Fujii, Piotr Futyma, Paweł Gać, Paweł Gajdzis, Maria Ganeva, Pankaj Garg, Rakesh Garg, Zbigniew Gąsior, Anita Gąsiorowska, Tomasz Gedrange, Ashraf Ghulam, Justyna Gil, Krystyna Głowacka, Robbert Gobbens, Upendarrao Golla, Dor Golomb, Tomasz Gołębiowski, Zhumei Gong, Małgorzata Goździk, Waldemar Goździk, Halina Grajeta, Alessandro Granito, Bianca Gregorio, Emilia Grosicka-Maciąg, Kinga Grzech-Leśniak, Bronisław Grzegorzewski, Teresa Grzelak, Grzegorz Grześk, Andrzej Grzybowski, Jakob Gubenšek, Sevin Güney, Shicheng Guo, Maciej Guziński, Jakub Hadzik, Min Hang, Hesam Hashemian, Olga Haus, Zbigniew Heleniak, Andrzej Hellmann, Piril Hepsomali, Tomasz Hirnle, Nguyen Hoai, Ladislav Hosák, András Hrabák, Tomasz Hrapkowicz, Jianzhang Hu, Rong Hu, Qiang Huang, Magdalena Hurkacz, Marek Hus, Lidia Hyla-Klekot, Joseph Irudayaraj, Arda Isik, Mehmet Işıkalan, Imen Ismail, Koni Ivanova, Teresa Jagła, Urmila Jagtap, Krzysztof Jamroziak, Anna Janas-Naze, Adrianna Janczura, Maurycy Jankowski, Radosław Januchowski, Monika Jasek, Marek Jasiński, Michał Jeleń, Michal Ješeta, Wiesław Jędrzejczak, Diana Jędrzejuk, Madeleine Johansson, Lee Jones, Karol Jopek, Sharma Joshi, Krystian Josiak, Adam Junka, Niu Junrong, Kamil Jurczyszyn, Adam Jurgoński, Radosław Kaczmarek, Tomasz Kaczmarzyk, Noha Kamel, Grzegorz Kamiński, Karol Kamiński, Piotr Kanclerz, Agnieszka Kapłon-Cieślicka, Habib Karim, Paweł Karpiński, Jarosław D. Kasprzak, Katarzyna Katulska, Andrzej Kawecki, Radosław Kaźmierski, Kushaan Khambata, Cheorl-Ho Kim, Brygida Knysz, Christopher Kobierzycki, Małgorzata Kobusiak-Prokopowicz, Altug Koc, Mehmet Kocaoğlu, Aleksandra Kołtuniuk, Tomasz Konopka, Wiesław Konopka, Grzegorz Kopeć, Agnieszka Kordek, Parastou Kordestani-Moghadam, Anna Korycka-Wołowiec, Michał Kosowski, Magdalena Koszewicz, Euphrosyni Koutsouraki, Jerzy Kowalczyk, Artur Kowalik, Magdalena Kowalik, Dariusz Kowalski, Katarzyna Koziak, Ewa Koziorowska-Gawron, Wiesława Kranc, Soňa Křížková, Tomasz Król, Leszek Królicki, Aleksandra Królikowska, Katarzyna Krzanowska, Anna Krzywonos-Zawadzka, Dorota Ksiądzyna, Paweł Kubasiewicz-Ross, Adriana Kubis-Kubiak, Piotr Kubler, Paweł Kuca, Tomasz Kucmin, Piotr Kuczera, Allison Kuipers, Radosław Kujawski, Julita Kulbacka, Wiktor Kuliczkowski, Michał Kulus, Anoop Kumar, Sonam Kumari, Maciej Kupczyk, Jacek Kusa, Anna Kusienicka, Irena Kustrzeba-Wójcicka, Damian Kuszewski, Michał Kuszewski, Halyna Kuznietsova, Amadeusz Kuźniarski, Xiang Lan, Sen-Yang Lang, Ewa Lange, Eryk Latoch, André Lázaro, Anna Lebedeva, Robert Lee, Nattawut Leelakanok, Christian Lehmann, Małgorzata Lelonek, Agnieszka Lepiesza, Aleksandra Lesiak, Marta Leśniczak-Staszak, Krzysztof Lewandowski, Łukasz Lewandowski, Łukasz Lewicki, Natalia Lewkowicz, Fang Li, Hui Li, Jian Li, Jing Li, Shuangdi Li, Che-Yu Lin, Pengchao Lin, Changquan Ling, Elizabeth Lippard, Luís Loureiro, Antonio José López, Wojciech Lubiński, Bastian Lubis, Kamila Ludwikowska, Andrey Lvov, Piotr Łacina, Izabela Łaczmańska, Daging Ma, Xinnan Ma, Bogusław B. Machaliński, Adam Maciejczyk, Jacek Mackiewicz, Paweł Madej,

Iddo Magen, Sadegh Mahdavi, Przemysław Majewski, Umberto Malapelle, Iwona Malinowska, Witold Malinowski, Bartosz Małkiewicz, Małgorzata Małodobra-Mazur, Krzysztof Małyszczak, Naresh Kumar Manda, Michele Manigrasso, Zenon Mariak, Lina Marin, Mirosław Markiewicz, Joana C. Marques, Richard Martin, Beatriz Martin-Perez, Iwona Maruniak-Chudek, Jarosław Marusiak, Jolanta Masiak, Mafalda Massara, Rafał Matkowski, Małgorzata Matusiewicz, Jacek Matys, Katarzyna Matysiak-Luśnia, Bogdan Mazur, Grzegorz Mazur, Henryk Mazurek, Maria Mazurkiewicz-Bełdzińska, Błażej Meczekalski, Miranda Mele, Katarzyna Michalska-Małecka, Olga Michel, Maria Miglino, Marta Migocka-Patrzałek, Anna Mika, Wioletta Mikulakova, Marcin Mikulewicz, Christos Miliotis, Marcin Misiek, Katarzyna Mizia-Stec, Agnieszka Młynarska, Nicola Mondanelli, Richard Moon, Piotr Morasiewicz, Daniel Morris, Ewa Mroczek, Jacek Musiał, Witold Musiał, Maria Nagai, Sharada Nalla, Grzegorz Nałęcz-Jawecki, Shyam Nandi, Anna Nasierowska-Guttmejer, Jacek Nasiłowski, Sagar Naskar, Joseph Nassif, Mariusz Nawrocki, Sergiusz Nawrocki, Urszula Nawrot, Bishal Nepal, Susan Nicola, Guimei Nie, Marek Niedziela, Piotr Niewiński, Przemysław Niewiński, Mohsen Nikbakht, Beata Nowak, Krzysztof Nowak, Michał Nowak, Marta Nowakowska-Kotas, Danuta Nowicka, Katarzyna Nowomiejska, Marta Obremska, Ewa Ocłoń, Berker Okay, Zofia Oko-Sarnowska, Paweł Olczyk, Agnieszka Olejnik, Robert Olszewski, Cem Onal, Hanna Osadnik, Marcin Osuchowski, Sevket Ozkaya, Radosław Pach, Anna Panasiuk, Konstantinos Papadopoulos, Bogusław Paradowski, Miłosz Parczewski, Joanna Pawlak, Krystyna Pawlas, Guido Pelletti, Rinaldo Pellicano, Bartosz Pencakowski, Hongliang Peng, Alvaro Perna, Cristian Persu, Ákos Pethő, Ferdinando Petrazzuoli, Roman Pfitzner, Beata Piątkowska-Jakubas, Mariusz Piechota, Aleksandra Piechota-Polańczyk, Joanna Pieczyńska, Paulina Pietras, Małgorzata Pietruska, Justyna Pigońska, Jian Ping, Hanna Piotrowska-Kempisty, Nicola Pirozzi, Wojciech Pluskiewicz, Elżbieta Płuciennik, Dorota Pojda-Wilczek, Mateusz Polaczek, Katarzyna Połtyn-Zaradna, Michał Pomorski, Rafał Poręba, Annamaria Porreca, Błażej Poźniak, Sumidtra Prathep, Marcin Protasiewicz, Tadeusz Przybyłowski, Piotr Radziwon, Reza Rahbarghazi, Rodryg Ramlau, Andrzej Rapak, Sanjay Rastogi, Krzysztof Reczuch, Alaa Redwan, Adam Reich, Nina Rembiałkowska, Matthias Riess, Waseem Rizvi, Keith Rochfort, Catalina Rojas-Solé, Jacek Roliński, Umberto Romeo, Dorota Różańska, Ingrid Różyło-Kalinowska, Lidia Rutkowska-Sak, Przemysław Rutkowski, Jolanta Saczko, Pranshu Sahgal, Fatima Saleh, Arun Kumar Sanapala, Javier Santabárbara, Hande Sar, Mehmet Sarier, Singaraju Sri Subrahmanya Sarma, Elżbieta Sarnowska, Naila Sattar, Sofie Saunier, Matthew Savoian, Grzegorz Sawicki, Vishal Saxena, Hale Sayan, Marek Sąsiadek, Ana Scocate, Zbigniew Serafin, Kalyan Sethi, Vishal Shelat, Wodong Shi, Jamil Shibli, Rafał Sibiak, Paweł Siekierski, Sonia Sifuentes-Franco, Santhi Silambanan, Scott E. Sills, Krzysztof Simon, Dona Sinha, Aleksander Siniarski, Rosalba Siracusa, Pasqualino Sirignano, Joanna Siuda, Tomasz Skirecki, Szymon Skoczyński, Andrzej Skorek, Mariusz Skowroński, Monika Skrzypiec-Spring, Jolanta Słowikowska-Hilczer, Krzysztof Słotwiński, Monika Służewska-Niedźwiedź, Jacek Smereka, Piotr Smolewski, Małgorzata Sobieszczańska, Grzegorz Sobota, Justyna Sokolska, Mateusz Sokolski, Francisco Solano, João Souza, Josip Spanjol, Eleonora Spekker, Marta Stafiniak, Agata Stanek, Bartłomiej Stańczykiewicz, Anna Starzyńska, Rafał Stec, Ludomir Stefańczyk, Cristina Stewart Bogsan, Maciej Stępnik, Rostyslav Stoika, Jan Styczyński, Lina Suarez, Halis Suleyman, Xuejun Sun, Anna Surdacka, Andrei Surguchov, Edyta Sutkowska, Ahmed Swalih, Ali Syed, Agata Szade, Krzysztof Szade, Anna Szewczyk, Adam Szpechciński, Aleksandra Szymczak, Andrzej Szyszka, Milena Ściskalska, Mariola Śliwińska-Mossoń, Robert Śmigiel, Paweł Tabakow, Aisha Tahir, Masaru Tanaka, Fenglian Tang, Rafał Tarkowski, Marziyeh Tavalaee, Yao Teng, Luca Testarelli, Dariusz Timler, Michał Tkaczyszyn, Tomasz Tokarek, Aleš Tomažič, Jacek Toporski, Mattia Tosi, Janusz Trzebicki, Przemysław Trzeciak, Mehmet Tuncer, Isaac Udo, Maciej Ugorski, Sadiq Umar, Zuhat Urakci, Wiktor Urbański, Marek Ussowicz, Manuel Valdano, Marina Valenzano, Stella Valenzuela, Bhavin Vasavada, Marta Wagner, Bożena Walewska-Zielecka, Marta Waliszewska-Prosół, Jianghua Wan, Rong Wang, Shaoxun Wang, Shuang Wang, Xinghuan Wang, Dorota Waśko-Czopnik, Gabriel Wcisło, Yudong Wei, Wojciech Widuchowski, Alicja Wiercińska-Drapało, Jolanta Wierzba, Mieszko Więckiewicz, Rafał Wiglusz, Markus Wilhelmi, Mark Willcox, Kamil Wojnicki, Beata Wojtczak, Maria Wołuń-Cholewa, Krzysztof Woźniak, Janusz Wójcik, Tomasz Wróbel, Xiangchun Wu, Ewa Wunsch, John Wynn-Jones, Lucjan Wyrwicz, Grzegorz Wystrychowski, Yong Xia, Gao Xiang, Liuling Xiao, Huan-Yu Xiong, Jinhua Xu, Ferda Yaman, Jun Yan, Qing Yang, Lin Yan-Ren, Weidong Yao, Yuanrong Yao, Yongjie Yin, Chun Yu, Nina Yu, Xiaojun Yu, Urszula Zaleska-Dorobisz, Rafał Załuski, Natalia Zaręba, Michał Zarobkiewicz, Ewa Zasadzka, Jan Zaucha, Renata Zaucha, Izabela Zawlik, Marcin Zeman, Hui Zhang, Jingyu Zhang, Qi Zhang, Tao Zhang, Wei Zhang, Ying Zhang, Yuan-Chuan Zhao, Liping Zhou, Yaoliang Zhou, Guoqi Zhu, Anna Zimny, Wojciech Zimoch, Nava Zisapel, Krzysztof Zub, Agnieszka Zubkiewicz-Kucharska, Danuta Zwolińska, Małgorzata Zwolińska-Wcisło, Robert Zymliński, Dorota Zyśko, Ewa Żurawska-Płaksej

COVID-19 pandemic as reflected in *Advances in Clinical and Experimental Medicine*

Krzysztof Kujawa[1,A–F], Marek Misiak[2,B–F], Donata Kurpas[3,A,B,E,F]

[1] Statistical Analysis Centre, Wroclaw Medical University, Poland
[2] Wroclaw Medical University Press, Poland
[3] Department of Family Medicine, Faculty of Medicine, Wroclaw Medical University, Poland

A – research concept and design; B – collection and/or assembly of data; C – data analysis and interpretation; D – writing the article; E – critical revision of the article; F – final approval of the article

Advances in Clinical and Experimental Medicine, ISSN 1899–5276 (print), ISSN 2451–2680 (online) *Adv Clin Exp Med*. 2022;31(12):1305–1307

Address for correspondence
Krzysztof Kujawa
E-mail: krzysztof.kujawa@umw.edu.pl

Funding sources
None declared

Conflict of interest
None declared

Acknowledgements
The authors would like to thank Iya Sudoplatova, PhD, for her assistance in translating the paper.

Received on December 13, 2022
Accepted on December 13, 2022

Published online on December 16, 2022

Abstract

The editorial demonstrates changes in the number and subject matter of papers dealing with issues related to the coronavirus disease 2019 (COVID-19), which were published in *Advances in Clinical and Experimental Medicine* (ACEM) during 3 years of the pandemic (2020–2022). In 2020, 24 such manuscripts were submitted to the editorial office, of which 9 were published; in 2021, 48 were submitted and 10 published, while in 2022, there were 34 articles submitted and 4 published. Authors of this editorial point out that while initially chances for publication of papers regarding COVID-19 were greater than papers covering other issues, the editors of ACEM gradually enforced the same requirements for COVID-19-related papers as for the others (the acceptance rate for these papers was 37.5% in 2020, 20.8% in 2021 and 11.8% in 2022). The published papers described, among other aspects, the relationship between COVID-19 and other diseases (e.g., pneumonia, Parkinson's disease and acute kidney injury) and methods of preventing severe acute respiratory syndrome coronavirus 2 (SARS-CoV-2) infection among healthcare staff. An emergency situation of pandemic called for disseminating the results of scientific research as promptly as possible; however, the proper answer to this challenge is not lowering and simplifying requirements for peer review, but releasing the results in a form of registered preprints, which allow for provisionally making the paper available for the scientific community while the peer review verification is still ongoing.

Key words: COVID-19, pandemic, SARS-CoV-2, scientific journal, preprint

Cite as
Kujawa K, Misiak M, Kurpas D. COVID-19 pandemic as reflected in *Advances in Clinical and Experimental Medicine*. *Adv Clin Exp Med*. 2022;31(12):1305–1307. doi:10.17219/acem/157447

DOI
10.17219/acem/157447

Introduction

In November 2022, 3 years will pass since COVID-19 disease has first been described. Rapid spread of the pandemic and the observed mortality – high for a disease caused by severe acute respiratory syndrome coronavirus 2 (SARS-CoV-2) – resulted in diverting the interest of many researchers to elucidating the etiology of this disease and establishing treatment methods. *Advances in Clinical and Experimental Medicine* (ACEM) is a scientific journal covering all clinical and experimental medicine as well as issues from other fields of knowledge related to medicine. Therefore, it was obvious that the emergence of a new disease – COVID-19 – and the subsequent spread of the pandemic in the whole world would be reflected in the thematic scope of submitted manuscripts and published papers. First articles pertaining this field started to reach the ACEM editorial office around March 11, 2020, when World Health Organization (WHO) declared the outbreak a pandemic.

Over the last 3 years, the number of publications relevant to this issue has increased massively. According to the Web of Science database searched with keywords „COVID-19" and „SARS-CoV-2", in 2019, 48 articles (both original papers and reviews) were published, in 2020 – 80,312 (sic!), in 2021 – 150,590, and in 2022 – 119,053 (as for October 31, 2022). There are already 313 papers (as for October 31, 2022) dated 2023. Papers on COVID-19 were cited unusually often – some even 15,000 times (sic!).[1–3] It is certainly safe to say that throughout the history of scientific medical journals no other subject became so popular in such a short time. Nevertheless, it has to be also strongly stressed that this phenomenon was neither a result of a trend similar in nature to fashion, nor an attempt made by many researchers to boost their career, but a proper response of the scientific community to a clear and present danger to the health and life of the entire world population. The research – undertaken first in China, where the virus was first isolated, and then in other countries – focused on the pathogen itself and its identified mutations, course of infection, possible complications and comorbidities, relationship between COVID-19 and other diseases, as well as – which can be particularly observed in papers published in ACEM – the impact of the pandemic on the possibilities of treating patients by doctors of various specialties, and issues related to preventing SARS-CoV-2 infection among healthcare staff (doctors, nurses, orderlies, other personnel).

Papers on COVID-19 published in ACEM

Advances in Clinical and Experimental Medicine, as a scientific journal, has had its share in disseminating relevant results of research on COVID-19/SARS-CoV-2. In 2020–2022 (as for October 31, 2022), a total of 106 papers covering various aspects of COVID-19 outbreak were submitted to the journal, of which 23 were published. The average acceptance rate for those papers amounted to 21.7% and was higher than the average acceptance rate for all manuscripts submitted in this period (16.2%). In 2020, 24 such manuscripts were submitted to the editorial office, of which 9 were published; in 2021, 48 were submitted and 10 published, while in 2022 there were 34 articles submitted and 4 published. If the acceptance rate is taken into consideration separately for the respective years, it can be observed that the editors of ACEM gradually enforced the same requirements for COVID-19-related papers as for other papers (the acceptance rate for COVID-19-related papers was 37.5% in 2020, 20.8% in 2021 and 11.8% in 2022 (as for October 31, 2022)). Therefore, it can be noted that in the 1st year of the pandemic, the novelty effect had a clear influence, but in the following 2 years the acceptance rate has decreased to a value similar to the average for all papers published in ACEM.

The thematic scope of the published papers was broad – in line with the general profile of the journal – and concerned, e.g., the relationship between COVID-19 and other diseases (e.g., pneumonia,[4,5] Parkinson's disease[6] and acute kidney injury[7]), and methods of preventing SARS-CoV-2 infection among healthcare staff.[8–11] The most cited COVID-19-related papers published in ACEM are studies by Wierzbicki et al. and Zubkiewicz-Kucharska et al.[9,12]

Preprints – prompt dissemination of results

The presented data clearly show 2 patterns. On the one hand, many important studies exploring diverse aspects of COVID-19 pandemic were published in ACEM and showed a persistent interest from among scientific community. On the other hand, such strong presence of this subject matter in the journal did not mean lowering the standards of scientific and linguistic assessment and verification of the submitted manuscripts, which could have been justified by the state of necessity. It is worth noting that a modern model of disseminating scientific papers allows for sharing particularly significant research results before their publication in a peer-reviewed scientific journal. It is of paramount importance that other investigators – and in some instances also health and state authorities, or even the general public – have the access to such papers immediately. Registered preprints are a tool that provides such possibility. They are made available – usually as PDF files with a DOI – on the websites of various universities and other research institutions, as well as on dedicated portals (e.g., https://www.researchsquare.com/). Such preprints are accordingly marked to make the readers aware that they are reading a text that is still to undergo peer review or is in the process of review. Therefore, while the paper is being reviewed and edited

to be published in a journal, the scientific community can offer their remarks or become inspired by the shared results, hypotheses and ideas. Various aspects of this problem in the context of COVID-19 pandemic have already been discussed in medical literature in the last 3 years.[13–20] The experiences of ACEM unambiguously exemplify that the outlined model of scientific communication (preprint followed by peer-reviewed publications), contrary to expediting the peer review process at the expense of its quality, is the right direction of developing scientific journals and a proper answer to challenges of the modern world as they are reflected in science and scientific publishing.

Where are we after 3 years?

The strategy of dealing with the influx of COVID-19-related manuscripts implemented by ACEM editorial office proved successful – we managed to publish several relevant papers without putting at stake the scientific integrity or editorial standard of our journal. The magnitude of this influx caused was certainly reflected in the journal – but was no excuse for inadequate result reporting, shortcomings regarding proper English or lack of originality. The rise of acceptance rate in the 1st pandemic year (2021) comes from a rapid shift in professional interests of our authors, as not only epidemiologists and virologists wrote about SARS-CoV-2. However, no temptation to lower the standards existed at any time because the authors also did not loosen their scientific rigor and many of them provided meticulously prepared manuscripts. The following remark could serve as a conclusion: In a sense, from the editors' point of view, COVID-19 pandemic was clearly an emergency situation, but not a state of necessity.

ORCID iDs

Krzysztof Kujawa https://orcid.org/0000-0003-2812-4702
Marek Misiak https://orcid.org/0000-0003-2208-2193
Donata Kurpas https://orcid.org/0000-0002-6996-8920

References

1. Huang C, Wang Y, Li X, et al. Clinical features of patients infected with 2019 novel coronavirus in Wuhan, China. *Lancet*. 2020;395(10223):497–506. doi:10.1016/S0140-6736(20)30183-5
2. Guan WJ, Ni ZY, Hu Y, et al. Clinical characteristics of coronavirus disease 2019 in China. *N Engl J Med*. 2020;382(18):1708–1720. doi:10.1056/NEJMoa2002032
3. Zhu N, Zhang D, Wang W, et al. A novel coronavirus from patients with pneumonia in China, 2019. *N Engl J Med*. 2020;382(8):727–733. doi:10.1056/NEJMoa2001017
4. Güçlü ÖA, Önal U, Akalın H, et al. Tocilizumab treatment in COVID-19: A prognostic study using propensity score matching [published online as ahead of print on August 11, 2022]. *Adv Clin Exp Med*. 2022. doi:10.17219/acem/151912
5. Öztürk R, Tazegul G. Real-world diagnostic value of a nationwide standardized COVID-19 triage chart in Turkey. *Adv Clin Exp Med*. 2022;31(9):965–971. doi:10.17219/acem/149243
6. Holland C, Garner I, Simpson J, et al. Impacts of COVID-19 lockdowns on frailty and wellbeing in older people and those living with long-term conditions. *Adv Clin Exp Med*. 2021;30(11):1111–1114. doi:10.17219/acem/144135
7. Adamczak M, Surma S, Więcek A. Acute kidney injury in patients with COVID-19: Epidemiology, pathogenesis and treatment. *Adv Clin Exp Med*. 2022;31(3):317–326. doi:10.17219/acem/143542
8. Matusiak Ł, Szepietowska M, Krajewski P, Białynicki-Birula R, Szepietowski J. Face masks use during the COVID-19 pandemic: Differences in attitudes and practices between medical and non-medical students. A survey of 2256 students in Poland. *Adv Clin Exp Med*. 2020;29(10):1201–1203. doi:10.17219/acem/126295
9. Wierzbicki J, Nowacki M, Chrzanowska M, et al. Additive manufacturing technologies enabling rapid and interventional production of protective face shields and masks during the COVID-19 pandemic. *Adv Clin Exp Med*. 2020;29(9):1021–1028. doi:10.17219/acem/126296
10. Arnabat-Dominguez J, Del Vecchio A, Todea C, et al. Laser dentistry in daily practice during the COVID-19 pandemic: Benefits, risks and recommendations for safe treatments. *Adv Clin Exp Med*. 2021;30(2):119–125. doi:10.17219/acem/130598
11. Madej M, Sebastian A, Morgiel E, et al. The assessment of the risk of COVID-19 infection and its course in the medical staff of a COVID-only and a non-COVID hospital. *Adv Clin Exp Med*. 2022;31(9):981–989. doi:10.17219/acem/149292
12. Zubkiewicz-Kucharska A, Seifert M, Stępkowski M, Noczyńska A. Diagnosis of type 1 diabetes during the SARS-CoV-2 pandemic: Does lockdown affect the incidence and clinical status of patients? *Adv Clin Exp Med*. 2021;30(2):127–134. doi:10.17219/acem/130359
13. Guterman EL, Braunstein LZ. Preprints during the COVID-19 pandemic: Public health emergencies and medical literature. *J Hosp Med*. 2020;15(10):634–636. doi:10.12788/jhm.3491
14. Massarani L, Neves LFF. Reporting COVID-19 preprints: Fast science in newspapers in the United States, the United Kingdom and Brazil. *Cien Saude Colet*. 2022;27(3):957–968. doi:10.1590/1413-81232022273.20512021
15. van Schalkwyk F, Dudek J. Reporting preprints in the media during the COVID-19 pandemic. *Public Underst Sci*. 2022;31(5):608–616. doi:10.1177/09636625221077392
16. Älgå A, Eriksson O, Nordberg M. The development of preprints during the COVID-19 pandemic. *J Intern Med*. 2021;290(2):480–483. doi:10.1111/joim.13240
17. Clyne B, Walsh KA, O'Murchu E, et al. Using preprints in evidence synthesis: Commentary on experience during the COVID-19 pandemic. *J Clin Epidemiol*. 2021;138:203–210. doi:10.1016/j.jclinepi.2021.05.010
18. Brierley L. Lessons from the influx of preprints during the early COVID-19 pandemic. *Lancet Planet Health*. 2021;5(3):e115–e117. doi:10.1016/S2542-5196(21)00011-5
19. Fraser N, Brierley L, Dey G, et al. The evolving role of preprints in the dissemination of COVID-19 research and their impact on the science communication landscape. *PLoS Biol*. 2021;19(4):e3000959. doi:10.1371/journal.pbio.3000959
20. Brierley L, Nanni F, Polka JK, et al. Tracking changes between preprint posting and journal publication during a pandemic. *PLoS Biol*. 2022;20(2):e3001285. doi:10.1371/journal.pbio.3001285

Accuracy of machine learning algorithms for the assessment of upper-limb motor impairments in patients with post-stroke hemiparesis: A systematic review and meta-analysis

Jorge Fernando Ambros-Antemate[1,A,B,D,F], Adriana Reyes-Flores[1,B,D,F], Liliana Argueta-Figueroa[2,A,D–F], Rafael Ramírez-Ramírez[1,B,D,F], Marciano Vargas-Treviño[3,C,E,F], Jaime Gutiérrez-Gutiérrez[3,C,E,F], Eduardo Pérez-Campos Mayoral[4,B,E,F], Eduardo Pérez-Campos[4,B,E,F], Luis Angel Flores-Mejía[5,C,E,F], Rafael Torres-Rosas[6,A,D–F]

[1] School of Medicine and Surgery, Benito Juárez Autonomous University of Oaxaca, Mexico
[2] CONACyT- School of Dentistry, Benito Juárez Autonomous University of Oaxaca, Mexico
[3] School of Biological Systems and Technological Innovation, Benito Juárez Autonomous University of Oaxaca, Mexico
[4] Center for Research UNAM-UABJO, Benito Juárez Autonomous University of Oaxaca, Mexico
[5] School of Public Health, Imperial College, London, United Kingdom
[6] Immunology Laboratory, Cencer for Health and Diseases Sciences Research, School of Dentistry, Benito Juárez Autonomous University of Oaxaca, Mexico

A – research concept and design; B – collection and/or assembly of data; C – data analysis and interpretation;
D – writing the article; E – critical revision of the article; F – final approval of the article

Advances in Clinical and Experimental Medicine, ISSN 1899–5276 (print), ISSN 2451–2680 (online) *Adv Clin Exp Med*. 2022;31(12):1309–1318

Address for correspondence
Rafael Torres-Rosas
E-mail: rtorres.cat@uabjo.mx

Funding sources
None declared

Conflict of interest
None declared

Acknowledgements
The authors would like to thank The National Council on Science and Technology (CONACyT) for providing the scholarships (No. 764816, No. 746138, No. 776919), the Investigadoras e Investigadores por México CONACYT program, and Postgraduate Division and Dentistry School, Benito Juárez Autonomous University of Oaxaca, Mexico, for their support, as well as Cuerpo académico "Investigación en Salud" UABJO-CA-63.

Received on March 31, 2022
Reviewed on May 25, 2022
Accepted on August 3, 2022

Published online on September 1, 2022

DOI
10.17219/acem/152596

Abstract

Background. The assessment of motor function is vital in post-stroke rehabilitation protocols, and it is imperative to obtain an objective and quantitative measurement of motor function. There are some innovative machine learning algorithms that can be applied in order to automate the assessment of upper extremity motor function.

Objectives. To perform a systematic review and meta-analysis of the efficacy of machine learning algorithms for assessing upper limb motor function in post-stroke patients and compare these algorithms to clinical assessment.

Materials and methods. The protocol was registered in the International Prospective Register of Systematic Reviews (PROSPERO) database. The review was carried out according to the Preferred Reporting Items for Systematic Reviews and Meta-Analyses (PRISMA) guidelines and the Cochrane Handbook for Systematic Reviews of Interventions. The search was performed using 6 electronic databases. The meta-analysis was performed with the data from the correlation coefficients using a random model.

Results. The initial search yielded 1626 records, but only 8 studies fully met the eligibility criteria. The studies reported strong and very strong correlations between the algorithms tested and clinical assessment. The meta-analysis revealed a lack of homogeneity ($I^2 = 85.29\%$, $Q = 48.15$), which is attributable to the heterogeneity of the included studies.

Conclusions. Automated systems using machine learning algorithms could support therapists in assessing upper extremity motor function in post-stroke patients. However, to draw more robust conclusions, methodological designs that minimize the risk of bias and increase the quality of the methodology of future studies are required.

Key words: stroke, machine learning, computer-assisted diagnosis

Cite as
Ambros-Antemate JF, Reyes-Flores A, Argueta-Figueroa L, et al. Accuracy of machine learning algorithms for the assessment of upper-limb motor impairments in patients with post-stroke hemiparesis: A systematic review and meta-analysis. *Adv Clin Exp Med*. 2022;31(12):1309–1318. doi:10.17219/acem/152596

Introduction

According to the World Health Organization (WHO), 15 million people worldwide suffer a stroke every year.[1] Of these, approx. 5 million are left with a disability that limits their capacity to perform daily activities. They are also prone to becoming depressed or stressed due to limitations of their motor functions.[2]

Because of these conditions, patients have to participate in rehabilitation programs aimed at improving their quality of life. These programs support them in regaining motor function in the areas affected by the stroke.[3] First, it is necessary to assess the degree of impairment to properly select the best therapeutic options.[4] There are numerous motor assessment tests to evaluate the degree of upper limb disability, including the Fugl–Meyer Assessment[5] and the Wolf Motor Function Test.[6] In general, each test consists of a series of tasks to be performed by the patient, and the therapist evaluates those tasks using measures based on their observations. However, motor assessments require prior training of the examiners; therefore, in many cases, the evaluation tends to be subjective.[7] To avoid this problem, there is a great interest in the development of automated systems aimed at achieving objective and quantitative assessments for rehabilitation after strokes. Automated quantitative assessment systems can be used with home-based systems that assist patients in evaluating improvements during home-based exercise programs.

Thanks to technological advances, significant progress has been made in recent years in measuring and analyzing vital signs and human movement through artificial intelligence (AI).[8–10] Furthermore, AI has provided a technical basis for the automation of many processes,[11] such as rehabilitation[12] and evaluation of upper limb motor function.

Objectives

Based on these points, the main objective of this study was to perform a systematic review and meta-analysis of the efficacy of machine learning algorithms in assessing upper limb motor function in post-stroke patients, and compare these algorithms to clinical assessment.

Materials and methods

Study protocol and record

The systematic review was conducted according to the Preferred Reporting Items for Systematic Reviews and Meta-Analyses (PRISMA) guidelines[13] and the Cochrane Handbook for Systematic Reviews of Interventions.[14] In addition, the review protocol was published in the International Prospective Register of Systematic Reviews (PROSPERO) with the registration number PROSPERO 2021 CRD42021257217 (https://www.crd.york.ac.uk/prospero/display_record.php?ID=CRD42021257217).

Eligibility criteria, information sources and search strategy

The articles included assessed upper limb motor function in post-stroke patients through machine learning algorithms compared to standard clinical assessment. The outcomes of interest were diagnostic accuracy, specificity, and/or sensitivity. Articles were excluded if they assessed motor function to predict patient recovery time; case series and literature reviews were also excluded. The patient-intervention-comparison-outcome (PICO) strategy was used to identify the key words used (Table 1). The electronic search was performed in May 2021 and updated in October 2021. The information sources and algorithms used in each database are shown in Table 1.

Selection process

Three authors (JFAA, ARF and RRR) independently reviewed the registries obtained by the search. Duplicate records were removed using Mendeley Desktop v. 1.19.8 Reference Manager (Elsevier, Amsterdam, the Netherlands).[15] Studies that met the eligibility criteria by reading the title and abstract were retrieved in full text. Any disagreement was addressed by another reviewer (LAF) who made the final decision. The selection process is summarized in the PRISMA flowchart (Fig. 1).

Data collection process and data items

The relevant data of the included articles were collected in a standardized Microsoft Excel 2019 spreadsheet (Microsoft Corp., Redmond, USA). The data included study design, characteristics of the population, type of machine learning algorithm, data acquisition device, reference test, relative sensitivity, relative specificity, and confidence intervals. Three reviewers were responsible for data extraction (MVT, JGG and LAFM). When there were disagreements, the reviewers held discussions until reaching a consensus. The researchers of the original articles were contacted via e-mail for missing or additional details.

Assessment of risk of bias and quality of the included studies

Three reviewers (EPCM, EPC and ARF) assessed the risk of bias of the included studies following Chapter 8 of the Cochrane Handbook for Systematic Reviews of Interventions.[14] Additionally, the reviewers performed a quality assessment of the studies using the modified QUADAS-2 tool (Table 2),[16] which encompasses the following 5 domains: sample selection, index test, reference standard, flow rate, and time.

Table 1. Patient, intervention, comparison, outcome (PICO) strategy and algorithms used for the systematic review

Population	Post-stroke patients with hemiparesis of the upper-limb motor impairments.
Intervention	Algorithms of machine learning.
Comparison	Clinical evaluation assessment: Fugl–Meyer assessment, Wolf Motor Function Test, Modified Ashworth Scale, Chedoke–McMaster Stroke, or Motor Assessment Scale.
Outcomes	Diagnostic: Accuracy, specificity or sensibility.
Study design	Randomized clinical trial, non-randomized clinical trial, case-control study, or cohort study.
Eligibility criteria	Studies published in English and Spanish.
Electronic databases	PubMed, IEEE Xplore, ScienceDirect, Taylor & Francis Online, Wiley Online Library, and Google Scholar.
Focused question	Is there any evidence for the application of machine learning algorithms in the assessment of upper-limb motor impairments in patients with post-stroke hemiparesis?
Number of registers found for each database	Algorithms used for search strategy adapted for each database
PubMed; October 16, 2020 32 records	("machine learning" OR "learning, machine" OR "transfer learning" OR "learning, transfer" OR "neural network" OR "deep learning" OR "knowledge bases" OR "hierarchical learning" OR "expert systems" OR "fuzzy logic" OR "computer vision" OR "artificial intelligence" OR "support vector machine") AND ("motor" OR "motor function" OR "activities, motor" OR "activity, motor" OR "motor activities") AND ("evaluation" OR "assessment" OR "quantify" OR "quantitative" OR "scoring") AND ("extremities, upper" OR "upper extremities" OR "membrum superius" OR "upper limb" OR "limb, upper" OR "limbs, upper" OR "upper limbs" OR "extremity, upper" OR "upper-limb") AND ("stroke" OR "cerebrovascular accident")
Google Scholar; October 16, 2020 1390 records	"machine learning" AND "motor function" AND ("evaluation" OR "assessment" OR "quantitative") AND "upper limb" AND "stroke"
IEEE Xplore; December 1, 2020 4 records	"machine learning" AND "motor function" AND ("evaluation" OR "assessment" OR "quantitative") AND "upper limb" AND "stroke"
ScienceDirect; December 15, 2020 39 records	"machine learning" AND "motor function" AND ("evaluation" OR "assessment" OR "quantitative") AND "upper limb" AND "stroke"
Taylor & Francis Online; December 18, 2020 29 records	"machine learning" AND "motor function" AND ("evaluation" OR "assessment" OR "quantitative") AND "upper limb" AND "stroke"
Wiley Online Library; December 22, 2020 132 records	"machine learning" AND "motor function" AND ("evaluation" OR "assessment" OR "quantitative") AND "upper limb" AND "stroke"

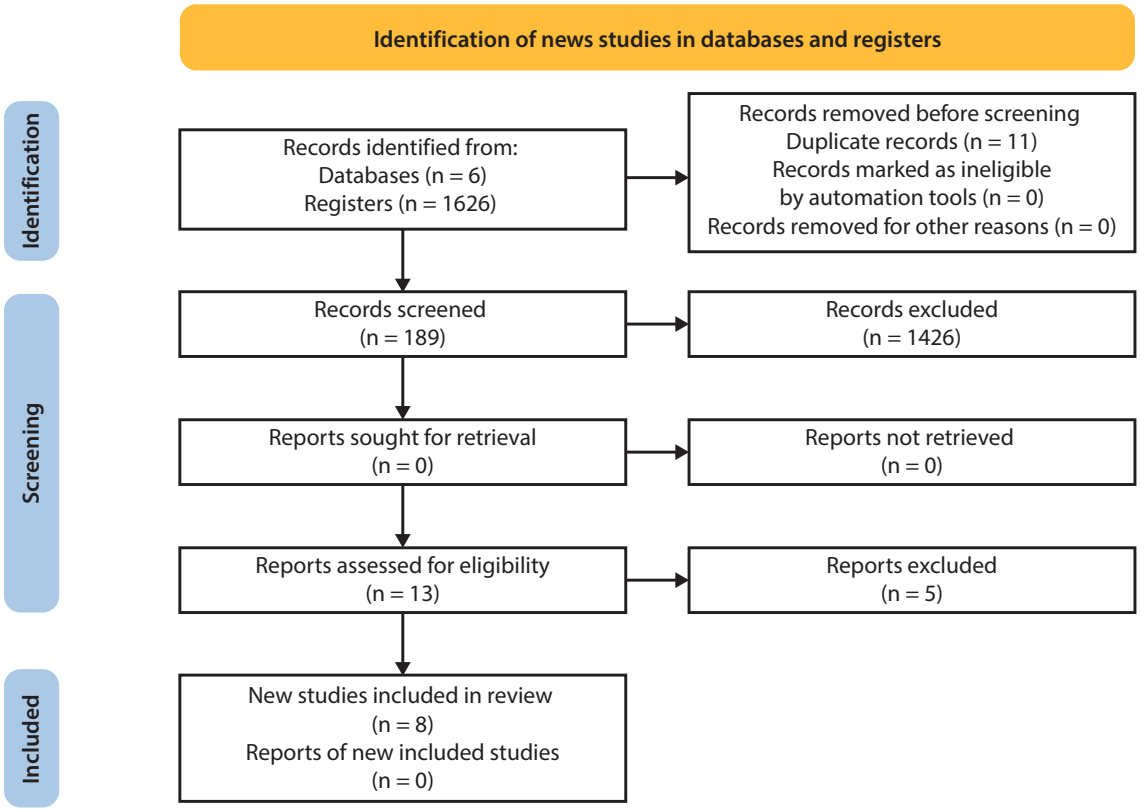

Fig. 1. Preferred Reporting Items for Systematic Reviews and Meta-Analyses (PRISMA) flow diagram of the selection process of the studies included in the systematic review

Table 2. QUADAS-2 modification

Domain name	Questions
Risk of bias	
1. Patient selection	1. Was a random or a consecutive sample of patients enrolled? 2. Was a case-control design avoided? 3. Were the exclusions made avoided?
2. Index test	1. Is there a sample calculation and the minimum necessary number of patients used?* 2. Was it previously specified if a threshold was used to define the positivity or negativity of the index test?
3. Benchmark	1. Is the reference test likely to correctly assess the target condition? 2. Were the reference test results interpreted without knowledge of the index test results?
4. Flow and Times	1. Was there an appropriate interval between the index test and the reference test? 2. Was the same reference test applied to all individuals? 3. Were all patients included in the analysis?
Applicability	
1. Patient selection	Is there a concern that the application or interpretation of the test being assessed does not match the review question?
2. Index test	Is there a concern that driving the index test or interpretation does not match the review question?
3. Benchmark	Is there a concern that the target condition, classified as such through the reference test, differs from the population to which the question was referred?

* This element was modified.

In case of disagreements in the assessment of risk of bias, the differences were resolved by consensus of the research group.

Summary of results

A formal narrative synthesis concerning the accuracy of the machine learning algorithms to determine the level of upper limb impairment was performed.

Meta-analysis

In order to assess the accuracy of the machine learning algorithms in determining the level of upper limb impairment, correlation coefficients were explored. The meta-analysis was performed using the metafor package (v. 3.0-2) of the R software program (R Development Core Team, 2011; R Foundation for Statistical Computing, Vienna, Austria) with the data from the correlation coefficients, using a random model. In addition, a test for funnel plot asymmetry and a likelihood ratio test for publication bias were performed using the metafor and weight packages, respectively.

Results

Selection and characteristics of the studies

The initial search yielded 1626 records. Eleven duplicate records were eliminated, leaving 1615 records that were reviewed by title and abstract. As a result of this review, 189 records related to the research question were identified. Of these, 13 full-text studies were assessed, but only 8 met the eligibility criteria (Fig. 1). All articles had an observational study design.

Results of the individual studies

Data acquisition

The researchers used different modalities for data acquisition in the included studies. Some researchers applied more than one device, while others used a single device. Of these, the most common was surface electromyography (sEMG), followed by electroencephalography (EEG), Microsoft Kinect, inertial measurement unit (IMU), accelerometer, flex sensors, and cell phone.

For sEMG, data are obtained through noninvasive electrodes, which measure the time and intensity of the electrical signals from the muscles. Among the included studies, Wang et al.,[17] Li et al.[18] and Zhou et al.[19] used this device.

Zhang et al. used EEG, which involves placing electrodes on the scalp. Each electrode sends a signal to a device called an electroencephalograph, which displays the rhythmic fluctuation of the brain's electrical activity (brain waves) in real time.[20]

An IMU is an electronic device that measures and reports velocity, orientation and, in some models, gravitational forces. Data are obtained from a combination of accelerometers, gyroscopes and magnetometers. Inertial measurement units are small devices that are placed noninvasively on the patient's skin to obtain motion data in 3 dimensions. Among the included studies, Li et al.[18] used an MPU-9250 device (InvenSense, San Jose, USA), while Zhang et al.[21] used an MPU-6050 device (Xsens Technologies, Los Angeles, USA).

Kim et al. used Microsoft Kinect (Microsoft Corp., Redmond, USA).[22] This device has cameras for motion and depth detection. It was initially developed as a video game device for Microsoft Xbox console; it tracks players' movements while they interact with a game. The Kinect consists

of an infrared light projector and a red-green-blue (RGB) video camera. The reflected infrared light is converted into depth data and calibrated with RGB data to distinguish shapes.

Yu et al. used an ADXL345 accelerometer and flex sensors.[23] An accelerometer is an electronic device that measures the vibration or acceleration of the movement of a structure. The force generated by the vibration or change in motion (acceleration) is detected, and an electrical charge is generated that is proportional to the force exerted on it. Accelerometers also play an important role in determining orientation and direction. Flex sensors are small strips composed of polymeric ink with embedded conductive particles; their function is to measure the resistivity when the sensor is flexed. Subsequently, the resistance value is converted into joint rotation angles.

Finally, Song et al. used an accelerometer and gyroscope integrated into a cell phone (iPhone 7, running an iOS 11.2.5 operating system; Apple Inc., Cupertino, USA).[24] Through this device, the researchers obtained the position and location of the hand in 3 dimensions.

Machine learning algorithms

The machine learning algorithms used for the assessment of motor function are briefly described below.

The machine learning algorithms using supervised learning included the support vector machine (SVM), which was employed by Wang et al.[17] and Zhou et al.[19] Support vector machine is a learning-based method for solving classification and regression problems. This algorithm is a decision function based on the hyperplane concept, a boundary that distinguishes several points in different classes and separates them.[25] In the same sense, Wang et al. used the backpropagation neural network (BPNN).[17] This algorithm applies the concept of gradient descent. Given an artificial neural network and an error function, this method calculates the gradient of the error function concerning the weights of the neural network. Wang et al.[17] and Zhou et al.[19] applied the random forest (RF) algorithm, which is a set of decision trees that are independent of each other. The advantage of the RF algorithm is that it can be used for both classification and regression problems, which constitute the majority of the current machine learning systems.

Continuing with supervised learning algorithms, Zhang et al. employed the convolutional neural network (CNN).[20] This type of neural network processes its layers by emulating the visual cortex of the human eye to recognize different features in the inputs. Convolutional neural network incorporates several specialized hidden layers into a hierarchy. The first layers can detect simple patterns, such as lines, curves and others; this is then specialized to deeper layers that recognize increasingly complex shapes. In the same way, Li et al. applied the least absolute shrinkage and selection operator (LASSO), which is a regression analysis method used to model the relationship between a dependent variable (which can be a vector) and one or more explanatory variables.[18] On the other hand, Kim et al. applied the artificial neural network (ANN), which is a computational learning system that uses a network of functions to understand and translate data input (usually patterns and relationships) into a desired output.[22] The concept of artificial neural network was inspired by human biology and how neurons in the human brain interconnect to understand human sensory inputs. Likewise, Zhou et al. applied linear discriminant analysis (LDA), which is based on the rule of maximum a posteriori probability and Bayesian principles, to find a linear combination of features that characterize or separate 2 or more classes of objects or events.[19]

Finally, Zhang et al. applied the K-nearest neighbor (KNN), which classifies an unknown sample by initially calculating the distance from that sample to all training samples.[21] This algorithm is used to rank values by looking for the "most similar" (closest) data points learned in the training stage and estimating new points based on that ranking. Similarly, Yu et al. used extreme learning machine (ELM).[23] This algorithm includes several hidden neurons in which the input weights are randomly assigned. In this type of network, data only go in one direction through a series of layers. It is implemented fully automatically without iterative tuning, and, in theory, no user intervention is required. Likewise, Song et al. applied the decision tree (DT).[24] This algorithm is the most frequently used in classification and regression problems, in which categorical or continuous input and output variables are used. Decision tree is composed of a root node, several internal nodes and several terminal nodes. The goal of the tree is to make the optimal choice at the end of each node. The name itself suggests that this technique uses a flowchart as a tree structure to show the predictions that result from a series of splits based on the features of the inputs.

Correlation with clinical analysis

In the included studies, the algorithms that showed a very strong correlation with the Fugl–Meyer Assessment test were CNN,[20] DT,[24] SVM,[19] and ELM.[23] The algorithms that presented a strong correlation were the framework with the union of SVM, BPNN, and RF,[17] LASSO,[18] and ANN.[22] Finally, the KNN algorithm presented a strong correlation with the Brunnstrom evaluation scale (Table 3).[21]

Risk of bias and quality assessment

At the QUADAS-2 assessment, 100% of the included studies showed a high risk of bias, whereas the applicability section showed a low risk of bias in 100% of the studies. In addition, 87.5% of the studies did not describe how the patients in the sample were enrolled; therefore, domain 1 showed a high risk of bias (Fig. 2).

Table 3. Characteristics of the individual studies and their results

Study ID	Population	Machine learning algorithm/reference test	Data acquisition device	Result
Wang et al.[17]	Patients with stroke: male n = 9 female n = 6; Healthy subjects: male n = 10 female n = 5	SVM BPNN RF FMA-UE	surface electro-myography	Correlation with FMA-UE Pearson correlation = –0.87, p < 0.0001 True positive rate: SVM = 0.9982 BPNN = 0.9749 RF = 0.9583 Sensitivity and specificity: no data
Zhang et al.[20]	Patients with chronic stroke: n = 12; Healthy subjects: n = 14	CNN FMA-UE	electroencephalo-graphy	Correlation with FMA-UE Pearson correlation = 0.9921, p < 0.0001 Sensitivity and specificity: no data
Li et al.[18]	Patients with chronic stroke: n = 18; Healthy subjects: n = 16	LASSO FMA-UE	Inertial Measurement Unit MPU-9250; surface electro-myography	Correlation with FMA-UE Pearson correlation = 0.8736, p = no data Sensitivity and specificity: no data
Kim et al.[22]	Patients with chronic stroke: n = 41	ANN FMA-UE	Microsoft Kinect	Correlation with FMA-UE Pearson correlation = 0.799, p < 0.0001 Sensitivity and specificity: no data
Zhang et al.[21]	Patients with chronic stroke: n = 21; Healthy subjects: n = 8	KNNs Brunnstrom stages	Inertial Measurement Unit MPU-6050	Correlation with the Brunnstrom stages of recovery r = 0.862, p < 0.001 Sensitivity and specificity: no data
Yu et al.[23]	Patients with chronic stroke: n = 24	ELM FMA-UE	Accelerometer ADXL345; flex sensor	Correlation with FMA-UE Coefficient of determination = 0.918, p = no data Sensitivity and specificity: no data
Song et al.[24]	Patients with chronic stroke: n = 10	DT FMA-UE	cell phone	Correlation with FMA-UE Pearson correlation = 0.97, p < 0.01 Sensitivity and specificity: no data
Zhou et al.[19]	Patients with chronic stroke: n = 6; Healthy subjects: n = 11	SVM LDA RF FMA-UE	surface electro-myography	Correlation with FMA-UE Pearson correlation = 0.93, p < 0.05 Sensitivity and specificity: no data

SVM – support vector machine; BPNN – backpropagation neural network; RF – random forest; CNN – convolutional neural network; LASSO – least absolute shrinkage and selection operator; ANN – artificial neural network; KNNs – K-nearest neighbors; ELM – extreme learning machine; DT – decision tree; LDA – linear discriminant analysis; FMA-UE – Fugl–Meyer Assessment for Upper Extremity.

Meta-analysis

The results of the meta-analysis suggest that there is a correlation between clinical assessment (Fugl–Meyer Assessment and Brunnstrom's evaluation scale) and machine learning algorithms in the evaluation of upper limb motor function (Fisher's z_r (95% confidence interval (95% CI)) = 1.62 (1.24–2.00), p < 0.001). In addition, the absence of homogeneity was observed (I^2 = 85.29%, Q = 48.15), which is attributable to the heterogeneity of the studies. The result of the test for funnel plot asymmetry was z = 1.1914, p = 0.2335, limit estimate (as sei ≥ 0): b = 0.7919 (95% CI: –0.6242–2.2080), as shown in Fig. 3A,B. In addition, a likelihood ratio test was conducted comparing the adjusted model, including the selection to its unadjusted random-effects counterpart. The Vevea and Hedges weight-function model resulted in a likelihood ratio of χ^2 = 0.3062, p = 0.58. Taken together, this suggests that there was no publication bias.

Discussion

A wide variety of machine learning algorithms are described in this systematic review. Out of the 8 included studies, 6 (75.0%) used only one algorithm to assess motor function; 3 of these presented a very strong correlation[20,23,24] and 3 showed a strong correlation[18,21,22] between the algorithms for motor assessment and clinical assessment. Two (25.0%) of the studies employed 3 algorithms: Zhou et al. showed a very strong correlation[19] and Wang et al. reported a strong correlation[17] between motor assessment algorithms and clinical evaluation. The evidence is not conclusive concerning whether better results are obtained with the exclusive use of a single algorithm or with a combination of algorithms. This is contrary to Wang et al., who are in favor of combined use.[17]

In machine learning, the number of samples required for training the machine learning model depends on the complexity of both the problem to be solved and the algorithm developed.[26] Although there is no established minimum

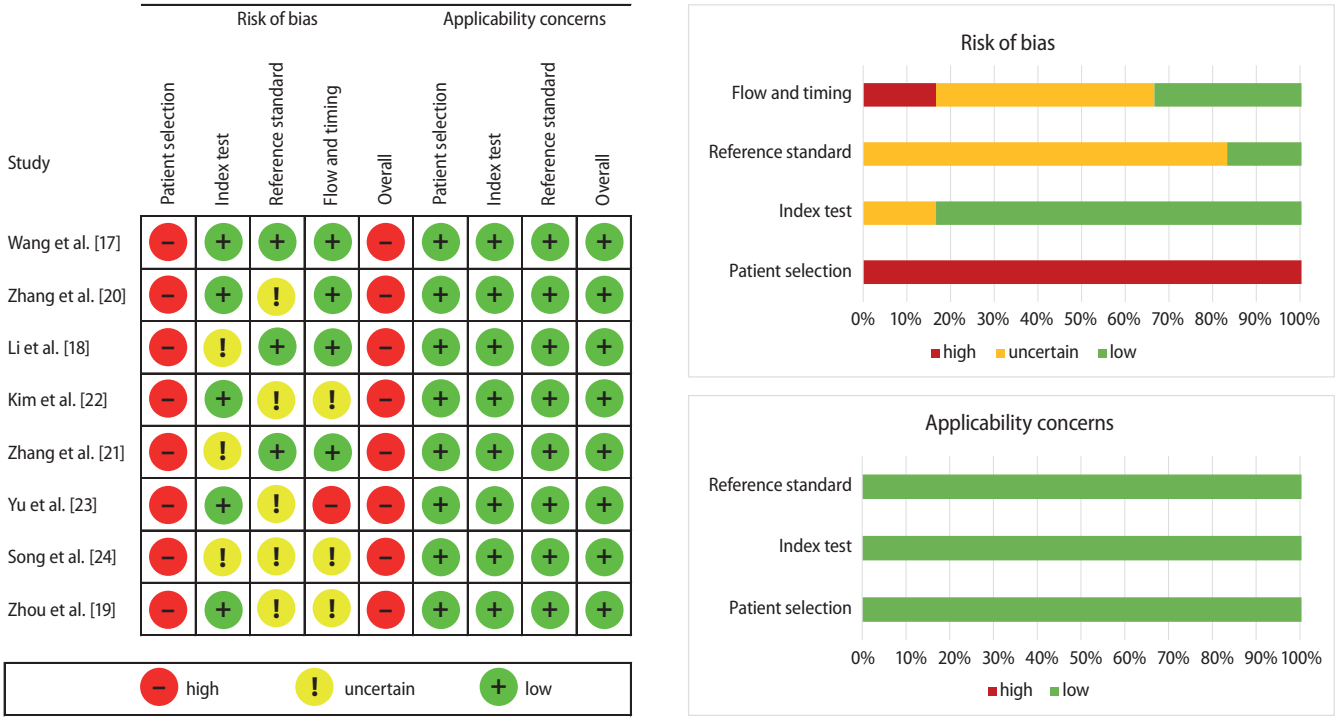

Fig. 2. Risk of bias assessment of the included studies using QUADAS-2

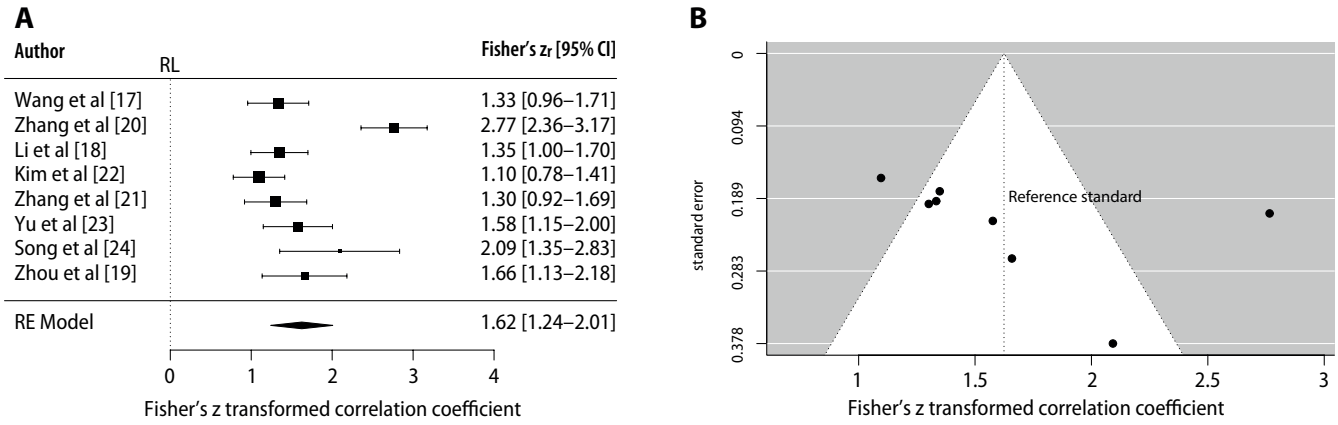

Fig. 3. Meta-analysis. A. Forest plot; B. Funnel plot, reference line (RL)

RE – random effects; 95% CI – 95% confidence interval.

number of training samples,[27] there are experiments that have indicated that increasing the size of the dataset improves performance.[27–29] Therefore, once the algorithm starts to detect patterns, it is best to increase the sample size. Of the included studies, 4 did not report the number of samples used for training,[18,21,22,24] while the rest reported using 992,[19] 1080,[17] 1680,[23] and 1960[20] samples; however, they did not justify the sample size used.

Data acquisition was performed using various sensors in the training of the algorithm and the evaluation of the upper limb motor function. Some are readily available (cell phone[24] and inertial sensors[18,21,23]), while others are specialized equipment that would limit their use to healthcare units (electromyography[17–19] and electroencephalography[20]).

The gold standard for evaluating motor function is clinical assessment, for which various assessment tools are available. These tools assess either general motor function (Medical Research Council (MRC) Scale and Fugl–Meyer Assessment) or specific areas of impairment (upper limb function, trunk function, gait ability, and spasticity). In this regard, the MRC Scale, the Frenchay Arm Test, and the Action Research Arm Test (ARAT) are specific to the upper limb motor function.[30]

The Fugl–Meyer Assessment is a performance-based index of the stroke-specific impairment.[31] It is designed to assess motor functioning, sensation, balance, joint range of motion, and joint pain in patients with post-stroke hemiplegia. It is the most commonly used scale in clinical assessments of the upper limb.[32,33] Thus, 87.5% of the studies

used the Fugl–Meyer Assessment for Upper Extremity (FMA-UE). The only study that did not use the FMA-UE was the study by Zhang et al.,[21] who used the Brunnstrom's evaluation scale.[34] It rates the recovery stage of the upper and lower extremities and hands in levels. The stages are classified from I to VI of recovery, whereby I indicates that the patient has low or absent movement, and VI indicates that the patient can perform voluntary movements.

As can be seen, the reported studies present at least a strong correlation with standard clinical tests. Therefore, the proposed evaluation systems have the potential to support therapists in the objective measurement of the upper limb motor function. Although the meta-analysis found a good relationship between machine learning algorithms and clinical assessment, it also showed a high heterogeneity.

The literature proposes that home-based rehabilitation can offer potential benefits,[35–37] such as performing the exercises according to the patient's schedule, providing flexibility of location and time, and receiving remote feedback and follow-up by the therapist. The home-based rehabilitation is possible to implement by having motor function evaluation systems, such as those presented in this review.

To the best of our knowledge, there are no systematic reviews in the literature evaluating the correlation between the clinical assessment of the upper limb motor function and machine learning algorithms in post-stroke patients.

Duque et al. conducted a systematic review that included studies focused on evaluating movement analysis in patients with stroke, Parkinson's disease, spinal cord injury, Huntington's disease, multiple sclerosis, and cerebral palsy, as well as in premature infants and the elderly.[38] However, their review did not perform the risk of bias assessment or a meta-analysis. Furthermore, it only focused on describing the devices used for data acquisition and the machine learning algorithms.

There are narrative reviews regarding the use of capture sensors and machine learning to perform automated assessments in home-based rehabilitation programs.[39] Caramiaux et al. described machine learning models for motor learning and their adaptive capabilities.[40] Moon et al. conducted a scoping review to explore the use of artificial neural networks in neurorehabilitation in various pathologies, including stroke, particularly in the prediction of variables such as functional recovery and rehospitalization.[41] In the same vein, Sirsat et al. performed a narrative review about the use of machine learning in stroke patients, grouping them according to their use for the identification of associated risk factors, diagnosis, treatment, and prognosis.[42] In summary, current reviews studying the application of machine learning in stroke patients focus on its use as a plausible tool for prediction and classification of neurological and motor impairments, as well as the assessment of rehabilitation progress.

Limitations

For more than a decade, the number of publications in basic science and clinical trials has grown exponentially. Clinical trials are considered the best evidence of solving a health problem. Unfortunately, some basic science results are not necessarily reflected in clinical practice.[43] Furthermore, several publications have divergent results despite presenting characteristics that superficially seem similar, or they use different variables to measure the impact of the intervention.[44,45] Hence the importance of evidence-based medicine aimed at determining the validity and analyzing the dataset of published studies through systematic reviews.

This systematic review encountered limitations, such as small sample sizes and a risk of bias in the included studies. In addition, the results of the meta-analysis showed high heterogeneity, probably due to the diversity of the statistical tests used in the correlation and different algorithms used in the studies. In addition, this review was limited to analyzing studies focused on the evaluation of the upper limb motor function, so studies analyzing the lower limb motor function were not considered. The exclusion of studies focused on the lower limbs could lead to a limitation, since both limbs have similar ranges of mobility; however, the inclusion of both limbs may have increased the heterogeneity of the review.

Conclusions

The results of the studies included in this systematic review show strong correlations between machine learning algorithms and clinical assessment scores of the upper limb. This correlation indicates a possible application to assist therapists in improving the efficacy of individualized diagnosis of motor function in post-stroke patients. The algorithms also serve as feedback to facilitate the training process for patient rehabilitation. Finally, studies with a representative sample, low risk of bias and better methodological quality are required to reach more robust conclusions.

ORCID iDs

Jorge Fernando Ambros-Antemate
https://orcid.org/0000-0003-1309-6147
Adriana Reyes-Flores https://orcid.org/0000-0002-5757-6495
Liliana Argueta-Figueroa https://orcid.org/0000-0002-1044-6757
Rafael Ramírez-Ramírez https://orcid.org/0000-0003-3729-2150
Marciano Vargas-Treviño https://orcid.org/0000-0002-2090-9727
Jaime Gutiérrez-Gutiérrez https://orcid.org/0000-0002-7713-3165
Eduardo Pérez-Campos Mayoral
https://orcid.org/0000-0002-6032-7609
Eduardo Pérez-Campos https://orcid.org/0000-0001-6720-7952
Luis Angel Flores-Mejía https://orcid.org/0000-0001-8157-5233
Rafael Torres-Rosas https://orcid.org/0000-0002-5934-003X

References

1. World Health Organization, World Bank. *World Report on Disability*. Geneva, Switzerland: World Health Organization; 2011. https://apps.who.int/iris/handle/10665/44575. Accessed October 19, 2021.
2. Das J, Rajanikat GK. Post stroke depression: The sequelae of cerebral stroke. *Neurosci Biobehav Rev*. 2018;90:104–114. doi:10.1016/j.neubiorev.2018.04.005
3. Le Danseur M. Stroke rehabilitation. *Crit Care Nurs Clin North Am*. 2020;32(1):97–108. doi:10.1016/j.cnc.2019.11.004
4. Futrell M, Rozzi SL. Principles of rehabilitation. *Prim Care*. 2020;47(1):87–103. doi:10.1016/j.pop.2019.10.004
5. Gladstone DJ, Danells CJ, Black SE. The Fugl–Meyer assessment of motor recovery after stroke: A critical review of its measurement properties. *Neurorehabil Neural Repair*. 2002;16(3):232–240. doi:10.1177/154596802401105171
6. Wolf SL, Catlin PA, Ellis M, Archer AL, Morgan B, Piacentino A. Assessing Wolf motor function test as outcome measure for research in patients after stroke. *Stroke*. 2001;32(7):1635–1639. doi:10.1161/01.STR.32.7.1635
7. Tanaka K, Yano H. Errors of visual judgement in precision measurements. *Ergonomics*. 1984;27(7):767–780. doi:10.1080/00140138408963550
8. Kringle EA, Knutson EC, Engstrom C, Terhorst L. Iterative processes: A review of semi-supervised machine learning in rehabilitation science. *Disabil Rehabil Assist Technol*. 2020;15(5):515–520. doi:10.1080/17483107.2019.1604831
9. Tack C. Artificial intelligence and machine learning applications in musculoskeletal physiotherapy. *Musculoskelet Sci Pract*. 2019;39:164–169. doi:10.1016/j.msksp.2018.11.012
10. Perezcampos Mayoral C, Gutiérrez Gutiérrez J, Cano Pérez JL, et al. Fiber optic sensors for vital signs monitoring: A review of its practicality in the health field. *Biosensors (Basel)*. 2021;11(2):58. doi:10.3390/bios11020058
11. O'Neil O, Gatzidis C, Swain I. A state of the art survey in the use of video games for upper limb stroke rehabilitation. In: Ma M, Jain LC, Anderson P, eds. *Virtual, Augmented Reality and Serious Games for Healthcare 1*. Berlin, Germany: Springer Berlin Heidelberg; 2014:345–370. doi:10.1007/978-3-642-54816-1_18
12. Beristain-Colorado MDP, Ambros-Antemate JF, Vargas-Treviño M, et al. Standardizing the development of serious games for physical rehabilitation: Conceptual framework proposal. *JMIR Serious Games*. 2021;9(2):e25854. doi:10.2196/25854
13. Moher D, Liberati A, Tetzlaff J, Altman DG. Preferred reporting items for systematic reviews and meta-analyses: The PRISMA statement. *PLoS Med*. 2009;6(7):e1000097. doi:10.1371/journal.pmed.1000097
14. Higgins JPT, Thomas J, Chandler J, et al., eds. *Cochrane Handbook for Systematic Reviews of Interventions*. 2nd ed. Hoboken, USA: Wiley; 2019. doi:10.1002/9781119536604
15. Mendeley. *Reference Management Software and Researcher Network*; 2015. https://www.mendeley.com/download-reference-manager/windows. Accessed October 10, 2021.
16. Whiting PF, Rutjes AWS, Westwood ME, et al. QUADAS-2: A revised tool for the quality assessment of diagnostic accuracy studies. *Ann Intern Med*. 2011;155(8):529–536. doi:10.7326/0003-4819-155-8-201110180-00009
17. Wang C, Peng L, Hou ZG, Li J, Zhang T, Zhao J. Quantitative assessment of upper-limb motor function for post-stroke rehabilitation based on motor synergy analysis and multi-modality fusion. *IEEE Trans Neural Syst Rehabil Eng*. 2020;28(4):943–952. doi:10.1109/TNSRE.2020.2978273
18. Li Y, Zhang X, Gong Y, Cheng Y, Gao X, Chen X. Motor function evaluation of hemiplegic upper-extremities using data fusion from wearable inertial and surface EMG sensors. *Sensors (Basel)*. 2017;17(3):582. doi:10.3390/s17030582
19. Zhou Y, Zeng J, Jiang H, Li Y, Jia J, Liu H. Upper-limb functional assessment after stroke using mirror contraction: A pilot study. *Artif Intell Med*. 2020;106:101877. doi:10.1016/j.artmed.2020.101877
20. Zhang X, D'Arcy R, Menon C. Scoring upper-extremity motor function from EEG with artificial neural networks: A preliminary study. *J Neural Eng*. 2019;16(3):036013. doi:10.1088/1741-2552/ab0b82
21. Zhang Z, Fang Q, Gu X. Objective assessment of upper limb mobility for post-stroke rehabilitation. *IEEE Trans Biomed Eng*. 2015;63(4):859–868. doi:10.1109/TBME.2015.2477095
22. Kim WS, Cho S, Baek D, Bang H, Paik NJ. Upper extremity functional evaluation by Fugl–Meyer assessment scoring using depth-sensing camera in hemiplegic stroke patients. *PLoS One*. 2016;11(7):e0158640. doi:10.1371/journal.pone.0158640
23. Yu L, Xiong D, Guo L, Wang J. A remote quantitative Fugl–Meyer assessment framework for stroke patients based on wearable sensor networks. *Comput Methods Programs Biomed*. 2016;128:100–110. doi:10.1016/j.cmpb.2016.02.012
24. Song X, Chen S, Jia J, Shull PB. Cellphone-based automated Fugl–Meyer assessment to evaluate upper extremity motor function after stroke. *IEEE Trans Neural Syst Rehabil Eng*. 2019;27(10):2186–2195. doi:10.1109/TNSRE.2019.2939587
25. Mechelli A, Viera S, eds. *Machine Learning: Methods and Applications to Brain Disorders*. San Diego, USA: Elsevier; 2019. ISBN: 978-012815-739-8.
26. Lantz B. *Machine Learning with R*. Birmingham, UK: Packt Publishing; 2013. ISBN: 978-1-78216-214-8.
27. Andonie R. Extreme data mining: Inference from small datasets. *Int J Comput Commun Control*. 2010;5(3):280–291. doi:10.15837/ijccc.2010.3.2481
28. Prusa J, Khoshgoftaar TM, Seliya N. The effect of dataset size on training tweet sentiment classifiers. In: *2015 IEEE 14th International Conference on Machine Learning and Applications (ICMLA)*. Miami, USA: IEEE; 2015:96–102. doi:10.1109/ICMLA.2015.22
29. Balki I, Amirabadi A, Levman J, et al. Sample-size determination methodologies for machine learning in medical imaging research: A systematic review. *Can Assoc Radiol J*. 2019;70(4):344–353. doi:10.1016/j.carj.2019.06.002
30. Cuadrado ÁA. Rehabilitation of the stroke: Evaluation, prognosis and treatment [in Spanish]. *Galicia Clín*. 2009;70(3):25–40. https://dialnet.unirioja.es/descarga/articulo/4208262.pdf. Accessed October 19, 2021.
31. Gladstone DJ, Danells CJ, Black SE. The Fugl–Meyer assessment of motor recovery after stroke: A critical review of its measurement properties. *Neurorehabil Neural Repair*. 2002;16(3):232–240. doi:10.1177/154596802401105171
32. Santisteban L, Térémetz M, Bleton JP, Baron JC, Maier MA, Lindberg PG. Upper limb outcome measures used in stroke rehabilitation studies: A systematic literature review. *PLoS One*. 2016;11(5):e0154792. doi:10.1371/journal.pone.0154792
33. Gor-García-Fogeda MD, Molina-Rueda F, Cuesta-Gómez A, Carratalá-Tejada M, Alguacil-Diego IM, Miangolarra-Page JC. Scales to assess gross motor function in stroke patients: A systematic review. *Arch Phys Med Rehabil*. 2014;95(6):1174–1183. doi:10.1016/j.apmr.2014.02.013
34. Brunnstrom S. Motor testing procedures in hemiplegia: Based on sequential recovery stages. *Phys Ther*. 1966;46(4):357–375. doi:10.1093/ptj/46.4.357
35. Chen Y, Abel KT, Janecek JT, Chen Y, Zheng K, Cramer SC. Home-based technologies for stroke rehabilitation: A systematic review. *Int J Med Inform*. 2019;123:11–22. doi:10.1016/j.ijmedinf.2018.12.001
36. Langan J, DeLave K, Phillips L, Pangilinan P, Brown S. Home-based telerehabilitation shows improved upper limb function in adults with chronic stroke: A pilot study. *J Rehabil Med*. 2013;45(2):217–220. doi:10.2340/16501977-1115
37. Anderson C, Mhurchu CN, Rubenach S, Clark M, Spencer C, Winsor A. Home or hospital for stroke rehabilitation? Results of a randomized controlled trial. II: Cost minimization analysis at 6 months. *Stroke*. 2000;31(5):1032–1037. doi:10.1161/01.STR.31.5.1032
38. Duque E, Trefftz H, Srivastava S. Objective assessments of human motor ability of the upper limb: A systematic review. *Technol Disabil*. 2021;33(1):29–44. doi:10.3233/TAD-200263
39. Liao Y, Vakanski A, Xian M, Paul D, Baker R. A review of computational approaches for evaluation of rehabilitation exercises. *Comput Biol Med*. 2020;119:103687. doi:10.1016/j.compbiomed.2020.103687
40. Caramiaux B, Françoise J, Liu W, Sanchez T, Bevilacqua F. Machine learning approaches for motor learning: A short review. *Front Comput Sci*. 2020;2:16. doi:10.3389/fcomp.2020.00016
41. Moon S, Ahmadnezhad P, Song HJ, et al. Artificial neural networks in neurorehabilitation: A scoping review. *NeuroRehabilitation*. 2020;46(3):259-269. doi:10.3233/NRE-192996
42. Sirsat MS, Fermé E, Câmara J. Machine learning for brain stroke: A review. *J Stroke Cerebrovasc Dis*. 2020;29(10):105162. doi:10.1016/j.jstrokecerebrovasdis.2020.105162

43. Manzo-Toledo A, Torres-Rosas R, Mendieta-Zerón H, Arriaga-Pizano L, Argueta-Figueroa L. Hydroxychloroquine in the treatment of COVID-19 disease: A systematic review and meta-analysis. *Med J Indones*. 2021; 30(1):20–32. doi:10.13181/mji.oa.205012
44. Castro-Gutiérrez MEM, Argueta-Figueroa L, Fuentes-Mascorro G, Moreno-Rodríguez A, Torres-Rosas R. Novel approaches for the treatment of necrotic immature teeth using regenerative endodontic procedures: A systematic review and meta-analysis. *Appl Sci*. 2021; 11(11):5199. doi:10.3390/app11115199
45. Ávila-Curiel BX, Gómez-Aguirre JN, Gijón-Soriano AL, Acevedo-Mascarúa AE, Argueta-Figueroa L, Torres-Rosas R. Complementary interventions for pain in patients with temporomandibular joint disorders: A systematic review [in Spanish]. *Rev Int de Acupunt*. 2020;14(4): 151–159. doi:10.1016/j.acu.2020.10.004

Carotid contrast-enhanced ultrasonography combined with sirtuin-3 in the diagnosis of plaques in carotid atherosclerosis

Aiyun Zhou[E,F], Wan Zhu[A–D], Pan Xu[E], Chunxiao Zhao[E], Liping Jiang[E], Wenxin Yuan[E]

Department of Ultrasonography, The First Affiliated Hospital of Nanchang University, China

A – research concept and design; B – collection and/or assembly of data; C – data analysis and interpretation;
D – writing the article; E – critical revision of the article; F – final approval of the article

Advances in Clinical and Experimental Medicine, ISSN 1899–5276 (print), ISSN 2451–2680 (online) *Adv Clin Exp Med*. 2022;31(12):1319–1326

Address for correspondence
Aiyun Zhou
E-mail: zhouaiyuntt@163.com

Funding sources
None declared

Conflict of interest
None declared

Received on December 8, 2021
Reviewed on April 21, 2022
Accepted on July 28, 2022

Published online on September 9, 2022

Abstract

Background. Carotid atherosclerosis (CAS) is one of the main causes of ischemic stroke. Currently, the clinical evidence for contrast-enhanced ultrasonography (CEUS) as a method for diagnosing CAS is still inadequate. Sirtuin-3 (SIRT3) is associated with the inflammation response; however, few studies have evaluated SIRT3 in CAS.

Objectives. To investigate the role of SIRT3 in CAS patients and its diagnostic value for unstable plaques when combined with CEUS.

Materials and methods. This is a prospective observational study including 517 CAS patients who were admitted to our hospital from January 2015 to December 2020. All patients received a normal Doppler ultrasound, CEUS and magnetic resonance imaging (MRI). The latter was used as the gold standard in evaluating plaque conditions. Serum SIRT3 levels were measured using an enzyme-linked immunosorbent assay (ELISA). Serum levels of total cholesterol (TC), triglycerides (TG), high-density lipoprotein cholesterol (HDL-ch), low-density lipoprotein cholesterol (LDL-ch), C-reactive protein (CRP), and interleukin (IL)-6 levels were measured and recorded.

Results. Patients with severe CAS showed significantly higher levels of CRP, IL-6, TC, and LDL-ch, a higher frequency of unstable plaques, as well as a lower level of HDL-ch. In patients with severe CAS and CAS patients with stable plaques, the levels of SIRT3 were markedly lower. Patients with a high expression of SIRT3 showed significantly lower levels of CRP, IL-6, TC and LDL-ch, and higher levels of HDL-ch, as well as a lower frequency of unstable plaques. Receiver operating characteristic (ROC) curves showed that the combination of CEUS and SIRT3 could achieve high sensitivity and specificity in the diagnosis of unstable plaques. High levels of C-reactive protein, IL-6, TC, TG and LDL-ch, as well as low levels of SIRT3 and HDL-ch, and current smoking were risk factors of unstable plaques in CAS patients.

Conclusions. A low expression of SIRT3 predicted a higher risk for unstable plaques in CAS patients. The combination of CEUS and SIRT3 is a potential strategy for diagnosing unstable plaques.

Key words: plaques, contrast-enhanced ultrasonography, carotid atherosclerosis, SIRT3

Cite as
Zhou A, Zhu W, Xu P, Zhao C, Jiang L, Yuan W. Carotid contrast-enhanced ultrasonography combined with sirtuin-3 in the diagnosis of plaques in carotid atherosclerosis. *Adv Clin Exp Med*. 2022;31(12):1319–1326. doi:10.17219/acem/152471

DOI
10.17219/acem/152471

Background

Carotid atherosclerosis (CAS) is one of the main causes of ischemic stroke.[1,2] As reported in a recent study, in 2020, the global prevalence of increased carotid intima-media thickness (IMT) was approx. 27.6% and the prevalence of carotid plaques was approx. 21.1% in people aged 30–79 years.[3] In rural northeast China, the prevalence of CAS and carotid plaques can be as high as 33.1% and 31.5%, respectively.[4] Since CAS can remain asymptomatic for many years, the early diagnosis is very important in preventing severe consequences, such as stroke.[5,6]

Currently, imaging studies are the main strategy for diagnosing CAS, including computed tomography (CT) scans, Doppler ultrasounds, magnetic resonance imaging (MRI), etc.[7–9] Among these methods, contrast-enhanced ultrasonography (CEUS) was developed in the recent decade. It utilizes resonated ultrasound waves from circulating microbubbles to produce superior angiography-like images for vascular visualization.[10] In recent years, some studies have shown the application of CEUS in diagnosing CAS plaques.[11,12] However, the clinical evidence is still inadequate.

Except for imaging methods, serum biomarkers are also important indices for the diagnosis and prediction of CAS.[13] Biomarkers such as inflammatory factors (C-reactive protein (CRP), interleukins (ILs)), lipid-related factors (high-density lipoprotein cholesterol (HDL-ch) and low-density lipoprotein cholesterol (LDL-ch)), endothelial and cell adhesion factors (VCAM-1, ICAM-1), etc., have all been widely studied.[14,15] Sirtuin-3 (SIRT3) belongs to the sirtuin family. Studies have found SIRT3 to be associated with inflammation and correlated with the development of cardiovascular diseases, such as myocardial ischemia-reperfusion injury.[16,17] However, up to now, few studies have focused on the clinical significance of SIRT3 in CAS patients and its potential value in predicting the condition of plaques.

Objectives

We performed an observational study to investigate the role of SIRT3 in CAS patients and its diagnostic value for unstable plaques when combined with CEUS. Our research might provide new insights into diagnosing unstable plaques and identifying biomarkers in CAS patients.

Materials and methods

Subjects

This is a prospective observational study including 517 CAS patients who were admitted to our hospital from January 2015 to December 2020. All patients diagnosed with CAS underwent a MRI to confirm the diagnosis. All patients also had a normal Doppler ultrasound and CEUS to evaluate the plaques. The exclusion criteria were as follows: 1) patients with stroke, coronary syndrome, and other severe cardiovascular or cerebrovascular diseases, such as cardiogenic cerebral embolism; 2) patients who were allergic to the contrast agent; 3) patients with cancer or dysfunction of the kidney or liver. All patients were allocated into the mild-moderate CAS or the severe CAS group according to the IMT, plaque condition and degree of arterial stenosis. Patients with an IMT > 1.0 mm with arterial stenosis <70% were allocated to the mild-moderate CAS group, while patients with multiple plaques and arterial stenosis ≥70% to the severe CAS group. Written informed consent was obtained from all patients. The present study was approved by the ethics committee at the First Affiliated Hospital of Nanchang University, China (approval No. NCDXYY20150612).

Imaging measurements for plaques

All patients received a normal Doppler ultrasound, CEUS and MRI. The IMT was measured using an Acuson-Aspen Color Doppler ultrasound diagnostic instrument (GE Healthcare, Boston, USA) with a probe frequency of 7.5 MHz. The IMT of bilateral common carotid arteries was measured proximally and distally to the bifurcation as well as at the bifurcation. Plaques were observed and classified as stable (strong echo or medium echo) or unstable (mixed echo or low echo) plaques based on the echo condition.

Contrast-enhanced ultrasonography was used to further evaluate the conditions of the plaques using the Toshiba Aplio500 instrument (Toshiba, Tokyo, Japan) with a probe frequency of 5–14 MHz and a mechanical index (MI) of 0.08 MHz. SonoVue (Bracco, Geneva, Switzerland) was used as the contrast agent. Briefly, after the observation of the plaque, 1.0 mL of SonoVue suspension (dissolved in normal saline) was injected into a peripheral vein by rapid bolus injection, followed by an injection of 5 mL of normal saline. According to the measurement of teh plaques using CEUS, patients were described using 5 grades: grade 0 – no enhancement; grade 1 – an enhancement for adventitia but not the inner plaque; grade 2 – a small amount of scattered punctate enhancement within the plaquel; grade 3 – a linear enhancement extending into the plaque; and grade 4 – an intraplaque diffusion enhancement.

Magnetic resonance imaging was used as the gold standard to evaluate plaque conditions using a GE Discovery MR750w 3.0T MRI scanner (GE Healthcare). Briefly, after the full exposure of the neck blood vessels, the exact location of the carotid bifurcation and the plaques was obtained using 2D-TOF scanning. Then, axial scanning of the plaques was performed using T1WI, T2WI, 3D-T0F, and enhanced T1WI. For measurement of plaques, the signal-to-noise ratio (SNR) and imaging conditions

were analyzed and plaques were divided into different types according to the American Heart Association (AHA) classification. Types I, II, III, VII, and VIII were considered stable while all other types were regarded as unstable.[18]

Measurements of serum SIRT3 and other laboratory indices

The measurement of serum SIRT3 was conducted using a commercially available enzyme-linked immunosorbent assay (ELISA) kit (Lengton Bioscience, Shanghai, China), according to the manufacturer's instructions. Serum levels of total cholesterol (TC), triglycerides (TG), HDL-ch, LDL-ch, CRP, and interleukin (IL)-6 were measured using an automatic biochemical analyzer (Hitachi 7600; Hitachi Corporation, Tokyo, Japan).

Statistical analyses

The distribution of the data was analyzed using the Kolmogorov–Smirnov method. Non-normally distributed data were expressed as a median, interquartile range (IQR) and range. All continuous data included in this study had a non-normal distribution. The comparison between the 2 groups was conducted using the Mann–Whitney U test. Rates were analyzed using the χ^2 test. A receiver operating characteristic (ROC) curve was used for the diagnostic analysis, and Youden's index was used for selecting the cutoff value. Logistic regression was used to analyze the risk of unstable plaques. The Hosmer–Lemeshow test was used to measure the model's goodness-of-fit. A value of $p < 0.05$ was considered statistically significant. All calculations were performed using SPSS v. 18.0 (SPSS Inc., Chicago, USA).

Results

Basic characteristics of all patients

The study included a total of 517 CAS patients, with 311 (60.15%) cases of mild-moderate CAS and 206 (39.85%) cases of severe CAS. A total of 293 cases (56.67%) had stable plaques and 224 cases (43.33%) had unstable plaques. As shown in Table 1, severe CAS patients showed a significantly higher expression of CRP, IL-6, TC, and LDL-ch (all with a p-value <0.001), while the expression of HDL-ch was markedly lower in severe CAS patients ($p < 0.001$). Additionally, severe CAS patients showed a higher frequency of unstable plaques compared to mild-moderate patients ($p < 0.001$). The ratio of patients with a history of coronary heart disease was significantly higher in severe CAS patients ($p = 0.008$). The typical imaging results were shown in Fig. 1. All the statistical calculation results for continuous data and logistic regressions are listed in the Supplementary Data (Table S1–S10).

Table 1. Basic characteristics of the patients

Characteristics	All CAS (n = 517)	Mild-moderate (n = 311)	Severe (n = 206)	U or χ^2	p-value*
Age [years]	54 (13, 37–70)	54 (13, 37–68)	54 (14, 39–70)	31871.50	0.923
BMI [kg/m^2]	27.03 (6.47, 20.28–33.72)	27.29 (7.07, 20.28–33.71)	26.45 (5.82, 20.30–33.72)	30079.00	0.240
Female sex (%)	252 (48.74)	152 (48.87)	100 (48.54)	0.002	0.963
Complications, n (%)					
Diabetes	108 (20.89)	57 (18.33)	51 (24.76)	1.233	0.269
Hypertension	90 (17.41)	50 (16.08)	40 (19.42)	0.382	0.537
History of coronary heart disease	67 (12.96)	24 (7.72)	43 (20.87)	7.057	0.008
History of stroke	67 (12.96)	35 (11.25)	32 (15.53)	0.790	0.374
Current smoker	169 (32.69)	100 (32.15)	69 (33.50)	0.041	0.839
Plaque, n (%)					
Stable	293 (56.67)	231 (74.28)	62 (30.10)	39.112	<0.001
Unstable	224 (43.33)	80 (25.72)	144 (69.90)		
CRP [mg/L]	8.37 (6.40, 2.17–23.71)	6.44 (3.48, 2.17–15.34)	12.96 (8.25, 6.16–23.71)	7026.50	<0.001
IL-6 [pg/mL]	10.05 (7.57, 3.92–26.24)	9.24 (4.60, 3.92–26.02)	12.55 (10.24, 4.13–26.24)	20053.50	<0.001
TC [mmol/L]	4.24 (0.67, 3.25–5.38)	4.12 (0.59, 3.25–5.38)	4.45 (0.71, 3.26–5.38)	19848.50	<0.001
TG [mmol/L]	1.44 (0.42, 0.93–2.02)	1.43 (0.41, 0.93–1.99)	1.45 (0.42, 0.97–2.02)	29956.50	0.212
LDL-ch [mmol/L]	2.93 (0.53, 2.17–3.80)	2.86 (0.53, 2.17–3.79)	3.02 (0.54, 2.20–3.80)	23236.50	<0.001
HDL-ch [mmol/L]	1.11 (0.09, 0.96–1.24)	1.13 (0.10, 0.97–1.24)	1.09 (0.09, 0.96–1.24)	23555.50	<0.001

BMI – body mass index; CAS – carotid atherosclerosis; IL-6 – interleukin 6; TC – total cholesterol; TG – triglycerides; LDL-ch – low-density lipoprotein cholesterol; HDL-ch – high-density lipoprotein cholesterol; * p-value was obtained by comparing the mild-moderate and severe CAS groups. All continuous data presented non-normal distribution (BMI, CRP, IL-6, TC, TG, LDL-ch and HDL-ch, and SIRT3), and were expressed by median (interquartile range (IQR)). The comparison between the 2 groups was conducted using Mann–Whitney U test. Rates were analyzed with χ^2 test.

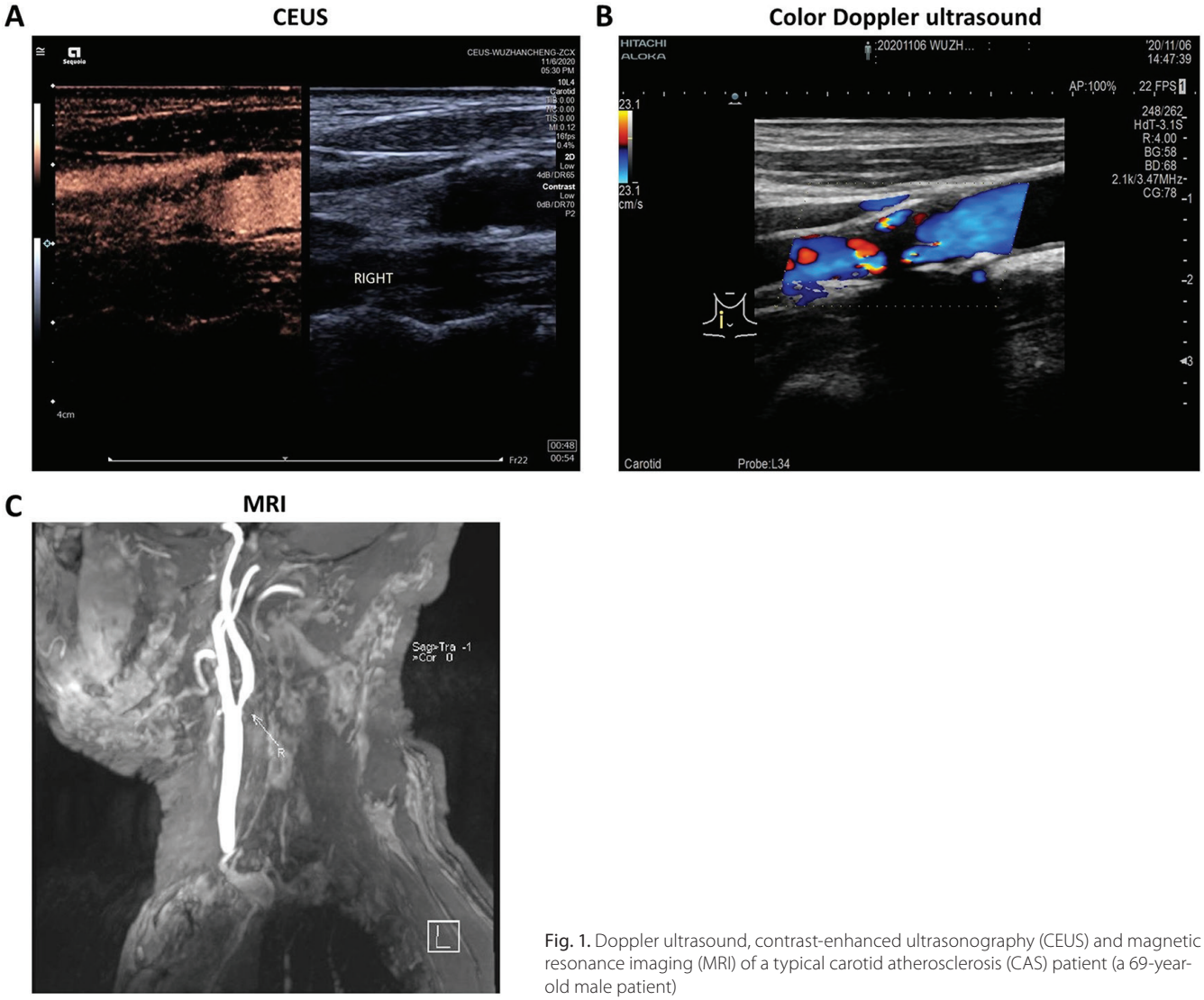

Fig. 1. Doppler ultrasound, contrast-enhanced ultrasonography (CEUS) and magnetic resonance imaging (MRI) of a typical carotid atherosclerosis (CAS) patient (a 69-year-old male patient)

SIRT3 was associated with the clinical outcomes of CAS patients

To further investigate the role of SIRT3 in CAS, serum SIRT3 levels were evaluated and compared. It was found that in severe CAS patients, the levels of SIRT3 were markedly lower than that of mild-moderate patients ($U = 22220.00$, $p < 0.001$, Fig. 2) Meanwhile, patients with unstable plaques showed a remarkably lower expression of SIRT3 compared to the patients with stable plaques ($U = 7899.00$, $p < 0.001$). Patients were further allocated into high or low SIRT3 expression groups, according to their median value (17.98 ng/mL). As shown in Table 2, patients with a high expression of SIRT3 showed significantly lower levels of CRP, IL-6, TC and LDL-ch, and higher levels of HDL-ch (all with a p-value < 0.001). The percentage of patients with unstable plaques was also lower in patients with higher SIRT3 levels ($p < 0.001$). These results indicate that SIRT3 might be associated with the clinical severity and plaque condition of CAS patients.

Diagnostic value of SIRT3 and CEUS for unstable plaques in CAS patients

Receiver operating characteristic curves were used to evaluate the diagnostic value of SIRT3 and CEUS for unstable plaques in CAS patients. Using a cutoff value of 17.14 ng/mL, SIRT3 showed the area under the curve (AUC) of 0.880 (95% confidence interval (95% CI): 0.852–0.907), with a sensitivity of 80.2% and specificity of 72.3% for diagnosis of unstable plaques. Meanwhile, CEUS grades with a cutoff value of 1.50 showed an AUC of 0.846 (95% CI: 0.810–0.882), achieving a sensitivity of 81.3% and specificity of 85.7% in diagnosing of unstable plaques. This result indicated that grades 0 and 1 were regarded as stable plaques, while unstable plaques were defined as grades 2–4. The cutoff values of SIRT3 and CEUS were combined and used for the diagnosis of unstable plaques. It was found that the combination of CEUS and SIRT3 could achieve a sensitivity of 94.20%, specificity of 69.28% and accuracy of 80.08% (Table 3, Fig. 3).

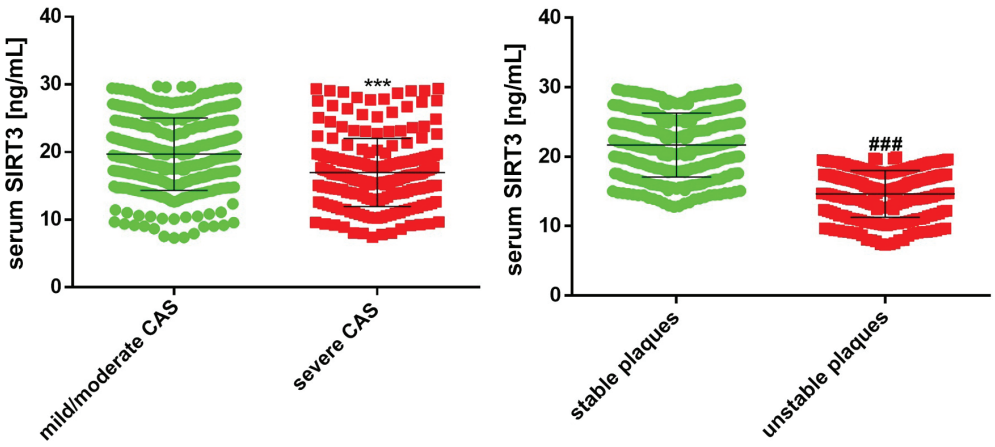

Fig. 2. Serum sirtuin-3 (SIRT3) levels in carotid atherosclerosis (CAS) patients with different severity and plaque conditions

*** $p < 0.001$ compared to mild/moderate CAS; ### $p < 0.001$ compared to stable plaques.

Table 2. Clinical characteristics of CAS patients with different expression of SIRT3

Characteristics	High SIRT3 (n = 257)	Low SIRT3 (n = 260)	U or χ^2	p-value*
Age [years]	54 (12.75, 37–69)	54 (13.00, 37–70)	32810.00	0.724
Female sex (%)	127 (49.42)	125 (48.08)	0.85	0.850
BMI [kg/m^2]	26.51 (6.36, 20.28–33.71)	27.08 (6.70, 20.30–33.72)	31614.00	0.290
Complications, n (%)				
Diabetes	49 (19.07)	59 (22.69)	0.397	0.529
Hypertension	48 (18.68)	42 (16.15)	0.223	0.637
History of coronary heart disease	26 (10.12)	41 (15.77)	1.416	0.234
History of stroke	29 (11.28)	38 (14.62)	0.495	0.482
Current smoker	73 (28.40)	96 (36.92)	1.650	0.199
Plaque, n (%)				
Stable	218 (84.82)	75 (28.85)	63.846	<0.001
Unstable	39 (12.54)	185 (89.81)		
CRP [mg/L]	6.67 (7.58, 2.17–23.07)	11.68 (4.22, 2.23–23.71)	16691.50	<0.001
IL-6 [pg/mL]	8.61 (9.79, 3.92–26.24)	13.11 (3.96, 4.25–26.23)	16276.50	<0.001
TC [mmol/L]	4.08 (0.74, 3.25–5.30)	4.47 (0.56, 3.26–5.38)	17177.00	<0.001
TG [mmol/L]	1.43 (0.44, 0.93–1.99)	1.45 (0.41, 0.96–2.02)	31918.00	0.380
LDL-ch [mmol/L]	2.79 (0.56, 2.17–3.80)	3.06 (0.47, 2.20–3.79)	19790.50	<0.001
HDL-ch [mmol/L]	1.13 (0.09, 0.96–1.24)	1.10 (0.10, 0.96–1.24)	24039.50	<0.001

SIRT3 – sirtuin-3; BMI – body mass index; CAS – carotid atherosclerosis; CRP – C-reactive protein; IL-6 – interleukin 6; TC – total cholesterol; TG – triglycerides; LDL-ch – low-density lipoprotein cholesterol; HDL-ch – high-density lipoprotein cholesterol; * p-value was obtained by comparison between SIRT3 high/low CAS groups. All continuous data presented non-normal distribution (BMI, CRP, IL-6, TC, TG, LDL-ch and HDL-ch, and SIRT3), and were expressed by median (interquartile range (IQR)). The comparison between the 2 groups was conducted using Mann–Whitney U test. Rates were analyzed using χ^2 test.

Risk factors for unstable plaques using logistic regression analysis

Binary logistic regression was employed to analyze risk factors for unstable plaques using a back-step method. After adjusting the model, we conducted multivariate logistic regressions evaluating age, body mass index (BMI), CRP, IL-6, and SIRT3 (model 1), sex and medical history (model 2), or the lipid metabolism factors – TC, TG, LDL-ch, and HDL-ch (model 3), using the entry method. The p-values of the Hosmer–Lemeshow tests for the 3 models were 0.983, 0.783 and 0.911, respectively. The results of each model are listed in Table 4. It was found that high levels of CRP, IL-6, TC, TG and LDL-ch, as well as low levels of SIRT3 and HDL-ch, and current smoking were all risk factors for unstable plaques in CAS patients (Table 4).

Discussion

Since CAS is closely associated with and is a main inducer of stroke, the early diagnosis of CAS is of great significance. We conducted an observational study to demonstrate

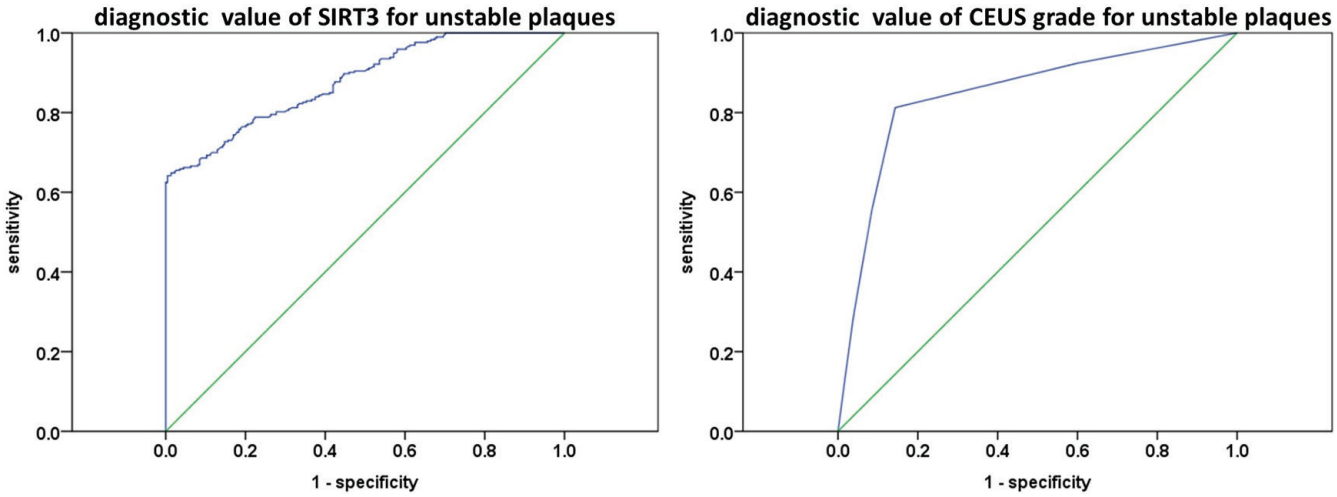

Fig. 3. Receiver operating characteristic (ROC) curve for the diagnostic value of sirtuin-3 (SIRT3) and contrast-enhanced ultrasonography (CEUS) (grade) in the diagnosis of unstable plaques

Table 3. Diagnostic value of SIRT3 and CEUS for the diagnosis of unstable plaques in CAS patients

Methods	True positive	False positive	True negative	False negative	Sensitivity	Specificity	Accuracy
Doppler ultrasound	150	77	216	74	66.96%	73.72%	70.79%
CEUS	182	42	251	42	81.25%	85.67%	83.75%
SIRT3	162	58	235	62	72.32%	80.20%	76.79%
CEUS+SIRT3	211	90	203	13	94.20%	69.28%	80.08%

SIRT3 – sirtuin-3; CEUS – contrast-enhanced ultrasonography; CAS – carotid atherosclerosis; * sensitivity = true positive/(true positive + false negative) × 100%; specificity = true negative/(true negative + false positive) × 100%; accuracy = (true positive + true negative)/(true positive + false negative + false positive + true negative) × 100%.

Table 4. Logistic regression for risk factors of unstable plaques

Variables	Hosmer– Lemeshow test	Wald	OR	95% CI	p-value
Model 1					
Age	0.983	3.603	0.925	0.854–1.003	0.058
BMI		0.222	1.037	0.893–1.204	0.637
CRP		39.226	2.648	1.952–3.592	<0.001
IL-6		24.906	1.682	1.371–2.063	<0.001
SIRT3		25.056	0.554	0.440–0.698	<0.001
Model 2					
Sex	0.783	0.177	1.078	0.758–1.533	0.674
Diabetes		0.979	0.804	0.522–1.238	0.322
Hypertension		0.758	1.232	0.770–1.972	0.384
History of coronary heart disease		1.892	0.694	0.413–1.168	0.169
History of stroke		0.001	1.010	0.583–1.752	0.971
Current smoker		5.293	0.629	0.424–0.934	0.021
Model 3					
TC	0.911	61.080	1.008	1.006–1.010	<0.001
TG		5.050	1.002	1.000–1.003	0.025
LDL-ch		42.322	1.004	1.003–1.006	<0.001
HDL-ch		30.696	0.138	0.068–0.278	<0.001

OR – odds ratio; 95% CI – 95% confidence interval; SIRT3 – sirtuin-3; BMI – body mass index; CRP – C-reactive protein; IL-6 – interleukin 6; TC – total cholesterol; TG – triglycerides; LDL-ch – low-density lipoprotein cholesterol; HDL-ch – high-density lipoprotein cholesterol.

that serum levels of SIRT3 were correlated with clinical outcomes, especially for severity and plaque stability. The combination of CEUS and SIRT3 might also be a potential diagnostic method for unstable plaques.

The application of CEUS is now widely accepted for the diagnosis of many cardiovascular and cerebrovascular diseases, including CAS.[19] Hamada et al. demonstrated that by using CEUS, physicians could observe a higher percentage of ulcerated findings in patients with plaque rupture.[20] Oura et al. showed that both CEUS and superb microvascular imaging had high sensitivity and specificity in the diagnosis of intraplaque neovascularization.[21] In other research, it was found that CEUS and multi-detector computed tomography angiography were the most accurate in the diagnosis of CAS, in which CEUS had a sensitivity and specificity of 94.1% and 97.95%, respectively, for the diagnosis of plaque ulceration.[22] A recent study reported that the combination of CEUS and erythrocyte sedimentation rate (ESR) in the diagnosis of Takayasu's arteritis could achieve a sensitivity and specificity of 81.1% and 81.5%, respectively.[23] In the present study, we found that CEUS could be used in the diagnosis of unstable plaques with a sensitivity of 81.25% and specificity of 85.67%, which was consistent with the above studies. We also found that the combination of CEUS and SIRT3 could achieve a sensitivity of 94.20%, a specificity of 69.28%, and an accuracy of 80.8% in the diagnosis of unstable plaques.

Sirtuin-3 is a member of the sirtuin family which has been associated with the inflammatory response in several studies.[24,25] Recently, researchers found that SIRT3 plays an important role in cardiovascular diseases. A recent study showed that SIRT3 could prevent myocardial ischemia-reperfusion injury by reducing oxidative stress and cell apoptosis.[26] Eid et al. demonstrated that the upregulation of both SIRT1 and SIRT3 was associated with improvements in myocardial ischemia-reperfusion injury.[27] In another study, Gaul et al. found that a deficiency of SIRT3 promoted arterial thrombosis, which is the main cause of plaque formation.[28] All of these studies indicated that SIRT3 is a key factor in the development of CAS. However, up to now, no clinical studies focused on the role of SIRT3 in CAS patients have been conducted. In our research, we found a low expression of SIRT3 in severe CAS patients and CAS patients with unstable plaques. In addition, a lower expression of SIRT3 predicted a higher risk for unstable plaques in CAS patients.

Limitations

Our study had some limitations. We obtained a limited sample size from a single center, which may limit the scientific value of this research. We did not consider how SIRT3 influences the formation of plaques; this issue requires more in vivo and in vitro studies.

Conclusions

In conclusion, this study demonstrated that SIRT3 was downregulated in severe CAS patients and CAS patients with unstable plaques. A low expression of SIRT3 predicted a higher risk for unstable plaques in CAS patients. The combination of CEUS and SIRT3 showed good sensitivity and specificity for the diagnosis of unstable plaques and might be a potential strategy in the clinic.

Supplementary data

The original statistical data of data distribution, Mann–Whitney U test and logistic regression are shown in Supplementary tables (https://doi.org/10.5281/zenodo.6993618).

The Supplementary material includes:

Table S1. Data distribution analysis for all continuous data in this study.

Table S2. Results of Mann–Whitney U test in table 1 and the left panel of figure 2.

Table S3. Results of Mann–Whitney U test in the right panel of figure 2.

Table S4. Results of Mann–Whitney U test in table 2.

Table S5. Hosmer–Lemeshow test of logistic regression model 1.

Table S6. Results of logistic regression model 1.

Table S7. Hosmer–Lemeshow test of logistic regression model 2.

Table S8. Results of logistic regression model 2.

Table S9. Hosmer–Lemeshow test of logistic regression model 3.

Table S10. Results of logistic regression model 3.

ORCID iDs

Aiyun Zhou https://orcid.org/0000-0002-4459-3384
Wan Zhu https://orcid.org/0000-0002-2692-1874
Pan Xu https://orcid.org/0000-0002-3891-6095
Chunxiao Zhao https://orcid.org/0000-0003-2315-8874
Liping Jiang https://orcid.org/0000-0001-7862-6909
Wenxin Yuan https://orcid.org/0000-0001-9701-2777

References

1. Ji X, Leng XY, Dong Y, et al. Modifiable risk factors for carotid atherosclerosis: A meta-analysis and systematic review. *Ann Transl Med*. 2019;7(22):632. doi:10.21037/atm.2019.10.115
2. Bytyçi I, Shenouda R, Wester P, Henein MY. Carotid atherosclerosis in predicting coronary artery disease: A systematic review and meta-analysis. *Arterioscler Thromb Vasc Biol*. 2021;41(4):e224–e237. doi:10.1161/ATVBAHA.120.315747
3. Song P, Fang Z, Wang H, et al. Global and regional prevalence, burden, and risk factors for carotid atherosclerosis: A systematic review, meta-analysis, and modelling study. *Lancet Glob Health*. 2020;8(5):e721–e729. doi:10.1016/S2214-109X(20)30117-0
4. Xing L, Li R, Zhang S, et al. High burden of carotid atherosclerosis in rural Northeast China: A population-based study. *Front Neurol*. 2021;12:597992. doi:10.3389/fneur.2021.597992
5. Pang Y, Zhang B, Xing D, et al. Increased risk of carotid atherosclerosis for long-term exposure to indoor coal-burning pollution in rural area, Hebei Province, China. *Environ Pollut*. 2019;255(Pt 2):113320. doi:10.1016/j.envpol.2019.113320

6. Spannella F, Di Pentima C, Giulietti F, et al. Prevalence of subclinical carotid atherosclerosis and role of cardiovascular risk factors in older adults: Atherosclerosis and aging are not synonyms. *High Blood Press Cardiovasc Prev*. 2020;27(3):231–238. doi:10.1007/s40292-020-00375-0
7. Joh JH, Cho S. Cardiovascular risk of carotid atherosclerosis: Global consensus beyond societal guidelines. *Lancet Glob Health*. 2020;8(5): e625–e626. doi:10.1016/S2214-109X(20)30132-7
8. Van der Heiden K, Barrett HE, Meester EJ, et al. SPECT/CT imaging of inflammation and calcification in human carotid atherosclerosis to identify the plaque at risk of rupture [Published online ahead of print on July 27, 2021]. *J Nucl Cardiol*. 2021. doi:10.1007/s12350-021-02745-0
9. Lu MM, Peng P, Hatsukami TS, et al. A comparison of carotid atherosclerosis in symptomatic patients between 2002–2005 and 2012–2015 cohorts using multi-contrast magnetic resonance vessel wall imaging. *J Geriatr Cardiol*. 2021;18(8):623–630. doi:10.11909/j.issn.1671-5411.2021.08.006
10. Filis K, Toufektzian L, Galyfos G, et al. Assessment of the vulnerable carotid atherosclerotic plaque using contrast-enhanced ultrasonography. *Vascular*. 2017;25(3):316–325. doi:10.1177/1708538116665734
11. Yang F, Wang C. Consistency of superb microvascular imaging and contrast-enhanced ultrasonography in detection of intraplaque neovascularization: A meta-analysis. *PLoS One*. 2020;15(7):e0230937. doi:10.1371/journal.pone.0230937
12. Camps-Renom P, Prats-Sánchez L, Casoni F, et al. Plaque neovascularization detected with contrast-enhanced ultrasound predicts ischaemic stroke recurrence in patients with carotid atherosclerosis. *Eur J Neurol*. 2020;27(5):809–816. doi:10.1111/ene.14157
13. Martinez E, Martorell J, Riambau V. Review of serum biomarkers in carotid atherosclerosis. *J Vasc Surg*. 2020;71(1):329–341. doi:10.1016/j.jvs.2019.04.488
14. Fu Q, Wang X, Wu T, et al. Carotid atherosclerosis biomarkers in cardiovascular diseases prevention: A systematic review and bibliometric analysis. *Eur J Radiol*. 2020;129:109133. doi:10.1016/j.ejrad.2020.109133
15. Saba L, Moody AR, Saam T, et al. Vessel wall-imaging biomarkers of carotid plaque vulnerability in stroke prevention trials: A viewpoint from the carotid imaging consensus group. *JACC Cardiovasc Imaging*. 2020;13(11):2445–2456. doi:10.1016/j.jcmg.2020.07.046
16. Parodi-Rullán RM, Chapa-Dubocq XR, Javadov S. Acetylation of mitochondrial proteins in the heart: The role of SIRT3. *Front Physiol*. 2018;9:1094. doi:10.3389/fphys.2018.01094
17. Sun W, Liu C, Chen Q, Liu N, Yan Y, Liu B. SIRT3: A new regulator of cardiovascular diseases. *Oxid Med Cell Longev*. 2018;2018:7293861. doi:10.1155/2018/7293861
18. Jiang Y, Zhu C, Peng W, et al. Ex-vivo imaging and plaque type classification of intracranial atherosclerotic plaque using high resolution MRI. *Atherosclerosis*. 2016;249:10–16. doi:10.1016/j.atherosclerosis.2016.03.033
19. Rafailidis V, Huang DY, Yusuf GT, Sidhu PS. General principles and overview of vascular contrast-enhanced ultrasonography. *Ultrasonography*. 2020;39(1):22–42. doi:10.14366/usg.19022
20. Hamada O, Sakata N, Ogata T, Shimada H, Inoue T. Contrast-enhanced ultrasonography for detecting histological carotid plaque rupture: Quantitative analysis of ulcer. *Int J Stroke*. 2016;11(7):791–798. doi:10.1177/1747493016641964
21. Oura K, Kato T, Ohba H, Terayama Y. Evaluation of intraplaque neovascularization using superb microvascular imaging and contrast-enhanced ultrasonography. *J Stroke Cerebrovasc Dis*. 2018;27(9): 2348–2353. doi:10.1016/j.jstrokecerebrovasdis.2018.04.023
22. Rafailidis V, Chryssogonidis I, Xerras C, et al. A comparative study of color Doppler imaging and contrast-enhanced ultrasound for the detection of ulceration in patients with carotid atherosclerotic disease. *Eur Radiol*. 2019;29(4):2137–2145. doi:10.1007/s00330-018-5773-8
23. Ma LY, Li CL, Ma LL, et al. Value of contrast-enhanced ultrasonography of the carotid artery for evaluating disease activity in Takayasu arteritis. *Arthritis Res Ther*. 2019;21(1):24. doi:10.1186/s13075-019-1813-2
24. Koyama T, Kume S, Koya D, et al. SIRT3 attenuates palmitate-induced ROS production and inflammation in proximal tubular cells. *Free Radic Biol Med*. 2011;51(6):1258–1267. doi:10.1016/j.freeradbiomed.2011.05.028
25. Dikalova AE, Pandey A, Xiao L, et al. Mitochondrial deacetylase Sirt3 reduces vascular dysfunction and hypertension while Sirt3 depletion in essential hypertension is linked to vascular inflammation and oxidative stress. *Circ Res*. 2020;126(4):439–452. doi:10.1161/CIRCRESAHA.119.315767
26. Zhai M, Li B, Duan W, et al. Melatonin ameliorates myocardial ischemia reperfusion injury through SIRT3-dependent regulation of oxidative stress and apoptosis. *J Pineal Res*. 2017;63(2):e12419. doi:10.1111/jpi.12419
27. Eid RA, Bin-Meferij MM, El-Kott AF, et al. Exendin-4 protects against myocardial ischemia-reperfusion injury by upregulation of SIRT1 and SIRT3 and activation of AMPK. *J Cardiovasc Transl Res*. 2021;14(4): 619–635. doi:10.1007/s12265-020-09984-5
28. Gaul DS, Weber J, van Tits LJ, et al. Loss of Sirt3 accelerates arterial thrombosis by increasing formation of neutrophil extracellular traps and plasma tissue factor activity. *Cardiovasc Res*. 2018;114(8): 1178–1188. doi:10.1093/cvr/cvy036

Comparison of biomarker expression in oral lichen planus and oral lichenoid lesions

Małgorzata Radwan-Oczko[1,A–F], Anna Lis-Nawara[2,C–D], Agnieszka Hałoń[3,B,C,F], Julia Bar[2,A,C–F]

[1] Department of Oral Pathology, Wroclaw Medical University, Poland
[2] Department of Immunopathology and Molecular Biology, Wroclaw Medical University, Poland
[3] Department of Pathomorphology and Oncological Cytology, Wroclaw Medical University, Poland

A – research concept and design; B – collection and/or assembly of data; C – data analysis and interpretation; D – writing the article; E – critical revision of the article; F – final approval of the article

Advances in Clinical and Experimental Medicine, ISSN 1899–5276 (print), ISSN 2451–2680 (online) *Adv Clin Exp Med*. 2022;31(12):1327–1334

Address for correspondence
Malgorzata Radwan-Oczko
E-mail: malgorzata.radwan-oczko@umed.wroc.pl

Funding sources
None declared

Conflict of interest
None declared

Received on January 13, 2022
Reviewed on February 13, 2022
Accepted on July 27, 2022

Published online on Septemper 1, 2022

Abstract

Background. Oral lichen planus (OLP) and oral lichenoid lesions (OLL) comprise a group of oral mucosal disorders that have similar clinical and histological features.

Objectives. To compare the levels of investigated biomarkers in biopsied OLP and OLL, and to determine the pattern of biomarkers, which could be useful for the biological characterization of these 2 disorders.

Materials and methods. A total of 56 biopsy specimens in 2 groups were analyzed in this study. One group consisted of 25 idiopathic OLP lesions, and the other included 31 OLL from patients treated with antihypertensive and cardiac medications. The expression of protein p53, topoisomerase I (topo I), heat shock protein 90 (HSP90), and E-cadherin was analyzed using immunohistochemistry.

Results. The p53 protein expression showed a trend to a positive correlation with topo I expression in the total sample ($p = 0.067$, $R = 0.25$). The p53 protein and HSP90 expression was higher in the OLL group compared to the OLP group, but the difference was not statistically significant. No association was found between topo I and E-cadherin expression for either the OLP or OLL group.

Conclusions. The findings of this study suggest that the slightly higher protein p53 and HSP90 expression in the OLL group might be caused by the medications used. The slight association between p53 and topo I expression indicates that the cooperation between these proteins might be essential for the growth of OLP/OLL in general. We conclude that the overexpression of p53 protein and high expression of topo I found in both types of lesions might induce their biologically aggressive behavior.

Key words: p53, biomarkers, OLP, OLL

Cite as
Radwan-Oczko M, Bar J, Hałoń A, Lis-Nawara A. Comparison of biomarker expression in oral lichen planus and oral lichenoid lesions. *Adv Clin Exp Med*. 2022;31(12):1327–1334. doi:10.17219/acem/152429

DOI
10.17219/acem/152429

Background

Oral lichen planus (OLP) and oral lichenoid lesions (OLL) comprise a group of disorders of the oral mucosa. Oral lichen planus lesions are a chronic disorder most commonly affecting middle-aged adults, with a slight female predominance. Such lesions appear as white papules that coalesce to form reticular, annular or plaque-like patterns.[1,2] The etiology and pathogenesis of OLP are still not clear or fully explained. Studies suggest the presence of an immunological disorder in which $CD4^+$ (Th1) and $CD8^+$ (Tc) lymphocyte activation, as well as production of cytokines, such as interleukin-2 (IL-2), interferon gamma (IFN-γ) and tumor necrosis factor (TNF), can cause apoptosis of keratinocytes.[3–5] Recent studies have indicated that Th2 lymphocytes can also contribute to the pathogenesis of OLP.[6] The histopathological assessment of OLP lesions reveals hyperkeratosis, degeneration of the basal cell layer of the epithelium, hydropic degeneration of basal cells, infiltration of lymphocytes in the connective tissue, and acanthotic or atrophic epithelium.[1,2]

Oral lichenoid lesions are another type of lesion frequently observed in the oral mucosa. In certain patients, oral lichenoid drug reaction lesions can be caused by numerous medications, such as the majority of β-blockers, some angiotensin-converting enzyme inhibitors, some thiazide diuretics, nonsteroidal anti-inflammatory drugs, and oral hypoglycemic medications.[2,5,7] In a study by Balakumar et al. adverse drug reactions were identified in patients treated with combinations of β-adrenergic blockers and calcium-channel blockers in addition to β-adrenergic blockers and diuretics and coronary disease medications.[7] Similarly, Jinbu and Demitsu noted that nicorandil induced ulcerations on the sites typical of OLP lesions.[8] Farzin et al. found lichenoid reactions of linear striations on the buccal mucosa in 4.5% of 465 hypertensive patients being treated with antihypertensive medications.[9] An oral lichenoid drug reaction can occur at any time, even years after the beginning of treatment. In many cases, alternative medication options are not available. Oral lichenoid lesions often represent clinical and histological features of OLP, so diagnosis is often complicated.[2,9] Furthermore, there are no specific biomarkers helpful in distinguishing between OLP and OLL and predicting their behavior.[10–12]

Few studies have analyzed molecular markers that might be useful in identifying patients with progressive OLP growth.[11–13] They found that p53 protein and topoisomerase IIα expressions in OLP might be markers of proliferative activity.[10,11] Some data suggest that the overexpression of p53 protein in benign lesions might play a role in the early stages of oral carcinogenesis, and *TP53* mutations might be an important oncogenic event in malignantly transformed OLP.[3,11,14] A single study determined that focal loss of E-cadherin expression in OLP lesions might increase their progressive growth.[10] Similarly, it was noted that heat shock proteins are potentially involved in the pathogenesis of the inflammatory process, which is observed when OLP induces premalignant lesions.[10,13] There are no data on p53, topoisomerase I (topo I), heat shock protein 90 (HSP90), and E-cadherin expression in OLL, or comparative studies between OLP and OLL. Based on the data that OLP/OLL represent a heterogeneous group of inflammatory disorders that share common antigens and are characterized by similar clinical and histological features, it would be interesting to investigate biomarker patterns which would be useful for the biological characterization of these different lesions.[2]

Objectives

The aim of this study was to assess p53 protein, topo I, HSP90, and E-cadherin expression in OLP and OLL biopsy specimens, which could help distinguish between these 2 pathologies diagnostically.

Materials and methods

Patients and study group selection

A total of 56 patients with OLP who were referred to the oral pathology outpatient clinic between January 1, 2015 and May 31, 2019, were enrolled in the study. The clinical and histopathological diagnoses of OLP were made based on the World Health Organization (WHO) criteria defined in 1978 and modified in 2003.[15] Clinical investigation was performed by a specialist in periodontology and oral mucosal pathology, and histopathological investigation was performed by a specialist in pathomorphology. The patients were reviewed for demographic data, general health and type(s) of medication. A clinical investigation was carried out to record the clinical forms of the lesions and the sites involved.

Assuming that the lesions of some of the patients diagnosed with OLP could be related to medication side effects, 2 groups of patients were created. The 1st group (idiopathic OLP) consisted of 25 patients, and the 2nd group (OLL) of 31 patients whose lesions may have resulted from the treatment with antihypertensive and/or cardiovascular medications. Differences in the expression patterns of the 4 abovementioned biomarkers, which could be considered when making the diagnosis between these 2 pathologies, were evaluated.

The pathologist evaluating the molecular markers was blinded. All 56 biopsies were assessed without being divided into groups. After immunohistochemical evaluation, the data were described in accordance with the groups (OLP or OLL groups).

The study was conducted according to the principles of the Declaration of Helsinki and approved by the Ethics Committee of the Wroclaw Medical University, Poland (approval No. KB230/2016).

Antibodies

Immunohistochemical staining was performed with the following antibodies: mouse monoclonal antibody DO-7 (clone DO-7) that reacts with both the wild and mutant forms of unphosphorylated human p53 protein (Novocastra, Newcastle, UK); anti-topo I that binds to a region within the middle of the topo I molecule (clone 1D6; Novocastra); anti-HSP90 protein that recognizes protein corresponding to 306 amino acids of the C-terminus of the HSP90 molecule (clone JPB24; Novocastra); and anti-human cadherin (clone NCH-38) that recognizes the 120 kD mature form of E-cadherin (Dako, Copenhagen, Denmark).

Immunohistochemical staining

Immunohistochemical staining for the analyzed proteins was performed on paraffin-embedded OLP tissue specimens using the Universal Dako REAL EnVision Detection System, Peroxidase/DAB+, Rabbit/Mouse (Dako); the primary antibodies were anti-p53 protein, topo I, HSP90, and E-cadherin. The 5-µm sections of OLP were deparaffinized and boiled 2 × 5 min in a citrate buffer (pH = 6.0) at 800 W in a microwave. After that, the OLP sections were slowly cooled for 30 min. Nonspecific tissue endogenous peroxidase reactivity was blocked with Dako REAL Peroxidase Blocking Solution (Dako). The OLP specimens were incubated overnight with primary antibodies at 4°C. After washing the OLP specimens with 0.1 M Tris-buffered saline (TBS; pH = 7.4), they were incubated with Dako REAL EnVision/HRP, Rabbit/Mouse (Dako) for 30 min at room temperature. After washing the antigen-antibody with TBS, the reaction was visualized using 3,3 diaminobenzidine (Dako) as a chromogen. The sections were counterstained with hematoxylin and mounted. The incubation buffer (TBS) without primary antibodies was used as a negative control. Positive controls for each antibody were performed according to the manufacturer's recommendations.

Interpretation of immunohistochemical staining

The assessment of protein expression in the OLP tissues was scored semiquantitatively, taking into account the intensity of immunostaining and the number of cells showing immunoreactivity for the analyzed proteins. The number of cells exhibiting staining for p53 protein and topo I antibodies was assessed by counting 1000 cells in 10–15 randomly selected high-power fields. Heat shock protein 90 and E-cadherin expressions were analyzed by determining cytoplasmic/membrane immunostaining based on the intensity of immunostaining and the percentage of the stained OLP tissue area. The cases were scored as negative for all protein expressions when there was no immunostaining or variable weak positivity (<5% of cells).

Statistical analyses

The statistical significance between the means for the different groups was calculated using the nonparametric Mann–Whitney U test; the frequencies were calculated using the χ^2 test or Fisher's exact test.[16] The associations between p53 protein and HSP90, topo I and E-cadherin were analyzed using Spearman's rank correlation. Differences were considered statistically significant when $p < 0.05$. Statistical analysis was performed using Statistica v. 13.0 software (StatSoft Poland, Kraków, Poland) and PAST v. 4.05 (https://past.en.lo4d.com/windows).

Results

Comparison of clinical parameters between groups

There were 21 men and 35 women with mean age of 57.7 ±13.6 years and 65.5 ±9.4 years, respectively. Following anamnesis, the OLP group included 25 patients with a mean age of 57.0 years, and the OLL group included 31 patients with a mean age of 68.0 years; the patients in the OLP group were significantly younger ($p = 0.0001$; Table 1). There was a significantly higher number of women when all 56 patients were considered ($p = 0.04$), as well as when the 31 OLL patients were considered separately ($p = 0.04$). The duration of the lesions was similar in the OLP and OLL groups (38.6 months and 39.3 months, respectively). A comparison of the parameters evaluated between the groups revealed a significant difference in the median age, which was higher in the OLL group. In the OLL group, more patients showed shorter disease duration (below 34 months), whereas in the OLP group, more patients presented with longer disease duration (above 34 months). The observed differences between the OLL group and the OLP group were statistically significant ($p = 0.018$; Table 1).

Two clinical forms among all 56 lesions were found: white lesions of striae in 43 cases and erosions in 13 cases; there were no statistically significant differences in the prevalence of clinical forms between the OLP and OLL groups. In the assessment of site involvement, lesions were present on the buccal mucosa in 27 patients, at other sites (such as the gingiva or tongue) in 4 patients, and at 2 or 3 sites in 25 patients. No statistically significant difference was seen in site involvement between the groups (Table 1).

Comparison of p53, topo I, HSP90, and E-cadherin expression between groups

The p53 expression was found in 19/56 (33.0%) of the oral lesions. Nuclear accumulation of p53 protein showed a trend to higher expression in the OLL group compared to the OLP group (Table 2). In the majority of cases

Table 1. Demographic parameters in oral lichenoid lesions (OLL) and oral lichen planus (OLP) groups

Parameters	OLL group (n = 31) median (25Q–75Q) mean ±SD	OLP group (n = 25) median (25Q–75Q) mean ±SD	Test value	p-value
Age [years]	68.0 (64.0 ±71.0)	57.0 (45.0 ±62.0)	3.46	0.0001*
Lesions presence duration [months]	38.6 ±19.9	39.3 ±18.9	0.87	0.386*
Lesions presence duration, patients (n)				
≤34 months	21	9	5.61	0.018**
>34 months	10	16		
Lesions presence clinical forms, patients with (n):				
White striae	23	20	0.26	0.609**
Erosive form	8	5		
Lesions presence – sites involved, patients with (n):				
Buccal mucosa involved	13	14	–	0.55***
Other site involved	3	1		
General involvement	15	10		

* U Mann–Whitney (test value – Z); ** χ^2 test; *** exact Fisher's test; 25Q – lower quartile; 75Q – upper quartile; SD – standard deviation.

in both groups, p53 expression was found in a low percentage of basal and suprabasal epithelial cells (Fig. 1A,B). Topoisomerase I expression was found in 42/56 specimens (75.0%), HSP90 in 28/56 specimens (50.0%) and E-cadherin in 37/56 specimens (66.1%); expressions were slightly higher in the OLL group than in the OLP group (Table 2).

Positive results for E-cadherin expression were obtained from 10–60% of immunoreactive tissue. Topoisomerase I expression revealed equal immunoreactivity in both groups and was observed in different tissue areas from 10–70% of tissue. The expression of HSP90 was slightly higher in the OLL group than in the OLP group (Fig. 1C–F). The intensity of topo I and HSP90 immunoreactivity was stronger in the OLL group than in the OLP group. Similarly, the range of E-cadherin immunopositivity was higher in the OLL group than in the OLP group (Fig. 1G,H).

Association between p53 protein and topo I, HSP90 and E-cadherin expression

The p53 protein expression showed a trend toward a positive correlation with top I expression only (of the biomarkers) when all patients were considered ($p = 0.067$, $R = 0.25$) (Table 3). Such a correlation between p53 and topo I expression was not observed when the 2 groups were considered separately. No correlation was observed between p53 protein expression and HSP90 and E-cadherin expression when the OLL and OLP groups were considered separately and when all cases were considered together (Table 3).

Discussion

Data on the identification of biomarkers of OLP and OLL, which could help explain their biological characteristics, are limited.[11–13] This study found no differences in terms of gender, forms and location of lesions between the OLP and OLL groups, which is consistent with other reports.[12,17] The differences in mean age between groups in this study are in contrast to the published data.[12,14] The reason why the patients in the OLL group were older might be that they had cardiac and vascular diseases. In the OLL group, a significantly higher number of patients had a longer duration of lesions, which could have been associated with the use of medications.

Table 2. P53, HSP90, topo I, and E-cadherin expression in oral lichenoid lesions (OLL) and oral lichen planus (OLP) groups

Biomarkers	Immunopositivity (% of positive cases)			
	OLL group (n = 31) [n, %]	OLP group (n = 25) [n, %]	Test value	p-value
p53	12 (38.7)	7 (28.0)	0.71	0.400
HSP90	18 (58.0)	10 (40.0)	1.81	0.177
E-cadherin	22 (70.9)	15 (60.0)	0.74	0.388
Topo I	24 (77.4)	18 (72.0)	0.64	0.642

HSP90 – heat shock protein 90; topo I – topoisomerase I. χ^2 test.

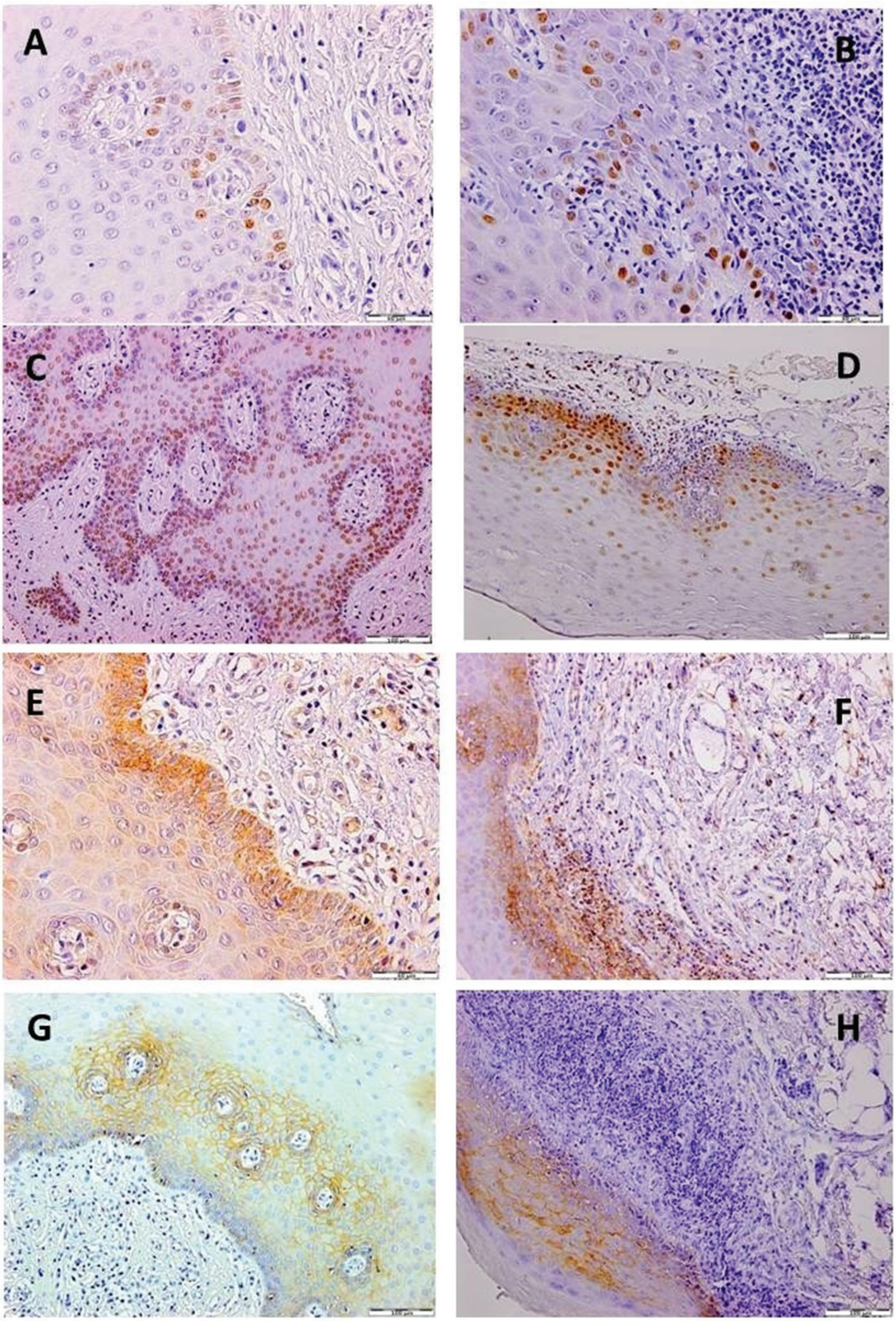

Fig. 1. Representative oral lichenoid lesions (OLL) and oral lichen planus (OLP) patients. A. Low number of keratinocytes and epithelial cells with p53 protein nuclear accumulation in OLP lesions; B. The p53 protein expression observed in a high number of cells in OLL; C. High number of cells showing topoisomerase I expression in OLP; D. Topoisomerase I immunostaining limited to deep layers of epithelial tissue in OLL; E. Heat shock protein 90 (HSP90) membrane/cytoplasmic expression detected in a high percentage of OLP tissue; F. The HSP90 membrane immunostaining observed in basal and suprabasal epithelial cells of patients with OLL; G. E-cadherin membrane expression in epithelial cells of untreated patients with OLP; H. E-cadherin expression in superficial epithelial tissue of OLL (the EnVision technique)

Fig. 1A,B,E: scale bar = 50 µm; Fig. 1C,D,F,G,H: scale bar = 100 µm.

Table 3. Correlation between p53 protein and HSP90, topo I and E-cadherin expression in the whole specimens, oral lichenoid lesions (OLL) and oral lichen planus (OLP) groups

Biomarkers	Number of cases	Spearman's R	p-value
P53 compared to HSP90			
Whole investigated group	56	0.16	0.225
OLP group	25	0.26	0.261
OLL group	31	0.07	0.671
P53 compared to topo I			
Whole investigated group	56	0.25	0.067
OLP group	25	0.15	0.509
OLL group	31	0.27	0.114
P53 compared to E-cadherin			
Whole investigated group	56	0.13	0.344
OLP group	25	0.34	0.139
OLL group	31	0.06	0.715

HSP90 – heat shock protein 90; topo I – topoisomerase I. Spearman's rank correlation.

In order to explore the differences between the OLP and OLL groups, the biomarkers p53, topo I, HSP90, and E-cadherin were analyzed.[10,11,18] As with previous reports, the expression of p53 was observed in a small number of cases in this study.[11,18] Consistent with existing studies, we consider that the heterogeneous pattern of p53 expression (ranging from weak to strong intensity of p53 immunostaining) observed in this study indicates that cases with strong nuclear accumulation of p53 protein are the result of gene alteration or protein structural changes which occur during the early stages of a premalignant lesion.[10,14,18] Our clinical observations of the OLP patients did not show any development of premalignant lesions. There are no reports in the literature regarding p53 protein expression in OLL patients taking antihypertensive or cardiac medications, which was analyzed in this study. The findings of this study revealed significant differences in p53 protein expression, which was higher in the OLL group; this could be explained as being related to ongoing medical treatment. Moreover, p53 protein expression might be a result of p53 protein activation after DNA damage by drugs used in the patients' therapy, which might reflect protective mechanisms, such as DNA repair, rather than gene alteration.[14] However, this observation needs to be confirmed by *TP53* gene status analysis.[16] Nevertheless, we postulate that the risk of progressive growth might be higher in the OLL group (that had greater p53 expression) than in the idiopathic OLP patients, due to loss of the suppressive role of p53 protein.[18,19] We found an association with high proliferative activity based on topo I expression and p53 protein nuclear accumulation in the sample as a whole but not when the OLL group alone was examined. We are unable to prove the prognostic value of the p53 protein due to the short time of clinical observation of the treated/untreated OLP patients. Nevertheless, the results of this study are supported by Bermejo-Fenoll et al. to an extext; their retrospective study found an association between p53 protein expression and malignancy of OLP lesions.[20] They found the development of squamous cell carcinoma (SCC) in 5 out of 550 patients with OLP; 3 of these 5 cases were being treated for hypertension, so they were diagnosed as OLL.[19] Giuliani et al. described overall malignant transformation in 1.4% of cases, including 1.37% for OLP and 2.43% for OLL in large groups, and concluded that p53 expression can cause progression from healthy oral tissue to malignancy; thus, p53 may be an early diagnostic sign of carcinogenesis.[21]

In this study, specimens showing the expression of topo I in a high number of cells indicated that this enzyme might characterize the subgroup of OLP that has high proliferative activity and leads to a progressive growth of these lesions. This hypothesis is supported by other studies which showed that high topo I expression in benign tumors increased the risk of malignancy.[22] As found in our study, similar topo I expression in specimens of both the OLP and OLL groups indicates that medications do not influence the cellular activity of oral epithelial cells. The lower expression of HSP90 in tissues from the OLP group might be associated with greater nuclear accumulation of p53 protein, which can form complexes with HSP90 in cells.[23,24] The lack of association between p53 protein and HSP90 expression in the study group as a whole, as well as in the OLP and OLL groups separately, suggests that HSP90 protein does not play a protective role against p53 protein in, for example, carcinoma tissue.[25]

The high E-cadherin expression observed in this study is consistent with other studies and indicates that high E-cadherin expression is important for tissue structure because this protein is highly expressed by normal oral epithelial cells in the spinous layer and basal layer.[26] Our results concerning equal E-cadherin expression in the OLP/OLL groups are somewhat in line with the the

study by Sargolzaei and Mohamadian, who did not observe significant differences in the expression of E-cadherin between OLP specimens with and without dysplasia.[12] However, there is research indicating that p53 protein expression reduces E-cadherin expression in oral SCC.[27] The lack of correlation between p53 protein and E-cadherin expression in the OLP specimens analyzed in this study suggests that there is no cooperation between these 2 proteins. This observation is consistent with a published report suggesting that the reduction of E-cadherin in OLP is associated with mild and moderate dysplasia.[26,27]

Limitations

The 1st limitation of this study is that the medications used by the OLL patients are not specified – not all classes of antihypertensive and cardiac medications cause OLL as a side effect. Moreover, there are new medications for which there are no published observations or investigations with regard to OLL. The 2nd limitation is the absence of a control group; tissue biopsies from healthy subjects would have been useful for comparison.

Conclusions

The results of this study suggest that high p53 protein and HSP90 expressions in the OLL of patients treated with cardiovascular medications could result not only from gene alterations but also from those medications. The impact of p53 protein on the biological behavior of oral cells might be different in idiopathic OLP compared to drug-related OLL. The association between p53 protein and topo I expression indicates that the association between these proteins might be essential for the growth and behavior of OLP/OLL. We conclude that the expression of p53 protein and topo I found in both types of lesion might induce their biologically aggressive behavior. However, to confirm these observations, future larger studies on the roles of these molecules in oral lesions are warranted.

ORCID iDs

Małgorzata Radwan-Oczko https://orcid.org/0000-003-4684-5722
Julia Bar https://orcid.org/0000-0002-3811-4834
Agnieszka Hałoń https://orcid.org/0000-0003-4240-7899
Anna Lis-Nawara https://orcid.org/0000-0003-4165-4652

References

1. Krupaa RJ, Sankari SL, Masthan KMK, Rajesh E. Oral lichen planus: An overview. *J Pharm Bioallied Sci*. 2015;7(Suppl 1):S158–S161. doi:10.4103/0975-7406.155873
2. Carrozzo M, Porter S, Mercadante V, Fedele S. Oral lichen planus: A disease or a spectrum of tissue reactions? Types, causes, diagnostic algorhythms, prognosis, management strategies. *Periodontol 2000*. 2019;80(1):105–125. doi:10.1111/prd.12260
3. Aghbari SMH, Abushouk AI, Attia A, et al. Malignant transformation of oral lichen planus and oral lichenoid lesions: A meta-analysis of 20095 patient data. *Oral Oncol*. 2017;68:92–102. doi:10.1016/j.oraloncology.2017.03.012
4. Akerzoul N, Chbicheb S. Pro-inflammatory cytokines and oral lichen planus. *Am J Clin Cancer Res*. 2018;4:1–6. http://www.ivyunion.org/index.php/ajcre/article/view/1245. Accessed October 1, 2020.
5. Cassol-Spanemberg J, Rodriguez-de Rivera-Campillo M, Otero-Rey E, Estrugo-Devesa A, Jane-Salas E, Lopez-Lopez J. Oral lichen planus and its relationship with systemic diseases: A review of evidence. *J Clin Exp Dent*. 2018;10(9):e938–e944. doi:10.4317/jced.55145
6. Yamauchi M, Moriyama M, Hayashida JN, et al. Myeloid dendritic cells stimulated by thymic stromal lymphopoietin promote Th2 immune responses and the pathogenesis of oral lichen planus. *PLoS One*. 2017;12(3):e0173017. doi:10.1371/journal.pone.0173017
7. Balakumar P, Kavitha M, Nanditha S. Cardiovascular drugs-induced oral toxicities: A murky area to be revisited and illuminated. *Pharmacol Res*. 2015;102:81–89. doi:10.1016/j.phrs.2015.09.007
8. Jinbu Y, Demitsu T. Oral ulcerations due to drug medications. *Jpn Dent Sci Rev*. 2014;50(2):40–46. doi:10.1016/j.jdsr.2013.12.001
9. Farzin M, Derafshi R, Ghapanchi J, Kafsh AZ, Rezaiee M. Oral manifestations of hypertension and rheumatic heart disease: A cross sectional study in elderly patients. *Asian J Med Pharm Res*. 2016;6(2):9–13. https://ajmpr.science-line.com/attachments/article/39/Asian%20J.%20Med.%20Pharm.%20Res.%206(2)%2009-13,%202016.pdf. Accessed June 15, 2020.
10. Sagari S, Sanadhya S, Doddamani M, Rajput R. Molecular markers in oral lichen planus: A systematic review. *J Oral Maxillofac Pathol*. 2016;20(1):115–121. doi:10.4103/0973-029X.180964
11. Farhadi S, Shahsavari F, Alf K. Comparison of expression of p53 and bcl-2 markers in oral lichen planus and oral squamous cell carcinoma. *J Res Dentomaxillofac Sci*. 2018;3(2):37–45. doi:10.29252/jrdms.3.2.37
12. Sargolzaei S, Mohamadian F. Immunohistochemical comparison of E-cadherin expression in oral lichen planus with and without dysplasia. *J Dental School*. 2017;35(1):26–31. doi:10.22037/jds.v35i1.24627
13. Chaiyarit P, Jintakanon D, Klanrit P, Siritapetawee M, Thongprasom K. Immunohistochemical analyses of survivin and heat shock protein 90 expression in patients with oral lichen planus: Immunohistochemical analyses of survivin and Hsp90. *J Oral Pathol Med*. 2009;38(1):55–62. doi:10.1111/j.1600-0714.2008.00713.x
14. Hadzi-Mihailovic M, Petrovic R, Raybaud H, Stanimirovic D, Ozar Koray M. Expression and role of p53 in oral lichen planus patients. *J BUON*. 2017;22(5):1278–1286. PMID:29135114.
15. van der Meij EH, van der Waal I. Lack of clinicopathologic correlation in the diagnosis of oral lichen planus based on the presently available diagnostic criteria and suggestions for modifications. *J Oral Pathol Med*. 2003;32(9):507–512. doi:10.1034/j.1600-0714.2003.00125.x
16. Hammer Ø, Harper DAT, Ryan PD. PAST: Paleontological statistics software package for education and data analysis. *Palaeontol Electron*. 2001;4(1):9. https://palaeo-electronica.org/2001_1/past/past.pdf. Accessed May 10, 2022.
17. Irani S, Esfahani AM, Ghorbani A. Dysplastic change rate in cases of oral lichen planus: A retrospective study of 112 cases in an Iranian population. *J Oral Maxillofac Pathol*. 2016;20(3):395–399. doi:10.4103/0973-029X.190911
18. Agha-Hosseini F, Mirzaii-Dizgah I, Miri-Zarandi NS. Unstimulated salivary p53 in patients with oral lichen planus and squamous cell carcinoma. *Acta Med Iran*. 2015;53(7):439–443. PMID:26520632.
19. Lambrus BG, Holland AJ. A new mode of mitotic surveillance. *Trends Cell Biol*. 2017;27(5):314–321. doi:10.1016/j.tcb.2017.01.004
20. Bermejo-Fenoll A, Sanchez-Siles M, López-Jornet P, Camacho-Alonso F, Salazar-Sanchez N. Premalignant nature of oral lichen planus. A retrospective study of 550 oral lichen planus patients from south-eastern Spain. *Oral Oncol*. 2009;45(8):e54–e56. doi:10.1016/j.oraloncology.2009.01.009
21. Giuliani M, Troiano G, Cordaro M, et al. Rate of malignant transformation of oral lichen planus: A systematic review. *Oral Dis*. 2019;25(3):693–709. doi:10.1111/odi.12885
22. Nikitakis NG, Pentenero M, Georgaki M, et al. Molecular markers associated with development and progression of potentially premalignant oral epithelial lesions: Current knowledge and future implications. *Oral Surg Oral Med Oral Pathol Oral Radiol*. 2018;125(6):650–669. doi:10.1016/j.oooo.2018.03.012
23. Faraji Lamouki M, Abbaszadeh H, Gholinia H. Study of HSP27 expression in two types of oral lichen planus. *J Adv Biotech Res*. 2018;9(1):617–625. https://bipublication.com/files/ijabr20189189Mojtaba.pdf. Accessed January 1, 2021.

24. Chang WC, Tsai PT, Lin CK, Shieh YS, Chen YW. Expression pattern of heat shock protein 90 in patients with oral squamous cell carcinoma in northern Taiwan. *Br J Oral Maxillofac Surg*. 2017;55(3):281–286. doi:10.1016/j.bjoms.2017.01.008
25. Chatterjee S, Burns TF. Targeting heat shock protein in cancer: A promising therapeutic approach. *Int J Mol Sci*. 2017;18(9):1978. doi:10.3390/ijms18091978
26. de Freitas Silva BS, de Castro CA, von Zeidler SLV, de Sousa SCOM, Batista AC, Yamamoto-Silva FP. Altered β-catenin expression in oral mucosal dysplasia: A comparative study. *J Appl Oral Sci*. 2015;23(5):472–478. doi:10.1590/1678-775720150150
27. Fan CC, Wang TY, Cheng YA, et al. Expression of E-cadherin, Twist, and p53 and their prognostic value in patients with oral squamous cell carcinoma. *J Cancer Res Clin Oncol*. 2013;139(10):1735–1744. doi:10.1007/s00432-013-1499-9

Early biomarkers predicting outcome in a porcine model of acetaminophen intoxication: A pilot study

Christian Thiel[1,A–F], Ulrika Lischner[1,A–F], Matthias Morgalla[2,A–C,E,F], Andreas Peter[3,B,C,E,F], Martin Schenk[1,A–F], Alfred Königsrainer[1,A,C,E,F], Karolin Thiel[1,A–F]

[1] Department of General, Visceral and Transplant Surgery, University Hospital Tübingen, Germany
[2] Department of Neurosurgery, University Hospital Tübingen, Germany
[3] Division of Endocrinology, Diabetology, Angiology, Nephrology, Pathobiochemistry and Clinical Chemistry, Department of Internal Medicine, University Hospital Tübingen, Germany

A – research concept and design; B – collection and/or assembly of data; C – data analysis and interpretation; D – writing the article; E – critical revision of the article; F – final approval of the article

Advances in Clinical and Experimental Medicine, ISSN 1899–5276 (print), ISSN 2451–2680 (online) *Adv Clin Exp Med*. 2022;31(12):1335–1342

Address for correspondence
Karolin Thiel
E-mail: karolin.thiel@med.uni-tuebingen.de

Funding sources
None declared

Conflict of interest
None declared

Acknowledgements
We would like to thank T.O. Greiner, A. Stolz and M. Seitzer for their excellent veterinarian and technical assistance, as well as Mary Heaney Margreiter and Martina Nowak-Machen for their kind contribution to the preparation of the manuscript. We acknowledge the support by the Open Access Publishing Fund of University of Tübingen, Germany.

Received on November 30, 2021
Reviewed on June 29, 2022
Accepted on August 3, 2022

Published online on September 1, 2022

Cite as
Thiel C, Lischner U, Morgalla M, et al. Early biomarkers predicting outcome in a porcine model of acetaminophen intoxication: A pilot study. *Adv Clin Exp Med*. 2022;31(12):1335–1342. doi:10.17219/acem/152595

DOI
10.17219/acem/152595

Abstract

Background. Acetaminophen intoxication has become the leading cause of acute liver failure (ALF) in Europe and the USA.

Objectives. To identify early biomarkers in order to predict the development of ALF in a porcine model of acetaminophen intoxication.

Materials and methods. Six German Landrace pigs received a single acetaminophen bolus of 1 g/kg body weight via a jejunal catheter. Cytokines and laboratory parameters were analyzed at 8-hour intervals for a total of 40 h.

Results. Three of the 6 animals survived the intoxication. The nonsurviving animals had an increase in serum lactate and interleukin (IL)-6, with a simultaneous decrease in prothrombin time (PT) and albumin concentration 8 h after intoxication. In all nonsurviving animals, elevated levels of tumor necrosis factor alpha (TNF-α) at baseline before intoxication and during the course of ALF were observed. The acetaminophen serum concentrations and toxicokinetics did not differ between the nonsurviving and surviving animals. Methemoglobinemia was proportional to the administered doses and acetaminophen blood levels, but methemoglobinemia did not affect survival.

Conclusions. Tumor necrosis factor alpha, IL-6, lactate, prothrombin time, and albumin blood concentration were identified as early predictors of outcome after acetaminophen intoxication. An elevated TNF-α level before acetaminophen exposure was the earliest prognostic marker for a lethal outcome. Therefore, it could serve as a very early indicator of prognosis.

Key words: cytokines, acute liver failure, prognostic markers, porcine model, acetaminophen intoxication

Background

Acetaminophen (Paracetamol®) intoxication has become the number one cause of acute liver failure (ALF) in Europe and the USA.[1,2] It is very important to make the diagnosis at an early stage so that specific treatment can be applied.[3] An overdose of acetaminophen, either deliberate or accidental, does not necessarily result in ALF. On the other hand, therapeutic doses of acetaminophen may cause severe hepatic injury in certain patients. Several risk factors, including concomitant use of other drugs, comorbidities, advanced age, and specific variants of genes encoding metabolic enzymes, are known to increase the probability of developing ALF.[4–8] Alcohol consumption is another crucial factor, but it plays a somewhat contradictory role.[9] While chronic alcoholism has been postulated to increase acetaminophen-related hepatotoxicity, acute administration of ethanol seems to protect against acetaminophen-induced liver injury.[10,11] Prognostic scores, such as the King's College Criteria for patients with ALF following acetaminophen intoxication, are commonly used to distinguish between patients who are likely to recover spontaneously and those who might require emergency liver transplantation as the only therapeutic life-saving option.[12] However, these late prognostic scores are based on clinical and laboratory data obtained after the onset of ALF. To date, there are no clinical tests or biomarkers to predict which individuals are prone to develop ALF from acetaminophen exposure before the onset of clinical disease.

The ideal biomarkers for predicting acetaminophen-induced liver failure should be easy to measure in a routine clinical setting using precisely quantifiable blood or urine markers, with results available within a short time. Certain cytokines, which are known to be promising candidates for novel biomarkers in drug-induced liver injury, fulfil all these criteria.[13] The balance of pro- and anti-inflammatory cytokines is discussed as modulating hepatic injury exacerbation or regeneration.[13] Several studies in patients suffering from ALF have reported elevated levels of inflammatory cytokines, such as interleukin (IL)-6, IL-8, IL-10, and tumor necrosis factor alpha (TNF-α).[14–16]

Objectives

The aim of this study was to analyze cytokine levels and ALF-related laboratory parameters before and over the course of acetaminophen-induced ALF in a porcine model in order to identify biomarkers for early prediction of the clinical outcome of acute acetaminophen poisoning.

Materials and methods

Animal care

The study was reviewed and approved by the Institutional Review Board for animal experiments of the Tübingen Regional Council, Germany (approval No. C3/09). National and institutional guidelines for the care and use of laboratory animals were used. All experiments were conducted in compliance with the standards outlined in the Guide for the Care and Use of Laboratory Animals and under the supervision of a veterinarian who set the guiding principles to minimize animal suffering.

Six female German Landrace pigs weighing 33.7 ±2.8 kg (range: 29.0–37.5 kg) and aged approx. 8 weeks underwent a laparotomy and consecutive acetaminophen administration.

During an adaptation period of 1 week, the animals were kept in cages in the Research Animal Care Facility at a temperature of approx. 20°C and relative humidity of approx. 60% with natural day–night cycles, in accordance with the European Union directive 2007/526/EG and the European Union guideline 2010/63/EU. They received a standard diet and tap water ad libitum. In the evening before the surgical procedure, the pigs were deprived of food (not water). Before the onset of the experiment, all animals were examined by a veterinarian, and no abnormalities were found.

Premedication, anesthesia protocols, intensive care treatment, and algorithms for standardized intensive care management have been reported in detail in previous studies.[17,18] Briefly, the animals received intramuscular premedication of atropine 0.1% (0.05 mg/kg), ketamine (14 mg/kg), azaperone (2 mg/kg), and midazolam (0.5 mg/kg). After oral intubation, ventilation was performed using a pressure-controlled ventilation machine. Continuous intravenous anesthesia was maintained with ketamine (15 mg/kg/h), fentanyl (0.02 mg/kg/h) and midazolam (0.9 mg/kg/h). The animals remained under general anesthesia for a total observation period of 40 h following acetaminophen administration.

Surgical procedures

Briefly, the internal carotid artery (Leadercath; Vygon, Écouen, France) and jugular veins (Multi-Lumen Central Venous Catheter; Arrow International, Reading, USA) were instrumented to measure mean arterial pressure (MAP) and central venous pressure (CVP), respectively. The abdominal cavity was entered through a midline incision. A jejunal catheter (Gentle-Flo™; Tyco Healthcare, Tullamore, Ireland) was implanted in the upper jejunum for acetaminophen administration, and a urinary catheter (Gentle-Flo™; Tyco Healthcare) was placed by cystostomy. The abdomen was then closed in a standard fashion.

Acetaminophen administration and acute liver failure

Immediately after the closure of the abdomen, the animals received a single bolus of acetaminophen of 1000 mg/kg through the jejunal catheter. For this purpose, commercially available acetaminophen tablets were crushed with a tablet mortar and dissolved in 10 mL of physiological sodium chloride solution. After the administration of the solution, the jejunal catheter was flushed with 50 mL of sodium chloride solution.

The onset of ALF syndrome was determined by the presence of coagulopathy, as shown by a decline in prothrombin time (PT, Quick) to below 30%.

Critical care management

Standard hemodynamic monitoring was used and recorded throughout the entire experiment, and included electrocardiography, oxygen saturation, MAP, CVP, and core body temperature. Arterial blood gas analysis (ABL 800; Radiometer, Copenhagen, Denmark), including the measurement of hemoglobin, methemoglobin, hematocrit, acid base balance, lactate, serum electrolytes, and blood glucose levels, was recorded hourly and directly corrected as required, while ventilation parameters were adjusted accordingly. General anesthesia was sustained with a continuous infusion of ketamine 15 mg/kg/h, fentanyl 0.02 mg/kg/h and midazolam 0.9 mg/kg/h. Urinary output was monitored, and volume resuscitation and vasopressor use were performed according to a standard protocol, as previously described.[17] After a total observation period of 40 h from the administration of acetaminophen, the surviving pigs were euthanized with a single intravenous bolus of 10 mL of T-61 (Intervet, Unterschleißheim, Germany). One mL of T-61 consists of 5 mg of tetracaine hydrochloride, 50 mg of mebezonium iodide and 200 mg of embutramide.

Biochemical analyses

All blood samples were collected through the internal carotid catheter and analyzed by the certified Central Laboratories of University Hospital Tübingen (Division of Endocrinology, Diabetology, Angiology, Nephrology, Pathobiochemistry, and Clinical Chemistry, Department of Internal Medicine), Germany. Laboratory parameters were obtained before and every 8 h after acetaminophen administration until death (or a maximum of 40 h). Acetaminophen levels were determined with an enzymatic assay performed on a fully automated biochemical analyzer (ACTM Flex® reagent cartridge, Cat. No. DF88; Dimension Xpand Plus; Siemens Healthcare Diagnostics, Eschborn, Germany) in an accredited laboratory. The certified assay has a range of 0.0–300.0 µg/mL (0.0–1985.4 µmol/L) and a total coefficient of variation of 4.44% (serum)/1.45% (plasma).

Samples with results in excess of 300.0 µg/mL (1985.4 µmol/L) were repeated following dilution. Albumin, total plasma protein, aspartate aminotransferase (AST) activity, and lactate concentration were measured on the ADVIA 1800 Clinical Chemistry Analyzer, and the ADVIA 2120 Hematology Analyzer was used for blood cell counts (both from Siemens Healthcare Diagnostics). Coagulation tests were performed on the ACL TOP 700 Hemostasis Testing System (Instrumentation Laboratory, Kirchheim, Germany). Tumor necrosis factor alpha and IL-6 (both R&D Systems, Minneapolis, USA), as well as hepatocyte growth factor (HGF) and epidermal growth factor (EGF) (both from Cusabio Biotech, Wuhan, China) plasma concentrations were analyzed using specific porcine enzyme-linked immunosorbent assay (ELISA) kits. The sample analysis was conducted within 1 h of blood withdrawal.

Pathological examinations

Immediately post mortem, a liver biopsy specimen of 1.0 × 1.0 × 0.5 cm from the lobus hepatis sinister lateralis was obtained from all 6 animals and fixed in 4% formaldehyde. Hematoxylin and eosin (H&E) were used to stain the specimens, and the POL HRP-006 Polymer Kit, monoclonal mouse antihuman Ki-67, antigen clone MIB-1 Code M7240, and Mouse IgGX 0931 for Ki-67 were used for immunostaining (Zytomed Systems GmbH, Berlin, Germany, and Agilent, Santa Clara, USA). Liver sections were examined and photographed with a Zeiss Axiovert 135 Microscope (Carl Zeiss AG, Jena, Germany).

Pharmacokinetic profile

The elimination half-life (t1/2el) was calculated. For this purpose, the acetaminophen concentration data were log transformed (logarithmus naturalis) and plotted against time. A trend line was calculated using linear regression. The slope in the equation shows the elimination rate constant (kel). To obtain the half-life of the elimination phase, the formula t1/2el = 0.693/kel was used.[19]

Statistical analyses

The mean values obtained before, during and after the administration of acetaminophen were compared using the Wilcoxon test (JMP® 12.0; SAS Institute, Cary, USA). A value of $p < 0.05$ was considered statistically significant. Results in the manuscript and figures are reported as mean and standard deviation (SD).

Results

Manifestation of acute liver failure

Three of the 6 animals developed ALF followed by multiple organ failure and subsequent death after 24 h, 25 h and 38 h. The other 3 of the 6 animals survived the administration of acetaminophen. A significant deterioration of MAP occurred 12 h after acetaminophen administration (51 ±5 mm Hg in nonsurviving animals compared to 72 ±1 mm Hg in surviving animals ($p < 0.05$, Wilcoxon test)). Changes in hemodynamic parameters and selected laboratory values during the experiment are presented in Table 1.

Histology of the liver

At autopsy, the H&E-stained liver biopsies in the nonsurviving animals demonstrated progressive centrilobular necrosis (Fig. 1A) in contrast to a small amount of necrosis around the central vein in an otherwise intact lobule of the liver in the surviving animals (Fig. 1B). Figure 1C shows necrotic cell nuclei and no evidence of Ki-67 expression in a representative nonsurviving animal specimen at the end of the experiment. In the surviving animals, a total of 35 ±15 Ki-67-positive cells/lobule of the liver were observed (Fig. 1D).

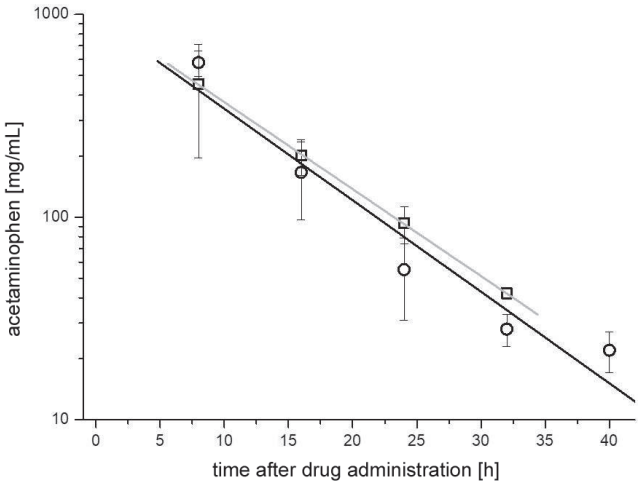

Fig. 2. Mean acetaminophen blood concentration in relation to time after drug administration

□ – nonsurviving animals; ○ – surviving animals.

Acetaminophen serum concentrations

The mean acetaminophen blood concentrations 8 h after receiving the bolus of 1000 mg/kg were 454 ±258 mg/L in the nonsurviving animals and 578 ±83 mg/L in the surviving animals; there was no statistically significant difference

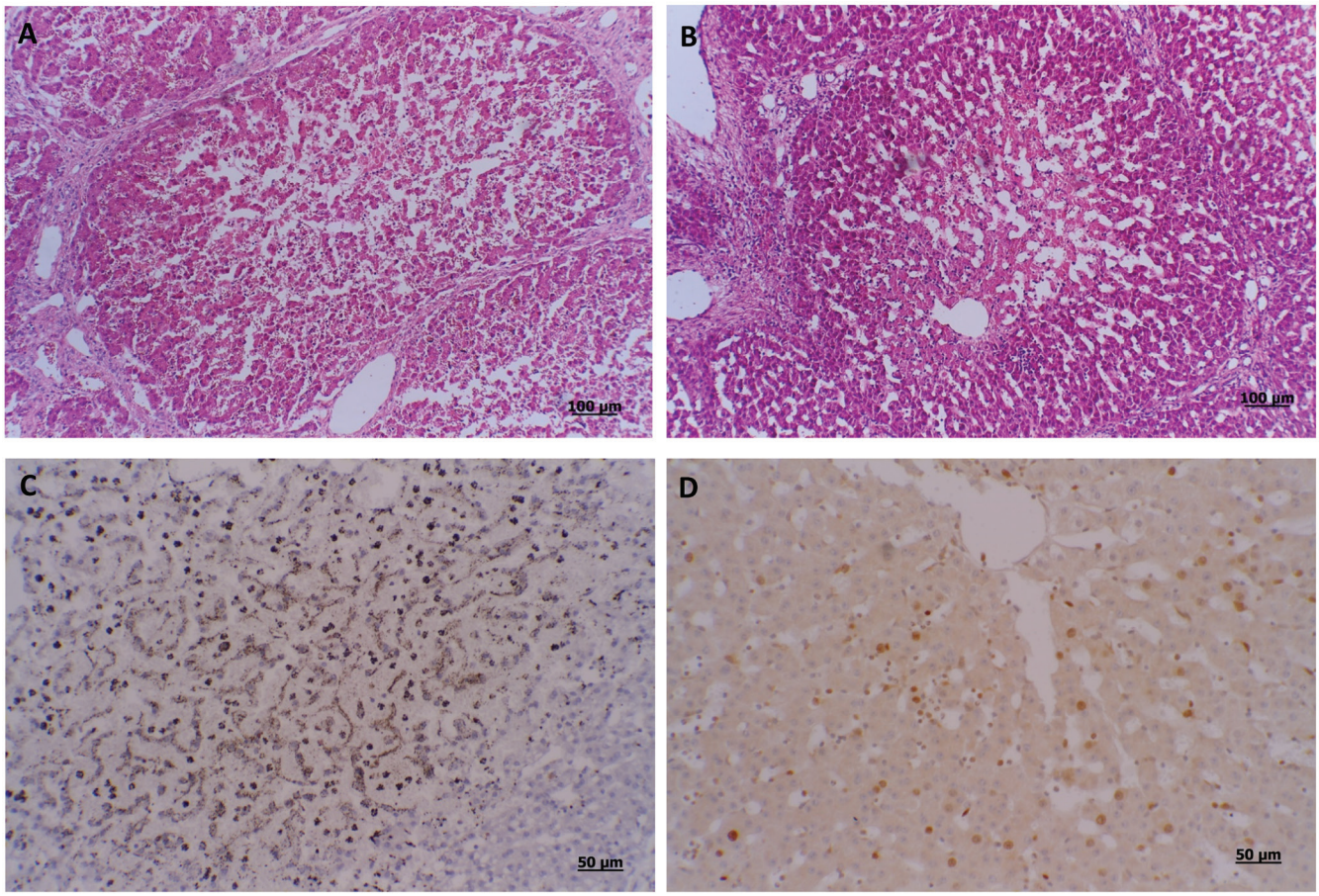

Fig. 1. Light microscope preparations (hematoxylin and eosin (H&E) staining) of post-mortem liver biopsies in nonsurviving (A) and surviving animals (B) and Ki-67 immunostaining in nonsurviving (C) and surviving animals (D)

between the groups in this regard (Fig. 2). The pharmacokinetic profiles were similar for both groups (kel in nonsurviving animals: −0.0989, resulting in a half-life of 7.0 h; kel in surviving animals: −0.10396, resulting in a half-life of 6.7 h).

Cytokines and growth factors

The baseline TNF-α levels before receiving the acetaminophen bolus were significantly higher in the group of nonsurviving animals (200 ±95 pg/mL compared to 28 ±26 pg/mL in the surviving animals; $p < 0.05$, Wilcoxon test, Fig. 3A). The concentration of TNF-α in the nonsurviving animals remained higher than in the surviving animals throughout the experiment. In the group of surviving animals, the TNF-α concentration increased to 120 ±60 pg/mL 8 h after drug administration, followed by a steady decline to 32 ±29 pg/mL at the end of the monitoring period.

The baseline IL-6 concentrations did not differ significantly between the groups (Fig. 3B). An increase in IL-6 levels to 1676 ±790 pg/mL was observed in the nonsurviving animals after 8 h, and IL-6 concentrations remained significantly elevated during the observation period. The surviving animals showed slightly elevated IL-6 values (443 ±388 pg/mL) at the time of drug administration, which decreased to below the initial values over the observed time (121 ±107 pg/mL after 32 h). The EGF concentrations oscillated from 0 ng/mL to 2 ng/mL and the HGF concentrations were approx. 1500 ng/mL in both groups.

Acute liver failure-related laboratory parameters

All biochemical parameters at baseline were within the physiological range reported earlier for German Landrace pigs.[20] The PT values in the nonsurviving animals

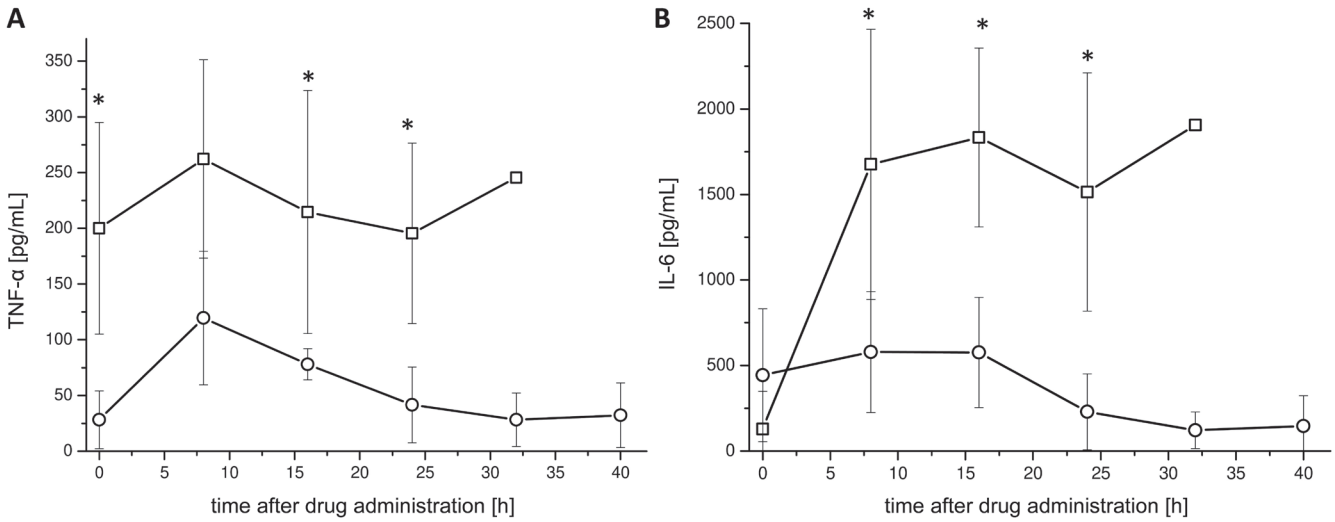

Fig. 3. Course of tumor necrosis factor alpha (TNF-α) (A) and interleukin (IL)-6 (B) in relation to time after drug administration

□ – nonsurviving animals (n = 3 at 24 h, n = 1 at 32 h); ○ – surviving animals (n = 3); * $p < 0.05$, Wilcoxon test.

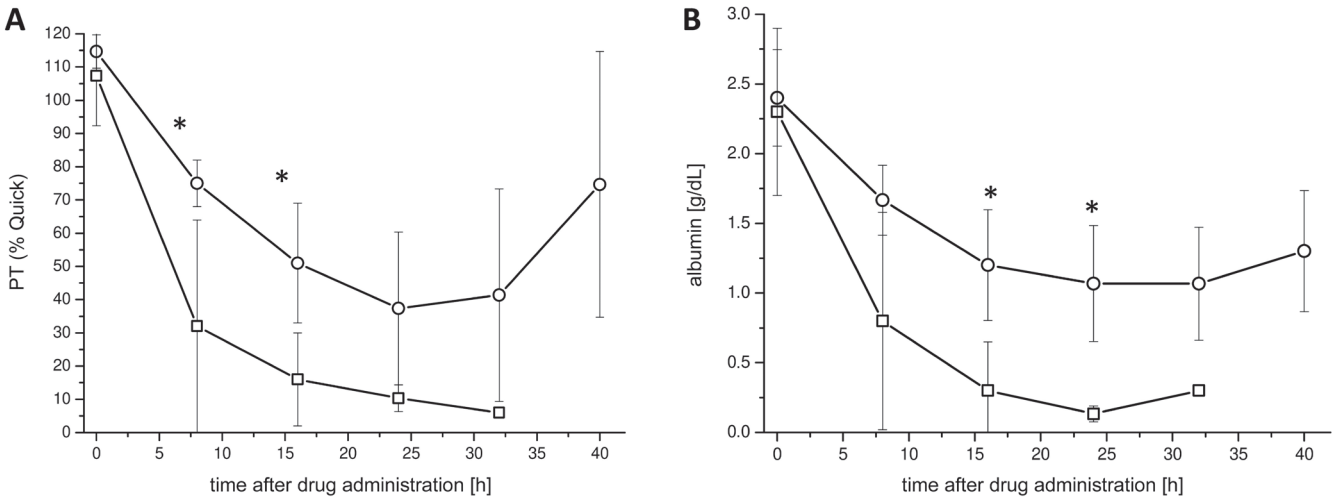

Fig. 4. Course of prothrombin time (A) and albumin (B) in relation to time after drug administration

□ – nonsurviving animals (n = 3 at 24 h, n = 1 at 32 h); ○ – surviving animals (n = 3); * $p < 0.05$, Wilcoxon test.

declined continuously, demonstrating the onset of ALF after 8 h of acetaminophen administration, and remained constantly below 30% during the observation period (Fig. 4A). The surviving animals showed a decline in PT values after the administration of acetaminophen, but their mean values remained above 30% and recovered to 75 ±40% after 40 h.

The baseline albumin concentrations ranged between 2.3 mg/dL and 2.4 mg/dL in both groups (Fig. 4B). Sixteen hours after drug administration, the nonsurviving animals showed significantly lower albumin concentrations than the surviving animals (0.3 ±0.4 mg/dL compared to 1.2 ±0.4 mg/dL; $p < 0.05$, Wilcoxon test).

Aspartate aminotransferase activity did not differ between the nonsurviving and surviving animals during the entire observation period and showed a gradual increase (before drug administration: 53 ±24 U/L; after 8 h: 52 ±21 U/L; after 16 h: 72 ±36 U/L; after 24 h: 191 ±175 U/L; after 32 h: 524 ±515 U/L; and after 40 h: 603 ±627 U/L).

Immediately before the administration of acetaminophen, the average lactate concentrations were 2.0 ±0.7 mmol/L in the surviving animals and 2.0 ±1.4 mmol/L in the nonsurviving animals. Eight hours after drug administration, the mean lactate concentration in the nonsurviving animals increased to 5.0 ±2.2 mmol/L, while it decreased to 1.3 ±0.9 mmol/L in the surviving animals ($p < 0.05$, Wilcoxon test). In the last 12 h before death, the lactate concentrations reached levels above 10 mmol/L in the nonsurviving animals.

Methemoglobinemia occurred during the first 4 h after acetaminophen administration (18.6 ±8.7% in the nonsurviving animals and 10.8 ±8.0% in the surviving animals; the difference was not statistically significant). Twenty-four hours after drug administration, the methemoglobin levels decreased to 2.8 ±3.4% in the surviving animals and 6.9 ±4.0% in the nonsurviving animals.

Discussion

Acetaminophen is a potentially harmful medication with pronounced variability in individual tolerance. The toxic metabolite of acetaminophen is N-acetyl-p-benzoquinone imine (NAPQI), which can be reduced to a nontoxic metabolite by glutathione in therapeutic doses.[21] However, NAPQI in higher doses can deplete glutathione and then covalently bind to mitochondrial proteins, leading to oxidative stress, inflammation, mitochondrial dysfunction, and cell death. Understanding of the mechanism involved in this procedure is essential for analyzing existing and prospective biomarkers.

The critical dose of acetaminophen for developing severe liver injury in humans is 4000 mg in 24 h.[21] In pigs, 1000 mg/kg body weight was identified as a critical dose by Artwohl et al. in 1988.[22] In their study, animals receiving 500–1000 mg/kg of acetaminophen survived, while animals receiving a dose of 1000–2000 mg/kg died within 6.5 h due to methemoglobinemia.

Thus, patients who are prone to developing ALF after acetaminophen intoxication should be identified as early as possible in order to ultimately prevent acetaminophen-induced ALF and increase their likelihood of survival. The purpose of this study was to measure blood cytokine levels and ALF-related laboratory parameters in a porcine model of acetaminophen overdose in order to guide the search for early biomarkers that could discriminate between susceptibility and tolerance to acetaminophen.

The prominent finding of this study is that an elevated baseline level of TNF-α seems to predict an increased susceptibility to acetaminophen-induced ALF. The TNF-α levels in the nonsurviving animals remained higher than in the surviving animals. It is known that TNF-α blood levels are increased in ALF[23–25] and correlate directly with disease activity and overall prognosis.[14,26] However, it is not clear why the animals differed in TNF-α before the treatment was initiated and what might have induced the expression of TNF-α. The animals were young (approx. 8 weeks old), healthy and obtained from the same farmer. Clinical examination by the veterinarian before commencing the experiments showed no clinical signs or symptoms of illness. All laboratory parameters, including liver enzymes and infection parameters at baseline, were within the physiological range for German Landrace pigs, which makes pre-existing subclinical or undetected liver damage or infection unlikely.

Our data suggest that elevated TNF-α blood concentrations at baseline might accelerate disease progression. Further investigation is needed to clarify whether an elevation of TNF-α at baseline directly affects the outcome by enhancing toxic acetaminophen effects or indicates an epiphenomenon. However, an elevated baseline TNF-α level could potentially serve as an early and easily obtainable prognostic marker for determining a risk–benefit ratio for the development of ALF after the administration of acetaminophen.

The nonsurviving animals had a significant increase in IL-6 after acetaminophen administration, and even though the IL-6 levels decreased steadily within 16 h after acute exposure, the IL-6 concentrations remained higher than in the surviving animals throughout the course of the experiment. In contrast, HGF and EGF levels did not differ between the surviving and nonsurviving animals.

To examine the histological signs of liver damage and determine regeneration potential, we performed liver biopsies at the end of the experiment. All of the surviving animals showed a large quantity of Ki-67-positive cells as a marker of regeneration, in contrast to the nonsurviving animals, that showed centrilobular necrosis and no signs of Ki-67 expression.

Bernal et al. identified an increased blood lactate concentration as an early predictor of outcome in acetaminophen-induced ALF and proposed a modification to the King's College Criteria in order to include blood lactate concentrations with cutoff values of 3.5 mmol/L measured early after admission and 3.0 mmol/L after

Table 1. Hemodynamic parameters and laboratory values of selected biochemical parameters before and after drug administration

Time after drug administration [h]	0		8		16		24		32		40	
Group	non-surv	surv	non-surv	surv	non-surv	surv	non-surv	surv	non-surv	surv	non-surv	surv
Number of animals	3	3	3	3	3	3	3	3	1	3	0	3
Heart rate [bpm]	79 ±27	62 ±17	126 ±18	93 ±113	116 ±25	87 ±15	145 ±31	75 ±11	126	69 ±8	–	66 ±9
Oxygen saturation [%]	100 ±0	100 ±1	95 ±5	98 ±1	98 ±3	100 ±0	95 ±7	100 ±0	100	99 ±1	–	99 ±2
Mean arterial pressure [mm Hg]	62 ±6	59 ±9	69 ±11	84 ±112	51 ±6	67 ±5	46 ±1	71 ±6	44	75 ±6	–	80 ±11
Central venous pressure [mm Hg]	8 ±2	8 ±3	11 ±5	10 ±2	12 ±2	10 ±4	14 ±3	11 ±5	11	12 ±6	–	10 ±4
Hemoglobin [g/dL]	9.1 ±0.6	9.7 ±0.8	8.7 ±1.6	8.8 ±1.8	8.2 ±1.2	9.4 ±0.8	7.0 ±1.4	8.8 ±0.2	7.5	8.6 ±0.6	–	9.1 ±0.4
Methemoglobin [%]	0.7 ±0.1	1.4 ±0.2	24.9 ±16.7	11.5 ±6.4	10.9 ±6.6	3.5 ±4.7	6.9 ±4.0	2.8 ±3.4	1.5	3.1 ±3.9	–	2.8 ±3.5
Hematocrit [%]	27 ±1	29 ±3	26 ±5	27 ±6	24 ±4	29 ±3	21 ±5	26 ±1	22	26 ±2	–	27 ±2
pH	7.47 ±0.02	7.47 ±0.02	7.33 ±0.07	7.37 ±0.05	7.31 ±0.03	7.39 ±0.06	7.33 ±0.06	7.42 ±0.04	7.27	7.40 ±0.02	–	7.42 ±0.07
Natrium [mmol/L]	140 ±1	140 ±3	148 ±4	146 ±4	155 ±3	146 ±3	161 ±6	151 ±7	158	156 ±1	–	153 ±6
Potassium [mmol/L]	4.1 ±0.3	3.9 ±0.8	3.2 ±0.9	3.5 ±0.5	3.5 ±0.4	3.8 ±0.3	3.9 ±0.8	3.6 ±0.1	5.5	3.3 ±0	–	3.7 ±0.1
Blood glucose [mmol/L]	6.5 ±2.5	7.0 ±1.7	7.3 ±1.5	6.2 ±1.5	5.8 ±1.0	6.1 ±1.3	6.7 ±1.7	5.7 ±1.1	5	5.8 ±0.1	–	4.8 ±0.6

Non-surv – nonsurviving animals; surv – surviving animals.

volume resuscitation.[27] In the current study, the lactate concentrations in the surviving animals remained between 0.9 mmol/L and 1.3 mmol/L, while the nonsurviving animals had peak lactate levels of 5.0 ±1.2 mmol/L as early as 8 h after acetaminophen administration. The French guidelines on the management of liver failure in general intensive care unit recommend monitoring lactate levels as well as the results of arterial blood gas analysis.[3]

Multiple animal studies with different species have linked the production of methemoglobin as a toxic by-product in acetaminophen-induced ALF with lethal outcomes.[22,28,29] Interestingly, in another porcine experiment, methemoglobinemia correlated directly with administered doses and blood levels of acetaminophen.[28] In a further porcine study, acetaminophen levels higher than 250 mg/L were seen to increase serum methemoglobin levels.[30] In our study, the concentration of acetaminophen rose to nearly 600 mg/L and methemoglobinemia occurred during the first 4 h after acute exposure. However, under standardized intensive care therapy, methemoglobin began to decrease continuously, even after the animals developed the typical hemodynamic and laboratory signs of ALF. The methemoglobin levels were slightly higher in the nonsurviving animals than in the surviving animals, but did not differ to a statistically significant degree. The presence of methemoglobinemia did not affect survival in this study.

After receiving an acetaminophen bolus of 1 g/kg body weight, the serum acetaminophen concentrations increased to 600 mg/L, which was previously described as a hepatotoxic concentration in humans.[31] The acetaminophen serum concentrations and elimination of acetaminophen did not differ between the surviving and nonsurviving animals. Even though acetaminophen is known to be a dose-dependent toxicant, it has been shown that acetaminophen dosing information in patients with ALF is an unreliable predictor of survival.[32] Furthermore, the total ingested dose did not influence survival in this study. Thus, it seems unlikely that acetaminophen serum concentration is the sole driving force that determines the clinical outcome.

Limitations

The small sample size and lack of a control group, which are factors of the pilot nature of the study, are clear limitations of this study. Therefore, larger investigations including controls are needed to validate the present data. In addition, the study did not analyze further acetaminophen metabolites, levels of NAPQI bound to proteins, or glutathione, and did not assess enzymes linked to oxidative stress.

Conclusions

In summary, TNF-α, IL-6, lactate, PT, and albumin blood concentration were identified as early predictors of outcome after acetaminophen intoxication. On the contrary, methemoglobinemia, acetaminophen serum

concentration, AST activity, and plasma HGF and EGF concentration did not differ between animals that were susceptible to acetaminophen and those who survived the acute phase of the poisoning.

An elevated TNF-α plasma concentration before the exposure to acetaminophen was the earliest prognostic plasma marker suggesting lethal outcome, and thus could possibly serve as a very early prognostic marker. Further studies in larger study groups and with human samples obtained from clinical cases are warranted.

ORCID iDs

Christian Thiel https://orcid.org/0000-0001-8880-4860
Matthias Morgalla https://orcid.org/0000-0003-4772-2871
Martin Schenk https://orcid.org/0000-0002-0402-7708
Alfred Königsrainer https://orcid.org/0000-0002-2301-4080
Karolin Thiel https://orcid.org/0000-0002-7328-7589

References

1. Lee WM. Acetaminophen-related acute liver failure in the United States. *Hepatol Res*. 2008;38:S3–S8. doi:10.1111/j.1872-034X.2008.00419.x
2. Simpson KJ, Bates CM, Henderson NC, et al. The utilization of liver transplantation in the management of acute liver failure: Comparison between acetaminophen and non-acetaminophen etiologies. *Liver Transplant*. 2009;15(6):600–609. doi:10.1002/lt.21681
3. Paugam-Burtz C, Levesque E, Louvet A, et al. Management of liver failure in general intensive care unit. *Anaesth Crit Care Pain Med*. 2020; 39(1):143–161. doi:10.1016/j.accpm.2019.06.014
4. Canbay A, Tacke F, Hadem J, Trautwein C, Gerken G, Manns MP. Acute liver failure: A life-threatening disease. *Dtsch Arztebl Int*. 2011;108(42): 714–720. doi:10.3238/arztebl.2011.0714
5. Krähenbühl S, Brauchli Y, Kummer O, et al. Acute liver failure in two patients with regular alcohol consumption ingesting paracetamol at therapeutic dosage. *Digestion*. 2007;75(4):232–237. doi:10.1159 /000111032
6. Schmidt LE, Dalhoff K. Concomitant overdosing of other drugs in patients with paracetamol poisoning. *Br J Clin Pharmacol*. 2002;53(5): 535–541. doi:10.1046/j.1365-2125.2002.01564.x
7. Strnad P, Zhou Q, Hanada S, et al. Keratin variants predispose to acute liver failure and adverse outcome: Race and ethnic associations. *Gastroenterology*. 2010;139(3):828–835. doi:10.1053/j.gastro.2010.06.007
8. Bernal W, Auzinger G, Dhawan A, Wendon J. Acute liver failure. *Lancet*. 2010;376(9736):190–201. doi:10.1016/S0140-6736(10)60274-7
9. Larson AM, Polson J, Fontana RJ, et al. Acetaminophen-induced acute liver failure: Results of a United States multicenter, prospective study. *Hepatology*. 2005;42(6):1364–1372. doi:10.1002/hep.20948
10. Riordan SM, Williams R. Alcohol exposure and paracetamol-induced hepatotoxicity. *Addict Biol*. 2002;7(2):191–206. doi:10.1080/135562 10220120424
11. Prescott LF. Paracetamol, alcohol and the liver. *Br J Clin Pharmacol*. 2000;49(4):291–301. doi:10.1046/j.1365-2125.2000.00167.x
12. O'Grady JG. Postoperative issues and outcome for acute liver failure. *Liver Transpl*. 2008;14(S2):S97–S101. doi:10.1002/lt.21640
13. Laverty HG, Antoine DJ, Benson C, Chaponda M, Williams D, Park BK. The potential of cytokines as safety biomarkers for drug-induced liver injury. *Eur J Clin Pharmacol*. 2010;66(10):961–976. doi:10.1007/ s00228-010-0862-x
14. Berry PA, Antoniades CG, Hussain MJ, et al. Admission levels and early changes in serum interleukin-10 are predictive of poor outcome in acute liver failure and decompensated cirrhosis. *Liver Int*. 2010; 30(5):733–740. doi:10.1111/j.1478-3231.2010.02219.x
15. James LP, Simpson PM, Farrar HC, et al. Cytokines and toxicity in acetaminophen overdose. *J Clin Pharmacol*. 2005;45(10):1165–1171. doi:10. 1177/0091270005280296
16. Kerr R, Newsome P, Germain L, et al. Effects of acute liver injury on blood coagulation. *J Thromb Haemost*. 2003;1(4):754–759. doi:10.1046/j. 1538-7836.2003.00194.x
17. Thiel C, Thiel K, Etspueler A, et al. Standardized intensive care unit management in an anhepatic pig model: New standards for analyzing liver support systems. *Crit Care*. 2010;14(4):R138. doi:10.1186/ cc9196
18. Thiel C, Thiel K, Etspueler A, et al. A reproducible porcine model of acute liver failure induced by intrajejunal acetaminophen administration. *Eur Surg Res*. 2011;46(3):118–126. doi:10.1159/000323411
19. Rowland M, Tozer TN. *Clinical Pharmacokinetics and Pharmacodynamics: Concepts and Applications*. 4th ed. Philadelphia, USA: Lippincott William & Wilkins; 2010. ISBN: 978-0781750097.
20. Swindle MM. *Surgery, Anesthesia and Experimental Techniques in Swine*. Ames, USA: Iowa State University Press; 1998. ISBN: 978-0813818290.
21. Mitchell JR, Thorgeirsson SS, Potter WZ, Jollow DJ, Keiser H. Acetaminophen-induced hepatic injury: Protective role of glutathione in man and rationale for therapy. *Clin Pharmacol Ther*. 1974;16(4): 676–684. doi:10.1002/cpt1974164676
22. Artwohl JE, Henne-Bruns D, Carter E, Cera LM. Acetaminophen toxicosis: A potential model for acute liver failure in swine. *Vet Hum Toxicol*. 1988;30(4):324–328. PMID: 3176307.
23. Saiman Y, Friedman SL. The role of chemokines in acute liver injury. *Front Physiol*. 2012;3:213. doi:10.3389/fphys.2012.00213
24. Shah N, Montes de Oca M, Jover-Cobos M, et al. Role of toll-like receptor 4 in mediating multiorgan dysfunction in mice with acetaminophen induced acute liver failure. *Liver Transpl*. 2013;19(7):751–761. doi:10.1002/lt.23655
25. Antoniades CG, Berry PA, Wendon JA, Vergani D. The importance of immune dysfunction in determining outcome in acute liver failure. *J Hepatol*. 2008;49(5):845–861. doi:10.1016/j.jhep.2008.08.009
26. Streetz K, Leifeld L, Grundmann D, et al. Tumor necrosis factor α in the pathogenesis of human and murine fulminant hepatic failure. *Gastroenterology*. 2000;119(2):446–460. doi:10.1053/gast.2000.9364
27. Bernal W, Donaldson N, Wyncoll D, Wendon J. Blood lactate as an early predictor of outcome in paracetamol-induced acute liver failure: A cohort study. *Lancet*. 2002;359(9306):558–563. doi:10.1016/ S0140-6736(02)07743-7
28. Henne-Bruns D, Artwohl J, Broelsch C, Kremer B. Acetaminophen-induced acute hepatic failure in pigs: Controversical results to other animal models. *Res Exp Med (Berl)*. 1988;188(6):463–472. doi:10.1007/ BF01852004
29. Kelly JH, Koussayer T, He DE, et al. An improved model of acetaminophen-induced fulminant hepatic failure in dogs. *Hepatology*. 1992; 15(2):329–335. doi:10.1002/hep.1840150225
30. Newsome PN, Henderson NC, Nelson LJ, et al. Development of an invasively monitored porcine model of acetaminophen-induced acute liver failure. *BMC Gastroenterol*. 2010;10(1):34. doi:10.1186/1471-230X-10-34
31. Rumack BH, Matthew H. Acetaminophen poisoning and toxicity. *Pediatrics*. 1975;55(6):871–876. PMID: 1134886.
32. Gregory B, Larson AM, Reisch J, Lee WM; Acute Liver Failure Study Group. Acetaminophen dose does not predict outcome in acetaminophen-induced acute liver failure. *J Investig Med*. 2010;58(5):707–710. doi:10.231/JIM.0b013e3181db8764

Schaftoside improves cerebral ischemia-reperfusion injury by enhancing autophagy and reducing apoptosis and inflammation through the AMPK/mTOR pathway

Lin Zhang[1,2,3,A–D], Minghua Wu[1,3,A,D–F], Zhaoyao Chen[1,3,A–C,F]

[1] Department of Neurology, Affiliated Hospital of Nanjing University of Chinese Medicine, China
[2] Department of Neurology, Nanjing Integrated Traditional Chinese and Western Medicine Hospital Affiliated with Nanjing University of Chinese Medicine, China
[3] Department of Neurology, Jiangsu Province Hospital of Chinese Medicine, Nanjing, China

A – research concept and design; B – collection and/or assembly of data; C – data analysis and interpretation;
D – writing the article; E – critical revision of the article; F – final approval of the article

Advances in Clinical and Experimental Medicine, ISSN 1899–5276 (print), ISSN 2451–2680 (online) *Adv Clin Exp Med*. 2022;31(12):1343–1354

Address for correspondence
Minghua Wu
E-mail: minghuaw001@163.com

Funding sources
This study was funded by the project of the Natural Science Foundation of Jiangsu Province (BK20201095), National Administration of Traditional Chinese Medicine: Evidence-Based Capacity Building Project (2019XZZX-NB007), 333 high level talents training project in Jiangsu (Grant No. BRA 2016507) and Jiangsu Province Administration of Chinese Medicine (ZT202102).

Conflict of interest
None declared

Received on March 25, 2022
Reviewed on June 28, 2022
Accepted on July 19, 2022

Published online on September 22, 2022

Cite as
Zhang L, Wu M, Chen Z. Schaftoside improves cerebral ischemia-reperfusion injury by enhancing autophagy and reducing apoptosis and inflammation through the AMPK/mTOR pathway. *Adv Clin Exp Med*. 2022;31(12):1343–1354. doi:10.17219/acem/152207

DOI
10.17219/acem/152207

Abstract

Background. As a flavonoid compound, schaftoside (SS) possesses a wide range of pharmaceutical activities. Nonetheless, it is unclear whether SS has a neuroprotective effect in cerebral ischemia-reperfusion injury (CI/RI).

Objectives. To examine the neuroprotective effect of SS in CI/RI and explore the underlying mechanism.

Materials and methods. An in vivo middle cerebral artery occlusion (MCAO) was used to simulate CI/RI in rats. Oxygen glucose deprivation/reperfusion (OGD/R) of HT22 cells was used to establish a cellular model of CI/RI in vitro. Pathological changes were evaluated with hematoxylin and eosin (H&E) staining, apoptosis was measured using terminal deoxynucleotidyl transferase dUTP nick end labeling (TUNEL) staining and flow cytometry, and inflammatory factors were assessed using enzyme-linked immunosorbent assay (ELISA). Protein expression was detected using western blot or immunofluorescence.

Results. Our results indicated that SS attenuated CI/RI by improving neurologic deficits and reducing brain edema. Moreover, SS treatment blocked apoptosis and inflammation and enhanced autophagy in MCAO rats. Schaftoside was found to amplify the activation of adenosine monophosphate-activated protein kinase (AMPK)/mammalian target of rapamycin (mTOR) pathway induced by MCAO. Similarly, SS pretreatment increased cell viability and autophagy, and reduced apoptosis and inflammation in OGD/R-induced HT22 cells. The OGD/R enlarges the p-AMPK/AMPK ratio while restricting the p-mTOR/mTOR ratio, and it was found that SS further enhanced the effect of OGD/R on the AMPK/mTOR pathway. Rapamycin promoted the effect of SS on OGD/R-induced HT22 cells, while compound C produced the opposite results. Mechanistically, SS promoted autophagy and reduced apoptosis and inflammation through the regulation of the AMPK/mTOR signaling pathway.

Conclusions. The obtained results showed that SS protected against CI/RI through an autophagy-mediated AMPK/mTOR pathway when accessed in vitro and in vivo.

Key words: apoptosis, autophagy, inflammation, cerebral ischemia-reperfusion injury, schaftoside

Background

Stroke is a central nervous system disease resulting from an acute cerebral blood circulation disorder caused by stenosis, occlusion or rupture of internal cerebral arteries.[1,2] Based on the pathogeny, strokes are divided into ischemic or hemorrhagic, in which ischemic strokes account for about 80% of total strokes.[3] The 2019 Global Stroke Statistics reported that the incidence of strokes was ranked first in China.[4] So far, there are no desirable drugs or strategies for the treatment of ischemic stroke. Current stroke treatment strategies include drug thrombolysis, mechanical thrombolysis, intravascular surgery, and the use of neuroprotective agents.[5,6] So far, recombinant tissue plasminogen activators (rtPAs), such as alteplase and reteplase, are the only drugs approved by the Food and Drug Administration (FDA) for the treatment of ischemic stroke.[7] However, due to the narrow treatment time window (3–4.5 h) of rtPAs and their serious adverse reactions, especially on the brain tissue injury caused by recanalization after thrombolysis by inducing a cerebral ischemia-reperfusion injury (CI/RI), the clinical application of rtPAs is limited.[8] The CI/RI is considered to be cell damage caused by cerebral ischemia. When blood supply is restored, the oxygen supply is enhanced and the damage to brain cells is exacerbated, resulting in further deterioration caused by the disease.[9] In addition, the study revealed that the ventromedial prefrontal cortex (vmPFC) is involved in the acquisition of emotional conditioning (i.e., learning), and assessed how naturally occurring bilateral lesion centered in the vmPFC compromises the generation of a conditioned psychophysiological response during the acquisition of threat conditioning (i.e., emotional learning).[10,11] A recent study focused on the cognitive symptoms (i.e., dysfunction in attention and emotion perception) in neurologic and brain-damaged patients, and highlighted the role of specific dysfunctional brain regions, such as the amygdala and superior temporal sulcus (STS), in the recognition and identification of nonverbal communicative signals of emotion.[12] The pathogenesis of neuronal damage and impairment of brain areas after stroke involves an interaction of multiple factors and pathways. Therefore, studying the pathogenesis of CI/RI is conducive to developing safe and effective drugs aimed at treating ischemic stroke.

It has been confirmed that CI/RI induces nerve cell inflammation and apoptosis or autophagy that results in neurological dysfunction.[13–16] Autophagy is an important stress response pathway of lysosomal degradation.[17] Some studies have shown that autophagy possesses a neuroprotective effect in CI/RI.[18,19] Melatonin can improve CI/RI in diabetic mice, and the underlying mechanism involves autophagy enhancement mediated by SIRT1/BMAL1 signaling.[20] Apoptosis is a kind of programmed cell death. Moreover, autophagy could block the induction of apoptosis and reduce cell damage.[21] Astragaloside IV has been shown to protect against CI/RI through reducing apoptosis by promoting autophagy.[22] It has been reported that inflammation is enhanced in neurodegenerative diseases.[23] Studies have shown that inhibiting neuroinflammation is considered an important strategy for the prevention of CI/RI.[24,25] Hence, nerve cell apoptosis, inflammation and autophagy were analyzed in CI/RI in this paper.

Traditional Chinese medicine possesses numerous medicinal animal and plant resources.[26] Screening anti-CI/RI drugs derived from traditional Chinese medicine have the advantages of low toxicity and few side effects.[27,28] Schaftoside (SS) is a flavonoid found in a variety of Chinese herbal medicines, such as *Eleusine indica*.[29] Currently, SS has a wide range of pharmacological activities, including anti-inflammatory, antiviral and antioxidant properties, and the regulation of autophagy.[30] Polyphenols such as resveratrol can potentially lead to autophagy in many diseases.[31,32] It has been reported that the treatment with SS in α-melanocyte-stimulating hormone (α-MSH)-treated cells reduced the expression of tyrosinase and tyrosinase-related protein 1 (TRP1), and activated autophagy.[30] However, the effects of SS on CI/RI are still unclear.

In this paper, middle cerebral artery occlusion (MCAO) was used to simulate CI/RI in rats in vivo. Oxygen glucose deprivation/reperfusion (OGD/R) of HT22 cells was used to establish a cellular model of CI/RI in vitro. Subsequently, whether SS could alleviate a CI/RI was explored in vivo and in vitro. Moreover, the effects of SS on neuronal apoptosis, inflammation and autophagy were explored. Our results showed that SS activates the adenosine monophosphate-activated protein kinase (AMPK)/mammalian target of rapamycin (mTOR) pathway, thereby reducing apoptosis and inflammation and inducing autophagy, thus improving a CI/RI.

Objectives

We aimed to explore whether SS could alleviate CI/RI by reducing apoptosis and inflammation and inducing autophagy through the activation of the AMPK/mTOR pathway.

Materials and methods

Animal experiments

Male Sprague Dawley rats (200 g, n = 50) were obtained from the Shanghai Experimental Animal Co., Ltd. (Shanghai, China). All rats were placed in the same animal feeding facility (room temperature 18–26°C, relative humidity 40–70%, ventilation 8–12 times per hour, and light/dark cycles alternating every 12 h). As shown in Table 1, the rats were randomly divided into 5 groups (n = 10 in each group): 1) sham operation group (sham

Table 1. The full scheme of animal experiment

Group	Time [h]		
	1	2	25
Sham (n = 10)	ig. physiological saline	Sham	ip. 120 mg/kg pentobarbital sodium
Control (n = 10)	ig. physiological saline	MCAO	ip. 120 mg/kg pentobarbital sodium
SS-L (n = 10)	ig. 50 mg/kg SS	MCAO	ip. 120 mg/kg pentobarbital sodium
SS-M (n = 10)	ig. 100 mg/kg SS	MCAO	ip. 120 mg/kg pentobarbital sodium
SS-H (n = 10)	ig. 150 mg/kg SS	MCAO	ip. 120 mg/kg pentobarbital sodium

SS – schaftoside; SS-L – SS low-dose group; SS-M – SS medium-dose group; SS-H – SS high-dose group; MCAO – middle cerebral artery occlusion; ig. – intragastrically; ip. – intraperitoneally.

group) – rats were treated by gavage with the same volume of physiological saline 1 h before modeling; 2) MCAO group – 1 h before modeling the same volume of physiological saline was given by gavage; 3) SS low-dose group (SS-L group) – 1 h before modeling the rats were treated with 50 mg/kg SS by gavage; 4) SS medium-dose group (SS-M group) – 1 h before modeling the rats were treated with 100 mg/kg of SS by gavage; 5) SS high-dose group (SS-H group) – 1 h before modeling the rats were treated with 150 mg/kg of SS by gavage.[33] Except for the sham group, MCAO was performed. The rats were anesthetized by intraperitoneal (ip.) injections of 10% chloral hydrate (35 mg/kg), and then the left common carotid artery (CCA), external carotid artery (ECA) and internal carotid artery (ICA) were separated. Wires were hung at the distal end and proximal end of the CCA and ECA for standby. The ICA was temporarily clamped with an arterial clamp, and the proximal CCA and ECA were ligated. Then, we cut a small opening in the ECA 4 mm away from the bifurcation of the CCA. A nylon suture was inserted from the ECA to ICA and gently fastened to a wire that was wound around the distal end of the CCA. The nylon suture was gently pushed with tweezers until an insertion depth of 18 mm was reached and slight resistance was met. The nylon suture was firmly fastened to the wire at the distal end of the CCA. One hour after the embolization, the nylon suture was pulled out ligating the ECA and opening the ICA and CCA. In the sham operation group, a nylon suture was inserted at 5 mm depth to simulate the above procedure. The animal experiments were performed in accordance with the Guidelines for the Care and Use of Laboratory Animals and approved by the Animal Ethics Committee in Affiliated Hospital of Nanjing University of Traditional Chinese Medicine, Nanjing, China (approval No. 2021 DW-09-02)

Neurological evaluation

After 24 h of modeling, a neurological evaluation of the rats in each group was performed; the examiner was blinded according to the Bederson's method.[34] The rats were suspended 1 m above the ground by gently holding their tails, and the bending of their forelimbs was observed. Rats with forelimbs bilaterally extended to the floor and no other neurological defects were given a score of 0. Rats with any amount of consistent forelimb flexion and no other abnormality received a score of 1. The rats were then placed on a large sheet of soft plastic paper which they held onto tightly with their claws. The tail of each rat was held and a slight lateral pressure was applied from behind the rat's shoulder until the forelimb slid a few inches. This was repeated several times in each direction. Normal or slightly dysfunctional rats had equal sliding resistance in both directions. However, severely dysfunctional rats had a consistently reduced resistance to the lateral push toward the paretic side and received a score of 2. Next, the rats were allowed to move freely and their circling behavior was observed. Rats that circled to the paralytic side received a score of 3. These experiments were repeated 3 times.

Hematoxylin and eosin staining

After 24 h of modeling, the rats were euthanized by an injection of excessive anesthetic, and their hippocampal tissue was stripped. The hippocampal tissue was fixed using 10% paraformaldehyde for 24 h, dehydrated with increasing gradients of ethanol (50%, 70%, 85%, 95%, 100%), cleared with xylene for 2 h, embedded in paraffin, and 4-μm sections were obtained. The sections were then soaked in 100%, 95%, 85%, and 75% ethanol solutions for 5 min each, washed with distilled water for 5 min, stained with 2% hematoxylin for 5 min, stained with 0.5% eosin for 2 min, washed with distilled water for 30 s, soaked in 80% ethanol for 30 s, soaked in 95% ethanol for 2 min, soaked in absolute ethanol for 3 min, cleared for 3 min using xylene, and then sealed with neutral resin. The hippocampal tissue sections were observed using an light microscope (model BX41; Olympus Corp., Tokyo, Japan). Each experiment was repeated 3 times.

TUNEL staining

After dewaxing, the sections were treated in an oven at 65°C for 30 min, soaked in xylene for 10 min, and then soaked in decreasing gradients of ethanol (100%, 95%, 90%, 80%, 70%) for 3 min. The sections were treated with protease K for 30 min and then with 3% H_2O_2 for 10 min at room

temperature in the dark. After cleaning with phosphate-buffered saline (PBS) for 5 min, sections were incubated in a terminal deoxynucleotidyl transferase (TdT) enzyme buffer for 5 min and then placed in a wet box of TdT reaction solution at 37°C for 1 h. The reaction was then terminated using a termination reaction buffer. The 3,3′-diaminobenzidine (DAB) was used for visualization at room temperature for 10 min. The sections were then counterstained with hematoxylin at room temperature. The number of terminal deoxynucleotidyl transferase dUTP nick end labeling (TUNEL)-positive cells (brownish yellow) was measured using an light microscope (BX41; Olympus Corp.). The experiment was repeated 3 times.

Brain water content

At 24 h after reperfusion, the brains of the rats were collected after euthanasia and immediately weighed to obtain the wet weight. The brains were then put in an oven (100°C) for 72 h and weighed to obtain the dry weight. The brain water content was calculated using the following formula: (wet weight–dry weight)/wet weight × 100%. The experiment was repeated 3 times.

Immunofluorescence

The sections were heated at 65°C for 30 min in a microwave oven, dehydrated with xylene and ethanol, and then antigen repairing was performed using a microwave. After blocking with bovine serum albumin (BSA), LC3 and p62, antibodies were added to the sections and incubated overnight at 4°C. After rinsing, fluorescent-labeled secondary antibodies were added, 4′,6-diamidino-2-phenylindole (DAPI) was added to stain the nucleus, and an anti-fluorescence quenching agent was added to seal the sections. The results were observed using a Leica TCS SP5 microscope (Leica Microsystems, Wetzlar, Germany). The experiment was repeated 3 times.

The cells were fixed with 4% paraformaldehyde for 15 min, then pretreated with 0.5% Triton X-100 at room temperature for 20 min, sealed with goat serum for 30 min at room temperature, incubated overnight with the corresponding primary antibody in a wet box at 4°C, and incubated with the corresponding secondary antibody for 1 h in the dark at room temperature. Nuclear counterstaining was performed by incubating the sections with DAPI in the dark for 5 min. The sections were then sealed with an anti-fluorescence quenching agent, and the results were observed using a Leica TCS SP5 microscope (Leica Microsystems). The experiment was repeated 3 times.

Western blot

Hippocampal tissues and cells were lysed using radioimmunoprecipitation assay (RIPA) lysate containing phenylmethylsulfonyl fluoride (PMSF; Beyotime, Shanghai, China), and proteins were obtained by centrifugation at 12,000 g for 15 min at 4°C. The protein content was identified using a BCA detection kit (Beyotime). For each group, 30 μg of protein were separated on a 10% sodium dodecyl-sulfate polyacrylamide gel electrophoresis (SDS-PAGE) background and then blotted onto a polyvinylidene difluoride (PVDF) membrane. The membranes were blocked for 1 h using 5% skimmed milk powder at room temperature and then incubated with the corresponding primary antibody overnight at 4°C. Then, the membranes were incubated with the corresponding secondary antibody for 2 h at room temperature. ImageJ software (National Institutes of Health, Bethesda, USA; https://imagej.nih.gov/ij/download.html) was used to quantify the protein bands, and glyceraldehyde-3-phosphate dehydrogenase (GAPDH) was used as an internal control. The experiment was repeated 3 times.

Cell culture and group

Mouse hippocampal neuron cell line HT22 cells were obtained from the China Center for Type Culture Collection at Wuhan University, Wuhan, China. The HT22 cells were cultured in a Dulbecco's modified Eagle's medium (DMEM) containing 10% fetal bovine serum (FBS) and 5% CO_2 in an incubator at 37°C. The HT22 cells were then inoculated into 24-well plates at a concentration of 1×10^5/mL. The cells were randomly divided into a control group, OGD/R group, SS-L group, SS-M group, and SS-H group. The cells were pretreated with SS (at concentrations of 0.1 μM, 0.5 μM and 1 μM)[35] for 24 h before OGD/R. After 24 h of culturing, the cells in the OGD/R group and SS treatment groups were cultured in DMEM without glucose in a medium containing 95% N_2/5% CO_2 at 37°C. After 4 h, the cells were again incubated in DMEM with glucose and returned to the conditions of 95% air/5% CO_2 for 24 h at 37°C. The cells in the control group were incubated in the culture conditions as described above.

CCK-8

The cells were inoculated into the 96-well plates using a concentration of 8×10^4/mL. After culturing for 24 h, the medium was discarded and 110 μL of complete medium containing 10% Cell Counting Kit-8 (CCK-8) (Beyotime) were added to each well. The cells were incubated for 2 h at 37°C. Next, the absorbance value at 450 nm was measured using a microplate reader (Bio-Rad, Hercules, USA). The experiment was repeated 3 times.

Flow cytometry

The cells were collected and fixed overnight at 4°C using precooled 75% ethanol. The ethanol was then removed by centrifugation (1000 rpm, 5 min), and the cells were washed 3 times using PBS. The cells were then mixed with

5 μL of Annexin V/FITC and 10 μL of propidium iodide solution (20 μg/mL), and the degree of apoptosis was measured using a BD FACSCalibur™ Flow Cytometer (BD Biosciences, Franklin Lakes, USA) within 1 h of adding the mixture. The experiment was repeated 3 times.

ELISA

After adjusting the cell concentration to 8×10^4/mL, the cells were inoculated onto 96-well plates and cultured at 37°C for 24 h in a 5% CO_2 incubator. After the treatment of the cell as previously described, the cell supernatant was collected using centrifugation at 5000 rpm for 10 min. The amount of interleukin (IL)-1β, tumor necrosis factor alpha (TNF-α) and IL-6 was measured according to the instructions of the corresponding kit (Nanjing Jiancheng Bioengineering Institute, Nanjing, China). The experiment was repeated 3 times.

The animal serum was separated using centrifugation at 3000 rpm for 10 min. The amount of IL-1β, TNF-α and IL-6 in the serum of each group was detected according to the instructions to the corresponding kit. The experiment was repeated 3 times.

Statistical analyses

The data from each group were analyzed statistically using GraphPad Prism v. 5.0 (GraphPad Software, San Diego, USA). The measurement data were reported as the mean ± standard deviation (x ±SD). The normality of the distribution was tested using the Shapiro–Wilk test. Since all the distributions were normal, the Brown–Forsythe test was used to establish the equality of variances, and then significant differences between multiple groups were analyzed using a one-way analysis of variance (ANOVA), followed by Tukey's post hoc test. When the test standard had a value of $p < 0.05$, the difference was considered statistically significant. The results of the assumptions of the verifying tests and the results of the analyses are presented in the Supplementary Table (https://doi.org/10.5281/zenodo.6838287).

Results

SS treatment alleviated CI/RI and reduced apoptosis and inflammation in MCAO rats

The ability of SS to alleviate CI/RI was investigated in rats. The results of hematoxylin and eosin (H&E) staining showed that compared to the sham group, the MCAO group exhibited obvious interstitial edema, brain tissue structure disorder, partial cell necrosis, and increased inflammatory cell infiltration (Fig. 1A). However, compared to the MCAO group, the degree of brain tissue necrosis was reduced, cell structure was maintained, interstitial edema was mild, and inflammation was reduced in the SS treatment groups, and the improvement effect was dose-dependent (Fig. 1A). Compared to the sham group, the neurological score of the MCAO group significantly increased ($p < 0.05$; Fig. 1B). However, the treatment with SS effectively alleviated the MCAO-induced neurological deficit observed in the rats ($p < 0.05$; Fig. 1B). The brain edema seen in the MCAO group was more serious than in the sham group ($p < 0.05$), and the administration of SS significantly reduced the brain edema observed in MCAO rats ($p < 0.05$; Fig. 1C). The effects of SS on apoptosis and inflammation were explored in MCAO rats. The results of the TUNEL assay indicated that MCAO increased the number of apoptosis-positive cells in the hippocampus, and SS inhibited the MCAO-induced apoptosis (Fig. 1D). The results of the enzyme-linked immunosorbent assay (ELISA) assay showed that MCAO upregulated the amount of the inflammatory factors IL-1β, TNF-α and IL-6 in rat serum ($p < 0.05$). The treatment using SS reduced the levels of the inflammatory factors ($p < 0.05$, Fig. 1E,G). Therefore, SS treatment protected against CI/RI in MCAO rats.

SS enhanced autophagy and regulated the AMPK/mTOR pathway in MCAO rats

To evaluate the role of SS in the regulation of autophagy during CI/RI, the expression of autophagy markers LC3 and p62 was detected with immunofluorescence staining and western blot. The expression of LC3 in the hippocampus was increased by the MCAO, while the expression of p62 was decreased (Fig. 2A). The expression of LC3 was further enhanced and the expression of p62 was further decreased after SS treatment (Fig. 2A). In addition, MCAO also increased the LC3II/LC3I ratio and decreased p62 levels ($p < 0.05$). Similarly, the administration of SS further promoted the effects of the MCAO on the LC3II/LC3I ratio and the expression of p62 ($p < 0.05$, Fig. 2B–D). The AMPK/mTOR pathway plays an important role in the regulation of CI/RI.[36] Next, the regulatory effects of SS on the AMPK/mTOR pathway were assessed in the MCAO rats. Middle cerebral artery occlusion stimulated an increase in the p-AMPK/AMPK ratio and decreased the p-mTOR/mTOR ratio ($p < 0.05$, Fig. 2B,E,F). The above effects were significantly increased by SS treatment ($p < 0.05$, Fig. 2B,E,F). Therefore, SS enhanced autophagy and regulated the AMPK/mTOR pathway in MCAO rats.

SS attenuated OGD/R-induced HT22 cell injury

The effects of SS on OGD/R-induced HT22 injury were explored. Schaftoside (≤1 μM) was not cytotoxic to HT22 cells ($p < 0.05$, Fig. 3A). Our results showed that OGD/R reduced the viability of HT22 cells, and pretreatment with SS weakened this effect ($p < 0.05$, Fig. 3B). In addition, SS

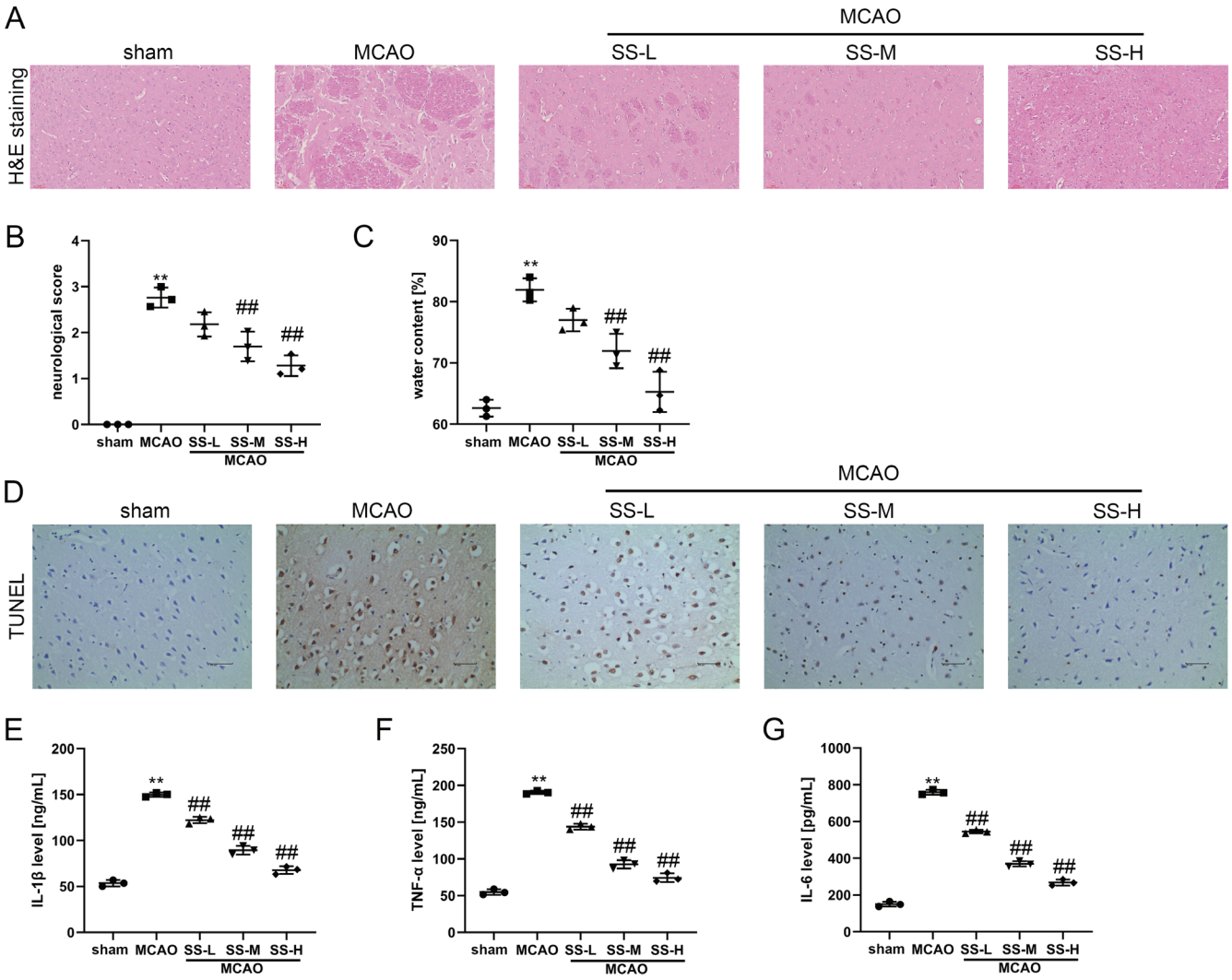

Fig. 1. Schaftoside (SS) protected against cerebral ischemia-reperfusion injury (CI/RI) and reduced apoptosis and inflammation. A. Hematoxylin and eosin (H&E) staining was performed on hippocampal tissue; B. Neurological evaluation of rats. The examiner was blinded according to the Bederson's method; C. Calculation of brain water content; D. Evaluation of apoptosis in hippocampal tissue using the terminal deoxynucleotidyl transferase dUTP nick end labeling (TUNEL) assay; E–G. Measurement of inflammation factors (interleukin (IL)-1β, tumor necrosis factor alpha (TNF-α) and IL-6) using enzyme-linked immunosorbent assay (ELISA)

SS-L – schaftoside low-dose group; SS-M – schaftoside medium-dose group; SS-H – schaftoside high-dose group; **p < 0.01 compared to sham group; ##p < 0.01 compared to the MCAO group.

treatment significantly alleviated OGD/R-induced apoptosis and inflammation in HT22 cells ($p < 0.05$, Fig. 3C–G). Besides, the immunofluorescence results illustrated that SS enhances OGD/R-induced autophagy in HT22 cells, which was demonstrated by the upregulation of LC3 levels (Fig. 4A). Moreover, after HT22 cells underwent OGD/R, the ratio of LC3II/LC3I was markedly increased ($p < 0.05$), while the expression of p62 was reduced ($p < 0.05$, Fig. 4B–D). The SS-induced LC3II/LC3I ratio was higher and the p62 level was lower than those in the OGD/R group ($p < 0.05$, Fig. 4B–D). Besides, SS treatment enhanced the p-AMPK/AMPK ratio and weakened the p-mTOR/mTOR ratio in OGD/R-induced HT22 cells ($p < 0.05$, Fig. 4B,E,F). These findings suggest that SS can reduce OGD/R-induced HT22 cell injury, and the AMPK/mTOR pathway may participate in the effects of SS on CI/RI.

SS improved the growth of HT22 cells by activating the AMPK/mTOR pathway

The mechanism of SS protection of HT22 cells was explored. To further determine the role of the AMPK/mTOR pathway in HT22 cells against OGD/R, the AMPK inhibitor compound C and mTOR inhibitor rapamycin were used. Schaftoside-induced inhibition of apoptosis and inflammation in HT22 cells against OGD/R were enhanced by rapamycin and blocked by compound C ($p < 0.05$, Fig. 5A–D). Rapamycin amplified SS-induced autophagy by reducing the LC3II/LC3I and p-mTOR/mTOR ratios, and upregulating p62 levels ($p < 0.05$). However, compound C showed the opposite effect ($p < 0.05$, Fig. 5F–J). Therefore, SS prevented HT22 cell injury induced by OGD/R by activating the AMPK/mTOR pathway.

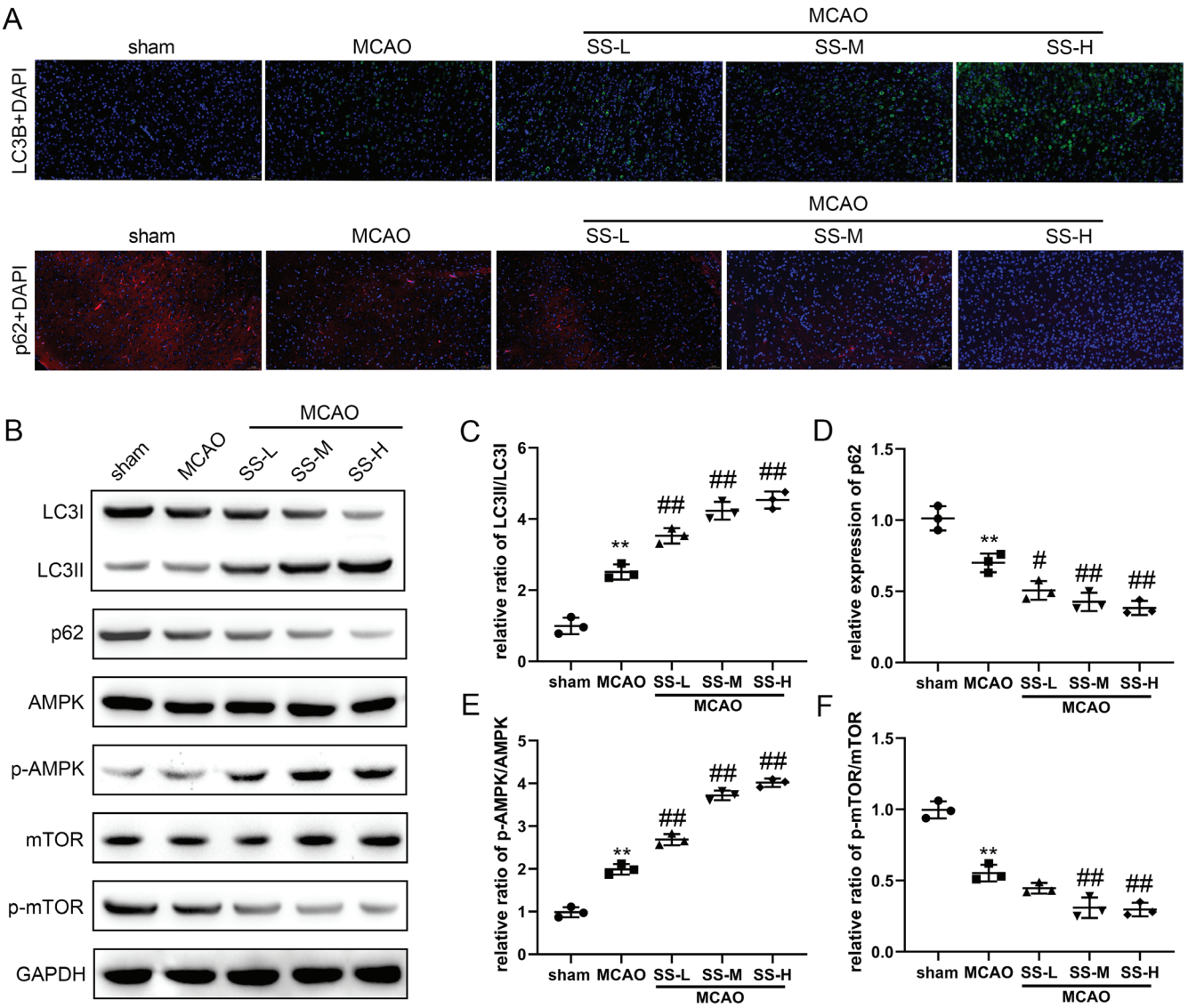

Fig. 2. Schaftoside (SS) promoted autophagy and activated the adenosine monophosphate-activated protein kinase (AMPK)/mammalian target of rapamycin (mTOR) pathway in middle cerebral artery occlusion (MCAO) rats. A. The expression of LC3 and p62 was detected with immunofluorescence assay; B–F. Related proteins of autophagy (LC3, p62) and the AMPK/mTOR pathway (AMPK, p-AMPK, mTOR, p-mTOR) were assessed using western blot

SS-L – schaftoside low-dose group; SS-M – schaftoside medium-dose group; SS-H – schaftoside high-dose group; DAPI – 4′,6-diamidino-2-phenylindole; GAPDH – glyceraldehyde-3-phosphate dehydrogenase; **p < 0.01 compared to the sham group; #p < 0.05 compared to the MCAO group; ##p < 0.01 compared to the MCAO group.

Discussion

Stroke is the leading cause of death and neurological dysfunction and places a heavy financial burden on the victims and health systems around the world. Previous studies have confirmed that CI/RI can lead to vascular injury, blood–brain barrier damage and a series of effects on neuronal injury. However, there is still a lot of work to be done to reduce the adverse effects of CI/RI. Despite continuous efforts to develop new treatment strategies (such as noninvasive brain stimulation techniques (NIBS)[37–39]), there are no effective treatment schemes for CI/RI. This study explored the potential neuroprotective effects of SS on brain I/R injuries and its mechanism.

Middle cerebral artery occlusion is a stable animal model for focal transient cerebral ischemia which is similar to human cerebral ischemia.[40] Therefore, MCAO is widely used in research on stroke pathology and neuroprotective drug screenings.[41] Neuronal death caused by CI/RI can lead to serious neurological deficits and cognitive impairments. After ischemia, the nutritional supply to neurons is blocked, including oxygen and glucose which play an important role in the growth of neurons.[42] Therefore, OGD/R-induced neuronal injury is used to simulate CI/RI in vitro.[43] In our study, we explored the effects of SS on CI/RI through an in vivo model of MCAO rats and the in vitro model of OGD/R-induced HT22 cells. Our findings suggested that SS reduced neuronal apoptosis and inflammation and

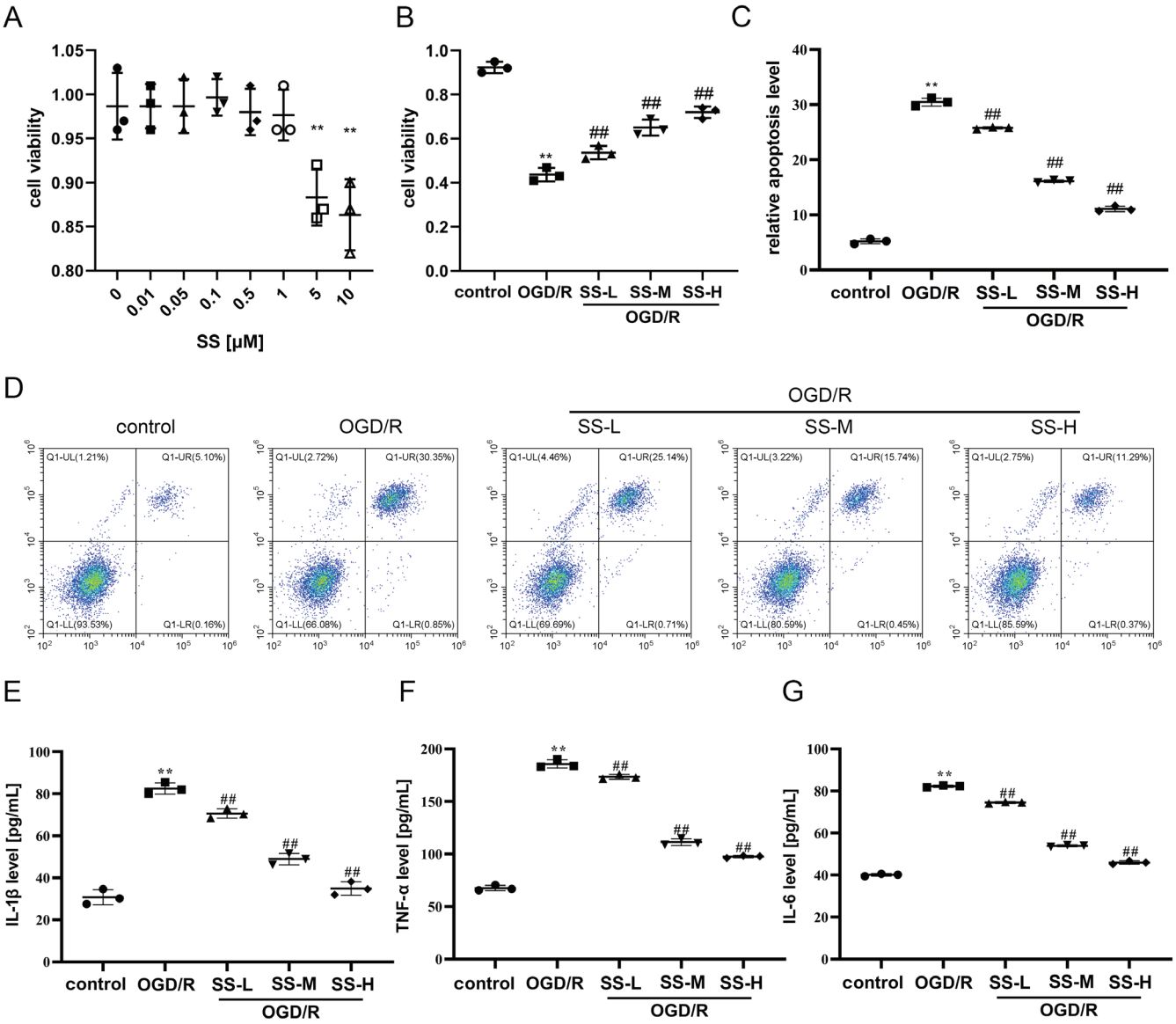

Fig. 3. Schaftoside (SS) increased cell viability and reduced apoptosis and inflammation in oxygen glucose deprivation/reperfusion (OGD/R)-induced HT22 cells. A,B. The cell viability was evaluated using the Cell Counting Kit-8 (CCK-8) assay; C,D. Cell apoptosis was measured using flow cytometry; E–G. Inflammation factors (interleukin (IL)-1β, tumor necrosis factor alpha (TNF-α) and IL-6) were measured using enzyme-linked immunosorbent assay (ELISA)

SS-L – schaftoside low-dose group; SS-M – schaftoside medium-dose group; SS-H – schaftoside high-dose group; **p < 0.01 compared to the control group; ##p < 0.01 compared to the OGD/R group.

promoted autophagy in MCAO rats and OGD/R-induced HT22 cells, and ist action was related to the activation of the AMPK/mTOR signaling pathway.

Apoptosis, also known as programmed cell death, is a process leading to cell death triggered by internal and external factors.[44] In recent years, scholars have found that CI/RI is closely related to apoptosis.[45,46] In addition, previous studies have confirmed that CI/RI causes inflammation, and reducing neuroinflammation is considered to be an important strategy to prevent CI/RI.[47,48] The upregulation of TREM2 can alleviate neurological dysfunction by inhibiting the inflammatory response and neuronal apoptosis in MCAO mice.[49] It was found that magnolol reduced the production of inflammatory factors and the expression and secretion of normal T cells in rats, and reduced brain injury in a rat I/R model.[50] Sappanone A effectively mitigated pathologic injury following cerebral infarction by reducing inflammation, oxidative stress and apoptosis in MCAO rats and OGD/R-induced PC12 cells.[51] Stigmasterol inhibits inflammation by regulating cyclooxygenase-2 (COX-2) and NF-κB (p65) expression and attenuates apoptosis by increasing the Bcl-2/Bax ratio and decreasing cleaved caspase-3 levels in rats with CI/RI.[52] Similarly, our results indicate that SS can inhibit apoptosis and inflammation in MCAO rats and OGD/R-induced HT22 cells.

Autophagy is a complex cellular metabolic process.[53] It is used as a metabolic self-defense process that differs from necrosis and apoptosis.[54] Autophagy is a complex

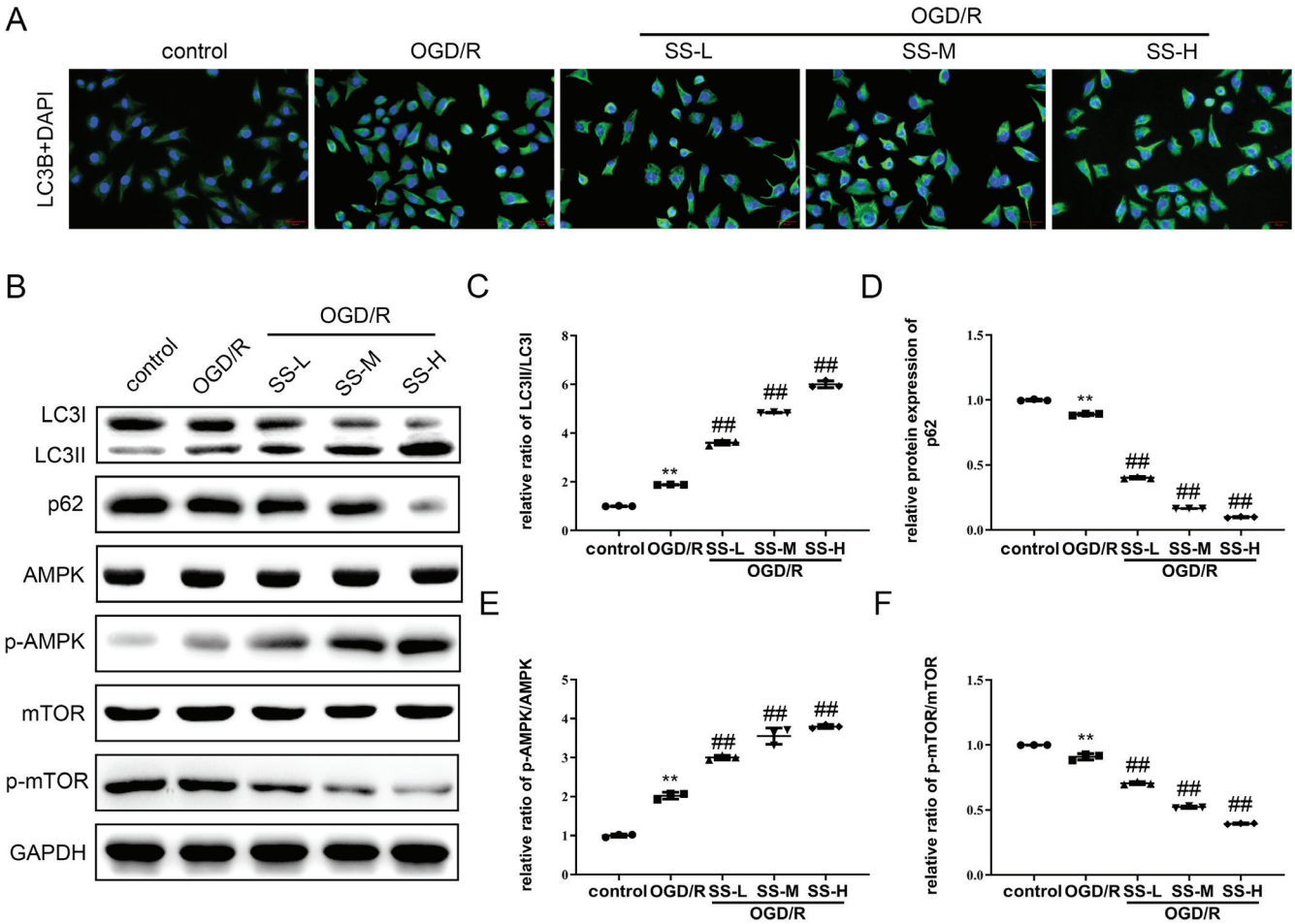

Fig. 4. Schaftoside (SS)-enhanced autophagy and activation of the adenosine monophosphate-activated protein kinase (AMPK)/mammalian target of rapamycin (mTOR) pathway in oxygen glucose deprivation/reperfusion (OGD/R)-induced HT22 cells. A. The expression of LC3 was measured with immunofluorescence assay; B–F. Related proteins of autophagy (LC3, p62) and the AMPK/mTOR pathway (AMPK, p-AMPK, mTOR, p-mTOR) were assessed using western blot

SS-L – schaftoside low-dose group; SS-M – schaftoside medium-dose group; SS-H – schaftoside high-dose group; DAPI – 4′,6-diamidino-2-phenylindole; GAPDH – glyceraldehyde-3-phosphate dehydrogenase; **p < 0.01 compared to the control group; ##p < 0.01 compared to the OGD/R group.

dynamic reaction, in which LC3 plays a significant role.[55] The transformation of LC3I to LC3II is considered to be a marker of autophagy.[56] The p62, as the substrate of autophagy, combines with LC3 and is degraded through a lysosomal pathway. It also plays a role in regulating autophagy.[57] Some scholars believe that autophagy plays a neuroprotective role in CI/RI.[58] Resveratrol inhibited the expression of NLRP3 proteins and their downstream inflammatory factors by activating the SIRT-autophagy pathway, and played a protective role in CI/RI.[59] Ibrutinib reduced cerebral infarction volume, alleviated neurological impairment and CI/RI, and promoted autophagy by activating the PI3K/AKT/mTOR pathway in diabetic mice.[60] The results of our study confirmed that SS increases the LC3II/LC3I ratio and decreases p62 expression in MCAO rats and OGD/R-induced HT22 cells, which suggests an increase in autophagic flux.

To study the molecular mechanism of SS in CI/RI, the AMPK/mTOR signaling pathway was evaluated. The AMPK is a serine/threonine protein kinase which is a key energy sensor to maintain metabolic homeostasis and has been proven to induce the activation of autophagy.[61,62] The mTOR is an important signaling molecule downstream from AMPK that plays a negative regulatory role in autophagy.[63,64] Eugenol enhanced autophagy via regulation of the AMPK/mTOR pathway, and inhibited apoptosis in MCAO rats and OGD/R-induced HT22 cells.[65] Remote limb biochemical postconditioning (RLPoC) played a neuroprotective role by activating the AMPK signaling pathway to induce autophagy.[66] These studies have confirmed that the AMPK/mTOR signaling pathway is also involved in the regulation of inflammation and apoptosis.[67,68] Tissue-type plasminogen activator (tPA) exerted neuroprotective effects by increasing the phosphorylation of AMPK, thereby inhibiting apoptosis and improving mitochondrial function.[69] Dexmedetomidine improved neuroinflammation in rats by activating the AMPK signaling pathway.[70] In our study, the phosphorylation of AMPK was enhanced and the phosphorylation of mTOR was reduced in MCAO rats and OGD/R-induced HT22 cells, which was amplified by SS. Compound C (AMPK inhibitor) and rapamycin (mTOR

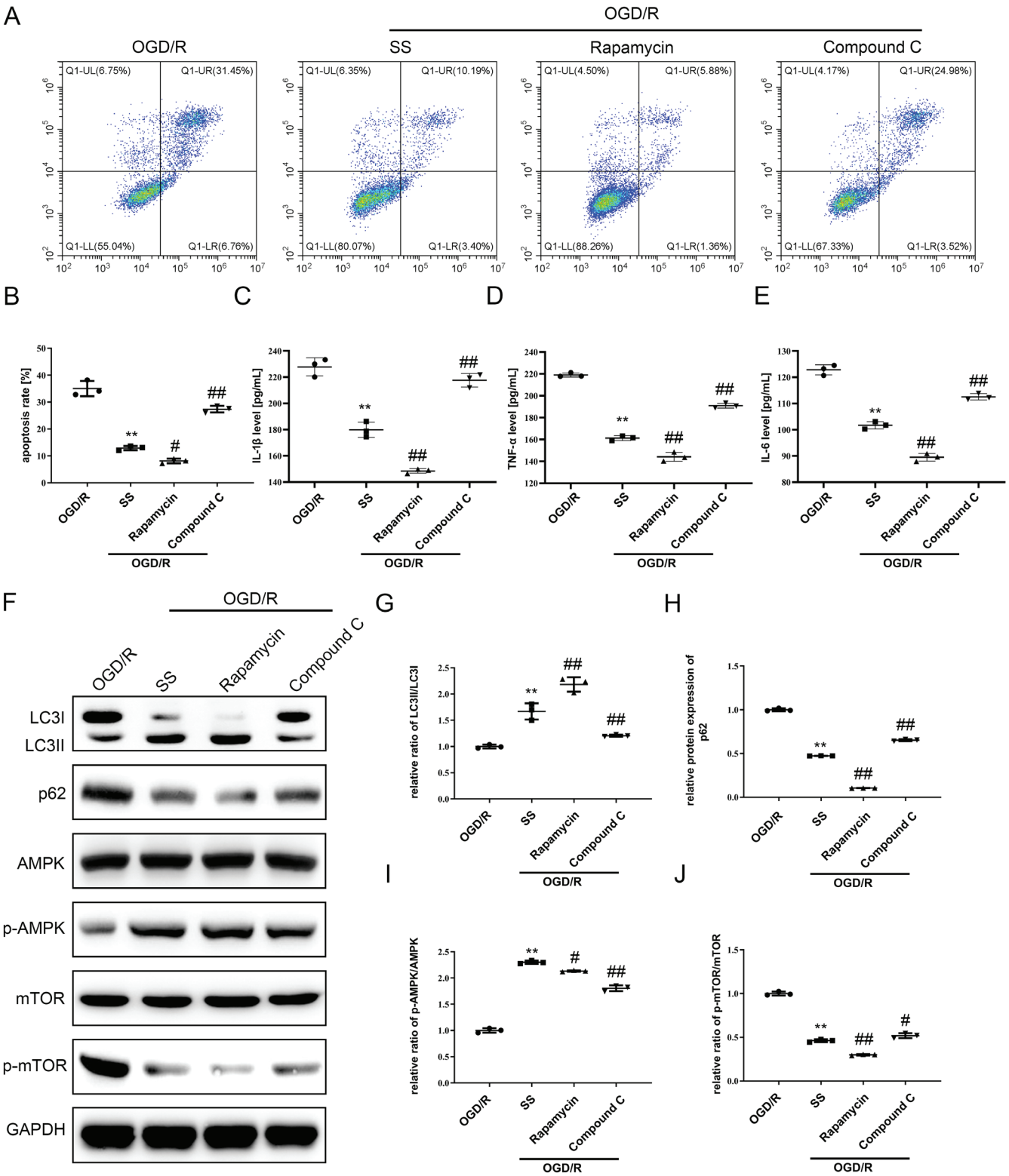

Fig. 5. Schaftoside (SS)-amplified autophagy and reduced apoptosis and inflammation through the regulation of the adenosine monophosphate-activated protein kinase (AMPK)/mammalian target of rapamycin (mTOR) pathway in oxygen glucose deprivation/reperfusion (OGD/R)-induced HT22 cells. A,B. Cell apoptosis was measured using flow cytometry; C–E. Inflammation factors (interleukin (IL)-1β, tumor necrosis factor alpha (TNF-α) and IL-6) were measured using enzyme-linked immunosorbent assay (ELISA); F–J. Related proteins of autophagy (LC3, p62) and the AMPK/mTOR pathway (AMPK, p-AMPK, mTOR, p-mTOR) were assessed with western blot

GAPDH – glyceraldehyde-3-phosphate dehydrogenase; **p < 0.01 compared to the OGD/R group; #p < 0.05 compared to the SS+OGD/R group; ##p < 0.01 compared to the SS+OGD/R group.

inhibitor) were used in our study. Our previous studies have demonstrated that SS reduced apoptosis and inflammation and promoted autophagy to resist CI/RI. Our results further confirmed that rapamycin enhances the protective effects of SS in CI/RI, but compound C reverses the beneficial effects of SS in CI/RI.

Limitations

There are some limitations in our study. Although we evaluated the protective effect of pretreatment with SS in CI/RI, the time window of the protective effects of SS needs to be investigated. In addition, whether SS could reduce CI/RI through the regulation of other signaling pathways requires further research.

Conclusions

Our study demonstrated that SS protected against CI/RI by inhibiting apoptosis and inflammation and promoting the activation of autophagy. The protective role of SS in CI/RI may be a result of the activation of the AMPK/mTOR signaling pathway. Our findings provide better insight into the function of SS in CI/RI, which could contribute to the clinical treatment of stroke.

Supplementary files

The data concerning verification of assumptions for the application of the ANOVA through ANOVA test and post hoc test with p-values are available at https://doi.org/10.5281/zenodo.6838287.

ORCID IDs

Lin Zhang https://orcid.org/0000-0002-0075-027X
Minghua Wu https://orcid.org/0000-0003-2855-2301
Zhaoyao Chen https://orcid.org/0000-0002-8441-5355

References

1. Guzik A, Bushnell C. Stroke epidemiology and risk factor management. *Continuum (Minneap Minn)*. 2017;23(1):15–39. doi:10.1212/CON.0000000000000416
2. Toman NG, Grande AW, Low WC. Neural repair in stroke. *Cell Transplant*. 2019;28(9–10):1123–1126. doi:10.1177/0963689719863784
3. Unnithan AKA, Das J, Mehta P. Hemorrhagic stroke. In: *StatPearls*. Treasure Island, USA: StatPearls Publishing; 2022. http://www.ncbi.nlm.nih.gov/books/NBK559173/. Accessed August 8, 2022.
4. Kim J, Thayabaranathan T, Donnan GA, et al. Global Stroke Statistics 2019. *Int J Stroke*. 2020;15(8):819–838. doi:10.1177/1747493020909545
5. Caprio FZ, Sorond FA. Cerebrovascular disease: Primary and secondary stroke prevention. *Med Clin North Am*. 2019;103(2):295–308. doi:10.1016/j.mcna.2018.10.001
6. Mair G, Wardlaw JM. Imaging of acute stroke prior to treatment: Current practice and evolving techniques. *Br J Radiol*. 2014;87(1040):20140216. doi:10.1259/bjr.20140216
7. Cramer SC. Recovery after stroke. *Continuum (Minneap Minn)*. 2020;26(2):415–434. doi:10.1212/CON.0000000000000838
8. Wardlaw JM, Murray V, Berge E, del Zoppo GJ. Thrombolysis for acute ischaemic stroke. *Cochrane Database Syst Rev*. 2014;2014(7):CD000213. doi:10.1002/14651858.CD000213.pub3
9. Liu R, Li H, Deng J, et al. QKI 6 ameliorates CIRI through promoting synthesis of triglyceride in neuron and inhibiting neuronal apoptosis associated with SIRT1-PPARγ-PGC-1α axis. *Brain Behav*. 2021;11(8):e2271. doi:10.1002/brb3.2271
10. Battaglia S, Garofalo S, di Pellegrino G, Starita F. Revaluing the role of vmPFC in the acquisition of Pavlovian threat conditioning in humans. *J Neurosci*. 2020;40(44):8491–8500. doi:10.1523/JNEUROSCI.0304-20.2020
11. Battaglia S. Neurobiological advances of learned fear in humans. *Adv Clin Exp Med*. 2022;31(3):217–221. doi:10.17219/acem/146756
12. Battaglia S, Fabius JH, Moravkova K, Fracasso A, Borgomaneri S. The neurobiological correlates of gaze perception in healthy individuals and neurologic patients. *Biomedicines*. 2022;10(3):627. doi:10.3390/biomedicines10030627
13. Xu J, Kong X, Xiu H, Dou Y, Wu Z, Sun P. Combination of curcumin and vagus nerve stimulation attenuates cerebral ischemia/reperfusion injury-induced behavioral deficits. *Biomed Pharmacother*. 2018;103:614–620. doi:10.1016/j.biopha.2018.04.069
14. Shi Y, Yi Z, Zhao P, Xu Y, Pan P. MicroRNA-532-5p protects against cerebral ischemia-reperfusion injury by directly targeting CXCL1. *Aging (Albany NY)*. 2021;13(8):11528–11541. doi:10.18632/aging.202846
15. Deng Z, Ou H, Ren F, et al. LncRNA SNHG14 promotes OGD/R-induced neuron injury by inducing excessive mitophagy via miR-182-5p/BINP3 axis in HT22 mouse hippocampal neuronal cells. *Biol Res*. 2020;53(1):38. doi:10.1186/s40659-020-00304-4
16. Wu MY, Yiang GT, Liao WT, et al. Current mechanistic concepts in ischemia and reperfusion injury. *Cell Physiol Biochem*. 2018;46(4):1650–1667. doi:10.1159/000489241
17. Galluzzi L, Green DR. Autophagy-independent functions of the autophagy machinery. *Cell*. 2019;177(7):1682–1699. doi:10.1016/j.cell.2019.05.026
18. Mo Y, Sun YY, Liu KY. Autophagy and inflammation in ischemic stroke. *Neural Regen Res*. 2020;15(8):1388–1396. doi:10.4103/1673-5374.274331
19. Ahsan A, Liu M, Zheng Y, et al. Natural compounds modulate the autophagy with potential implication of stroke. *Acta Pharm Sin B*. 2021;11(7):1708–1720. doi:10.1016/j.apsb.2020.10.018
20. Liu L, Cao Q, Gao W, et al. Melatonin ameliorates cerebral ischemia-reperfusion injury in diabetic mice by enhancing autophagy via the SIRT1-BMAL1 pathway. *FASEB J*. 2021;35(12):e22040. doi:10.1096/fj.202002718RR
21. Maiuri MC, Zalckvar E, Kimchi A, Kroemer G. Self-eating and self-killing: Crosstalk between autophagy and apoptosis. *Nat Rev Mol Cell Biol*. 2007;8(9):741–752. doi:10.1038/nrm2239
22. Zhang Y, Zhang Y, Jin XF, et al. The role of Astragaloside IV against cerebral ischemia/reperfusion injury: Suppression of apoptosis via promotion of P62-LC3-autophagy. *Molecules*. 2019;24(9):1838. doi:10.3390/molecules24091838
23. Tanaka M, Toldi J, Vécsei L. Exploring the etiological links behind neurodegenerative diseases: Inflammatory cytokines and bioactive kynurenines. *Int J Mol Sci*. 2020;21(7):2431. doi:10.3390/ijms21072431
24. Lambertsen KL, Finsen B, Clausen BH. Post-stroke inflammation: Target or tool for therapy? *Acta Neuropathol*. 2019;137(5):693–714. doi:10.1007/s00401-018-1930-z
25. Chamorro Á, Dirnagl U, Urra X, Planas AM. Neuroprotection in acute stroke: Targeting excitotoxicity, oxidative and nitrosative stress, and inflammation. *Lancet Neurol*. 2016;15(8):869–881. doi:10.1016/S1474-4422(16)00114-9
26. Ma Y, Zhou K, Fan J, Sun S. Traditional Chinese medicine: Potential approaches from modern dynamical complexity theories. *Front Med*. 2016;10(1):28–32. doi:10.1007/s11684-016-0434-2
27. Yang Y, Zhang M, Zhao J, Song S, Hong F, Zhang G. Effect of traditional Chinese medicine emotional therapy on post-stroke depression: A protocol for systematic review and meta-analysis. *Medicine (Baltimore)*. 2021;100(14):e25386. doi:10.1097/MD.0000000000025386
28. Gong X, Sucher NJ. Stroke therapy in traditional Chinese medicine (TCM): Prospects for drug discovery and development. *Phytomedicine*. 2002;9(5):478–484. doi:10.1078/09447110260571760
29. Liu M, Zhang G, Wu S, et al. Schaftoside alleviates HFD-induced hepatic lipid accumulation in mice via upregulating farnesoid X receptor. *J Ethnopharmacol*. 2020;255:112776. doi:10.1016/j.jep.2020.112776
30. Kim PS, Shin JH, Jo DS, et al. Anti-melanogenic activity of schaftoside in *Rhizoma Arisaematis* by increasing autophagy in B16F1 cells. *Biochem Biophys Res Commun*. 2018;503(1):309–315. doi:10.1016/j.bbrc.2018.06.021

31. Kou X, Chen N. Resveratrol as a natural autophagy regulator for prevention and treatment of Alzheimer's disease. *Nutrients*. 2017;9(9):927. doi:10.3390/nu9090927
32. Yang X, Jiang T, Wang Y, Guo L. The role and mechanism of SIRT1 in resveratrol-regulated osteoblast autophagy in osteoporosis rats. *Sci Rep*. 2019;9(1):18424. doi:10.1038/s41598-019-44766-3
33. Liu R, Meng C, Zhang Z, et al. Comparative metabolism of schaftoside in healthy and calcium oxalate kidney stone rats by UHPLC-Q-TOF-MS/MS method. *Anal Biochem*. 2020;597:113673. doi:10.1016/j.ab.2020.113673
34. Bieber M, Schuhmann MK, Volz J, et al. Description of a novel phosphodiesterase (PDE)-3 inhibitor protecting mice from ischemic stroke independent from platelet function. *Stroke*. 2019;50(2):478–486. doi:10.1161/STROKEAHA.118.023664
35. Zhou K, Wu J, Chen J, et al. Schaftoside ameliorates oxygen glucose deprivation-induced inflammation associated with the TLR4/Myd88/Drp1-related mitochondrial fission in BV2 microglia cells. *J Pharmacol Sci*. 2019;139(1):15–22. doi:10.1016/j.jphs.2018.10.012
36. Wang G, Wang T, Zhang Y, Li F, Yu B, Kou J. Schizandrin protects against OGD/R-induced neuronal injury by suppressing autophagy: Involvement of the AMPK/mTOR pathway. *Molecules*. 2019;24(19):3624. doi:10.3390/molecules24193624
37. Borgomaneri S, Battaglia S, Garofalo S, Tortora F, Avenanti A, di Pellegrino G. State-dependent TMS over prefrontal cortex disrupts fear-memory reconsolidation and prevents the return of fear. *Curr Biol*. 2020;30(18):3672–3679.e4. doi:10.1016/j.cub.2020.06.091
38. Hara T, Shanmugalingam A, McIntyre A, Burhan AM. The effect of non-invasive brain stimulation (NIBS) on attention and memory function in stroke rehabilitation patients: A systematic review and meta-analysis. *Diagnostics (Basel)*. 2021;11(2):227. doi:10.3390/diagnostics11020227
39. Borgomaneri S, Battaglia S, Sciamanna G, Tortora F, Laricchiuta D. Memories are not written in stone: Re-writing fear memories by means of non-invasive brain stimulation and optogenetic manipulations. *Neurosci Biobehav Rev*. 2021;127:334–352. doi:10.1016/j.neubiorev.2021.04.036
40. Tang H, Gamdzyk M, Huang L, et al. Delayed recanalization after MCAO ameliorates ischemic stroke by inhibiting apoptosis via HGF/c-Met/STAT3/Bcl-2 pathway in rats. *Exp Neurol*. 2020;330:113359. doi:10.1016/j.expneurol.2020.113359
41. Barthels D, Das H. Current advances in ischemic stroke research and therapies. *Biochim Biophys Acta Mol Basis Dis*. 2020;1866(4):165260. doi:10.1016/j.bbadis.2018.09.012
42. Wang Y, Li Y, Ma C, et al. LncRNA XIST promoted OGD-induced neuronal injury through modulating/miR-455-3p/TIPARP axis. *Neurochem Res*. 2021;46(6):1447–1456. doi:10.1007/s11064-021-03286-1
43. Ryou MG, Mallet RT. An in vitro oxygen–glucose deprivation model for studying ischemia-reperfusion injury of neuronal cells. In: Tharakan B, ed. *Traumatic and Ischemic Injury*. Methods in Molecular Biology. New York, USA: Springer New York; 2018:229–235. doi:10.1007/978-1-4939-7526-6_18
44. Xu X, Lai Y, Hua ZC. Apoptosis and apoptotic body: Disease message and therapeutic target potentials. *Biosci Rep*. 2019;39(1):BSR20180992. doi:10.1042/BSR20180992
45. Gong L, Tang Y, An R, Lin M, Chen L, Du J. RTN1-C mediates cerebral ischemia/reperfusion injury via ER stress and mitochondria-associated apoptosis pathways. *Cell Death Dis*. 2017;8(10):e3080. doi:10.1038/cddis.2017.465
46. Shi C, Jin J, Wang X, et al. Sevoflurane attenuates brain damage through inhibiting autophagy and apoptosis in cerebral ischemia-reperfusion rats. *Mol Med Rep*. 2019;21(1):123–130. doi:10.3892/mmr.2019.10832
47. Franke M, Bieber M, Kraft P, Weber ANR, Stoll G, Schuhmann MK. The NLRP3 inflammasome drives inflammation in ischemia/reperfusion injury after transient middle cerebral artery occlusion in mice. *Brain Behav Immun*. 2021;92:223–233. doi:10.1016/j.bbi.2020.12.009
48. Liu H, Wu X, Luo J, et al. Pterostilbene attenuates astrocytic inflammation and neuronal oxidative injury after ischemia-reperfusion by inhibiting NF-κB phosphorylation. *Front Immunol*. 2019;10:2408. doi:10.3389/fimmu.2019.02408
49. Wu R, Li X, Xu P, et al. TREM2 protects against cerebral ischemia/reperfusion injury. *Mol Brain*. 2017;10(1):20. doi:10.1186/s13041-017-0296-9
50. Huang S, Tai S, Chang C, Tu Y, Chang C, Lee E. Magnolol protects against ischemic-reperfusion brain damage following oxygen-glucose deprivation and transient focal cerebral ischemia. *Int J Mol Med*. 2018;41(4):2252–2262. doi:10.3892/ijmm.2018.3387
51. Wang M, Chen Z, Yang L, Ding L. Sappanone A protects against inflammation, oxidative stress and apoptosis in cerebral ischemia-reperfusion injury by alleviating endoplasmic reticulum stress. *Inflammation*. 2021;44(3):934–945. doi:10.1007/s10753-020-01388-6
52. Liang Q, Yang J, He J, et al. Stigmasterol alleviates cerebral ischemia/reperfusion injury by attenuating inflammation and improving antioxidant defenses in rats. *Biosci Rep*. 2020;40(4):BSR20192133. doi:10.1042/BSR20192133
53. Glick D, Barth S, Macleod KF. Autophagy: Cellular and molecular mechanisms. *J Pathol*. 2010;221(1):3–12. doi:10.1002/path.2697
54. Martínez-Borra J, López-Larrea C. Autophagy and self-defense. In: López-Larrea C, ed. *Self and Nonself*. New York, USA: Springer US; 2012:169–184. doi:10.1007/978-1-4614-1680-7_11
55. Tanida I, Ueno T, Kominami E. LC3 and autophagy. In: Deretic V, ed. *Autophagosome and Phagosome*. Totowa, USA: Humana Press; 2008:77–88. doi:10.1007/978-1-59745-157-4_4
56. Runwal G, Stamatakou E, Siddiqi FH, Puri C, Zhu Y, Rubinsztein DC. LC3-positive structures are prominent in autophagy-deficient cells. *Sci Rep*. 2019;9(1):10147. doi:10.1038/s41598-019-46657-z
57. Lamark T, Svenning S, Johansen T. Regulation of selective autophagy: The p62/SQSTM1 paradigm. *Essays Biochem*. 2017;61(6):609–624. doi:10.1042/EBC20170035
58. Huang YG, Tao W, Yang SB, Wang JF, Mei ZG, Feng ZT. Autophagy: Novel insights into therapeutic target of electroacupuncture against cerebral ischemia/reperfusion injury. *Neural Regen Res*. 2019;14(6):954–961. doi:10.4103/1673-5374.250569
59. He Q, Li Z, Wang Y, Hou Y, Li L, Zhao J. Resveratrol alleviates cerebral ischemia/reperfusion injury in rats by inhibiting NLRP3 inflammasome activation through Sirt1-dependent autophagy induction. *Int Immunopharmacol*. 2017;50:208–215. doi:10.1016/j.intimp.2017.06.029
60. Jin L, Mo Y, Yue EL, Liu Y, Liu KY. Ibrutinib ameliorates cerebral ischemia/reperfusion injury through autophagy activation and PI3K/Akt/mTOR signaling pathway in diabetic mice. *Bioengineered*. 2021;12(1):7432–7445. doi:10.1080/21655979.2021.1974810
61. Carling D. AMPK signalling in health and disease. *Curr Opin Cell Biol*. 2017;45:31–37. doi:10.1016/j.ceb.2017.01.005
62. Li Y, Chen Y. AMPK and autophagy. In: Qin ZH, ed. *Autophagy: Biology and Diseases*. Advances in Experimental Medicine and Biology. Singapore: Springer Singapore; 2019:85–108. doi:10.1007/978-981-15-0602-4_4
63. Inoki K, Kim J, Guan KL. AMPK and mTOR in cellular energy homeostasis and drug targets. *Annu Rev Pharmacol Toxicol*. 2012;52(1):381–400. doi:10.1146/annurev-pharmtox-010611-134537
64. Alers S, Löffler AS, Wesselborg S, Stork B. Role of AMPK-mTOR-Ulk1/2 in the regulation of autophagy: Cross talk, shortcuts, and feedbacks. *Mol Cell Biol*. 2012;32(1):2–11. doi:10.1128/MCB.06159-11
65. Sun X, Wang D, Zhang T, et al. Eugenol attenuates cerebral ischemia-reperfusion injury by enhancing autophagy via AMPK-mTOR-P70S6K pathway. *Front Pharmacol*. 2020;11:84. doi:10.3389/fphar.2020.00084
66. He JT, Li H, Yang L, Cheng KL. Involvement of endothelin-1, H2S and Nrf2 in beneficial effects of remote ischemic preconditioning in global cerebral ischemia-induced vascular dementia in mice. *Cell Mol Neurobiol*. 2019;39(5):671–686. doi:10.1007/s10571-019-00670-y
67. Liu X, Xu Y, Cheng S, et al. Geniposide combined with notoginsenoside R1 attenuates inflammation and apoptosis in atherosclerosis via the AMPK/mTOR/Nrf2 signaling pathway. *Front Pharmacol*. 2021;12:687394. doi:10.3389/fphar.2021.687394
68. Sun Z, Gu L, Wu K, et al. VX-765 enhances autophagy of human umbilical cord mesenchymal stem cells against stroke-induced apoptosis and inflammatory responses via AMPK/mTOR signaling pathway. *CNS Neurosci Ther*. 2020;26(9):952–961. doi:10.1111/cns.13400
69. Cai Y, Yang E, Yao X, et al. FUNDC1-dependent mitophagy induced by tPA protects neurons against cerebral ischemia-reperfusion injury. *Redox Biol*. 2021;38:101792. doi:10.1016/j.redox.2020.101792
70. Wang Z, Zhou W, Dong H, Ma X, He Z. Dexmedetomidine pretreatment inhibits cerebral ischemia/reperfusion-induced neuroinflammation via activation of AMPK. *Mol Med Report*. 2018;18(4):3957–3964. doi:10.3892/mmr.2018.9349

Protective effects of rectal ozone administration on colon anastomoses following radiotherapy

Tonguç Utku Yilmaz[1,A,D], Eda Yirmibeşoğlu Erkal[2,C], Saffet Çinar[3,D,E], Ceyla Eraldemir[4,B], Çiğdem Vural[5,E], Ezgi Uçar Taş[3,B], Nihat Zafer Utkan[3,F]

[1] Organ Transplantation Unit, Atakent Hospital, Acıbadem Mehmet Ali Aydınlar University, Turkey
[2] Department of Radiation Oncology, Faculty of Medicine, University of Kocaeli, Turkey
[3] Department of General Surgery, Faculty of Medicine, University of Kocaeli, Turkey
[4] Department of Biochemistry, Faculty of Medicine, University of Kocaeli, Turkey
[5] Department of Pathology, Faculty of Medicine, University of Kocaeli, Turkey

A – research concept and design; B – collection and/or assembly of data; C – data analysis and interpretation; D – writing the article; E – critical revision of the article; F – final approval of the article

Advances in Clinical and Experimental Medicine, ISSN 1899–5276 (print), ISSN 2451–2680 (online) *Adv Clin Exp Med*. 2022;31(12):1355–1364

Address for correspondence
Tonguç Utku Yilmaz
E-mail: drutkuyilmaz@yahoo.com

Funding sources
None declared

Conflict of interest
None declared

Received on December 27, 2021
Reviewed on March 15, 2022
Accepted on July 14, 2022

Published online on August 24, 2022

Abstract

Background. Anastomotic leakage (AL) following rectal surgery is associated with increased mortality and morbidity. Neoadjuvant radiotherapy disrupts the wound healing process in rectal surgery.

Objectives. To evaluate the effects of intra-rectal ozone application on rectal anastomoses after radiotherapy.

Materials and methods. This study was performed on animals. Thirty-two male Wistar rats were randomly divided into 4 groups: control group, ozone group, radiotherapy group, and radiotherapy/ozone group. Ozone was administered intrarectally in the ozone group and water was administered intrarectally in rthe control group for 5 days. The radiotherapy group received 20 Gy of pelvic radiotherapy. The radiotherapy/ozone group received 20 Gy of pelvic radiotherapy after the administration of ozone. Afterward, colon resection followed by an anastomosis were performed under general anesthesia in all groups. Anastomotic segments were resected to evaluate tissue hydroxyproline (HYP) and myeloperoxidase (MPO) levels, perform a histological evaluation, and measure bursting pressure.

Results. There were no statistically significant differences between groups regarding tissue MPO levels ($p = 0.55$). Tissue HYP levels were significantly decreased in the radiotherapy group ($p = 0.04$). Bursting pressure was found to be significantly lower in the radiotherapy group ($p < 0.05$). No significant differences were found between adhesion scores in the control and ozone groups. Exudate formation was significantly lower in the radiotherapy group ($p < 0.05$). The lowest macrophage scores were found in the radiotherapy group ($p < 0.05$). Fibroblast scores were the highest in the control group and the lowest in the radiotherapy group ($p < 0.05$).

Conclusions. Intra-rectal ozone application significantly improved the anastomotic healing process after radiation exposure.

Key words: colon anastomosis, ozone, radiotherapy, anastomotic leakage, rectal administration

Cite as
Yilmaz TU, Erkal EY, Çinar S, et al. Protective effects of rectal ozone administration on colon anastomoses following radiotherapy. *Adv Clin Exp Med*. 2022;31(12):1355–1364. doi:10.17219/acem/152121

DOI
10.17219/acem/152121

Background

Anastomoses are vital steps in colorectal cancer surgery since anastomotic failures can lead to drawbacks such as increased morbidity, increased mortality and potentially worse oncological outcomes.[1] Anastomotic leakage (AL) after colorectal surgery has been reported to occur at a rate of 3–12% in prospective studies.[2,3] Preoperative radiotherapy is a risk factor for AL.[4] Poor blood supply and decreased oxygen delivery lead to hypoxia and have been blamed for the increased risk of AL.[5] After radiotherapy, ischemia leads to oxidative stress and increased production of free oxygen radicals that are the main destructive factor.[6] The overexpression of factors such as tissue growth factor β, vascular endothelial growth factor, tumor necrosis factor, and pro-inflammatory cytokines after radiation lead to uncontrolled matrix accumulation.[7] The uncontrolled matrix accumulation results in fibrosis, AL or a stricture.[7] In order to decrease the deleterious effects of radiotherapy, several agents such as glutamine, steroid, sucralfate, and N-acetylcysteine have been used.[8,9] The aim of using these agents is to improve wound healing by decreasing inflammation and hypoxia. Successful anastomotic healing includes not only histological healing but also the ability of the previously injured bowel to withstand tensile forces. If sufficient tissue strength cannot be restored, the anastomosis may burst upon a challenge with intraluminal pressure.

Ozone, chemically known as O_3, is made up of 3 oxygen atoms and has several functions such as being antimicrobial, antioxidative, regulating the immune response, and causing epigenetic modifications.[10] Oxidative preconditioning by ozone shows its protective effects against free radicals.[11] Ozone promotes macrophage activity and accelerates epithelialization in the colon.[11] The increased epithelialization after ozone administration has been shown to be beneficial in trophic ulcers, burns, gingivitis, and furunculosis.[6] The main mechanisms of ozone in wound healing are attributed to its local antioxidant properties and ability to promote tissue repair. The ozone has been administered via different routes such as intravenous, intra-arterial, subcutaneous, intramuscular, intra-articular, and via an enema.[12] An ozone enema induces a significant increase in mucosal prostaglandin E_2 production during the early period and increases nitric oxide synthase activity during the later period. However, the amount and concentration of ozone in the enema are very important.

Objectives

This study aimed to show the protective effects of rectal ozone administration on colon anastomoses following radiotherapy. This study is the first experimental study evaluating rectal O_3 administration. The relationship between ozone therapy and radiotherapy is a new area for future clinical and experimental studies.

Materials and methods

The experiment was approved by the Animal Ethics Committee at The University of Kocaeli, Turkey (approval No. 10/2-2015). The National Institutes of Health (NIH) Guidelines for the Care and Use of Laboratory Animals were followed in handling of all animals.

Ozone

An ozone generator (Bozon N; Econica, Odessa, Ukraine) was used for producing ozone at a dose of 20 μg/mL. The injected mixture had a total volume of 2.5 mL. Five ozone applications performed once daily were used to achieve oxidative preconditioning. The flow rate of O_3 was maintained at 2 L/min. The gas mixture was composed of 96% O_2 and 4% O_3. Intra-rectal ozone applications were performed using 16 gauge silicone catheters that were inserted in the anus under sedation (using ether). The catheters were kept closed for 5 min after injection and then removed.

Animals and experiment

Thirty-two male Wistar rats weighing 300–450 g were housed individually in cages and given free access to regular rat meal and water both before and after the experiment. The animal rooms had no windows and were controlled for temperature (23 ±2°C) and light (12 h day and 12 h night). The rats were divided into 4 groups: control group, ozone group, radiotherapy group, and radiotherapy/ozone group. They were anesthetized with 100 mg/kg ketamine (Ketalar; Parke Davis Co. Inc., New Jersey, USA) and 5 mg/kg xylazine (Rompun; Bayer AG, Leverkusen, Germany) administrated intraperitoneally. The laparotomy procedure was performed through a standard 4-cm midline incision. A 1-cm resection of the left colon was performed from 2 to 3 cm above the peritoneal reflection. The continuity of the bowel was restored with an end-to-end anastomosis using 8–10 interrupted 6-0 monofilament Prolene sutures (Ethicon Ltd., Edinburgh, UK). Running sutures were used for abdominal and skin closure of the rats. The rats were euthanized with intracardiac blood collection.

In the control group, the intra-rectal water administration was performed for 5 days under ether sedation. Afterward, colon resection and anastomosis were performed. Five days after the colon resection and anastomosis, the rats were anesthetized for in vivo analytic procedures.

In the ozone group, the intra-rectal ozone administration was performed for 5 days under ether sedation. Five days after the last administration of ozone, the animals were anesthetized for colon resection and anastomosis. Five days after colon resection and anastomosis, the rats were anesthetized for in vivo analytic procedures. For in vitro analytic procedures, the animals were euthanized.

In the radiotherapy group, the animals underwent ether sedations for 5 days. Five days after the last sedation, the rats underwent radiotherapy. While under anesthesia, each rat was placed in prone position on a styrofoam board. For radiotherapy planning, a volumetric computed tomography (CT) scan was obtained using a CT scanner (SOMATOM Definition AS; Siemens, Munich, Germany). The rectum was contoured in its entirety to define the critical target volume (CTV) with uniform margins of 3 mm added in each direction in order to define the planning target volume (PTV). An isocentric technique was used to deliver a dose of 20 Gy using opposed anterior and posterior portals on a linear accelerator (Oncor; Siemens) with 6 Mv photons. Five days after radiotherapy, the animals were anesthetized for colon resection and anastomosis. Five days after colon resection and anastomosis, the rats were anesthetized for in vivo analytic procedures. For in vitro analytic methods, the animals were euthanized.

In the radiotherapy/ozone group, the intra-rectal ozone administration was performed for 5 days under ether sedation. Five days after the last administration of ozone, the animals underwent radiotherapy treatments as described above. Five days after radiotherapy, the animals were anesthetized for colon resection and anastomosis. Five days after colon resection and anastomosis, the rats were anesthetized for in vivo analytic procedures. For in vitro analytic methods, the animals were euthanized.

Analytic procedures

The existence of infection, dehiscence and intra-abdominal adhesions were regarded as complications. For grading intra-abdominal adhesions, the method described by Knightly et al. was used.[13] A grade of 0 indicated no adhesion; grade 1 – a single, thin, easily separable adhesion; grade 2 – less extensive but weak adhesions that withstood traction poorly; and grade 3 – numerous extensive visceral adhesions that involved the adjacent abdominal wall. Polypropylene sutures were used to identify the anastomotic line. Without removing adhesions, the burst pressure (BP) was measured in situ. The BP of each anastomosis was measured with a fluid pump (B. Braun, Frankfurt, Germany) working at 5 mL/min and a pressure transducer (Abbot Monitoring Kit Transpac II; Abbott Ireland Ltd., Sligo, Ireland) to determine the strength of the anastomosis. Colonic segments of at least 2 cm were prepared separately from the anastomosis. The infusion pump was inserted in the proximal part of the bowel segment using a 6-Fr catheter and the distal part was occluded using a 2-0 silk suture to avoid any air or fluid leak. Fluid was transferred from the catheter at a speed of 30 mL/h. The pressure was observed and leakage was viewed using a magnifying lens and identified by a sudden loss of pressure. After measuring the BP, the rats were euthanized. The anastomosis segment of the colon was resected. Half of the segment was fixed in 10% formaldehyde and embedded in paraffin. The other half was frozen for a subsequent determination of collagen content by hydroxyproline (HYP) measurements. Hydroxyproline measurements were performed using an enzyme-linked immunosorbent assay (ELISA) kit (Elabscience Biotechnology, Houston, USA) and the results were provided in ng/mg.[14] Myeloperoxidase (MPO) activity was measured by means of an ELISA kit (Hycult Biotech, Uden, the Netherlands) and the results were provided in ng/100 mg.[15]

After staining with hematoxylin and eosin (H&E), the anastomosis was evaluated histologically in a blinded fashion using the histological scoring described by de Roy van Zuidewijn et al.[16] The apposition of the wound edges of the mucosa and the muscularis mucosa were graded as 1 – good, 2 – moderate and 3 – poor to control for the surgical technique. The epithelialization of the wound healing procedure and the re-epithelialization of the mucosa were examined using a 7-point scale ranging from 1 – none to 7 – normal glandular mucosa. The regeneration of the muscularis propria was considered positive or negative (point scale, 1 = +, 2 = –). Other histological aspects such as necrosis, inflammatory exudate, granulation tissue, and the degree of granulocytes, macrophages and fibroblasts in the granulation tissue were evaluated. The histological parameters mentioned above were evaluated on a 4-point scale, as follows: 0 – negative, 1 – low, 2 – moderate, and 3 – high. Adhesion scoring was graded as 0 – weak adhesion, 1 – easily separable adhesion, 2 – moderate adhesion, and 3 – strong adhesion.

Statistical analyses

The statistical analysis was performed using IBM SPSS v. 22.0 software (IBM Corp., Armonk, USA). The Shapiro–Wilk test was used to determine whether the data fit a normal distribution. The Levene's statistic was used to assess the homogeneity of variance. A value of $p > 0.05$ was considered homogeneous (Table 1). One-way analysis of variance (ANOVA) was used to compare data with normal distribution. The Tukey's post hoc test was used for pairwise comparisons of the groups. Continuous variables showing non-normal distribution were compared using the Kruskal–Wallis test. A value of $p < 0.05$ was considered statistically significant for each test. For group comparisons, the Mann–Whitney U test with a Bonferroni correction was used. After the correction, a value of $p < 0.0083$ was considered statistically significant.

Results

All of the rats survived the surgery. As seen in Table 2, Fig. 1 and Fig. 2, the tissue MPO and HYP levels in the radiotherapy group were lower than in the other groups. Myeloperoxidase and HYP values were compared between the 4 groups using a one-way ANOVA test. There was

Table 1. Variance homogeneity of MPO, HYP and burst pressure

Variables	Levene's statistic	df1	df2	p-value
MPO levels	1.830	3	31	0.167*
HYP levels	2.025	3	31	0.135*
Burst pressure	2.187	3	31	0.112*

* p > 0.05 was considered sufficient for assumption of homogeneity of variance. MPO – myeloperoxidase; HYP – hydroxyproline; df – degrees of freedom.

Table 2. One-way analysis of variance (ANOVA) and post hoc Tukey's test of MPO and HYP values by groups

Dependent variable	Group (I)	F	df	Group (J)	Average difference (I–J)	p-value
MPO	control	4.686	31	ozone	68.65	0.621
				radiotherapy	110.24	0.064
				radiotherapy/ozone	–33.23	0.428
	ozone			control	–68.65	0.624
				radiotherapy	41.59	0.107
				radiotherapy/ozone	–101.88	0.996
	radiotherapy			control	–110.24	0.064
				ozone	–41.59	0.103
				radiotherapy/ozone	–143.47	0.153
	radiotherapy/ozone			control	33.23	0.424
				ozone	101.88	0.997
				radiotherapy	143.47	0.158
HYP	control	2.320	31	ozone	20.67	0.472
				radiotherapy	**498.46**	**0.000**
				radiotherapy/ozone	–88.67	0.771
	ozone			control	–20.67	0.479
				radiotherapy	**477.79**	**0.000**
				radiotherapy/ozone	–109.34	0.094
	radiotherapy			control	**–498.46**	**0.000**
				ozone	**–477.79**	**0.000**
				radiotherapy/ozone	**–587.13**	**0.000**
	radiotherapy/ozone			control	88.67	0.776
				ozone	109.34	0.098
				radiotherapy	**587.13**	**0.000**

MPO – myeloperoxidase; HYP – hydroxyproline; I – group designated for comparison; J – other groups compared; df – degrees of freedom. Values in bold show statistically significant differences between the groups. The value of p < 0.05 was considered sufficient for statistical significance.

no significant difference between MPO values between the groups (F (4.686), df = 31, p = 0.554). However, there was a statistically significant difference between HYP values (F (2.320), df = 31, p = 0.042). The Tukey's post hoc test revealed that there was a significant difference between the radiotherapy and other groups in comparison to the binary groups (Table 2). The mean MPO levels ± standard deviation (SD) (ng/mg) in the control, ozone, radiotherapy, and radiotherapy/ozone groups were 551.52 ±104.55, 482.87 ±141.07, 441.28 ±79.24, and 584.75 ±374.77, respectively. The mean HYP levels ±SD (ng/mg) in the control, ozone, radiotherapy, and radiotherapy/ozone groups were 1336.06 ±169.56, 1315.39 ±502.19, 837.60 ±258.20, and 1424.73 ±438.43, respectively.

Burst pressure values were compared between the 4 groups using a one-way ANOVA test. There was a statistically significant difference between BP values in the 4 groups (F (50.442), df = 31, p = 0.000) (Table 3, Fig. 3). The Tukey's post hoc test showed that there was a significant difference between the radiotherapy group and other groups (Table 3). The mean burst pressures ±SD (mm Hg) in the control, ozone, radiotherapy, and radiotherapy/ozone groups were 143.7 ±22.43, 162.5 ±36.47, 79.7 ±13.79, and 123.3 ±31.31, respectively.

The adhesion scores were found to be statistically significant and lower in the control and ozone groups compared to the other 2 groups (p < 0.05) (Table 4, Table 5).

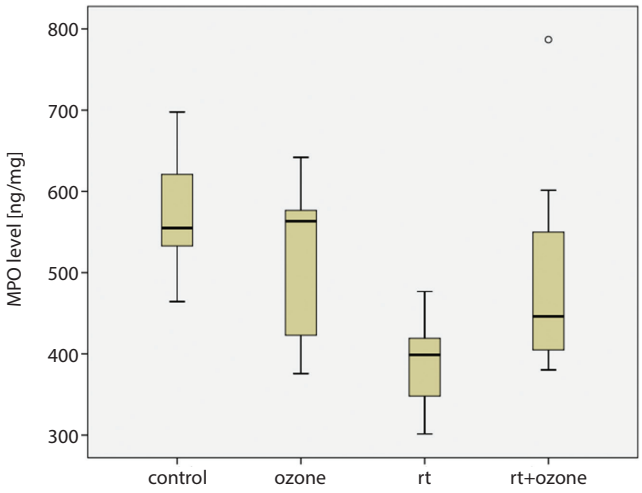

Fig. 1. Tissue myeloperoxidase (MPO) levels

rt – radiotherapy. An outlier was detected in 1 rat in the radiotherapy/ozone group.

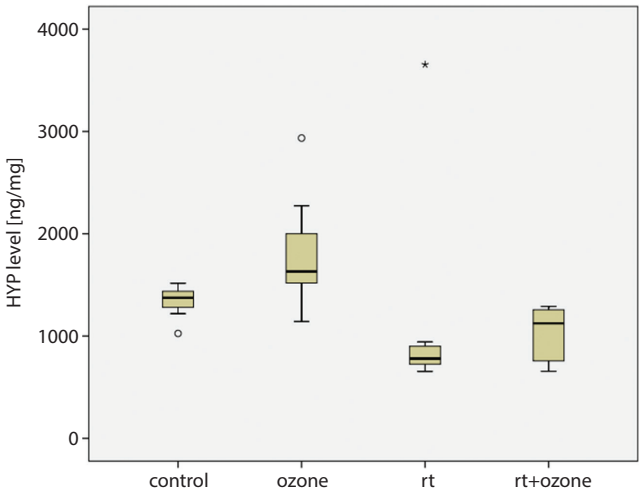

Fig. 2. Tissue hydroxyproline (HYP) levels

rt – radiotherapy. Outliers were detected in 1 rat in each of the control, ozone and radiotherapy groups.

Table 3. One-way analysis of variance (ANOVA) and post hoc Tukey's test of burst pressure values by groups

Dependent variable	Group (I)	F	df	Group (J)	Average difference (I–J)	p-value
Burst pressure	control	50.442	31	ozone	**–18.76**	**0.059**
				radiotherapy	**63.95**	**0.000**
				radiotherapy/ozone	**20.40**	**0.035**
	ozone			control	18.76	0.059
				radiotherapy	**82.71**	**0.004**
				radiotherapy/ozone	**39.16**	**0.007**
	radiotherapy			control	**–63.95**	**0.000**
				ozone	**–82.71**	**0.003**
				radiotherapy/ozone	**–43.55**	**0.001**
	radiotherapy/ozone			control	**–20.40**	**0.035**
				ozone	**–39.16**	**0.000**
				radiotherapy	**43.55**	**0.002**

I – group designated for comparison; J – other groups compared; df – degrees of freedom. Values in bold show statistically significant differences between the groups. The value of $p < 0.05$ was considered sufficient for statistical significance.

Upon histological evaluation of the groups, no tissue necrosis was observed. The scores of inflammatory exudate, macrophages, granulocytes, and fibroblasts in the radiotherapy group were significantly lower than those in the control group (Table 6, Table 7; $p < 0.05$). There were no significant differences among the groups regarding their tissue mucosa and muscularis propria apposition levels (Table 8, Table 9). The wound healing scores, except for the macrophage score of the radiotherapy/ozone and ozone groups were higher than those of the radiotherapy group but not statistically significant (Table 6). The macrophage scores of the radiotherapy/ozone group were significantly higher than those in the radiotherapy group (Table 5; $p < 0.05$). No statistically significant differences were found between the regeneration scores and re-epithelialization of the groups (Table 8, Table 10 and Table 11).

Discussion

Anastomosis is a complex process and one of the pivotal steps in the success of colorectal surgery.[1] Anastomotic wound healing is dynamic and involves multiple variables. Radiotherapy is a widely used treatment modality in the treatment of rectal cancer. Despite its widespread use, radiotherapy has many side effects.[4] Radiation has shown a negative effect on anastomotic healing in experimental and clinical studies.[3,4,17] Reducing the side effects of radiotherapy is one of the areas of interest in modern medicine. Therefore, the effects of ozone therapy in rats receiving radiotherapy are being investigated. Ozone therapy is a trending modality due to its hemostatic effects as well as its accelerating effects on tissue healing.[11,12] A controlled administration of O_3 can reduce the damage

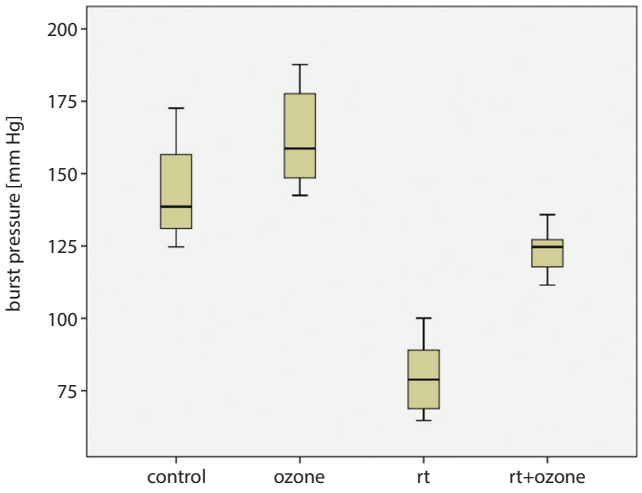

Fig. 3. Tissue burst pressure levels

rt – radiotherapy.

Table 4. Tissue adhesion scores*

Group	Median and SD	Adhesion
Control (n = 8)	median (Q1–Q3)	1 (0.25–0.75)
	SD	0.35
Ozone (n = 8)	median (Q1–Q3)	2.5 (2–3)
	SD	0.54
Radiotherapy (n = 8)	median (Q1–Q3)	3 (3–3)
	SD	0.62
Radiotherapy/ozone (n = 8)	median (Q1–Q3)	3 (3–3)
	SD	0.74
χ^2	overall	24.861
df (total)	overall	31
p-value	overall	0.013

Q1 – 1st quartile; Q3 – 3rd quartile; SD – standard deviation; df – degrees of freedom. * Kruskal–Wallis test was used and Mann– Whitney U test with Bonferroni correction was performed as post hoc test. A value of $p < 0.0083$ was considered sufficient for statistical significance.

Table 5. Adhesion score frequencies of the groups

Variable	Score	Control	Ozone	Radiotherapy	Radiotherapy/ozone
Adhesion	0	2 (25%)	0	0	0
	1	4 (50%)	0	0	0
	2	2 (25%)	4 (50%)	0	0
	3	0	4 (50%)	8 (100%)	8 (100%)

score 0 – weak adhesion; score 1 – easily separable adhesion; score 2 – moderate adhesion; score 3 – strong adhesion.

produced by reactive oxygen species (ROS) by maintaining the adaptation to O_3 oxidative preconditioning or stress. Here, the effects of ozone therapy on colonic anastomosis after radiotherapy were evaluated. For this reason, our study is an O_3 oxidative preconditioning study.

Anastomotic BP is one of the parameters that can show the safety and durability of an anastomosis. It can also provide information about the anastomotic collagen levels. Cronin et al. reported that the anastomotic BP is related to the collagen content.[18] Burst pressure was found to be significantly lower in the radiotherapy group compared to the other groups (Table 3, Fig. 3). This finding points to the negative effects of radiotherapy on anastomoses. The administration of ozone eliminated the negative effects of radiotherapy.

Hydroxyproline is the most important amino acid in collagen formation.[19] Different effects of radiotherapy on HYP levels have been reported in the literature. While some studies have shown that radiotherapy reduces the levels of HYP, others failed to show any relationship between radiotherapy and HYP levels.[20,21] In our study, the HYP level was lower in the radiotherapy group, as expected. Significant differences were found between other groups (Table 2, Fig. 2). The increased collagen synthesis with increased BP indicates that rectal O_3 administration improves wound healing.

Radiotherapy has been shown to play an important role in oxidative stress-related tissue toxicity and inflammation by increasing free oxygen radicals.[22] Under oxidative stress, it has been shown that MPO is secreted from the lysosomes of leukocytes.[23] Increased MPO activity causes tissue damage.[24,25] A reducing effect of ozone application on MPO levels was not detected in our study (Table 2, Fig. 1). Although the main mechanism of O_3 was thought to be related to nitric oxide pathways and antioxidative enzymes, our study did not provide any suggestion about this mechanism.[11] This might be a result of the administration route.

On the 5th day, there was no significant difference between the groups in terms of mucosal re-epithelialization and muscularis propria regeneration. Likewise, there was no significant difference between the groups in terms of their apposition scores (Table 8). These results show that epithelialization and regeneration are neither positively nor negatively affected by radiotherapy and ozone (Table 8). This shows that the dose of radiotherapy was suitable and the concentration of O_3 was not toxic. The most important parameter for the healing of mucosa and muscularis propria layers is the quality of the anastomosis technique.[1] In our study, all anastomoses were performed by a single investigator. No significant differences in adhesion scores were found in the control and ozone groups compared to the radiotherapy and radiotherapy/ozone groups (Table 5). The application of ozone might increase inflammation and accelerate the formation of tissue adhesions.

Table 6. Comparison of histological scores by groups*

Group	Median and SD	Necrosis	Granulation tissue	Inflammatory exudate	Macrophages	Granulocytes	Fibroblasts
Control (n = 8)	median (Q1–Q3)	0 (0–0)	1 (1–1)	0.5 (0–1)	2 (2–2.75)	1 (1–1.75)	2 (2–2.75)
	SD	0	0.51	0.53	0.69	0.64	0.69
Ozone (n = 8)	median (Q1–Q3)	0 (0–0.75)	1 (1–2)	1 (0.25–2)	2 (1.25–2)	2 (2–3)	2 (2–2)
	SD	0.37	0.53	0.75	0.48	0.48	0.37
Radiotherapy (n = 8)	median (Q1–Q3)	0 (0–0)	2 (1–2)	2.5 (2–3)	0.5 (0–1)	2 (2–2.75)	1 (1–1)
	SD	0.35	0.37	0.54	0.53	0.37	0.35
Radiotherapy/ ozone (n = 8)	median (Q1–Q3)	0 (0–0)	1 (1–1.75)	2 (1–2)	2 (1–2)	2 (1.25–2)	2 (1–2)
	SD	0	0.46	0.46	0.70	0.46	0.51
χ^2	overall	2.214	8.402	18.850	16.607	10.044	12.732
df (total)	overall	31	31	31	31	31	31
p-value	overall	0.574	**0.032**a**	**0.000**a,b,e**	**0.000**a,c,d**	**0.000**d**	**0.000**a**

Q1 – 1st quartile; Q3 – 3rd quartile; SD – standard deviation; df – degrees of freedom; * Kruskal–Wallis test was used and Mann–Whitney U test with Bonferroni correction was performed as post hoc test; ** $p < 0.0083$ was considered sufficient for statistical significance. Values in bold show statistically significant differences between groups. [a] – comparison between control group and radiotherapy group; [b] – comparison between control group and ozone group; [c] – comparison between radiotherapy and radiotherapy/ozone group; [d] – comparison between ozone group and radiotherapy group; [e] – comparison between control group and radiotherapy/ozone group.

Table 7. Histological score frequencies of the groups

Variable	Score	Control	Ozone	Radiotherapy	Radiotherapy/ozone
Necrosis	0	8 (100%)	6 (75%)	7 (87.5%)	8 (100%)
	1	0	2 (25%)	1 (12.5%)	0
	2	0	0	0	0
	3	0	0	0	0
Granulation tissue	0	1 (12.5%)	0	0	0
	1	7 (87.5%)	5 (62.5%)	3 (37.5%)	6 (75%)
	2	0	3 (37.5%)	3 (37.5%)	2 (25%)
	3	0	0	0	0
Inflammatory exudate	0	3 (37.5%)	2 (25%)	0	0
	1	5 (62.5%)	3 (37.5%)	0	6 (75%)
	2	0	3 (37.5%)	4 (50%)	2 (25%)
	3	0	0	4 (50%)	0
Macrophages	0	0	0	4 (50%)	0
	1	1 (12.5%)	2 (25%)	4 (50%)	3 (37.5%)
	2	4 (50%)	6 (75%)	0	4 (50%)
	3	3 (37.5%)	0	0	1 (12.5%)
Granulocytes	0	0	0	0	0
	1	6 (75%)	0	1 (12.5%)	2 (25%)
	2	2 (25%)	5 (62.5%)	5 (62.5%)	6 (75%)
	3	0	3 (37.5%)	2 (25%)	0
Fibroblasts	0	0	0	0	0
	1	2 (25%)	1 (12.5%)	7 (87.5%)	3 (37.5%)
	2	4 (50%)	7 (87.5%)	1 (12.5%)	5 (62.5%)
	3	2 (25%)	0	0	0

score 0 – negative; score 1 – low; score 2 – moderate; score 3 – high.

However, as the ozone was administered via the rectal route, there were no significant changes in the adhesion scores of the groups.

It is known that radiotherapy is an important cause of anastomosis leakage due to its effects on reducing tissue blood flow.[4] Decreased blood flow can cause tissue

Table 8. Mucosa and muscularis propria apposition levels. Re-epithelization of mucosa and regeneration of muscularis propria levels*

Group	Median and SD	Mucosa apposition	Muscularis propria apposition	Re-epithelization of mucosa	Regeneration of muscularis propria
Control (n = 8)	median (Q1–Q3)	2 (2–2.75)	2 (2–2)	1 (1–3.75)	1.5 (2–2)
	SD	0.48	0	1.25	0.53
Ozone (n = 8)	median (Q1–Q3)	2 (2–2)	2 (2–2)	1 (1–4.25)	2 (1.25–2)
	SD	0.57	0	1.49	0.48
Radiotherapy (n = 8)	median (Q1–Q3)	2 (2–2)	2 (2–2)	1 (1–1)	2 (1–2)
	SD	0.35	0.35	0	0.51
Radiotherapy/ ozone (n = 8)	median (Q1–Q3)	2 (2–2)	2 (2–2)	1 (1–2.75)	1 (1–2)
	SD	0.35	0	0.91	0.51
χ^2	overall	4.015	3	2.460	1.301
df (total)	overall	31	31	31	31
p-value	overall	0.694	0.457	0.483	0.549

Q1 – 1st quartile; Q3 – 3rd quartile; SD – standard deviation; df – degrees of freedom; * Kruskal–Wallis test was used and Mann–Whitney U test with Bonferroni correction was performed as post hoc test. A value of $p < 0.0083$ was considered sufficient for statistical significance.

Table 9. Mucosal and muscularis propria apposition frequencies of the groups

Variable	Score	Control	Ozone	Radiotherapy	Radiotherapy/ozone
Mucosa apposition	1	0	1 (12.5%)	0	0
	2	5 (62.5%)	6 (75%)	7 (87.5%)	7 (87.5%)
	3	3 (37.5%)	1 (12.5%)	1 (12.5%)	1 (12.5%)
Muscularis propria apposition	1	0	0	0	0
	2	8 (100%)	8 (100%)	7 (87.5%)	8 (100%)
	3	0	0	1 (12.5%)	0

score 1 – good; score 2 – moderate; score 3 – poor.

Table 10. Mucosal re-epithelialization frequencies of the groups

Variable	Score	Control	Ozone	Radiotherapy	Radiotherapy/ozone
Re-epithelization of mucosa	1	5 (62.5%)	5 (62.5%)	8 (100%)	5 (62.5%)
	2	0	1 (12.5%)	0	1 (12.5%)
	3	1 (12.5%)	0	0	2 (25%)
	4	2 (25%)	0	0	0
	5	0	2 (25%)	0	0
	6	0	0	0	0
	7	0	0	0	0

Scores: 1 – none; 2 – little, one-layer, cubic; 3 – large one-layer, cubic; 4 – almost complete, one-layer, cubic; 5 – complete, one-layer, cubic; 6 – one-layer, glandular; 7 – normal glandular mucosa.

Table 11. Muscularis propria regeneration frequencies of the groups

Variable	Score	Control	Ozone	Radiotherapy	Radiotherapy/ozone
Regeneration of muscularis propria	1	4 (50%)	2 (62.5%)	3 (37.5%)	5 (62.5%)
	2	4 (50%)	6 (12.5%)	5 (62.5%)	3 (12.5%)

score 1 – positive; score 2 – negative.

exudate, ischemia and necrosis.[4] The absence of necrosis showed that neither radiotherapy nor O_3 has toxic effects on the colon mucosa. Wound healing is composed of inflammatory exudate, macrophages, granulation tissue, and fibroblast formation. Macrophage and granulocyte cells are a group of cells that take part in the formation of granulation tissue.[15] Fibroblasts are the basic cells of connective tissue, taking part in collagen synthesis during the later stages of wound healing. In our study, all wound healing parameters decreased

in the radiotherapy groups. Although O_3 administration significantly improved wound healing in macrophages, granulocytes and fibroblast levels, granulation tissue formation also improved but was not statistically significant. This is probably due to not enough time for the formation of granulation tissue to occur. However, early wound healing parameters significantly improved with ozone administration when compared to radiotherapy. The negative effects of radiotherapy on wound healing have been shown in previous studies.[15,20] There are studies showing the effect of radiotherapy in preventing the migration of fibroblasts to the wound site.[26] These findings, together with a decrease in exudate formation and the differences in groups receiving ozone, support the hypothesis of our study, namely the positive effects of ozone therapy following radiotherapy (Table 6).

Tissue oxygenation is one of the most important factors for wound healing and, as a result, the prevention of AL. Tissue microvascular patency is the key factor for tissue oxygenation. Surgical devascularization, smoking and diabetes are risk factors for impairing tissue oxygenation. Several diagnostic measurements such as microfabricated oxygen sensors and near infrared spectroscopy have emerged.[27] Hyperbaric oxygen treatments have been shown to be beneficial in preventing AL and increasing transport to tissues.[28] Our study tried to determine if rectal ozone administration can reverse the harmful effects of radiotherapy. Local administration of ozone can improve healing disturbances that occur in the colon mucosa due to radiotherapy.[29] The main difference between our study and previous studies is the application method.[16] The rectal administration method can be translated to human studies and is the main difference between intraperitoneal administration. Besides systemic administration, local treatment can be regarded as an innovative beneficial approach to preventing AL.

The latest theory on the harmful effects of radiation resulting from major changes in the gastrointestinal microflora was put forward by Manichanh et al.[30] After radiotherapy, anaerobes are dominating the microflora of the colon and increasing the risk of leakage.[31] An increase in the amount of oxygen in the colon lumen can decrease the number of anaerobes.[32] Although not proven, the administration of ozone might reverse the harmful effects of radiotherapy on the microflora of the colon. The effect of ozone on the microflora of the colon is a subject of future investigation.

Limitations

The main limitation of our study is the small number of rats (n = 32) used. Another limitation is the absence of different time periods of sampling the rats rather than the 5th day. Also, a more detailed histological evaluation of the colon might have been performed.

Conclusions

As a result of this study, rectal administration of O_3 decreased the negative effects of radiotherapy on colon anastomoses by the O_3 oxidative preconditioning effect. This study is the first experimental study evaluating rectal O_3 administration and might be a subject of future clinical studies. The effect of ozone on tumor cells is a separate issue in the literature that requires more research.

ORCID iDs

Tonguç Utku Yilmaz https://orcid.org/0000-0002-2344-7783
Eda Yirmibeşoğlu Erkal https://orcid.org/0000-0002-6327-7037
Saffet Çinar https://orcid.org/0000-0003-3637-1922
Ceyla Eraldemir https://orcid.org/0000-0001-9410-8554
Çiğdem Vural https://orcid.org/0000-0002-9405-9112
Ezgi Uçar Taş https://orcid.org/0000-0002-2685-6013
Nihat Zafer Utkan https://orcid.org/0000-0002-2133-3336

References

1. Rutegård M, Rutegård J. Anastomotic leakage in rectal cancer surgery: The role of blood perfusion. *World J Gastrointest Surg*. 2015;7(11):289–292. doi:10.4240/wjgs.v7.i11.289
2. Mirnezami A, Mirnezami R, Chandrakumaran K, Sasapu K, Sagar P, Finan P. Increased local recurrence and reduced survival from colorectal cancer following anastomotic leak: Systematic review and meta-analysis. *Ann Surg*. 2011;253(5):890–899. doi:10.1097/SLA.0b013e3182128929
3. Espín E, Ciga MA, Pera M, et al. Oncological outcome following anastomotic leak in rectal surgery. *Br J Surg*. 2015;102(4):416–422. doi:10.1002/bjs.9748
4. Qin Q, Ma T, Deng Y, et al. Impact of preoperative radiotherapy on anastomotic leakage and stenosis after rectal cancer resection: Post hoc analysis of a randomized controlled trial. *Dis Colon Rectum*. 2016;59(10):934–942. doi:10.1097/DCR.0000000000000665
5. Vignali A, Gianotti L, Braga M, Radaelli G, Malvezzi L, Carlo VD. Altered microperfusion at the rectal stump is predictive for rectal anastomotic leak. *Dis Colon Rectum*. 2000;43(1):76–82. doi:10.1007/BF02237248
6. Gültekin FA, Bakkal BH, Sümer D, Köktürk F, Bektaş S. Effects of ozonated olive oil on acute radiation proctitis in rats. *Balkan Med J*. 2013;30(4):369–374. doi:10.5152/balkanmedj.2013.9158
7. Nguyen HQ, To NH, Zadigue P, et al. Ionizing radiation-induced cellular senescence promotes tissue fibrosis after radiotherapy. A review. *Crit Rev Oncol Hematol*. 2018;129:13–26. doi:10.1016/j.critrevonc.2018.06.012
8. Shukla PK, Gangwar R, Manda B, et al. Rapid disruption of intestinal epithelial tight junction and barrier dysfunction by ionizing radiation in mouse colon in vivo: Protection by *N*-acetyl-L-cysteine. *Am J Physiol Gastrointest Liver Physiol*. 2016;310(9):G705–G715. doi:10.1152/ajpgi.00314.2015
9. Vidal-Casariego A, Calleja-Fernández A, Cano-Rodríguez I, Cordido F, Ballesteros-Pomar MD. Effects of oral glutamine during abdominal radiotherapy on chronic radiation enteritis: A randomized controlled trial. *Nutrition*. 2015;31(1):200–204. doi:10.1016/j.nut.2014.08.003
10. Zeng J, Lu J. Mechanisms of action involved in ozone-therapy in skin diseases. *Int Immunopharmacol*. 2018;56:235–241. doi:10.1016/j.intimp.2018.01.040
11. León OS, Menéndez S, Merino N, et al. Ozone oxidative preconditioning: A protection against cellular damage by free radicals. *Mediators Inflamm*. 1998;7(4):289–294. doi:10.1080/09629359890983
12. Eliakim R, Karmeli F, Rachmilewitz D, Cohen P, Zimran A. Ozone enema: A model of microscopic colitis in rats. *Dig Dis Sci*. 2001;46(11):2515–2520. doi:10.1023/A:1012348525208
13. Knightly JJ, Agostino D, Cliffton EE. The effect of fibrinolysin and heparin on the formation of peritoneal adhesions. *Surgery*. 1962;52:250–258. PMID:14457251.
14. Elabscience. *Hydroxyproline (Hyp) Colorimetric Assay Kit (Alkali Hydrolysis Method)*. https://www.elabscience.com/Manual/biochemical_kits/E-BC-K061-S.pdf. Accessed December 20, 2020.

15. Hycult Biotech. *MPO, Rat, ELISA Kit*. https://www.hycultbiotech.com/hk105-01. Accessed December 20, 2020.
16. de Roy van Zuidewijn DB, Schillings PH, Wobbes T, de Boer HH. Histologic evaluation of wound healing in experimental intestinal anastomoses: Effects of antineoplastic agents. *Int J Exp Pathol*. 1992;73(4):465–484. PMID:1390194.
17. Taşdöven İ, Emre AU, Gültekin FA, et al. Effects of ozone preconditioning on recovery of rat colon anastomosis after preoperative radiotherapy. *Adv Clin Exp Med*. 2019;28(12):1683–1689. doi:10.17219/acem/110329
18. Cronin K, Jackson DS, Dunphy JE. Specific activity of hydroxyproline-tritium in the healing colon. *Surg Gynecol Obstet*. 1968;126(5):1061–1065. PMID:5652652.
19. Braskén P, Renvall S, Sandberg M. Fibronectin and collagen gene expression in healing experimental colonic anastomoses. *Br J Surg*. 1991;78(9):1048–1052. doi:10.1002/bjs.1800780908
20. Kerem M, Bedirli A, Karahacioglu E, et al. Effects of soluble fiber on matrix metalloproteinase-2 activity and healing of colon anastomosis in rats given radiotherapy. *Clin Nutr*. 2006;25(4):661–670. doi:10.1016/j.clnu.2006.01.028
21. Terzi C, Sevinç Aİ, Koçdor H, et al. Improvement of colonic healing by preoperative rectal irrigation with short-chain fatty acids in rats given radiotherapy. *Dis Colon Rectum*. 2004;47(12):2184–2194. doi:10.1007/s10350-004-0724-7
22. Kochhar R, Patel F, Sharma SC, et al. Radiation-induced proctosigmoiditis: Prospective, randomized, double-blind controlled trial of oral sulfasalazine plus rectal steroids versus rectal sucralfate. *Dig Dis Sci*. 1991;36(1):103–107. doi:10.1007/BF01300096
23. Ho E, Karimi Galougahi K, Liu CC, Bhindi R, Figtree GA. Biological markers of oxidative stress: Applications to cardiovascular research and practice. *Redox Biol*. 2013;1(1):483–491. doi:10.1016/j.redox.2013.07.006
24. Reiter RJ, Tan DX, Osuna C, Gitto E. Actions of melatonin in the reduction of oxidative stress: A review. *J Biomed Sci*. 2000;7(6):444–458. doi:10.1007/BF02253360
25. Erkol H, Kahramansoy N, Kordon O, Buyukasik O, Serin E, Ulas N. Effects of beta-glucan on hepatic damage caused by obstructive jaundice [in Turkish]. *Ulus Travma Acil Cerrahi Derg*. 2011;17(4):303–307. doi:10.5505/tjtes.2011.88964
26. Seifert WF, Wobbes T, Hoogenhout J, de Man BM, Huyben KMLC, Hendriks T. Intraoperative irradiation delays anastomotic repair in rat colon. *Am J Surg*. 1995;170(3):256–261. doi:10.1016/S0002-9610(05)80010-8
27. Marland J, Gray M, Argyle D, Underwood I, Murray A, Potter M. Post-operative monitoring of intestinal tissue oxygenation using an implantable microfabricated oxygen sensor. *Micromachines (Basel)*. 2021;12(7):810. doi:10.3390/mi12070810
28. Brouwer RJ, Engberts AC, Borger van der Burg BL, van Dongen TT, van Hulst RA, Hoencamp R. Meta-analysis on the effect of hyperbaric oxygen as adjunctive therapy in the outcome of anastomotic healing of experimental colorectal resections in rats. *Diving Hyperb Med*. 2018;48(3):173–185. doi:10.28920/dhm48.3.173-185
29. Reischl S, Wilhelm D, Friess H, Neumann PA. Innovative approaches for induction of gastrointestinal anastomotic healing: An update on experimental and clinical aspects. *Langenbecks Arch Surg*. 2021;406(4):971–980. doi:10.1007/s00423-020-01957-1
30. Manichanh C, Varela E, Martinez C, et al. The gut microbiota predispose to the pathophysiology of acute postradiotherapy diarrhea. *Am J Gastroenterol*. 2008;103(7):1754–1761. doi:10.1111/j.1572-0241.2008.01868.x
31. Brook I, Walker RI, Macvittie TJ. Effect of antimicrobial therapy on bowel flora and bacterial infection in irradiated mice. *Int J Radiat Biol Relat Stud Phys Chem Med*. 1988;53(5):709–716. doi:10.1080/09553008814551081
32. Makanyengo SO, Carroll GM, Goggins BJ, Smith SR, Pockney PG, Keely S. Systematic review on the influence of tissue oxygenation on gut microbiota and anastomotic healing. *J Surg Res*. 2020;249:186–196. doi:10.1016/j.jss.2019.12.022

Dexamethasone promotes osteoblast apoptosis through the Chk2/p53 signaling pathway

*Jie Zhu[1,A,D], *Tantan Zhao[1,B], Lunqing Zhu[1,B], Chunhua Yin[1,B,C], Yao Liu[1,C], Jianfeng Fang[1,B,C], Hansi Liang[2,E], Yunfang Zhen[1,E,F]

[1] Department of Orthopaedics, Children's Hospital of Soochow University, Suzhou, China
[2] Suzhou Key Laboratory for Tumor Immunology of Digestive Tract, The First Affiliated Hospital of Soochow University, Suzhou, China

A – research concept and design; B – collection and/or assembly of data; C – data analysis and interpretation;
D – writing the article; E – critical revision of the article; F – final approval of the article

Advances in Clinical and Experimental Medicine, ISSN 1899–5276 (print), ISSN 2451–2680 (online) *Adv Clin Exp Med*. 2022;31(12):1365–1374

Address for correspondence
Yunfang Zhen
E-mail: zhenyufang2021@163.com

Funding sources
The study has been supported by the National Natural Science Foundation of China (grant No. 82172520), the Suzhou Science and Technology Development Program of Medical Devices and New Medicine (grant No. SLT201935), the Suzhou Science and Technology Development Plan (grant No. SYS2019088), the Suzhou Health Personnel Training Program (grant No. GSWS2019016), the Jiangsu Provincial Natural Science Foundation of China (grant No. BE2016674), and the Suzhou Science and Technology Development Plan (grant No. SYS2020109).

Conflict of interest
None declared

* Jie Zhu and Tantan Zhao contributed equally to this work.

Received on September 2, 2021
Reviewed on December 27, 2021
Accepted on July 15, 2022

Published online on September 9, 2022

Cite as
Zhu J, Zhao T, Zhu L, et al. Dexamethasone promotes osteoblast apoptosis through the Chk2/p53 signaling pathway. *Adv Clin Exp Med*. 2022;31(12):1365–1374. doi:10.17219/acem/152150

DOI
10.17219/acem/152150

Abstract

Background. Glucocorticoids (GCs) are widely used to treat inflammatory or autoimmune diseases. However, several studies have reported that the use of GCs can lead to numerous complications, the most serious of which are osteoporosis and osteonecrosis of the femoral head (ONFH). Osteoblast apoptosis has been identified as an important event in the development of GC-induced osteoporosis and ONFH. However, the mechanisms underlying the regulation of these processes have not yet been explored.

Objectives. To observe the effect of dexamethasone (Dex) on the apoptosis of osteoblasts and explore its mechanism, as well as provide a new therapeutic idea for GC-induced osteoporosis and ONFH.

Materials and methods. Cell proliferation and apoptosis of MC3T3-E1 cells after Dex treatment were determined using the CellTiter-Glo® Luminescent Cell Viability Assay kit and Annexin V-FITC/PI Double Staining Apoptosis Detection Kit, respectively. The expression of caspase-3/cleaved caspase-3 and poly(ADP-ribose) polymerase (PARP)/cleaved PARP in MC3T3-E1 cells after Dex treatment was determined with western blotting. The expression of p53 and checkpoint kinase 2 (Chk2) in MC3T3-E1 cells after Dex treatment was analyzed using western blotting and polymerase chain reaction (PCR). The effects of p53 knockdown and Chk2 knockdown on Dex-induced apoptosis of MC3T3-E1 cells were also characterized.

Results. Dexamethasone remarkably inhibited cell growth and induced the apoptosis of MC3T3-E1 cells. We also observed that Dex induced osteoblast apoptosis by promoting p53 expression. The regulatory effect of Dex on p53 expression is mediated by the upregulation of Chk2, which interacted with p53 and inhibited p53 degradation. The knockdown of p53 alleviated Dex-induced MC3T3-E1 cell apoptosis by decreasing the expression of cleaved caspase-3 and cleaved PARP.

Conclusions. We demonstrated that Dex increased Chk2 protein expression, which stabilized the protein expression of p53, and in turn promoted osteoblast apoptosis.

Key words: dexamethasone, osteoblast apoptosis, Chk2/p53, glucocorticoid (GC)-induced osteoporosis, ONFH

Background

Glucocorticoids (GCs) are among the most commonly prescribed drugs. As they have anti-inflammatory and immunosuppressive properties, GCs are primarily used to treat inflammatory or autoimmune diseases, such as systemic lupus erythematosus and nephrotic syndrome.[1,2] However, recent studies have revealed that the use of GCs can cause many undesirable complications. Among these, osteoporosis and osteonecrosis of the femoral head (ONFH) are the most serious.[3–5] There is evidence that osteoblast apoptosis is an important event in the development of osteoporosis and ONFH induced by GCs.[6]

Dexamethasone (Dex) is a synthetic GC and its functions include inhibiting collagen and fibronectin synthesis[7] and activating collagenase synthesis.[8] Although Dex has been reported to induce apoptosis of osteoblasts and exert a modulatory effect on osteoblast proliferation,[9,10] the regulation of these mechanisms by Dex is yet to be characterized.

Checkpoint kinase 2 (Chk2) is an important regulator that can rapidly phosphorylate downstream effectors and lead to DNA damage.[11] When Chk2 is activated, it leads to alternative cell responses, such as programmed cell death.[12] The Chk2/p53 pathway can induce cell cycle arrest in DNA damage responses (DDRs) and activate p53-related apoptosis pathways.[13] It has been reported that Dex can cause cell apoptosis by upregulating the expression of p53 in MC3T3-E1 cells.[14] However, the role and mechanisms of the Chk2/p53 pathway in osteoblasts have not been determined. Accordingly, we aimed to characterize the molecular mechanisms underlying Dex promotion of osteoblast cell apoptosis.

Objectives

The objective of this study was to observe the effect of Dex on the apoptosis of osteoblasts and explore the underlying mechanisms. This could reveal a new therapeutic potential for GC-induced osteoporosis and ONFH.

Materials and methods

Reagents, plasmids and antibodies

The SuperScript™ First-Strand Synthesis System and TRIzol Reagent were acquired from Invitrogen (Grand Island, USA). The plasmids of shp53 and shChk2 were obtained from Open Biosystems (Thermo Fisher Scientific, Pittsburgh, USA). Antibodies against caspase-3, cleaved caspase-3, poly(ADP-ribose) polymerase (PARP), cleaved PARP, p53, p-p53 Ser15, p-p53 Ser20, ataxia telangiectasia mutated kinase and Rad3-related kinase (ATR), p-ATR Ser428, murine double minute 2 (MDM2), p-MDM2 Ser166, p-Chk2 Thr68, p-Chk1 Ser345, glyceraldehyde-3-phosphate dehydrogenase (GAPDH), and β-actin were purchased from Cell Signaling Technology (Danvers, USA). Dexamethasone was obtained from Sigma-Aldrich (St. Louis, USA). Cycloheximide (CHX) and MG132 were acquired from Calbiochem (San Diego, USA).

Cell culture

Osteoblast cells (MC3T3-E1) were obtained from the Institute of Biochemistry and Cell Biology (IBCB; Shanghai Institutes for Biological Sciences, Chinese Academy of Sciences, Shanghai, China). Dulbecco's modified Eagle's medium (DMEM) high glucose (Gibco, Waltham, USA) was used to maintain cells. It was synchronized by incubation in medium with extra 0.1% fetal bovine serum (FBS; NovaTech, Grand Island, USA) overnight, and cultured in medium with extra 10% FBS and penicillin-streptomycin solution (100 U/mL penicillin and 100 μg/mL streptomycin). The culture was maintained in a humidified incubator atmosphere with 5% CO_2 at 37°C.

Transfection

In this study, we used the PolyJet™ In Vitro DNA Transfection Reagent (SignaGen Laboratories, Rockville, USA) to transfect cells. In order to obtain stable transfected cells, the cells were cultured with hygromycin B, G418 or puromycin according to the transfected granules with different antibiotic resistance properties. Transfected cells were selected with hygromycin B, G418 or puromycin for 3–4 weeks. Before being used for further experiments, cells were cultured for at least 2 passages.

Cell proliferation assay

Adenosine triphosphate (ATP)ase analysis was used to evaluate the effect of Dex on viability of MC3T3-E1 cells. Cells were cultured in 96-well plates with a density of 3×10^3 cells per well and subsequently treated with 1 μM Dex for different durations (1–4 days). Treated cells were collected and analyzed with ATP Colorimetric/Fluorometric Assay Kit (Sigma-Aldrich), following the manufacturer's instructions.

Determination of cell apoptosis

The MC3T3-E1 cells were incubated to 70–80% confluence in 6-well plates. Before the Dex treatment, the culture medium was shifted to 0.1% FBS medium for 24 h. The cells were then treated with the designated concentration of Dex. After the treatment that lasted for 24 h, the cells were washed with phosphate-buffered saline (PBS) 3 times. Then, 100 μL of cells were incubated with equal volume of FITC-Annexin V/PI Assay Kit solution (Biosea Biotechnology, Beijing, China) in the dark for 30 min

at room temperature. The apoptosis rate was recorded using a flow cytometer (Bender MedSystems, Burlingame, USA).

Protein degradation experiments

The MC3T3-E1 cells were pretreated with the proteasome inhibitor MG132 at a concentration of 20 μM for 24 h. The MG132 was then removed and 100 μg/mL of synthetic inhibitor CHX were added to the culture medium – alone or in combination with 1 μM Dex in different time intervals (2 h, 4 h or 6 h). The levels of remaining p53 and GAPDH proteins were detected by means of western blot analysis.

Western blot analysis

Cells (1×10^6) were inoculated on 6-well plates and treated by the method described previously. Then, they were extracted with cell lysis buffer. For each sample, 60–80 μg of protein was subjected to sodium dodecyl sulfate-polyacrylamide gel electrophoresis (SDS-PAGE). The membrane was then incubated with primary antibodies overnight, followed by incubation with the alkaline phosphatase (AP)-conjugated secondary antibody. The ImageQuant™ TL software v. 8.1 (Cytiva, Marlborough, USA) was used to detect the density of the bands. The results shown in this study represent 3 independent experiments.

Quantitative reverse transcription-polymerase chain reaction (RT-PCR) for miRNA assay

The RNeasy Mini Kit (Qiagen, Valencia, USA) was used to extract total miRNAs. The MC3T3-E1 cells (1×10^6) were inoculated on 6-well plates and treated with 1 μM Dex for different time periods (1–3 h). For the reverse transcription, the amount of total RNA used was 1 μg. The expression of *p53* was amplified using the miScript PCR Kit (Qiagen) and analyzed using the 7900HT Fast Real-time PCR system (Applied Biosystems, Carlsbad, USA). The primers were: human *p53* (forward: 5'-ACCTATGGAAACTACTTCCTGAAA-3', reverse: 5'-CTGGCATTCTGGGAGCTTCA-3').

Statistical analyses

The experimental data were presented as mean ± standard deviation (M ±SD) and analyzed with IBM SPSS v. 19.0 statistical software (IBM Corp., Armonk, USA). The normality of the data was analyzed using the Shapiro–Wilk test, and the value of $p > 0.05$ indicated that the data were normally distributed. The Levene's test was used to analyze the homogeneity of variance, and the value of $p > 0.05$ indicated that the data conformed to homogeneity of variance. The one-way analysis of variance (ANOVA) test for repeated measures, followed by the post hoc least significant difference (LSD) test were used for overall comparisons between groups across multiple time points. The value of $p < 0.05$ was considered statistically significant.

Results

Dex significantly inhibited the proliferation of MC3T3-E1 cells and induced cell apoptosis

We used the ATPase analysis to evaluate the effect of Dex on the viability of MC3T3-E1 cells. Cells were cultured in the Dex dose range (1 μM). The Shapiro–Wilk test was used to analyze the normality of the data. As shown in Table 1, the data were normally distributed ($p > 0.05$). The homogeneity of variance test indicated that the data conform to homogeneity of variance (Table 2, $p > 0.05$). As shown in Fig. 1A, cell apoptosis had not yet started over the first 2 days and there was no statistically significant difference between the treatment groups (day 1: $F = 3.654$, $p = 0.196$; day 2: $F = 2.476$; $p = 0.256$). In contrast, cell viability was significantly reduced in Dex-treated cells on days 3 and 4 (day 3: $F = 73.491$, $p = 0.013$; day 4: $F = 123.085$; $p = 0.008$). Specific data points are shown in Table 3. We then used FITC-Annexin V/PI staining to detect the effect of Dex on apoptosis in MC3T3-E1 cells. As shown in Fig. 1B,

Table 1. Shapiro–Wilk test results of the effect of dexamethasone (Dex) on the viability of MC3T3-E1 cells (M ±SD)

Test	n	Data	Statistics	p-value
Medium control day 1	3	3.768 ±1.207	0.966	0.648
Medium control day 2	3	6.228 ±1.609	0.868	0.289
Medium control day 3	3	14.417 ±0.560	0.962	0.625
Medium control day 4	3	21.739 ±2.030	0.948	0.560
Dex 1 μM day 1	3	2.472 ±0.640	0.858	0.261
Dex 1 μM day 2	3	3.938 ±1.518	0.977	0.708
Dex 1 μM day 3	3	7.237 ±1.002	0.997	0.891
Dex 1 μM day 4	3	9.329 ±0.983	0.998	0.909

M ±SD – mean ± standard deviation.

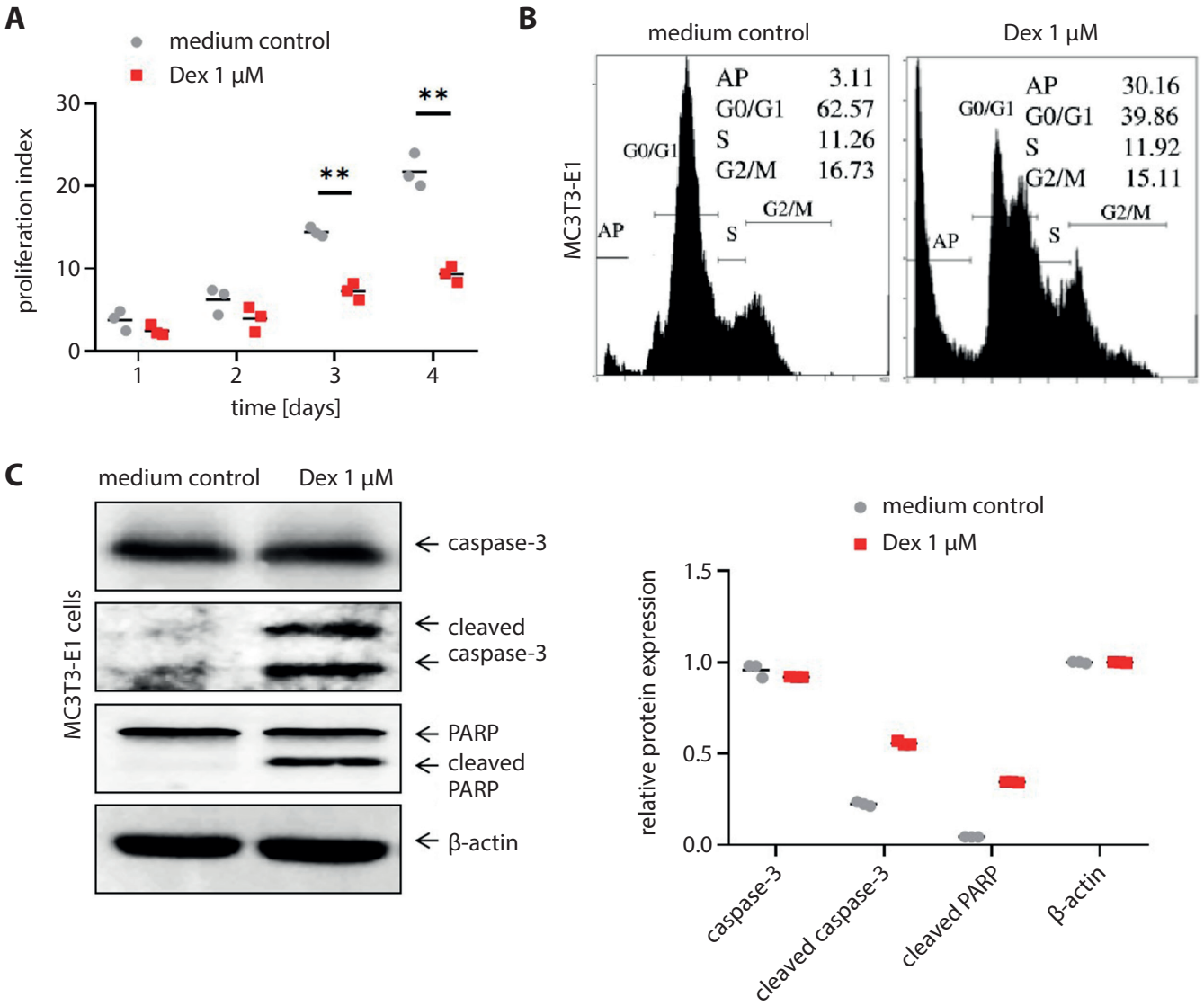

Fig. 1. Dexamethasone (Dex) significantly inhibited the proliferation of MC3T3-E1 cells and induced cell apoptosis. A. Cell viability was significantly reduced after Dex treatment (** $p < 0.01$ on day 3 and day 4); B. The cell apoptosis analysis on MC3T3-E1 cells after Dex treatment; C. Western blot analysis on the expression of caspase-3/cleaved caspase-3 and poly (ADP-ribose) polymerase (PARP)/cleaved PARP in MC3T3-E1 cells after Dex treatment

Table 2. Levene's test of the homogeneity of dexamethasone (Dex) with the viability of MC3T3-E1 cells

Test	Day 1	Day 2	Day 3	Day 4
F	1.268	0.064	0.662	1.934
p-value	0.323	0.813	0.461	0.237

Table 3. Comparison of cell viability at each time point of dexamethasone (Dex) administration with the viability of MC3T3-E1 cells

Test	Day 1	Day 2	Day 3	Day 4
F	3.654	2.476	73.491	123.085
p-value	0.196	0.256	0.013	0.008

Treatment factor main effect: $F = 112.41$, $p < 0.01$; time factor main effect: $F = 115.99$, $p < 0.01$; interaction between the 2 factors: $F = 23.76$, $p < 0.01$.

we found that the apoptosis rate of MC3T3-E1 cells significantly increased after 24 h of Dex treatment. Considering that PARP cleavage and caspase activation are typically associated with apoptosis, we used western blotting in order to detect the expression of these proteins in Dex-treated MC3T3-E1 cells. The results suggested that the cleavage of cleaved PARP and cleaved caspase-3 was increased by Dex treatment in MC3T3-E1 cells (Fig. 1C). Collectively, our results demonstrate that Dex can significantly inhibit the proliferation of MC3T3-E1 cells and induce the cell apoptosis.

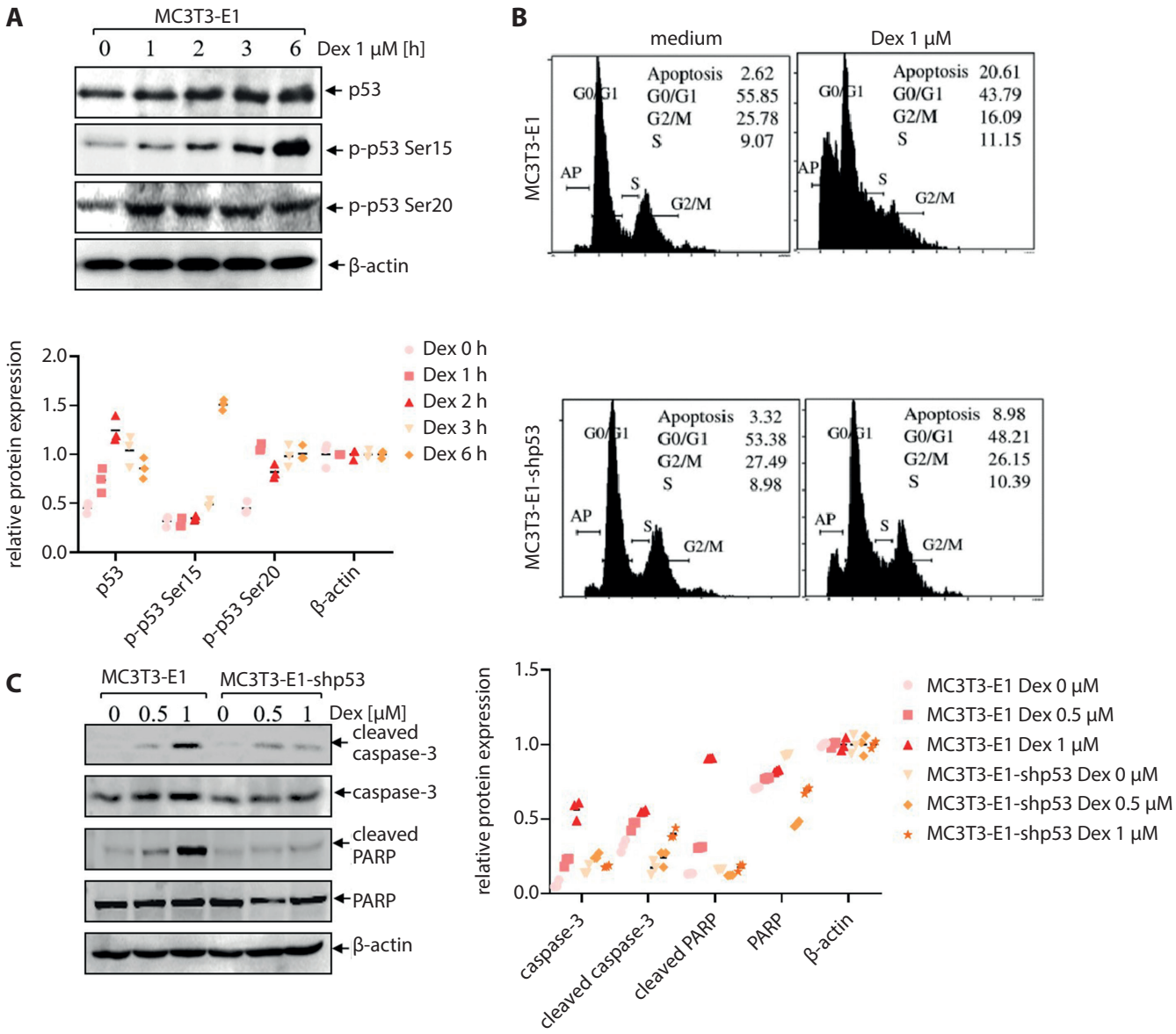

Fig. 2. The phosphorylation of p53 protein was important for the induction of apoptosis following dexamethasone (Dex) treatment. A. The expression of p53 protein phosphorylated at Ser15, Ser20 and total p53 protein in Dex-treated MC3T3-E1 cells; B. Cell apoptosis induced by Dex observed using flow cytometric analysis; C. Western blot analysis indicated that Dex-induced cleavage of poly (ADP-ribose) polymerase (PARP) and caspase-3 were blocked by p53 protein knockdown

Phosphorylation of p53 was crucial for apoptosis induction after Dex treatment

It has been reported that p53 protein is associated with caspase-dependent apoptosis.[15] In order to elucidate the molecular mechanisms underlying the apoptotic effect of Dex, western blotting was performed to determine whether p53 was involved in the cell apoptosis induced by Dex. As presented in Fig. 2A, the expression of total p53 protein and phosphorylated status of p53 protein at Ser15 and Ser20 were determined in MC3T3-E1 cells after Dex treatment. The phosphorylation level of p53 protein at Ser20 was significantly upregulated 1 h after the exposure. Similarly, the phosphorylation level of p53 protein at Ser15 slightly increased in the early treatment period (≤3 h) and significantly increased 6 h after treatment. The expression of total p53 protein showed a stable increase after Dex treatment and reached a peak within 2–6 h following the treatment. As phosphorylation at Ser20 usually contributes to the stabilization of p53 protein and results in the phosphorylation at Ser15,[10] we presumed that the Dex-induced p53 activation in MC3T3-E1 cells was also dependent on phosphorylation of Ser20.

To further confirm whether Dex-induced apoptosis requires p53 activation, we used shp53 MC3T3-E1 cells. The flow cytometry analysis demonstrated that the apoptosis induction rate of shp53 MC3T3-E1 cells induced by Dex was much lower than that of wild-type MC3T3-E1 cells (Fig. 2B). Western blot results indicated that the knockdown of p53 could block the cleavage

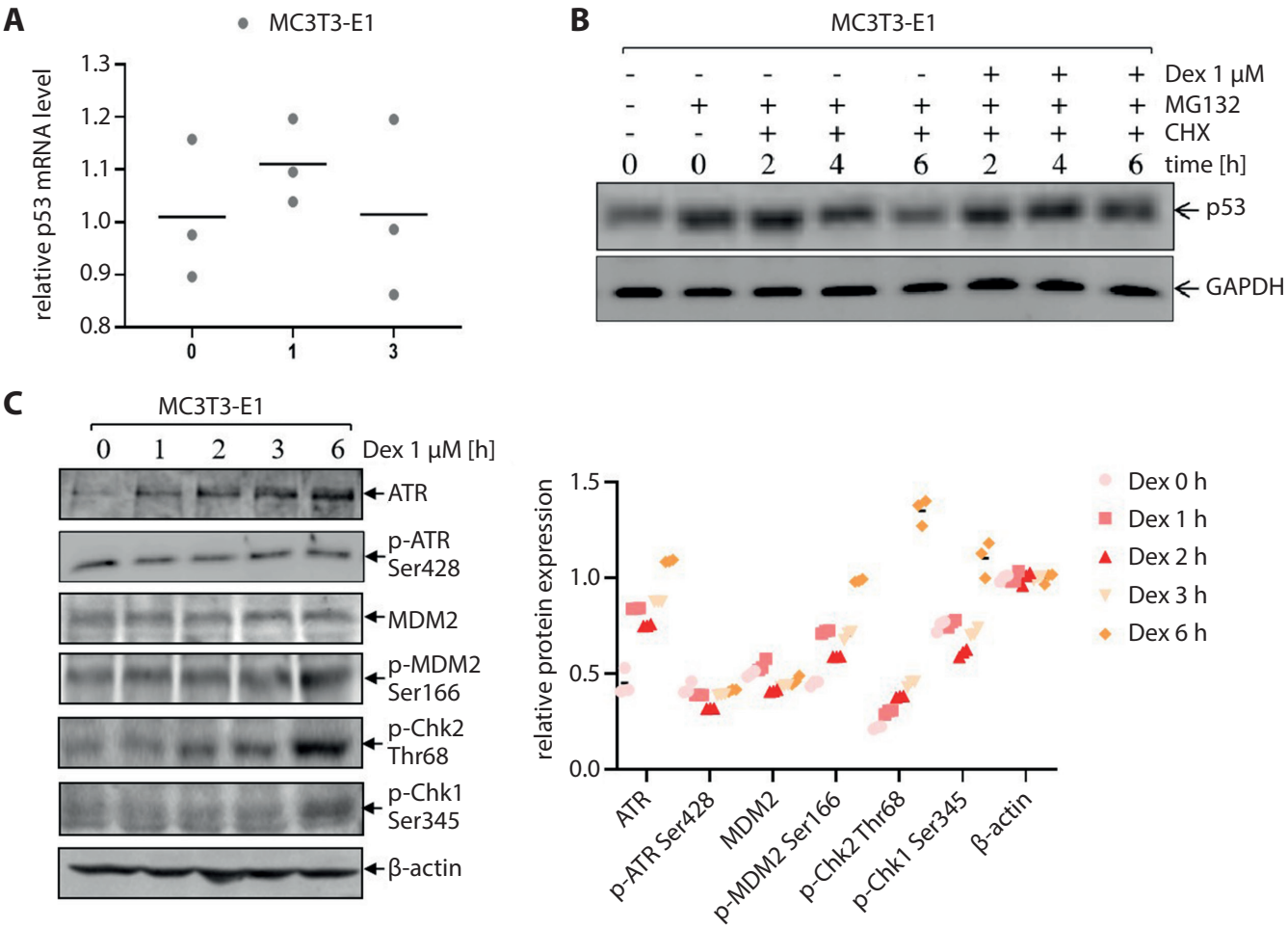

Fig. 3. Dexamethasone (Dex) induced caspase-dependent apoptosis by promoting p53 protein degradation. A. Quantitative polymerase chain reaction (qPCR) analysis of Dex-treated MC3T3-E1 cells; B. MC3T3-E1 cells were pretreated with MG132. Western blot analysis on the dynamics of p53 protein degradation induced by Dex; C. Western blot analysis on phosphorylation of ataxia telangiectasia mutated kinase and Rad3-related kinase (ATR) protein at Ser428, murine double minute 2 (MDM2) protein at Ser166, checkpoint kinase 2 (Chk2) protein at Ser345, and Chk2 protein at Thr68 in Dex-treated MC3T3-E1 cells

CHX – cycloheximide; GAPDH – glyceraldehyde-3-phosphate dehydrogenase.

of PARP and caspase-3 induced by Dex (Fig. 2C). Taken together, these results suggest that the activation of p53 protein is essential for cell apoptosis in MC3T3-E1 cells induced by Dex treatment.

Dex induced caspase-dependent apoptosis through promoting p53 protein degradation

In order to investigate the mechanism of Dex upregulation of p53 protein, we characterized the effect of Dex on the expression of *p53* mRNA level in MC3T3-E1 cells. The results of quantitative PCR have shown that Dex had no effect on the expression of *p53* mRNA level after 3 h of treatment (Fig. 3A). Therefore, we inferred that Dex might regulate the induction of p53 protein at the protein level instead.

In order to elucidate whether Dex was able to prevent p53 protein degradation, we pretreated MC3T3-E1 cells with the proteasome inhibitor MG132. The MG132 was subsequently removed and the synthetic inhibitor CHX was added into the medium, alone or in combination with Dex, for different time periods.[17] This experiment could provide a basis for further research on the effects of Dex on the degradation dynamics of p53 protein. After the cells were treated with both Dex and CHX for 4 h and 6 h, the expression level of p53 protein in the cells was much higher than in the cells treated with CHX alone (Fig. 3B). These results suggest that Dex was contributing to the accumulation of p53 by inhibiting its proteasome-mediated degradation.

Chk2 protein regulates p53 protein degradation during Dex treatment

The degradation of p53 protein can be regulated by many factors, such as MDM2, Chk1/2 and ATR.[18] For instance, studies have shown that the post-translational phosphorylation of MDM2 protein at Ser166 contributes to the degradation of p53 protein.[19,20] Accordingly,

we examined the phosphorylation of MDM2 at Ser166 in Dex-treated MC3T3-E1 cells. The expression of total MDM2 protein was not affected by Dex, while the phosphorylation level at Ser166 was slightly upregulated after Dex treatment at 6 h (Fig. 3C). These results suggested that Dex did not inhibit the phosphorylation of the MDM2 protein at Ser166. Therefore, it could not be explained why p53 protein accumulated in MC3T3-E1 cells after Dex treatment.

Several studies have shown that Chk1/2 can also affect the stabilization and activation of p53 protein by inducing its phosphorylation.[21] As phosphorylation of Chk1 protein at Ser345 or Chk2 protein at Thr68 is necessary for p53 protein activation,[22,23] we evaluated the phosphorylation state of both sites in Chk1 and Chk2 after Dex treatment. Western blot results show that Chk2 protein was phosphorylated at Thr68 after 2 h of Dex treatment and reached a peak after 6 h of treatment, while the phosphorylation level of Chk1 protein at Ser345 increased slightly after 6 h of Dex treatment (Fig. 3C). As p53 is phosphorylated at an early stage, we eliminated the possibility that Chk1 protein is directly involved in inducing p53 protein and hypothesized that Chk2 protein may have some functions in p53 protein stabilization and reactivation instead.

Chk2 protein led to p53-mediated cell apoptosis during Dex treatment

To illuminate the mechanisms underlying Chk2 promotion of p53 protein expression, MC3T3-E1 ShChk2 cells were used to analyze phosphorylation and expression levels of p53 protein after Dex treatment. Western blot analysis indicated that phosphorylated Chk2 protein was depleted in MC3T3-E1 ShChk2 cells compared to MC3T3-E1 cells (Fig. 4A). Importantly, the expression of p53 protein was inhibited in MC3T3-E1 ShChk2 cells induced by Dex and when Chk2 was knocked down, the phosphorylation of p53 protein at Ser15 and Ser20 was nearly eliminated. As the phosphorylation of p53 protein at Ser20 typically contributes to the stability of p53 protein, which leads to the phosphorylation of p53 protein at Ser15,[10] we predicted that Chk2 could regulate the phosphorylation of p53 protein at Ser15 and Ser20 and mediate Dex-induced p53 protein stabilization and accumulation. In order to investigate whether the accumulation of p53 mediated by Chk2 was the result of preventing the degradation of p53 protein, MC3T3-E1 ShChk2 cells were treated with MG132 and CHX. The results revealed that there was no effect of Dex on the inhibition of p53 protein degradation in MC3T3-E1 ShChk2 cells under the same conditions (Fig. 4B). Further studies revealed that Chk2 protein enhanced the stability of Dex-induced p53 protein expression. Similarly, the loss of Chk2 led to apoptosis (Fig. 4C) and caspase-3 cleavage (Fig. 4D). These results indicate that the expression of Chk2 protein was essential for the phosphorylation of p53 protein, which in turn increased p53 protein stabilization and accumulation, and thus resulted in cell apoptosis after Dex treatment.

Discussion

Dexamethasone has been reported to induce apoptosis of osteoblasts and exert a modulatory effect on their proliferation.[24] However, the regulation of these mechanisms by Dex has not been explored yet. Therefore, this study revealed a novel biological role of Dex in the induction of cell apoptosis and inhibition of colony formation in MC3T3-E1 cells. The mechanism studies demonstrated that Dex-mediated apoptosis was via the Chk2/p53 pathway. This finding suggests that Chk2/p53 might also serve as a potential intervention in ONFH treatment.

Dexamethasone can upregulate the expression of p53 protein in MC3T3-E1 cells and cause cell apoptosis.[25] However, the role and mechanism of the Chk2/p53 pathway on osteoblasts is yet to be elucidated. Interestingly, our results show that Dex-induced cell apoptosis in MC3T3-E1 cells was mediated by the accumulation of p53 protein. In particular, Dex could promote p53 protein stabilization by inducing Chk2 phosphorylation. Furthermore, our results strongly indicated that Dex can regulate p53 protein by preventing its degradation.

The degradation of p53 protein can be caused by a variety of factors, such as the activation of MDM2, Chk1, Chk2, and ATR.[26–28] Our study demonstrated that MDM2 and Chk1 were not direct regulators of Dex upregulation of p53 protein in MC3T3-E1 cells, but that the activation of Chk2 occurred relatively early. This suggested that Chk2 may involved in the induction of p53 protein by Dex treatment.

Limitations

Our research indicated the molecular mechanisms underlying Dex promotion of osteoblast cell apoptosis. However, there are 2 limitations of this study. First, we did not evaluate other effects of GCs (including Dex) in the treatment of inflammatory or autoimmune diseases. As a side effect of their clinical applications, GCs can cause osteonecrosis and ONFH.[29–31] Previous research had shown that the damaging effects of Dex on osteoblasts and ONFH are due to its role in inhibiting cell proliferation and promoting cell apoptosis.[32,33] Therefore, we only considered the effect of Dex on inhibiting cell proliferation and promoting cell apoptosis. Second, in this study, we demonstrated that Dex can inhibit MC3T3-E1 proliferation and induce apoptosis, but we did not evaluate other pathways in apoptosis induced by Dex. In our previous study, we found that Dex can upregulate the expression of p53 protein in MC3T3-E1 cells, thus causing cell apoptosis.[14] Various studies have shown that the Chk2/p53 pathway can induce growth inhibition and apoptosis.[34,35]

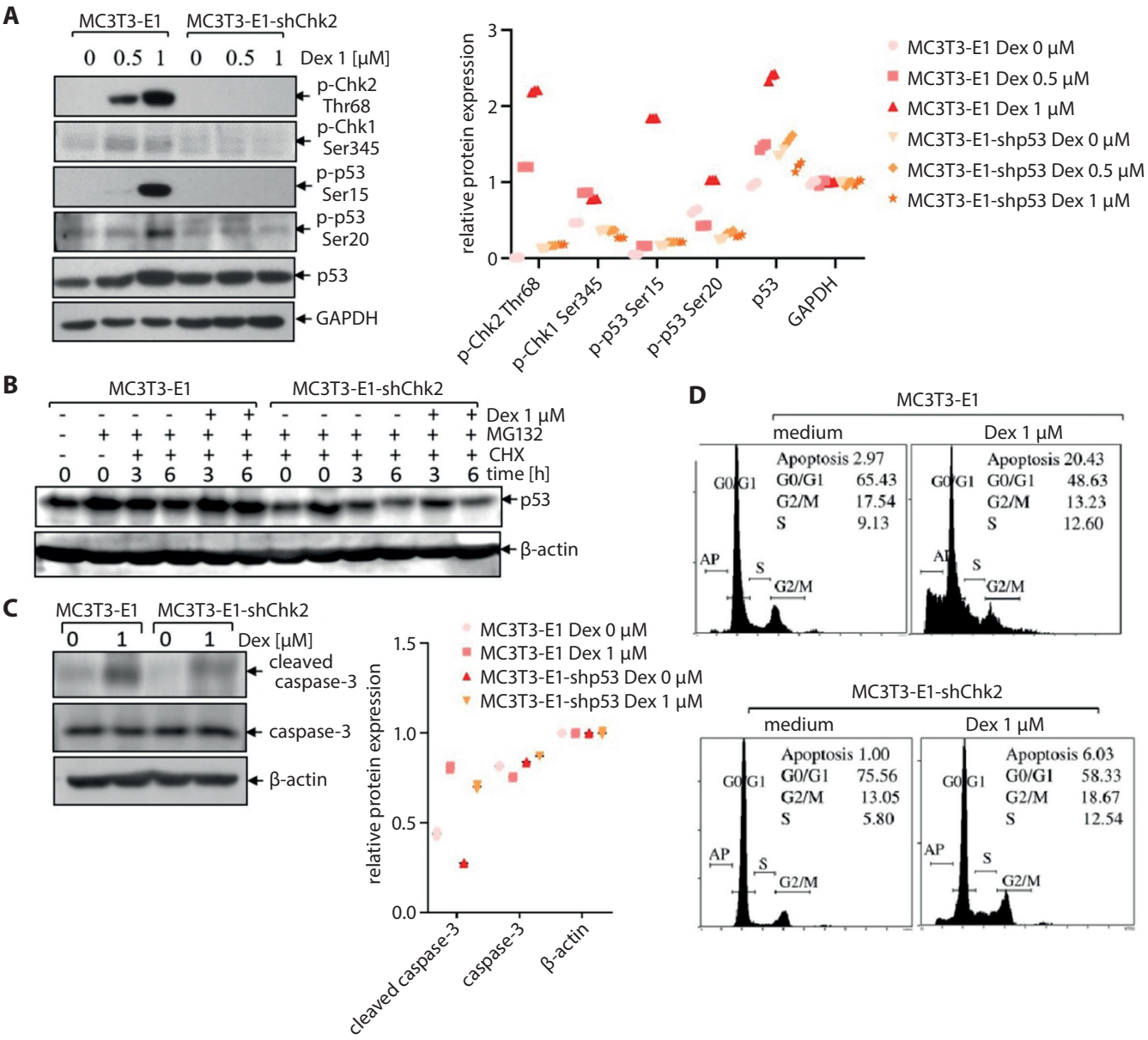

Fig. 4. Checkpoint kinase 2 (Chk2) led to p53-mediated apoptosis during dexamethasone (Dex) treatment. A. Phosphorylation and expression of p53 protein after Dex treatment of MC3T3-E1 ShChk2 cells; B. The effect of Dex inhibition of p53 protein degradation in MC3T3-E1 cells and MC3T3-E1 ShChk2 cells; C. Chk2 mediated Dex-induced p53 protein expression; D. Flow cytometry analysis on the apoptosis-inducing effects on MC3T3-E1 cells and MC3T3-E1 ShChk2 cells after Dex treatment

CHX – cycloheximide; GAPDH – glyceraldehyde-3-phosphate dehydrogenase.

In line with this, our results show that Dex can activate p53-mediated cell apoptosis in MC3T3-E1 cells through the Chk2/p53 signaling pathway. The practical implications of these results need to be further analyzed, particularly in clinical applications.

Conclusions

In summary, our studies demonstrated that Dex could promote cell apoptosis in MC3T3-E1 cells. Our investigation of apoptosis induction showed that Dex mediated the phosphorylation and activation of Chk2. Activated Chk2 leads to the accumulation of p53 protein through the Chk2/p53 signaling pathway, which in turn results in cell apoptosis. Our research can provide a new therapeutic avenue for GC-induced osteoporosis and ONFH.

The flowchart of this study was shown in Fig. 5.

ORCID iDs

Jie Zhu https://orcid.org/0000-0002-7708-7920
Tantan Zhao https://orcid.org/0000-0002-5186-3872
Lunqing Zhu https://orcid.org/0000-0002-3801-9773
Chunhua Yin https://orcid.org/0000-0003-2777-9766
Yao Liu https://orcid.org/0000-0001-9074-4940
Jianfeng Fang https://orcid.org/0000-0003-4647-2145
Hansi Liang https://orcid.org/0000-0002-8798-9610
Yunfang Zhen https://orcid.org/0000-0003-2496-3920

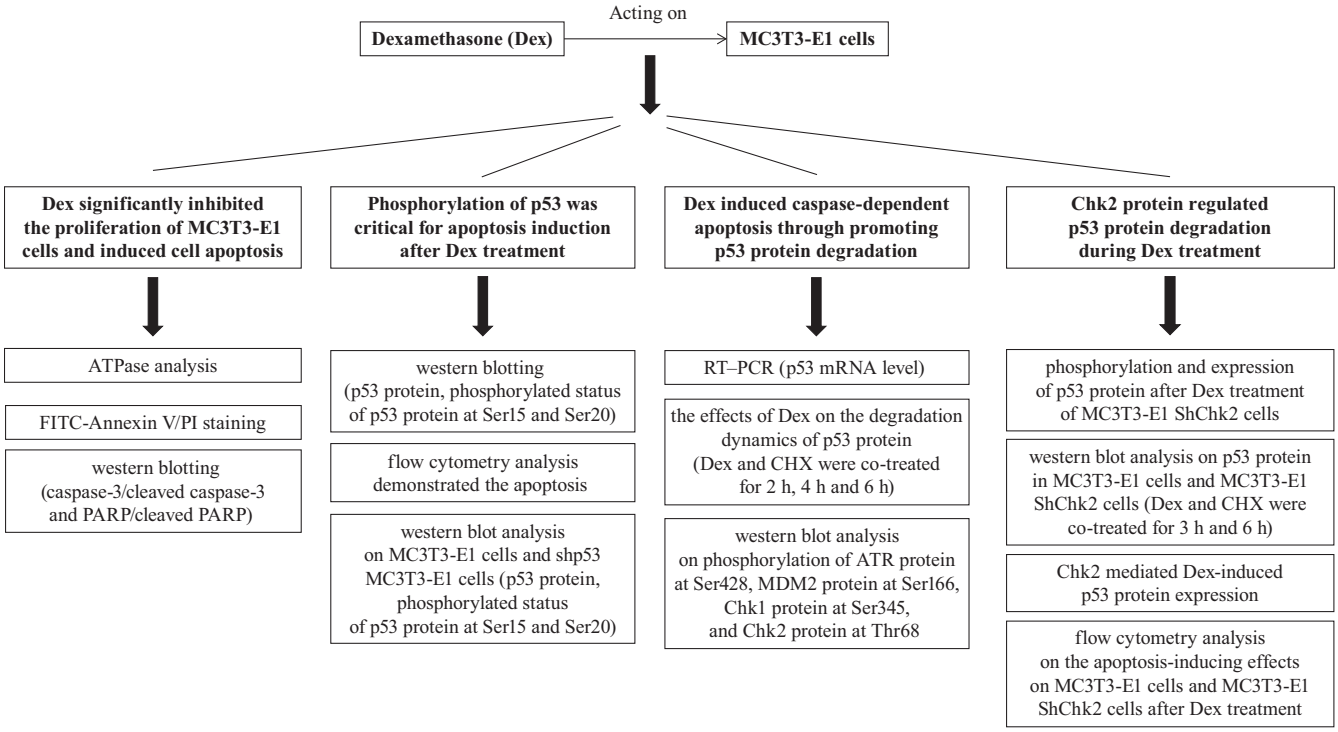

Fig. 5. Flowchart of the study

ATP – adenosine triphosphate; PARP – poly(ADP-ribose) polymerase; RT-PCR – reverse transcription-polymerase chain reaction; CHX – cycloheximide; ATR ataxia telangiectasia mutated kinase and Rad3-related kinase; MDM2 – murine double minute 2.

References

1. Gessi S, Merighi S, Borea PA. Glucocorticoid's pharmacology: Past, present and future. *Curr Pharm Des*. 2010;16(32):3540–3553. doi:10.2174/138161210793797915
2. Balsevich G, Abizaid A, Chen A, Karatsoreos IN, Schmidt MV. Stress and glucocorticoid modulation of feeding and metabolism. *Neurobiol Stress*. 2019;11:100171. doi:10.1016/j.ynstr.2019.100171
3. Adami G, Saag KG. Glucocorticoid-induced osteoporosis: 2019 concise clinical review. *Osteoporos Int*. 2019;30(6):1145–1156. doi:10.1007/s00198-019-04906-x
4. Lane NE. Glucocorticoid-induced osteoporosis: New insights into the pathophysiology and treatments. *Curr Osteoporos Rep*. 2019;17(1):1–7. doi:10.1007/s11914-019-00498-x
5. Buckley L, Humphrey MB. Glucocorticoid-induced osteoporosis. *N Engl J Med*. 2018;379(26):2547–2556. doi:10.1056/NEJMcp1800214
6. Xu J, Gong H, Lu S, Deasey MJ, Cui Q. Animal models of steroid-induced osteonecrosis of the femoral head: A comprehensive research review up to 2018. *Int Orthop*. 2018;42(7):1729–1737. doi:10.1007/s00264-018-3956-1
7. Filla MS, Dimeo KD, Tong T, Peters DM. Disruption of fibronectin matrix affects type IV collagen, fibrillin and laminin deposition into extracellular matrix of human trabecular meshwork (HTM) cells. *Exp Eye Res*. 2017;165:7–19. doi:10.1016/j.exer.2017.08.017
8. Huang Y, Cai GQ, Peng JP, Shen C. Glucocorticoids induce apoptosis and matrix metalloproteinase-13 expression in chondrocytes through the NOX4/ROS/p38 MAPK pathway. *J Steroid Biochem Mol Biol*. 2018;181:52–62. doi:10.1016/j.jsbmb.2018.03.001
9. Deng S, Dai G, Chen S, et al. Dexamethasone induces osteoblast apoptosis through ROS-PI3K/AKT/GSK3β signaling pathway. *Biomed Pharmacother*. 2019;110:602–608. doi:10.1016/j.biopha.2018.11.103
10. Zhang B, Yi J, Zhang CL, et al. MiR-146a inhibits proliferation and induces apoptosis in murine osteoblastic MC3T3-E1 by regulating Bcl2. *Eur Rev Med Pharmacol Sci*. 2017;21(17):3754–3762. PMID:28975995.
11. Mullee LI, Morrison CG. Centrosomes in the DNA damage response: The hub outside the centre. *Chromosome Res*. 2016;24(1):35–51. doi:10.1007/s10577-015-9503-7
12. Matt S, Hofmann TG. The DNA damage-induced cell death response: A roadmap to kill cancer cells. *Cell Mol Life Sci*. 2016;73(15):2829–2850. doi:10.1007/s00018-016-2130-4
13. Shkreta L, Michelle L, Toutant J, Tremblay ML, Chabot B. The DNA damage response pathway regulates the alternative splicing of the apoptotic mediator Bcl-x. *J Biol Chem*. 2011;286(1):331–340. doi:10.1074/jbc.M110.162644
14. Zhen YF, Wang GD, Zhu LQ, et al. P53 dependent mitochondrial permeability transition pore opening is required for dexamethasone-induced death of osteoblasts. *J Cell Physiol*. 2014;229(10):1475–1483. doi:10.1002/jcp.24589
15. Ranjan A, Iwakuma T. Non-canonical cell death induced by p53. *Int J Mol Sci*. 2016;17(12):2068. doi:10.3390/ijms17122068
16. Lee DH, Goldberg AL. Proteasome inhibitors: Valuable new tools for cell biologists. *Trends Cell Biol*. 1998;8(10):397–403. doi:10.1016/S0962-8924(98)01346-4
17. Pommier Y, Marchand C. Interfacial inhibitors of protein–nucleic acid interactions. *Curr Med Chem Anticancer Agents*. 2005;5(4):421–429. doi:10.2174/1568011054222337
18. Appella E, Anderson CW. Post-translational modifications and activation of p53 by genotoxic stresses. *Eur J Biochem*. 2001;268(10):2764–2772. doi:10.1046/j.1432-1327.2001.02225.x
19. Pabla N, Huang S, Mi QS, Daniel R, Dong Z. ATR-Chk2 signaling in p53 activation and DNA damage response during cisplatin-induced apoptosis. *J Biol Chem*. 2008;283(10):6572–6583. doi:10.1074/jbc.M707568200
20. Shieh SY, Ikeda M, Taya Y, Prives C. DNA damage-induced phosphorylation of p53 alleviates inhibition by MDM2. *Cell*. 1997;91(3):325–334. doi:10.1016/S0092-8674(00)80416-X
21. Zhou BP, Liao Y, Xia W, Zou Y, Spohn B, Hung MC. HER-2/neu induces p53 ubiquitination via Akt-mediated MDM2 phosphorylation. *Nat Cell Biol*. 2001;3(11):973–982. doi:10.1038/ncb1101-973
22. Ou YH, Chung PH, Sun TP, Shieh SY. p53 C-terminal phosphorylation by CHK1 and CHK2 participates in the regulation of DNA-damage-induced C-terminal acetylation. *Mol Biol Cell*. 2005;16(4):1684–1695. doi:10.1091/mbc.e04-08-0689

23. Abraham RT. Cell cycle checkpoint signaling through the ATM and ATR kinases. *Genes Dev*. 2001;15(17):2177–2196. doi:10.1101/gad.914401
24. Yanase T, Suzuki S, Goto K, et al. Aromatase in bone: Roles of vitamin D3 and androgens. *J Steroid Biochem Mol Biol*. 2003;86(3–5):393–397. doi:10.1016/S0960-0760(03)00349-2
25. Walia MK, Ho PM, Taylor S, et al. Activation of PTHrP-cAMP-CREB1 signaling following p53 loss is essential for osteosarcoma initiation and maintenance. *eLife*. 2016;5:e13446. doi:10.7554/eLife.13446
26. Chao CCK. Mechanisms of p53 degradation. *Clin Chim Acta*. 2015;438: 139–147. doi:10.1016/j.cca.2014.08.015
27. Haupt Y, Maya R, Kazaz A, Oren M. Mdm2 promotes the rapid degradation of p53. *Nature*. 1997;387(6630):296–299. doi:10.1038/387296a0
28. Rinaldi VD, Bloom JC, Schimenti JC. Oocyte elimination through DNA damage signaling from CHK1/CHK2 to p53 and p63. *Genetics*. 2020;215(2):373–378. doi:10.1534/genetics.120.303182
29. Fowler TW, Acevedo C, Mazur CM, et al. Glucocorticoid suppression of osteocyte perilacunar remodeling is associated with subchondral bone degeneration in osteonecrosis. *Sci Rep*. 2017;7(1):44618. doi:10.1038/srep44618
30. Woolf AD. An update on glucocorticoid-induced osteoporosis. *Curr Opin Rheumatol*. 2007;19(4):370–375. doi:10.1097/BOR.0b013e328133f5c7
31. Henneicke H, Gasparini SJ, Brennan-Speranza TC, Zhou H, Seibel MJ. Glucocorticoids and bone: Local effects and systemic implications. *Trends Endocrinol Metabol*. 2014;25(4):197–211. doi:10.1016/j.tem.2013.12.006
32. Ding H, Wang T, Xu D, Cha B, Liu J, Li Y. Dexamethasone-induced apoptosis of osteocytic and osteoblastic cells is mediated by TAK1 activation. *Biochem Biophys Res Commun*. 2015;460(2):157–163. doi:10.1016/j.bbrc.2015.02.161
33. Ma P, Gu B, Ma J, et al. Glimepiride induces proliferation and differentiation of rat osteoblasts via the PI3-kinase/Akt pathway. *Metabolism*. 2010;59(3):359–366. doi:10.1016/j.metabol.2009.08.003
34. Chen Z, Wang L, Yao D, et al. Wip1 inhibitor GSK2830371 inhibits neuroblastoma growth by inducing Chk2/p53-mediated apoptosis. *Sci Rep*. 2016;6:38011. doi:10.1038/srep38011
35. Zhou J, Zhang C, Sui X, et al. Histone deacetylase inhibitor chidamide induces growth inhibition and apoptosis in NK/T lymphoma cells through ATM-Chk2-p53-p21 signalling pathway. *Invest New Drugs*. 2018;36(4):571–580. doi:10.1007/s10637-017-0552-y

MMP-2 inhibition prevents platelet activation in ischemia/reoxygenation conditions

Kornela Jagoda Hałucha[A–D,F], Marta Banaszkiewicz[B,C,F], Alina Rak-Pasikowska[B,E,F], Iwona Bil-Lula[A,C,E,F]

Division of Clinical Chemistry and Laboratory Hematology, Department of Medical Laboratory Diagnostics, Faculty of Pharmacy with Division of Medical Analytics, Wroclaw Medical University, Poland

A – research concept and design; B – collection and/or assembly of data; C – data analysis and interpretation;
D – writing the article; E – critical revision of the article; F – final approval of the article

Advances in Clinical and Experimental Medicine, ISSN 1899–5276 (print), ISSN 2451–2680 (online) *Adv Clin Exp Med*. 2022;31(12):1375–1384

Address for correspondence
Iwona Bil-Lula
E-mail: iwona.bil-lula@umw.edu.pl

Funding sources
The research was partially performed in the Screening Laboratory of Biological Activity Test and Collection of Biological Material, Faculty of Pharmacy with Division of Medical Analytics, Wroclaw Medical University, Poland, supported by the ERDF Project within the Innovation Economy Operational Programme POIG.02.01.00-14-122/09. This research was financially supported by the Ministry of Health subvention according to number of STM.D010.20.130 from the IT Simple system of Wroclaw Medical University.

Conflict of interest
None declared

Acknowledgements
The authors would like to acknowledge Dr. Aneta Wrzyszcz for her valuable suggestions.

Received on December 17, 2021
Reviewed on March 26, 2022
Accepted on July 22, 2022

Published online on September 22, 2022

Cite as
Hałucha KJ, Banaszkiewicz M, Rak-Pasikowska A, Bil-Lula I. MMP-2 inhibition prevents platelet activation in ischemia/reoxygenation conditions. *Adv Clin Exp Med*. 2022;31(12):1375–1384. doi:10.17219/acem/152286

DOI
10.17219/acem/152286

Abstract

Background. Platelets play a fundamental role in myocardial infarction and the pathogenesis of ischemia/reoxygenation (I/R) injuries. They contain matrix metalloproteinases (MMPs) that are involved in arterial thrombosis. The MMP inhibitor doxycycline has been shown to exert protective effects in I/R injuries involving various organs and mechanisms.

Objectives. To explore the influence of doxycycline on platelet activation and MMP-2 activity during I/R.

Materials and methods. Platelets isolated from the blood of healthy human volunteers were subjected to chemical I/R conditions. The study included aerobic controls (AERO), I/R platelets and I/R platelets pretreated with doxycycline (I/R+D). The concentration of doxycycline used was standardized to 10 μM. The analysis of platelet activation markers and platelet microvesicles (PMVs) was performed using flow cytometry. Adenosine diphosphate (ADP)-induced and collagen-induced aggregation, as well as MMP-2 activity and its concentration in platelets were evaluated.

Results. Doxycycline decreased the expression of activated glycoprotein IIb/IIIa on platelets ($p = 0.043$). Additionally, an increased expression of CD63 was observed in buffers containing PMVs after doxycycline administration ($p = 0.043$). The ADP-dependent aggregation of I/R platelets was significantly lower in comparison to AERO ($p = 0.022$). Furthermore, there was a stronger tendency of enhanced ADP-dependent aggregation in I/R platelets pretreated with doxycycline compared to platelets that underwent I/R without doxycycline. Higher MMP-2 activity was observed in I/R+D platelets compared to I/R platelets ($p < 0.01$).

Conclusions. The inhibition of platelet MMP-2 by doxycycline attenuated platelet activation and protected platelets by preserving their aggregation ability.

Key words: ischemia, reperfusion, platelets, metalloproteinases, doxycycline

Background

In myocardial infarction (MI), platelets participate in thrombus formation and the microembolization from unstable plaque rupture and intravascular intervention. Moreover, in acute MI, the triggered inflammation, in addition to platelet–leukocyte and platelet–endothelium interactions, leads to the release of vasoconstrictor and pro-inflammatory molecules from platelet microvesicles (PMVs) and exosomes.[1] Changes in the shape of platelet and an enhancement in mean platelet volume have been observed in acute MIs.[2] Several studies have revealed that platelets activate and contribute to cardiac ischemia/reoxygenation injury (IRI),[1] critical limb ischemia[3] and ischemic strokes.[4] The impact of platelets on the reperfused myocardium depends on their activation status.[5] The activation of platelets leads to the release of PMVs and granules containing growth factors as well as pro-inflammatory and proapoptotic molecules.[1,6] Platelet microvesicles are membrane fragments from 0.1 μm to 1.0 μm in diameter that form from platelets and other cells due to cell activation or apoptosis. Platelet microvesicles express surface proteins characteristic of platelets, modulate intercellular interactions and have prothrombotic properties.[6] It is well known that platelet activation, aggregation and subsequent thrombus formation play a major role in the pathophysiological process that underlies MIs.

Matrix metalloproteinases (MMPs) are a family of zinc- and calcium-dependent proteolytic enzymes involved in vascular remodeling.[7] Platelets contain MMP-2, which is localized in the cytosol and is translocated to the extracellular space during platelet activation.[8] Platelet-derived MMP-2 amplifies the response of platelets to low concentrations of agonists such as collagen, arachidonic acid and adenosine diphosphate (ADP).[9–11] The MMP-2 is involved in the formation of an atherosclerotic plaque and is released from platelets in vivo after the exposure to a damaged vessel wall at the site of vascular injury.[12] The inactivation of MMP-2 genes in mice has been shown to protect against arterial thrombosis, indicating that MMP-2 plays a promoting role in arterial thrombosis and can lead to the formation of an occlusive thrombus.[11]

Regulation of platelet activation and agonist-induced aggregation by intracellular MMP-2 has been associated with glycoprotein (GP) IIb/IIIa receptors that bind to fibrinogen and von Willebrand factor.[13] Moreover, by binding MMP-2, GP IIb/IIIa receptors facilitate the MMP-2-dependent cleavage of platelet PAR-1 and subsequent platelet activation.[14]

Antiplatelet therapy is widely used with good efficiency in the treatment of MIs and ischemic strokes. Current antiplatelet therapy aimed at preventing cardiac IRI includes a cyclooxygenase (COX) inhibitor – aspirin. However, there is a group of patients resistant to aspirin. This resistance has been correlated with an increased level of plasma oxidative stress markers in patients with coronary artery disease (CAD).[15] Cangrelor and ticagrelor are inhibitors of the P2Y12 receptor and have shown to have protective effects independently of their anti-aggregatory effect.[16,17] The interaction with platelets is required for the cardiac protection of cangrelor.[16] Cardioprotection induced by ticagrelor was related to a ticagrelor-mediated release of sphingosine-1-phosphate and adenosine from platelets.[17] As antiplatelet therapy may have unexpected mechanisms of action and aspirin resistance, there is a need to search for new treatment options against IRI and to learn about new mechanisms of action of currently available drugs.

Doxycycline is a well-documented inhibitor of MMPs due to its ability to bind zinc and calcium ions. It is presumed that doxycycline can inhibit pro-MMP activation by suppressing oxidative stresses.[18] A protective effect of doxycycline was shown in the hearts and kidneys of rats subjected to IRI.[19,20] In addition, the protective role of doxycycline used at subthreshold doses (1 μM) in the combination with subthreshold doses of a myosin light chain 1 (MLC1) phosphorylation inhibitor has been described.[19]

Objectives

Doxycycline is a well-documented inhibitor of MMPs, and platelets contain and release MMP-2 upon activation.[1,2] Since MMP-2 may reinforce a platelet response to agonists such as collagen and ADP in atherosclerotic plaque formation, we aimed to evaluate if the inhibition of MMP-2 in platelets by doxycycline can reduce platelet activation and aggregation. In addition, we evaluated whether doxycycline could potentially reduce arterial thrombus formation during coronary vessel obstruction.

We examined the effects of doxycycline in doses ranging from 5 μM to 30 μM on platelet activation in ischemia/reoxygenation (I/R) conditions in order to establish the lowest effective drug concentration. We explored changes in activation, the release of PMVs, and aggregation of platelets subjected to doxycycline and I/R. We measured MMP-2 concentrations and activity in isolated platelets subjected to I/R to assess the impact of doxycycline on MMP-2 release from platelets.

Materials and methods

Materials

Blood was obtained from 15 healthy human volunteers who had not used any medications for at least 14 days. Blood was collected using the S-Monovette® 10 mL blood collection system containing 106 mM of sodium citrate (Sarstedt, Nümbrecht, Germany). The study was approved by the Ethics Committee of the Wroclaw Medical University, Poland (approval No. KB-165/2020).

Platelet isolation

The isolation of platelets was performed using the method described by Wrzyszcz et al.[21] For platelet isolation, a continuous density gradient medium (OptiPrep™; Sigma-Aldrich, St. Louis, USA) was used. In brief, to prevent platelet activation, a prostacyclin (PGI2; Sigma-Aldrich) was added to the blood (final concentration: 2 µg/mL). To obtain platelet-rich plasma (PRP), the blood was centrifuged at 200 g for 20 min at 22°C. The PRP was then diluted (1 part of PRP per 1 part of HEPES buffer (140 mM NaCl, 20 mM HEPES, pH 7.4)), layered onto the surface of the gradient (3 mL of PRP over 5 mL of density gradient) and centrifuged at 300 g for 20 min at 22°C. We allowed the rotor to decelerate without braking. The suspension was extracted except for the last 0.5 mL just above the pellet of cells (leukocytes, erythrocytes). After collection, the suspension was washed in a HEPES buffer with the addition of PGI2 (final concentration: 0.3 µg/mL). All samples were prepared in the same way. Isolated platelets were resuspended in a stabilizing buffer (5.5 mmol/L HEPES, 63.7 mmol/L $CaCl_2$, 5 mmol/L KCl, 2.1 mmol/L $MgCl_2$, 5.5 mmol/L glucose, and 10 mmol/L taurine enriched with 55 µmol/L $CaCl_2$ and 0.75 mg/mL bovine serum albumin (BSA)). The platelet count of the suspensions was quantified using a KX-21N (Sysmex, Kobe, Japan) hematology analyzer.

Chemical I/R protocol

The I/R procedure was performed on 12-well culture plates with inserts (with 1.0-µm pores and 0.4-µm pores; ThinCert™; Greiner Bio-One, Kremsmünster, Austria) dedicated for multi-well plates, in order to allow or prevent the PMVs from entering through the porous membrane. Additionally, the use of inserts made it possible to not have to centrifuge the platelets after each step of the procedure, which could affect their activation. Freshly isolated blood platelets were suspended in stabilizing buffer and placed in the insert. The buffer was added to the wells. The I/R procedure consisted of 3 stages: stabilization, ischemia and reoxygenation. The study included platelets untreated with I/R (AERO), platelets that underwent I/R, and platelets that underwent I/R with doxycycline (I/R+D) (Fig. 1). The concentration of doxycycline (selected from the range of 5–30 µM) was used to determine the lowest concentration that produced a reduction in the expression of platelet activation markers. The I/R+D platelets were pretreated with doxycycline 5 min before the I/R protocol. Appropriate buffers were added to the wells during the subsequent stages of the experiment, and the inserts with platelets were not removed from the wells for the duration of the experiment. During the first phase, a stabilizing buffer was added to the wells. After 15 min, the buffer was removed and the platelets were exposed to ischemia

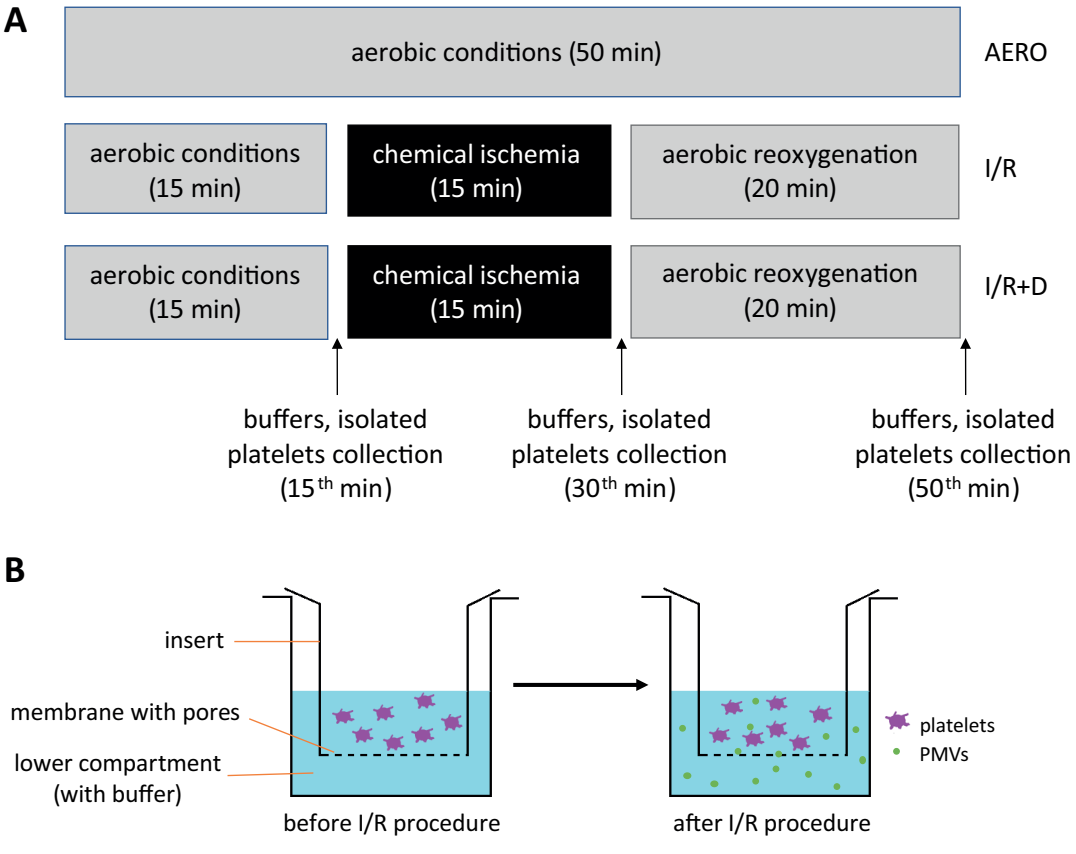

Fig. 1. A. Experimental protocol for aerobic controls (AERO), ischemia/reoxygenation (I/R), and I/R platelets pretreated with doxycycline (I/R+D) groups; B. Platelet microvesicles (PMVs) migrating through the insert with a porous membrane

for 15 min by using a fresh portion of stabilizing buffer with 4.4 mmol/L of 2-deoxyglucose to prevent glycolysis and 4.0 mmol/L of sodium cyanide as a cell respiratory inhibitor. After 15 min, the buffer used for ischemia was removed and a fresh portion of stabilizing buffer was added for 20 min to simulate a reoxygenation process. The buffers and isolated platelets were collected for cytometric analysis before and after ischemia, as well as after reoxygenation. An aggregation of isolated platelets was performed immediately after reoxygenation. The rest of the buffers and isolated platelets were stored at –80°C until further analysis.

Flow cytometry analysis of platelet activation markers

The state of platelet activation was determined by measuring the surface expression of P-selectin (CD62P), activated GP IIb/IIIa (PAC-1) and CD63 antigen. The platelets and the buffers (potentially containing PMVs) were fixed immediately after the collection with 1% paraformaldehyde in phosphate-buffered saline (PBS) for 30 min at 4°C, centrifuged (1200 g for 5 min), washed in PBS, and then resuspended in Stain Buffer (BD Biosciences, Franklin Lakes, USA). The fixed samples were incubated with fluorescently-labeled monoclonal antibodies: fluorescein isothiocyanate conjugated anti-human CD41/CD61 (clone PAC-1), phycoerythrin conjugated anti-human CD62P (clone AK-4), and phycoerythrin-Cy7 conjugated anti-human CD63 antigen (clone H5C6) or a fluorescently labeled nonspecific mouse IgG antibody (isotype control) for 20 min at room temperature (all antibodies were from BioLegend, San Diego, USA). Finally, the samples were washed, centrifuged, resuspended in PBS, and analyzed within 3 h. The PMVs were analyzed by setting gates based on 0.5-µm calibration beads. The analysis was performed using CyFlow Space (Sysmex) and 20,000 events were collected per sample.

Platelet aggregation

Platelet aggregation was carried out on each collected platelet suspension using light transmission aggregometry (Chrono-Log Corporation, Havertown, USA). Aggregation was performed according to the Platelet Physiology Subcommittee of the International Society on Thrombosis and Haemostasis (SSC/ISTH) recommendations for the standardization of light transmission aggregometry at 37°C, with constant stirring of platelet samples at 1000 rpm using a disposable stirrer.[22] Suspensions of platelets were adjusted to a count of 250×10^3/µL. After 1 min of incubation with fibrinogen (Sigma-Aldrich; final concentration: 200 µg/mL) at 37°C, the aggregation was induced by adding the appropriate agonist. The following agonists were used: 5.02 µg/mL collagen and 10.26 µM ADP (all from HYPHEN BioMed, Neuville-sur-Oise, France). The aggregation curve and the maximum platelet aggregation were recorded over 6 min after the agonist addition.

Gelatin zymography

The activity of MMP-2 was evaluated with gelatin zymography of the platelets after the I/R procedure. The samples were thawed just before use and protein concentrations were determined using the Bradford Protein Assay (Bio-Rad, Hercules, USA). Gelatin zymography was performed with the modification, as previously described.[23] After electrophoresis (Mini-Protean II; Bio-Rad) in 7.5% sodium dodecyl sulfate–polyacrylamide gel electrophoresis (SDS-PAGE) with copolymerized gelatin (1 mg/mL; Sigma-Aldrich), the gels were washed 3 times in 2.5% Triton X-100 for 20 min to remove SDS and then incubated in an enzyme assay buffer (0.05 M Tris-HCl, pH 7.5, 5 mM $CaCl_2$, 0.2 M NaCl, 0.05% NaN_3) at 37°C for 18 h. After incubation, the gels were stained with a mixture of 0.3% Coomassie brilliant blue (CBB) R-250 and 0.2% CBB G-250. The gels were scanned using a densitometer (GS-800; Bio-Rad) and analyzed based on standard activity using Quantity One software (Bio-Rad). The relative activity of MMP-2 was expressed in arbitrary units (AU) as an activity per µg of total protein.

Platelet homogenization

Platelet pellets were suspended in a homogenization buffer (150 mM NaCl, 50 mM Tris-HCl pH 7.4, 1% Triton® X-100, Protease Inhibitor Cocktail without ethylenediaminetetraacetic acid (EDTA) set III (Sigma-Aldrich)) on ice. The cells underwent 3 cycles of freezing in liquid nitrogen and thawing at 37°C, and then were homogenized mechanically on ice (3 × 10 s) using a hand-held homogenizer. Cell homogenates were centrifuged for 5 min (14,000 g at 4°C) to collect the supernatant. The supernatants were stored at –80°C and thawed prior to analysis.

Analysis of MMP-2 concentrations in platelets

The MMP-2 content of platelet homogenates was measured using the quantitative Quantikine enzyme-linked immunosorbent assay (ELISA) Assay for Total MMP-2 (R&D Systems, Minneapolis, USA) according to the manufacturer's instructions. Before ELISA, total protein concentrations were measured using the Bradford Protein Assay (Bio-Rad). The MMP-2 concentrations in platelets were expressed as ng per µg of total protein.

Statistical analyses

Statistical analyses of the results were performed in Statistica 13 (StatSoft Inc., Tulsa, USA). Only the zymography results showed a normal distribution (K-S test $p > 0.2$; Lilliefors correction $p > 0.2$). The F test to check the variance homogeneity was performed, the variance of the zymography results was homogeneous ($p = 0.893$, $F = 1.155$).

The results were then analyzed using the appropriate test: parametric t-test (normal data distribution) and nonparametric (non-normal data distribution) Friedman's analysis of variance (ANOVA) by ranks test with the Dunn's post hoc test or paired Wilcoxon test. The correlation was assessed using the Spearman's test. The results were expressed as mean ± standard error of the mean (M ±SEM). A value of $p < 0.05$ was considered statistically significant.

Results

Working doxycycline concentrations

The surface expression of activated GP IIb/IIIa was significantly lower in I/R+D platelets compared to I/R platelets in the following concentrations of doxycycline: 30 μM, 20 μM and 10 μM (paired Wilcoxon test: $p = 0.046$, $T = 1$; $p = 0.025$, $T = 2$; and $p = 0.036$, $T = 3$, respectively; Fig. 2). Moreover, the surface expression of P-selectin was significantly lower in I/R+D platelets compared to I/R platelets in a concentration of 30 μM (Friedman's ANOVA by ranks test: $p = 0.011$, $\chi^2 = 9$, degrees of freedom (df) = 2) and 20 μM (Friedman's ANOVA by ranks test: $p = 0.030$, $\chi^2 = 7$, df = 2), as was CD63 in concentration of 30 μM (Friedman ANOVA by ranks test: $p = 0.042$, $\chi^2 = 6.333$, df = 2, data not shown). A decreased expression of the above markers was not observed for platelets pretreated with 5 μM of doxycycline. Therefore, the lowest active drug concentration used in the study was 10 μM, based on the reduction of the expression of GP IIb/IIIa receptor on the platelet's surface.

An influence of doxycycline on surface expression of platelet activation markers

The decrease in activated GP IIb/IIIa surface expression in I/R+D platelets compared to I/R platelets of approx. 7.5% (paired Wilcoxon test: $p = 0.043$, $T = 0$) was

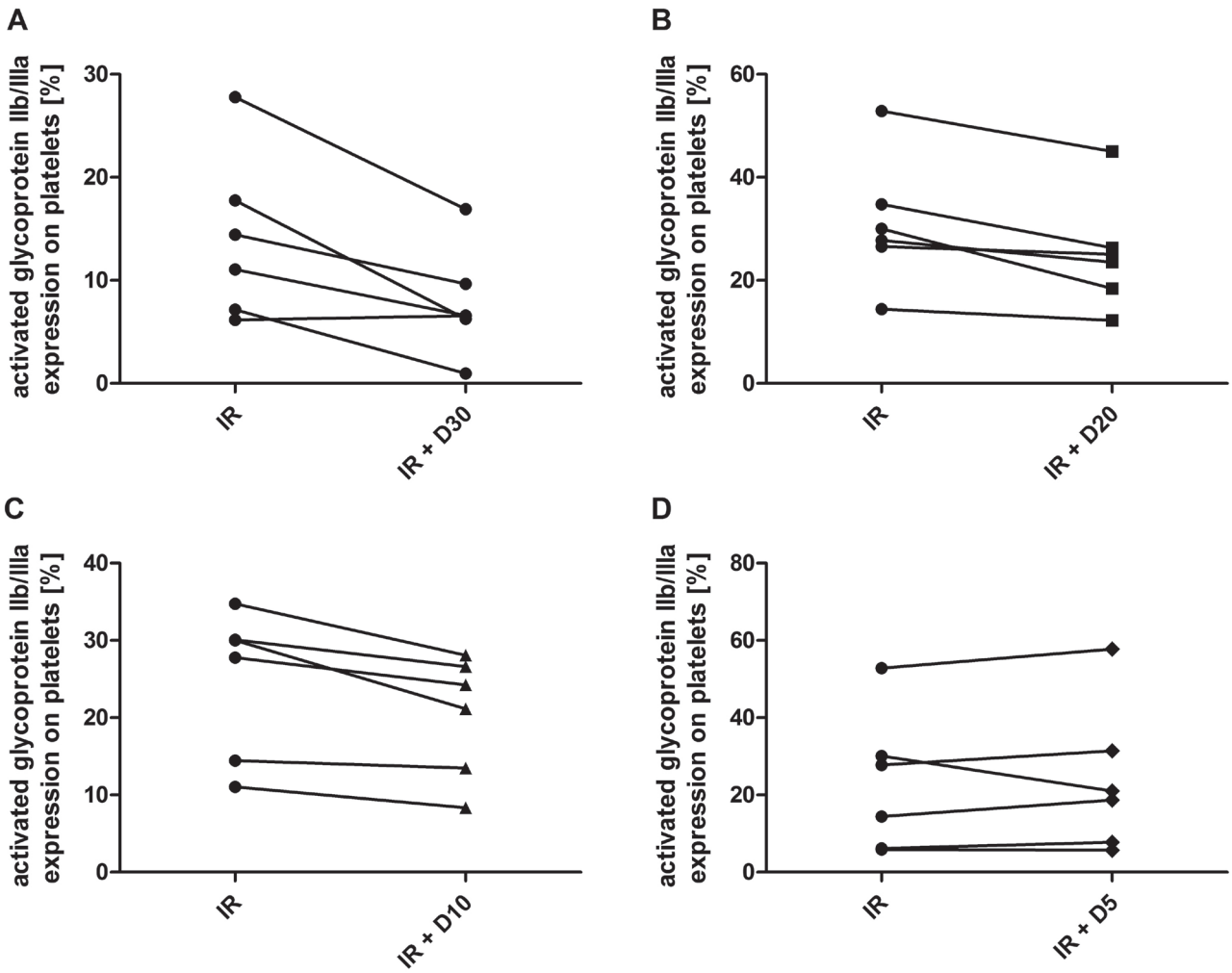

Fig. 2. Expression of activated glycoprotein IIb/IIIa on platelets pretreated with different concentrations of doxycycline: 30 μM (A), 20 μM (B), 10 μM (C), and 5 μM (D) after the ischemia/reoxygenation (I/R) procedure. The differences between I/R and 30 μM, 20 μM, and 10 μM of doxycycline (paired Wilcoxon test): A. 30 μM: $p = 0.046$, $T = 1$; B. 20 μM: $p = 0.025$, $T = 2$; C. 10 μM: $p = 0.036$, $T = 3$; n = 6/group

AERO – aerobic control; I/R – platelets underwent ischemia/reoxygenation; I/R+D30/20/10 – platelets underwent I/R following pretreatment with 30 μM, 20 μM and 10 μM of doxycycline, respectively.

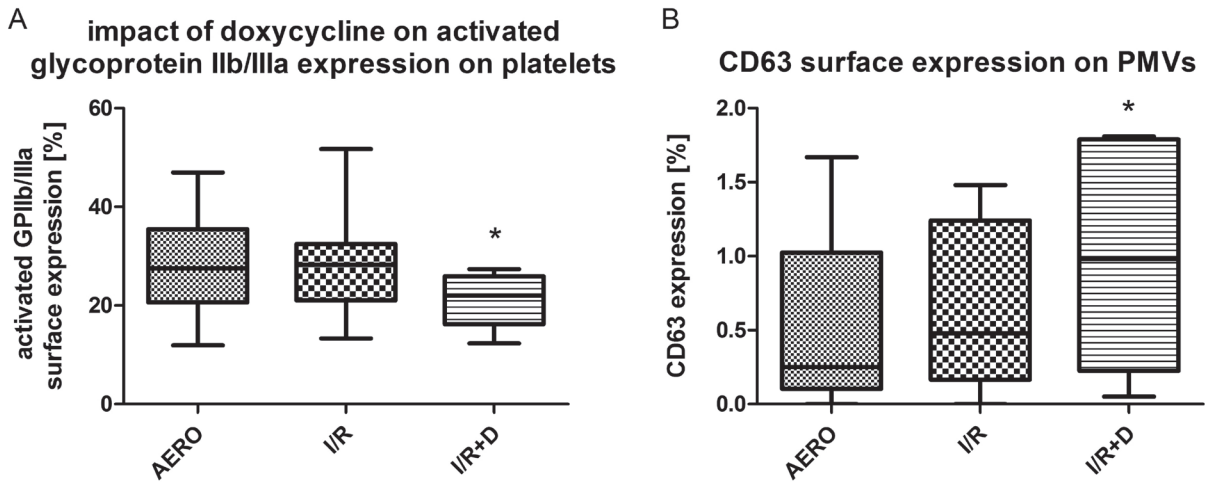

Fig. 3. Expression of activated glycoprotein (GP) IIb/IIIa on platelets after the ischemia/reoxygenation (I/R) procedure (A) and of CD63 on platelet microvesicles (PMVs) in the buffers after I/R procedure using pores with a diameter of 1.0 μm (B)

AERO – aerobic control; I/R – platelets underwent ischemia/reoxygenation; I/R+D – platelets underwent I/R following pretreatment with 10 μM of doxycycline; * $p < 0.05$. Data are expressed as median (middle line), box as 25th–75th percentiles, whiskers indicate minimum and maximum values (paired Wilcoxon test): A. $p = 0.043$, $T = 0$, $n = 7$/group; B. $p = 0.043$, $T = 0$, $n = 5$/group.

observed (Fig. 3A). Changes in the binding of P-selectin (paired Wilcoxon test: $p = 0.075$, $T = 2$) and CD63 (paired Wilcoxon test: $p = 0.463$, $T = 7$) based on the platelets exposure to doxycycline was not observed.

Interesting results were obtained after the last step of the procedure. Cytometric analysis of the buffers showed an increased surface expression of CD63 on PMVs after using inserts with a pore diameter of 1.0 μm in the I/R+D series compared to the I/R series (paired Wilcoxon test: $p = 0.043$, $T = 0$; Fig. 3B). No significant changes in CD63 surface expression were observed in buffers after using inserts with a pore diameter of 0.4 μm, which significantly reduced the transfer of PMVs into the buffer. In addition, there was a trend towards a higher expression of activated GP IIb/IIIa and P-selectin in buffers analyzed after the last step of the procedure in the I/R+D series compared to the I/R series, regardless of the diameter of insert used.

An influence of I/R and doxycycline on platelet aggregation

The aggregation was performed in platelets taken from inserts with a pore diameter of 1.0 μm, which significantly reduced the presence of PMVs in the inserts. Adenosine diphosphate (ADP)-dependent aggregation of platelets that underwent I/R and I/R with doxycycline was significantly lower in comparison to aerobic controls (Friedman's ANOVA by ranks test: $p = 0.022$, $\chi^2 = 7.684$, $df = 2$; Dunn's multiple comparisons post hoc tests: I/R compared to AERO: $p = 0.0003$, I/R+D compared to AERO: $p = 0.0417$). Additionally, there was a strong tendency for an enhanced ADP-dependent aggregation of I/R+D platelets compared to I/R platelets. The collagen-dependent aggregation showed no significant changes after the use of doxycycline (Fig. 4).

An impact of doxycycline on MMP-2 activity and concentration in platelets

Zymogram analysis revealed a 36% higher MMP-2 activity in I/R+D platelets compared to I/R platelets (t-test: $p = 0.007$, $t = 6.771$, $df = 3$) when 1.0-μm diameter inserts were used (potential MMP-2 in PMVs was eliminated; Fig. 5A). The examination of MMP-2 concentrations in platelets revealed a strong tendency (Friedman's ANOVA by ranks test: $p = 0.091$, $\chi^2 = 4.8$, $df = 2$) for higher MMP-2 levels in platelets treated with doxycycline (Fig. 5B). Additionally, a correlation between MMP-2 activity and the expression of activated GP IIb/IIIa on I/R+D platelets was observed but was not significant due to the small sample size ($p = 0.233$, Fig. 6). Interestingly, the use of a 0.4-μm pore size insert did not change the MMP-2 activity in platelets between series. Additionally, no differences in MMP-2 activity were noticed between the studied groups after the ischemia stage. The activity and concentration of MMP-2 were undetectable in buffers.

Discussion

The protective effects of doxycycline against ischemia have been shown to involve various organs and mechanisms. Doxycycline displays a protective effect by inhibiting MMP-2 in myocardial IRI studies.[19] In cerebral ischemia, the protection of doxycycline was associated with MMP-9, MMP-2 and PKCδ inhibition and upregulation of tight junction proteins.[24,25] Another protective mechanism of doxycycline was presented in a model using rat hepatocytes, where the protection against hypoxia and cell death was associated with the inhibition of mitochondrial calcium uniporters.[26] Tetracyclines have therapeutic

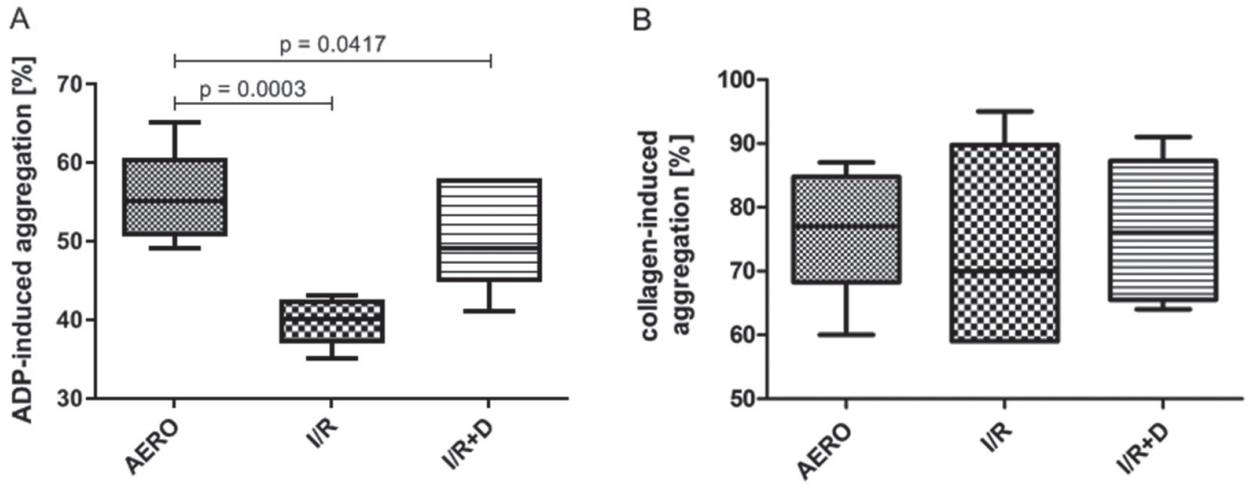

Fig. 4. Platelet aggregation after the ischemia/reoxygenation (I/R) procedure induced by adenosine diphosphate (ADP) (A) and collagen (B)

AERO – aerobic control; I/R – platelets underwent ischemia/reoxygenation; I/R+D – platelets underwent I/R following pretreatment with 10 μM of doxycycline. Data are expressed as median (middle line), box as 25th–75th percentiles, whiskers indicate minimum and maximum values; Friedman analysis of variance (ANOVA) by ranks test (A): $\chi^2 = 7.684$, df = 2, p = 0.022; Dunn's multiple comparisons post hoc test: I/R compared to AERO: p = 0.0003; I/R+D compared to AERO: p = 0.0417; n = 6/group (A); n = 6/group (B).

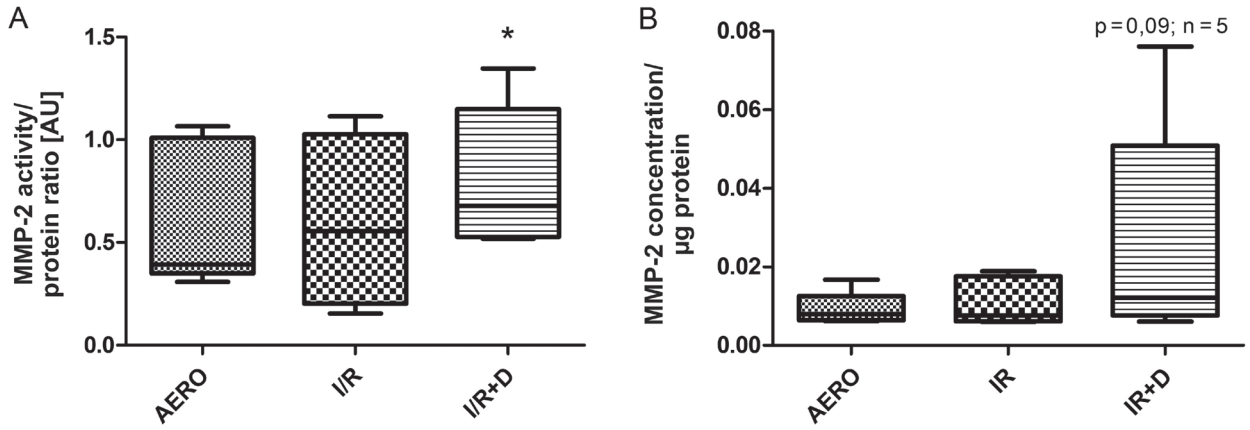

Fig. 5. The MMP-2 activity (A) and concentration (B) in platelets normalized to protein concentrations

AERO – aerobic control; I/R – platelets underwent ischemia/reoxygenation; I/R+D – platelets underwent I/R following pretreatment with 10 μM of doxycycline; * p < 0.05. Data are expressed as median (middle line), box as 25th–75th percentiles, whiskers indicate minimum and maximum values; A. t-test: p = 0.007, t = 6.771, df = 3; B. Friedman analysis of variance (ANOVA) by ranks test: p = 0.091, $\chi^2 = 4.8$, df = 2; I/R+D compared to AERO and I/R; n = 5/group (A); n = 5/group (B).

potential in cardiovascular diseases, especially in cardiac IRI, due to the involvement of MMP-2 in the degradation of cardiac contractile proteins, including troponin I.[27] The MMP-2 inhibition by doxycycline improved the recovery of cardiac mechanical function and led to a reduced endothelial permeability in cardiac IRI.[27] Additionally, doxycycline was able to protect cardiac tissue using a much lower concentration when combined with myosin light chain kinase inhibitors than doxycycline alone.[19] In addition to cardiac IRI, the protective effects of doxycycline against IRI have also been demonstrated in the kidneys and the nervous system.[24,28] In a rat stroke model, doxycycline preserved the function of blood–brain barrier and attenuated cerebral infarction.[24] The numerous in vitro and animal model studies suggesting that doxycycline can protect various organs against IRI and cell death have resulted

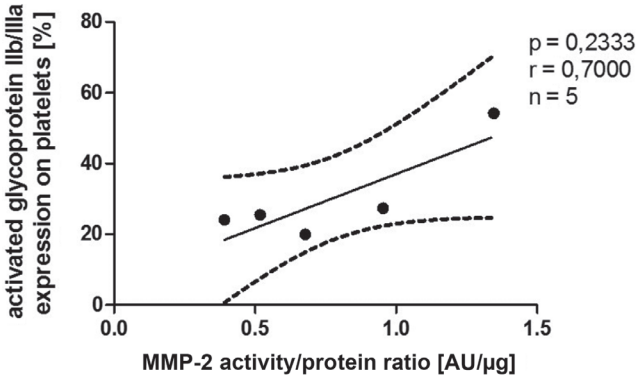

Fig. 6. Correlation between MMP-2 activity in platelets and activated glycoprotein IIb/IIIa expression on platelets pretreated with doxycycline after the ischemia/reoxygenation (I/R) procedure

Spearman's correlation: p = 0.233, r = 0.7, n = 5.

in clinical trials evaluating doxycycline in the treatment of I/R. Patients with ST-elevation myocardial infarction (STEMI) and left ventricular (LV) dysfunction treated with timely primary percutaneous intervention and short-term treatment with doxycycline were shown to have decreased infarct sizes and severities and a reduction in LV dysfunction and remodeling.[29] These changes were associated with plasma levels of tissue inhibitors of metalloproteinase 2 (TIMP-2), since doxycycline therapy resulted in higher plasma levels of TIMP-2.[29] In patients with active CAD, subantimicrobial doses of doxycycline reduced the levels of C-reative protein (CRP), interleukin 6 (IL-6) and pro-MMP-9. The authors suggested that doxycycline may potentially exert beneficial effects on inflammation and prevent coronary plaque rupture events.[30]

In this study, we demonstrated that doxycycline decreased platelet activation in I/R conditions. Doxycycline reduces platelet activation by decreasing the expression of GP IIb/IIIa on platelets. At the moment, we do not know the mechanism of action of doxycycline. In our study, we demonstrated that I/R platelets pretreated with doxycycline presented higher activity and concentration of MMP-2 than I/R platelets without doxycycline. The MMP-2 is released from platelets as a result of their activation.[8] Moreover, MMP-2 was shown to regulate platelet activation and aggregation by the interaction between MMP-2 and GP IIb/IIIa.[13] Our findings confirmed that the mechanism of doxycycline underlying platelet activity is based on the interaction of MMP-2 and platelet GP IIb/IIIa in I/R conditions. Furthermore, the released MMP-2 mediates the activation of consecutive platelets by increasing the expression of P-selectin, one of the platelet activation markers.[31] The increased activity and concentration of MMP-2 in platelets subjected to I/R+D, as well as the lack of increase in the concentration and activation of MMP-2 in the extracellular space and the decreased activity of platelets, prove the mechanism of action of doxycycline in our model. Similar results were demonstrated in the in vitro model of knockout mice, MMP-2$^{-/-}$, where the inactivation of the *MMP-2* gene impaired P-selectin expression and decreased the formation of platelet/leukocyte aggregates upon in vivo activation.[11] We showed that doxycycline's mechanism of action on platelets arises from the blocking of MMP-2 release from platelets, leading to a decrease in the expression of activated GP IIb/IIIa on platelets, a key player in thrombus formation contributing to MI. The intracellular-active MMP-2 was shown to affect the activation and aggregation of platelets through the hydrolytic activation of talin, which is associated with the activation of GP IIb/IIIa.[13] Platelets release pro-MMP-2 and the active form of MMP-2 at the site of vascular damage in vivo. The amount of MMP-2 released locally is capable of enhancing the response of platelets to a stimulus.[12] Additionally, platelets are a major source of MMP-2 in acute coronary syndrome (ACS) patients.[31] The MMP-2 contributed to cardiac contractile dysfunction following I/R through the degradation of cardiac contractile proteins. We have shown that doxycycline prevents platelet activation by inhibiting MMP-2 release. Given the participation of MMP-2 in the degradation of cardiac contractile proteins and the fact that platelets were the source of MMP-2, it seems that doxycycline may prevent cardiac injury through the regulation of platelet MMP-2.

Previous data have shown that MMP-2 released from platelets was able to facilitate ADP-, collagen- and thrombin-induced aggregation, although MMP-2 alone did not induce resting platelet aggregation.[10] On the other hand, high concentrations of MMP-2 inhibited collagen-induced aggregation of platelets.[9] We demonstrated that doxycycline did not affect collagen-induced platelet aggregation. Our results are partially consistent with a study using healthy rats, where intravenous administration of doxycycline resulted in no changes in ADP and collagen-induced platelet aggregation after 15 min.[32] Our results also revealed that doxycycline had a strong tendency to enhance ADP-induced platelet aggregation in I/R. This finding is opposite to another study using healthy dogs, in which doxycycline administered at therapeutic antimicrobial concentrations had no effect on platelet aggregation using 2 agonists: ADP and platelet-activating factor (PAF).[33] Another study reported a positive correlation between levels of ADP-induced aggregation and GP IIb/IIIa content in healthy volunteers and patients with ACS within the first hour upon admission to the hospital. However, after a few days, there was no correlation between ADP-induced aggregation and GP IIb/IIIa content in ACS patients.[34] Discrepancies in the results obtained by us and other researchers may be both due to the dose of doxycycline and the final concentration of agonist. Additionally, in our research, in addition to the use of doxycycline, platelets were also exposed to I/R, which undoubtedly affected them in a different way than after the use of doxycycline alone. Also, collagen is a strong agonist. Therefore, it is possible that slight changes in platelet aggregation caused by doxycycline may not have significantly affected their response to this agonist. We showed that ADP-induced platelet aggregation capacity decreased when platelets were subjected to I/R and I/R with doxycycline compared to platelets in aerobic conditions. Interestingly, I/R platelets pretreated with doxycycline presented a strong tendency to increase ADP-induced platelet aggregation capacity compared to I/R platelets without the drug. It seems that as a result of I/R, the aggregation capacity of platelets is reduced and their function is impaired, similar to the case of, for example, the storage of platelets.[35] At the same time, the use of doxycycline had a protective effect on the maintenance of platelet function in I/R.

Platelets microvesicles, as mentioned, are released from platelets during their activation in response to stimulants such as oxidative stress.[6] Vélez et al. showed that in STEMI, the PMV fibrinogen is upregulated; therefore, PMVs may be involved in the excessive platelet aggregation responsible

for atherothrombosis.[36] Jung et al. showed that in STEMI patients, circulating PMV levels are correlated with the degree of ischemia.[37] In this research, we used inserts with 2 different pore diameters: 1.0 μm to allow the PMVs enter the buffers and 0.4 μm to prevent penetration by most of the PMVs. For this reason, the use of the appropriate pore size allowed us to study the changes resulting from the presence or absence of PMVs, since MI triggers PMVs, which contain pro-inflammatory, proapoptotic and prothrombotic properties.[6] By using inserts allowing the separation of platelets from PMVs, we confirmed the release of PMVs in I/R conditions. We demonstrated that platelets pretreated with doxycycline showed enhanced CD63 expression on PMVs after I/R in comparison to PMVs from platelets without doxycycline when 1.0-μm inserts were used. According to our knowledge, there is no evidence explaining the interaction between CD63 and doxycycline. Tetraspanin CD63, present on lysosomes and membranes of dense granules in resting platelets, is expressed on platelet membranes as a result of their activation. The CD63 is a common platelet-derived exosomal marker that is also present on PMVs.[6,38] However, pharmacotherapy, especially antiplatelet drugs, have been shown to reduce the level of PMVs released.[6] This effect may be dose-dependent since low-dose acetylsalicylic acid therapy did not reduce the release of PMVs into the microcirculation.[39] Additionally, PMVs may be a potential biomarker for the response to antiplatelet therapy. As in the case of clopidogrel, increased levels of circulating PMVs were observed in ACS patients with a high on-treatment platelet reactivity compared to patients with a low on-treatment reactivity on clopidogrel.[40] In our model, we observed an increase in the expression of CD63 on PMVs, which may be related to concentrations of doxycycline being not sufficient to reduce the release of PMVs.

Enhanced activation and aggregation of platelets is a well-established component of the pathophysiology of MIs. This study revealed a new possibility for the application of doxycycline in antiplatelet therapy.

Limitations

A limitation of our study is the small sample size, which could have affected the results. Therefore, further research on this topic should be based on a larger number of cases.

Conclusions

In our research, we showed that the inhibition of platelet MMP-2 by doxycycline attenuated platelet activation and protected platelets by preserving their aggregation ability. The use of doxycycline in cardiac IRI may indicate a two-fold benefit: first, protection of cardiac contractile proteins, and second, prevention of platelet activation and unwanted aggregation. Doxycycline should be taken into consideration for antiplatelet therapy and MI prevention.

ORCID IDs

Kornela Jagoda Hałucha https://orcid.org/0000-0002-0465-4912
Marta Banaszkiewicz https://orcid.org/0000-0002-1248-3244
Alina Rak-Pasikowska https://orcid.org/0000-0002-6864-043X
Iwona Bil-Lula https://orcid.org/0000-0002-2769-0166

References

1. Ziegler M, Wang X, Peter K. Platelets in cardiac ischaemia/reperfusion injury: A promising therapeutic target. *Cardiovasc Res*. 2019; 115(7):1178–1188. doi:10.1093/cvr/cvz070
2. Amraotkar AR, Song DD, Otero D, et al. Platelet count and mean platelet volume at the time of and after acute myocardial infarction. *Clin Appl Thromb Hemost*. 2017;23(8):1052–1059. doi:10.1177/1076029616683804
3. Wisman PP, Teraa M, de Borst GJ, Verhaar MC, Roest M, Moll FL. Baseline platelet activation and reactivity in patients with critical limb ischemia. *PLoS One*. 2015;10(7):e0131356. doi:10.1371/journal.pone.0131356
4. Schmalbach B, Stepanow O, Jochens A, Riedel C, Deuschl G, Kuhlenbäumer G. Determinants of platelet-leukocyte aggregation and platelet activation in stroke. *Cerebrovasc Dis*. 2015;39(3–4):176–180. doi:10.1159/000375396
5. Mirabet M, Garcia-Dorado D, Inserte J, et al. Platelets activated by transient coronary occlusion exacerbate ischemia-reperfusion injury in rat hearts. *Am J Physiol Heart Circ Physiol*. 2002;283(3):H1134–H1141. doi:10.1152/ajpheart.00065.2002
6. Badimon L, Suades R, Fuentes E, Palomo I, Padró T. Role of platelet-derived microvesicles as crosstalk mediators in atherothrombosis and future pharmacology targets: A link between inflammation, atherosclerosis, and thrombosis. *Front Pharmacol*. 2016;7:293. doi:10.3389/fphar.2016.00293
7. Galis Z, Khatri J. Matrix metalloproteinases in vascular remodeling and atherogenesis: the good, the bad, and the ugly. *Circ Res*. 2002;90:251–262. doi:10.1161/hh0302.105345
8. Sawicki G, Sanders E, Salas E, Wozniak M, Rodrigo J, Radomski M. Localization and translocation of MMP-2 during aggregation of human platelets. *Thromb Haemost*. 1998;80(11):836–839. doi:10.1055/s-0037-1615367
9. Sawicki G, Salas E, Murat J, Miszta-Lane H, Radomski MW. Release of gelatinase A during platelet activation mediates aggregation. *Nature*. 1997;386(6625):616–619. doi:10.1038/386616a0
10. Falcinelli E, Guglielmini G, Torti M, Gresele P. Intraplatelet signaling mechanisms of the priming effect of matrix metalloproteinase-2 on platelet aggregation. *J Thromb Haemost*. 2005;3(11):2526–2535. doi:10.1111/j.1538-7836.2005.01614.x
11. Momi S, Falcinelli E, Giannini S, et al. Loss of matrix metalloproteinase 2 in platelets reduces arterial thrombosis in vivo. *J Exp Med*. 2009; 206(11):2365–2379. doi:10.1084/jem.20090687
12. Falcinelli E, Giannini S, Boschetti E, Gresele P. Platelets release active matrix metalloproteinase-2 in vivo in humans at a site of vascular injury: Lack of inhibition by aspirin. *Br J Haematol*. 2007;138(2):221–230. doi:10.1111/j.1365-2141.2007.06632.x
13. Soslau G, Mason C, Lynch S, et al. Intracellular matrix metalloproteinase-2 (MMP-2) regulates human platelet activation via hydrolysis of talin. *Thromb Haemost*. 2014;111(1):140–153. doi:10.1160/TH13-03-0248
14. Sebastiano M, Momi S, Falcinelli E, Bury L, Hoylaerts MF, Gresele P. A novel mechanism regulating human platelet activation by MMP-2–mediated PAR1 biased signaling. *Blood*. 2017;129(7):883–895. doi:10.1182/blood-2016-06-724245
15. Kranzhofer R, Ruef J. Aspirin resistance in coronary artery disease is correlated to elevated markers for oxidative stress but not to the expression of cyclooxygenase (COX) 1/2, a novel COX-1 polymorphism or the PIA 1/2 polymorphism. *Platelets*. 2006;17(3):163–169. doi:10.1080/09537100500441101
16. Cohen MV, Yang XM, White J, Yellon DM, Bell RM, Downey JM. Cangrelor-mediated cardioprotection requires platelets and sphingosine phosphorylation. *Cardiovasc Drugs Ther*. 2016;30(2):229–232. doi:10.1007/s10557-015-6633-2
17. Penna C, Aragno M, Cento AS, et al. Ticagrelor conditioning effects are not additive to cardioprotection induced by direct nlrp3 inflammasome inhibition: Role of RISK, NLRP3, and redox cascades. *Oxid Med Cell Longev*. 2020;2020:1–12. doi:10.1155/2020/9219825

18. Ramamurthy NS, Vernillo AT, Greenwald RA, et al. Reactive oxygen species activate and tetracyclines inhibit rat osteoblast collagenase. *J Bone Miner Res*. 1993;8(10):1247–1253. doi:10.1002/jbmr.5650081013
19. Cadete VJJ, Sawicka J, Bekar LK, Sawicki G. Combined subthreshold dose inhibition of myosin light chain phosphorylation and MMP-2 activity provides cardioprotection from ischaemic/reperfusion injury in isolated rat heart. *Br J Pharmacol*. 2013;170(2):380–390. doi:10.1111/bph.12289
20. Cortes AL, Gonsalez SR, Rioja LS, et al. Protective outcomes of low-dose doxycycline on renal function of Wistar rats subjected to acute ischemia/reperfusion injury. *Biochim Biophys Acta Mol Basis Dis*. 2018;1864(1):102–114. doi:10.1016/j.bbadis.2017.10.005
21. Wrzyszcz A, Urbaniak J, Sapa A, Woźniak M. An efficient method for isolation of representative and contamination-free population of blood platelets for proteomic studies. *Platelets*. 2017;28(1):43–53. doi:10.1080/09537104.2016.1209478
22. Cattaneo M, Cerletti C, Harrison P, et al. Recommendations for the standardization of light transmission aggregometry: A consensus of the working party from the Platelet Physiology Subcommittee of SSC/ISTH. *J Thromb Haemost*. 2013;11(6):1183–1189. doi:10.1111/jth.12231
23. Krzywonos-Zawadzka A, Franczak A, Sawicki G, Bil-Lula I. Mixture of MMP-2, MLC, and NOS inhibitors affects NO metabolism and protects heart from cardiac I/R injury. *Cardiol Res Pract*. 2020;2020:1561478. doi:10.1155/2020/1561478
24. Wang Z, Xue Y, Jiao H, Liu Y, Wang P. Doxycycline-mediated protective effect against focal cerebral ischemia-reperfusion injury through the modulation of tight junctions and PKCδ signaling in rats. *J Mol Neurosci*. 2012;47(1):89–100. doi:10.1007/s12031-011-9689-x
25. Lee H, Park JW, Kim SP, Lo EH, Lee SR. Doxycycline inhibits matrix metalloproteinase-9 and laminin degradation after transient global cerebral ischemia. *Neurobiol Dis*. 2009;34(2):189–198. doi:10.1016/j.nbd.2008.12.012
26. Schwartz J, Holmuhamedov E, Zhang X, Lovelace GL, Smith CD, Lemasters JJ. Minocycline and doxycycline, but not other tetracycline-derived compounds, protect liver cells from chemical hypoxia and ischemia/reperfusion injury by inhibition of the mitochondrial calcium uniporter. *Toxicol Appl Pharmacol*. 2013;273(1):172–179. doi:10.1016/j.taap.2013.08.027
27. Castro MM, Kandasamy AD, Youssef N, Schulz R. Matrix metalloproteinase inhibitor properties of tetracyclines: Therapeutic potential in cardiovascular diseases. *Pharmacol Res*. 2011;64(6):551–560. doi:10.1016/j.phrs.2011.05.005
28. Moser MAJ, Sawicka K, Sawicka J, et al. Protection of the transplant kidney during cold perfusion with doxycycline: Proteomic analysis in a rat model. *Proteome Sci*. 2020;18(1):3. doi:10.1186/s12953-020-00159-3
29. Cerisano G, Buonamici P, Gori AM, et al. Matrix metalloproteinases and their tissue inhibitor after reperfused ST-elevation myocardial infarction treated with doxycycline: Insights from the TIPTOP trial. *Int J Cardiol*. 2015;197:147–153. doi:10.1016/j.ijcard.2015.06.024
30. Brown DL, Desai KK, Vakili BA, Nouneh C, Lee HM, Golub LM. Clinical and biochemical results of the metalloproteinase inhibition with subantimicrobial doses of doxycycline to prevent acute coronary syndromes (MIDAS) pilot trial. *Arterioscler Thromb Vasc Biol*. 2004;24(4):733–738. doi:10.1161/01.ATV.0000121571.78696.dc
31. Gresele P, Falcinelli E, Loffredo F, et al. Platelets release matrix metalloproteinase-2 in the coronary circulation of patients with acute coronary syndromes: Possible role in sustained platelet activation. *Eur Heart J*. 2011;32(3):316–325. doi:10.1093/eurheartj/ehq390
32. Bengmark S, Göransson G, Zoucas E. Defects in hemostasis produced by antibiotics: An in vivo study in the rat. *Eur Surg Res*. 1981;13(4):290–298. doi:10.1159/000128196
33. Webb JF, Schilling TF. Zebrafish in comparative context: A symposium. *Integr Comp Biol*. 2006;46(5):569–576. doi:10.1093/icb/icl017
34. Yakushkin VV, Zyuryaev IT, Khaspekova SG, Sirotkina OV, Ruda MY, Mazurov AV. Glycoprotein IIb-IIIa content and platelet aggregation in healthy volunteers and patients with acute coronary syndrome. *Platelets*. 2011;22(4):243–251. doi:10.3109/09537104.2010.547959
35. Sperling S, Vinholt PJ, Sprogøe U, Yazer MH, Frederiksen H, Nielsen C. The effects of storage on platelet function in different blood products. *Hematology*. 2019;24(1):89–96. doi:10.1080/10245332.2018.1516599
36. Vélez P, Parguiña A, Ocaranza-Sánchez R, et al. Identification of a circulating microvesicle protein network involved in ST-elevation myocardial infarction. *Thromb Haemost*. 2014;112(4):716–726. doi:10.1160/TH14-04-0337
37. Jung C, Sörensson P, Saleh N, Arheden H, Rydén L, Pernow J. Circulating endothelial and platelet derived microparticles reflect the size of myocardium at risk in patients with ST-elevation myocardial infarction. *Atherosclerosis*. 2012;221(1):226–231. doi:10.1016/j.atherosclerosis.2011.12.025
38. van der Zee PM, Biró É, Ko Y, et al. P-Selectin- and CD63-exposing platelet microparticles reflect platelet activation in peripheral arterial disease and myocardial infarction. *Clin Chem*. 2006;52(4):657–664. doi:10.1373/clinchem.2005.057414
39. Lubsczyk B, Kollars M, Hron G, Kyrle PA, Weltermann A, Gartner V. Low dose acetylsalicylic acid and shedding of microparticles in vivo in humans. *Eur J Clin Invest*. 2010;40(6):477–482. doi:10.1111/j.1365-2362.2010.02299.x
40. Kafian S, Mobarrez F, Wallén H, Samad B. Association between platelet reactivity and circulating platelet-derived microvesicles in patients with acute coronary syndrome. *Platelets*. 2015;26(5):467–473. doi:10.3109/09537104.2014.940304

Clinical implications of a diagnosis of taurodontism: A literature review

Janusz Pach[1,A–F], Piotr A. Regulski[2,A–C,E,F], Jacek Tomczyk[3,B,C,E,F], Izabela Strużycka[4,A,B,E,F]

[1] Department of Comprehensive Dentistry, Medical University of Warsaw, Poland
[2] Department of Dental and Maxillofacial Radiology, Medical University of Warsaw, Poland
[3] Institute of Biological Sciences, Cardinal Stefan Wyszyński University, Warszawa, Poland
[4] Department of Comprehensive Dentistry, Medical University of Warsaw, Poland

A – research concept and design; B – collection and/or assembly of data; C – data analysis and interpretation; D – writing the article; E – critical revision of the article; F – final approval of the article

Advances in Clinical and Experimental Medicine, ISSN 1899–5276 (print), ISSN 2451–2680 (online) *Adv Clin Exp Med*. 2022;31(12):1385–1389

Address for correspondence
Piotr A. Regulski
E-mail: piotr.regulski@wum.edu.pl

Funding sources
None declared

Conflict of interest
None declared

Received on March 19, 2022
Reviewed on June 9, 2022
Accepted on July 14, 2022

Published online on August 24, 2022

Abstract

Taurodontism is a morphological anomaly involving multirooted teeth that is characterized by a vertical shift of the pulp chamber and shortening of the roots. The literature was analyzed to determine the impact of a diagnosis of taurodontism on dental treatment. A total of 85 full-text publications from the years 2005–2021 were analyzed and 20 publications were included in this research. The endodontic treatment of a taurodont tooth is challenging due to the apical displacement of the pulpal chamber floor and the incorrect configuration of the root canal system, or the presence of additional canals. In terms of prosthetics, the use of taurodont teeth as abutments is not recommended as they lack stability due to shorter roots. The extraction of taurodont teeth can be complicated due to an apical shift of the root furcation. In periodontology, taurodont teeth can have a better prognosis as there is less chance of furcation involvement. From an orthodontic point of view, it is important to note that taurodont teeth are not sufficiently embedded in the alveolus and have a greater tendency for root resorption. With regard to genetic diseases, it has been reported that this anomaly can exist as an isolated feature. However, the majority of authors agree that taurodontism is associated with conditions such as Down syndrome, Klinefelter syndrome, cleft lip and palate, hypodontia, amelogenesis imperfecta, and others. From a clinical standpoint, it is very important to diagnose taurodontism before treatment. A diagnosis of taurodontism can be important in the early diagnosis of malformations that commonly occur with this condition.

Key words: genetic diseases, endodontics, dental pulp cavity, tooth cervix

Cite as
Pach J, Regulski PA, Tomczyk J, Strużycka I. Clinical implications of a diagnosis of taurodontism: A literature review. *Adv Clin Exp Med*. 2022;31(12):1385–1389. doi:10.17219/acem/152120

DOI
10.17219/acem/152120

Introduction

Taurodontism is a morphological anomaly involving multirooted teeth. It can affect both deciduous and permanent teeth.[1–3] Taurodontism most commonly affects the permanent molars of the mandible.[4] However, some authors contend that this anomaly is found more frequently in the maxilla and second molars, and is less frequently seen in the first molars of the mandible.[3] Taurodontism can occur unilaterally or bilaterally.

A taurodont tooth is characterized by an apical displacement of the pulpal floor and shortening of the roots. A lack of constriction at the cementoenamel junction (CEJ) is a characteristic feature.[3] On clinical examination, a taurodont tooth is not visibly different from the other teeth, as this anomaly is only detected on radiographic imaging.

The origin of the name "taurodontism" comes from the Latin term "taurus" which means bull and the Greek term "odous" which means tooth.[3] Taurodontism was first observed by Henry Pickerill in 1909.[3,5,6] The name of the condition was coined by Arthur Keith in 1913.[2–9] Since its identification, de Terra has discovered these misshaped teeth in prehistoric humans.[8] There are reports stating that the term "taurodontism" was first used by Dragutin Gorjanović-Kramberger who found this anomaly in neanderthal remains in Krapina (Croatia).[3] In modern populations, the prevalence of taurodontism varies depending on the population studied. This condition has been observed in 8% of Jordanians, 46% of Chinese, 5% of Israelis, and 10% of the Dutch.[10] However, it should be considered that the aforementioned differences may result from the use of different diagnostic criteria.[11]

The etiology of this condition has not been clearly explained. Many authors assume that the anomaly forms in early fetal life due to the failure of Hertwig's epithelial sheath diaphragm to invaginate at the proper horizontal level.[1,3,5,7,11–14] Some authors report that this anomaly may be associated with an aberration of a gene on the X chromosome that is responsible for enamel development,[3,4,15] or that it may be inherited in an autosomal dominant fashion.[4]

Objectives

The objective of this study was to analyze the available publications in order to assess the impact of the presence of taurodontism on various aspects of dental treatment (endodontology, prosthetics, surgery, periodontology, and orthodontics) and the association of taurodontism with various malformations.

Material and methods

The PubMed database was searched covering the years 2005–2021, and the keyword "taurodontism" was used. This resulted in identifying 243 publications, of which 158 were rejected after an analysis of the abstracts. The exclusion criteria included a lack of relation to the topic, non-English text and nonavailability of the abstract and article. A total of 85 full-text articles were analyzed. The inclusion criteria consisted of the subject of the article evaluating the impact of taurodontism on endodontic, prosthetics, dental surgery, periodontological and orthodontic treatment, or describing the association of taurodontism with other malformations. Full-text articles were excluded if they were not relevant to the subject of this work. Sixty-five articles were rejected and 20 were included in this research (Fig. 1). Particular attention was paid to the clinical relevance of the cases described. The conclusions of the authors were categorized into endodontics, prosthetics, dental surgery, periodontology, and orthodontics. We analyzed the points of view of the authors concerning the coexistence of taurodontism and other genetic diseases and systemic disorders.

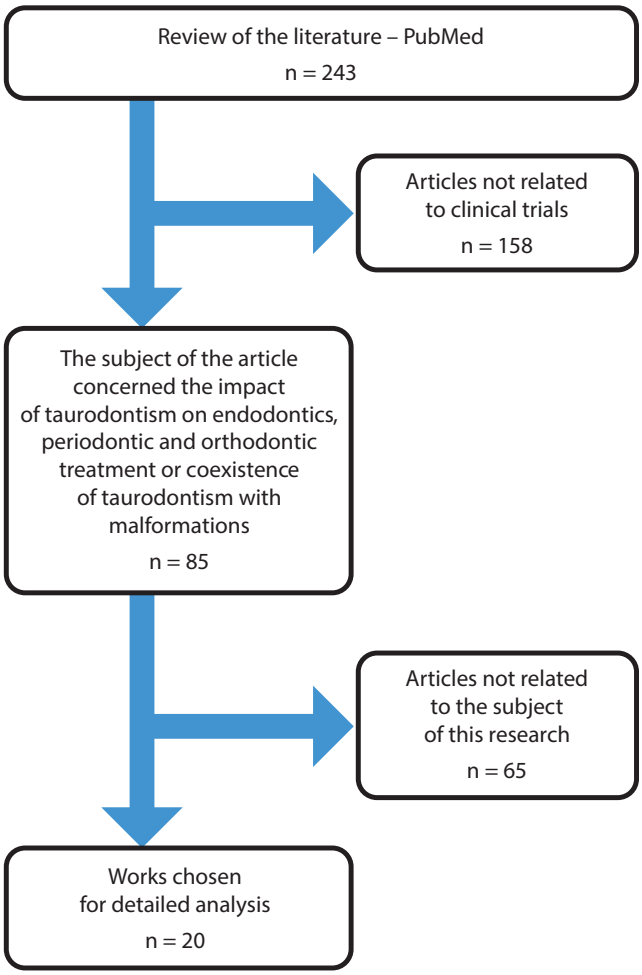

Fig. 1. Flow diagram for publications qualified for the review

Results

The endodontic treatment of taurodont teeth is complex and difficult because of the apical displacements of the pulpal chamber floor, which makes it harder to find the localization of the root canals.[5,6,11,15,16] Taurodont teeth often have an incorrect configuration of the root canal system and additional canals (Fig. 2,3). Increased bleeding during pulp chamber trepanation may be mistaken for perforation[1]; however, due to root shortening and the apical displacement of the pulpal chamber, floor perforations can occur.[3,12,17] The complexity of the root canal system makes its instrumentation almost impossible. Because of this, the authors recommend the use of sodium hypochlorite to dissolve the remaining pulp that cannot be removed with instruments.[13,18] Kulkarni et al. described a case of a patient who underwent root canal irrigation of tooth 37 with 2.5% sodium hypochlorite, 17% aqueous ethylene diamine tetra-acetic acid (EDTA) solution, 2% chlorhexidine gluconate, and saline.[4] According to Bharti et al., an irrigation with 5% sodium hypochlorite for 20 min–2 h can completely dissolve the pulp.[19] However, Prakash et al. recommended the irrigation with sodium hypochlorite be limited to single-use to minimize the detrimental effects in the periapical tissues.[8]

From an endodontist's standpoint, it is very helpful to use an endodontic magnifier and endodontic microscope during the treatment of taurodont teeth.[19] By using these modern optical devices, the operating field is better illuminated and the picture becomes deeper and clearer. The endodontic microscope provides up to ×40 magnification of the operating field, which significantly minimizes the risk of complications when finding hard-to-reach root canal orifices. The use of an endodontic microscope also makes it possible to check the dryness, cleanliness and shape of the root canals. An additional challenge during endodontic treatment is the difficult procedure of root canal filling. Mohan et al. proposed a modified technique of root canal filling, based on connecting the side condensation of the apical area with the vertical condensation of the extended pulp chamber.[2,19] As a result of the vertical shift of the pulp chamber, the diagnosis of a taurodont tooth may be difficult, as the pulp viability test may not be conclusive.[3]

Taurodont teeth are less useful as abutments in prosthetic treatment because the shortened roots do not provide adequate anchorage in the alveolus and, therefore, do not adequately resist lateral forces.[3,5,16] According to some authors, taurodont teeth are a contraindication for the use of root-crown posts.[12]

With regard to dental surgery, it should be taken into account that the extraction of a taurodont tooth may be more difficult because of the apical shift of the furcation, the root apical area being shorter and thinner,[5,16] and the roots having a widened dimension in the 1/3 of their length (Fig. 2).[3,5,17] Paradoxically, due to their large crown and short roots, such teeth are less seated in the alveolus, and thus may be easier to extract than their cynodont counterparts.[1,2,15]

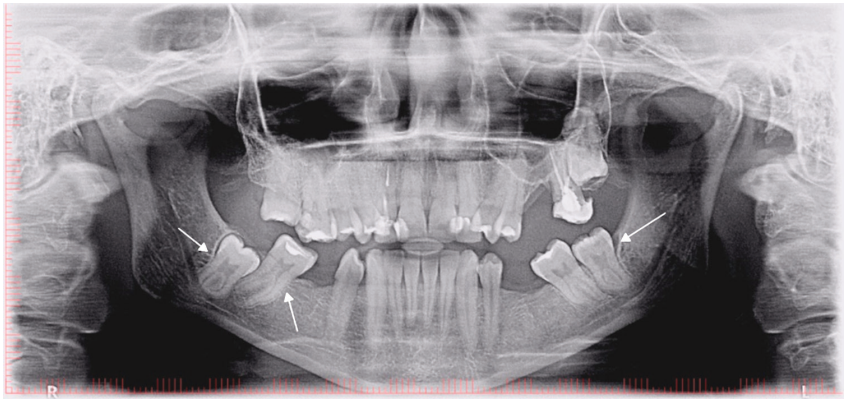

Fig. 2. Panoramic radiograph with taurodont teeth 38, 47 and 48

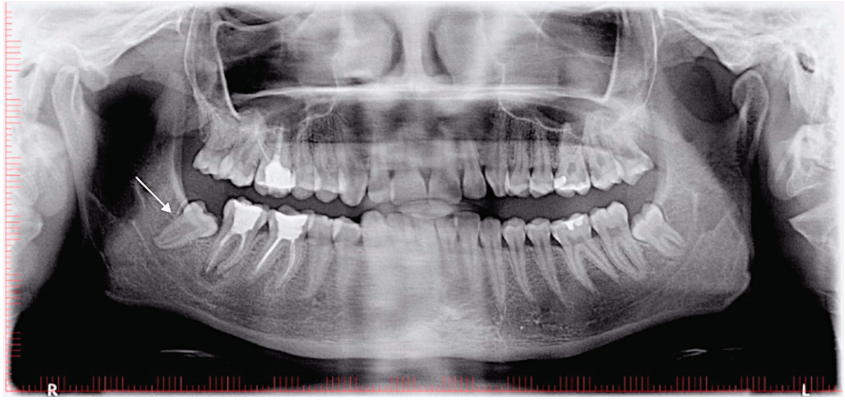

Fig. 3. Panoramic radiograph with taurodont tooth 48

In periodontal treatment, taurodont teeth appear to have a better prognosis than cynodont teeth, as the probability of involvement of the furcation in taurodont teeth is significantly smaller.[5,15,16] However, if this does occur, then the prognosis becomes questionable.[16]

A diagnosis of taurodontism is important before making decisions about orthodontic treatment. Due to the reduced surface area of the roots, it may be necessary to reduce the anchorage value of the root in the alveolus.[3,16] From the point of view of an orthodontist, it is very important to know the link between the occurrence of facial and dental malformations. During orthodontic treatment, taurodont teeth may have an excessive tendency for root resorption.[14]

The opinions of researchers are divided on the question of whether taurodontism coexists with other genetic diseases. Some authors report that taurodontism is an anomaly that may be observed as an isolated feature,[15] or as a coexisting feature with other genetic diseases such as tricho-dento-osseus syndrome and Klinefelter syndrome.[7,16–18] There are reports stating that taurodontism occurs more frequently in people with a cleft lip and palate.[3,7,10,11] Also, correlations with disorders such as hypodontia, amelogenesis imperfecta and Down syndrome have been observed.[1–3,9,10,13,19] The authors agree with the hypothesis that the prevalence of taurodontism increases as the number of X chromosomes increases, indicating that the expression of the defect and the number of X chromosomes may be correlated. Furthermore, it has been suggested that the X chromosomal gene responsible for the development of enamel may also be responsible for the development of taurodontism.[15] Puttalingaiah et al. studied patients from central India and were able to prove a correlation between taurodontism and tooth agenesis.[20] In the population studied, they noted a prevalence of 7.5% for this association. Chetty et al. investigated and described a relationship between the occurrence of taurodontism and the existence of genetic abnormalities in the bone structure of a South African population.[17] They found that out of 23 people with osteogenesis imperfecta (OI) type XI, 43.48% showed signs of taurodontism in their permanent teeth. Contrary to this, a study of the Danish population has shown taurodontism to only occur in persons with mild OI. Taurodontism has also been diagnosed in association with Torg–Winchester syndrome and Pyle disease.[17]

The prevalence of this dental anomaly reported in the literature is variable due to the use of different study methods. Studies in the literature report values ranging from 0.1% to 55% of the total number of patients examined, including values of 0.1% to 9.9% in patients without known systemic diseases. The proportion of patients with systemic diseases and congenital malformations (Down syndrome, Klinefelter syndrome, oligodontia, or cleft lip and palate) diagnosed with taurodontism was high (from 19.4% to 55%).[3]

Discussion

Taurodontism is a relatively rare tooth anomaly in modern humans.[3,16] However, there are studies showing that this malformation can occur in 0.25–11.3% of the population.[11] Most of the authors of the analyzed publications agree that the occurrence of this defect is related to ethnicity.[2,3,5–7,9,10,16] For example, this anomaly has been reported in up to 46% of young Chinese people.[3,10] Even using panoramic radiographs and cone beam computed tomography (CBCT), the occurrence of this anomaly, especially its milder forms (hypotaurodontism), can be overlooked. Therefore, a thorough biometric analysis of the available images is very important.[7,12,15,16]

There are several ways to diagnose taurodontism. In 1928, Shaw classified the subtypes of this disease as hypo-, meso- and hypertaurodontism, based on the relative shift of the pulpal floor. This subjective assessment has often led to a misdiagnosis of this anomaly.[4] In 1978, Shifman and Chanannel (Fig. 4), and later Kim Seow and Lai (Fig. 5), developed taurodontal indices in order to determine the occurrence of taurodontism and classify it based on a biometric study, as shown radiographically (Fig. 2,3).[3] Determining taurodontism consists of dividing the distance between the lowest point of the pulp chamber roof and the highest point of the pulpal floor by the distance between the lowest point of the pulp chamber roof and the apex, and then multiplying the result by 100. When this value is equal to or greater than 20, the patient is said to have a taurodont tooth. Values from 20 to 29.9 classify the tooth as a hypotaurodont, values from 30 to 39.9 classify it as a mesotaurodont, and values from 40 to 75 identify it as a hypertaurodont.

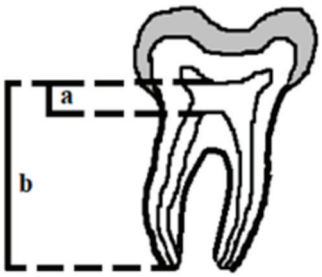

Fig. 4. Index of Shifman and Chanannel equal to a×100/b

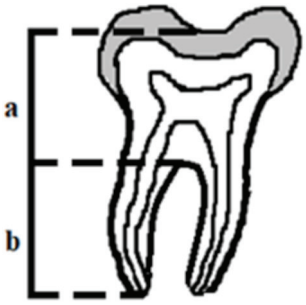

Fig. 5. Index of Seow and Lai equal to a/b

The 2nd index used to identify taurodontism calculates the crown-to-root ratio of the tooth. This is accomplished by measuring the distance from the deeper furrow on the occlusal surface of the furcation and comparing it to the distance from the furcation to the apex. A result from 1.1 to 1.29 indicates hypotaurodontism, from 1.3 to 2.0 indicates mesotaurodontism and above 2.0 indicates hypertaurodontism.[3,13]

The ability to diagnose taurodontism is particularly useful in endodontics, especially regarding meso- and hypertaurodont teeth. The treatment of such teeth is very complicated and requires much more commitment from the clinician.[11,18] Due to the considerable elongation of the pulp chamber and consequently, the shortening of the root canals, it is much more difficult to localize and avoid perforation. However, it is possible to observe increased hemorrhaging during trepanation, which can suggest a perforation.[13]

Conclusions

The literature suggests that from the clinician's point of view, the diagnosis of taurodontism before treatment is crucial for its success. The complications of endodontic treatment are mostly caused by this defect; however, the possibility of this anomaly should be considered in other areas of dentistry. The diagnosis of taurodontism is important in the early diagnosis of some malformations with which it may be correlated. Therefore, the clinical usefulness of an imaging examination in patients at risk of developing systemic genetic diseases due to medical family history should be emphasized. Genetic testing should be performed in cases where the clinician suspects a genetic disease and where taurodontism has been confirmed, especially in Klinefelter syndrome where it may be asymptomatic at first; however, the risk of tumors development is increased in the case of initially asymptomatic Klineferter syndrome.

ORCID IDs

Janusz Pach https://orcid.org/0000-0001-9308-2313
Piotr A. Regulski https://orcid.org/0000-0002-3692-3582
Jacek Tomczyk https://orcid.org/0000-0002-0605-665X
Izabela Strużycka https://orcid.org/0000-0002-7058-3614

References

1. Bafna Y, Kambalimath HV, Khandelwal V, Nayak P. Taurodontism in deciduous molars. *BMJ Case Rep*. 2013;2013:bcr2013010079. doi:10.1136/bcr-2013-010079
2. Mohan RPS, Verma S, Agarwal N, Singh U. Taurodontism. *BMJ Case Rep*. 2013;2013:bcr2012008490. doi:10.1136/bcr-2012-008490
3. Kalina A, Rożniatowski P, Regulski P, Turska-Szybka A. The occurrence and intensity of taurodontism among patients in the Hospital of the Infant Jesus: Biometric analysis of panoramic radiographs. *Dent Med Probl*. 2015;52(4):455–461. doi:10.17219/dmp/59227
4. Kulkarni G, Rajeev K, Ambalavanan P, Kidiyoor K. Successful endodontic management of hypo, meso and hypertaurodontism: Two case reports. *Contemp Clin Dent*. 2012;3(Suppl 2):S253–S256. doi:10.4103/0976-237X.101108
5. Patil S, Doni B, Kaswan S, Rahman F. Prevalence of taurodontism in the North Indian population. *J Clin Exp Dent*. 2013;5(4):e179–e182. doi:10.4317/jced.51118
6. Parupalli K, Solomon R, Karteek B, Polasa S. Application of cone-beam computed tomography in the analysis and management of intricate internal anatomy of hyper- and mesotaurodontic teeth. *J Conserv Dent*. 2020;23(2):211–214. doi:10.4103/JCD.JCD_175_19
7. Jogendra Sai Sankar A, Sreedevi E, Satya Gopal A, Naga Lakshmi M. A rare condition of bimaxillary primary molar taurodontism. *J Dent (Shiraz)*. 2017;18(2):153–156. PMID:28620641.
8. Prakash R, Chenduran V, Ballal S, Velmurugan N, Kandaswamy D. Endodontic management of taurodontic teeth. *Indian J Dent Res*. 2005;16(4):177–181. doi:10.4103/0970-9290.29900
9. Melo Filho MR, Nogueira dos Santos LA, Barbosa Martelli DR, et al. Taurodontism in patients with nonsyndromic cleft lip and palate in a Brazilian population: A case control evaluation with panoramic radiographs. *Oral Surg Oral Med Oral Pathol Oral Radiol*. 2015;120(6):744–750. doi:10.1016/j.oooo.2015.08.005
10. Çolak H, Tan E, Bayraktar Y, Hamidi MM, Çolak T. Taurodontism in a Central Anatolian population. *Dent Res J (Isfahan)*. 2013;10(2):260–263. doi:10.4103/1735-3327.113367
11. Janani M, Rahimi S, Shahi S, Aghbali A, Zand V. Endodontic treatment of a hypertaurodont mandibular second molar: A case report. *Iran Endod J*. 2011;6(3):133–135. PMID:23130066.
12. Vashisth P, Dwivedi S, Arora S, Mayall S. Multiple bilateral taurodontic teeth in primary dentition: A case report. *Int J Clin Pediatr Dent*. 2013;6(2):132–133. doi:10.5005/jp-journals-10005-1205
13. Simsek N, Keles A, Ocak M. Endodontic treatment of hypertaurodontism with multiple bilateral taurodontism. *J Conserv Dent*. 2013;16(5):477–479. doi:10.4103/0972-0707.117497
14. Wojtasińska-Chebel P, Iwanecka-Zduńczyk M, Machorowska-Pieniążek A. Taurodontism: Literature review and case reports. *Forum Ortodontyczne*. 2010;6(2):37–46. https://publisherspanel.com/api/files/view/31385.pdf. Accessed August 17, 2022.
15. Jayashankara C, Shivanna AK, Sridhara K, Kumar PS. Taurodontism: A dental rarity. *J Oral Maxillofac Pathol*. 2013;17(3):478. doi:10.4103/0973-029X.125227
16. Hegde V, Anegundi RT, Pravinchandra K. Biometric analysis: A reliable indicator for diagnosing taurodontism using panoramic radiographs. *J Clin Diagn Res*. 2013;7(8):1779–1781. doi:10.7860/JCDR/2013/5543.3274
17. Chetty M, Roomaney IA, Beighton P. Taurodontism in dental genetics. *BDJ Open*. 2021;7(1):25. doi:10.1038/s41405-021-00081-6
18. Jamshidi D, Adl A, Sobhnamayan F, Bolurian M. Root canal treatment of a hypertaurodont mandibular second molar: A case report. *J Dent Res Dent Clin Dent Prospects*. 2015;9(1):57–59. doi:10.15171/joddd.2015.012
19. Bharti R, Chandra A, Tikku A, Arya D. Prevalence of taurodont molars in a North Indian population. *Indian J Dent*. 2015;6(1):27–31. doi:10.4103/0975-962X.151700
20. Puttalingaiah V, Agarwal P, Miglani R, Gupta P, Sankaran A, Dube G. Assessing the association of taurodontism with numeric dentition anomalies in an adult central Indian population. *J Nat Sci Biol Med*. 2014;5(2):429–433. doi:10.4103/0976-9668.136222

New biochemical, immune and molecular markers in lung cancer: Diagnostic and prognostic opportunities

Karol Marschollek[1,A–D], Anna Brzecka[2,D–F], Anna Pokryszko-Dragan[1,A,D–F]

[1] Department of Neurology, Wroclaw Medical University, Poland
[2] Department of Pulmonology and Lung Oncology, Wroclaw Medical University, Poland

A – research concept and design; B – collection and/or assembly of data; C – data analysis and interpretation;
D – writing the article; E – critical revision of the article; F – final approval of the article

Advances in Clinical and Experimental Medicine, ISSN 1899–5276 (print), ISSN 2451–2680 (online) *Adv Clin Exp Med*. 2022;31(12):1391–1411

Address for correspondence
Karol Marschollek
E-mail: karol.marschollek@gmail.com

Funding sources
None declared

Conflict of interest
None declared

Received on March 26, 2022
Reviewed on June 27, 2022
Accepted on July 25, 2022

Published online on August 24, 2022

Abstract

Lung cancer is one of the most common neoplasms and the leading cause of cancer-related deaths worldwide. Despite recent progress in understanding the pathomechanisms of lung cancer, it is frequently associated with late diagnosis, high incidence of metastases and poor response to treatment. Thus, there is extensive research in the field of biomarkers that aims to optimize management of lung cancer. The aim of this study was to review the current perspectives of a wide spectrum of circulating molecules that seem promising as new potential biomarkers of lung cancer. Among these, biochemical (active proteins), immunological (immunocompetent cells, cytokines, chemokines, and antibodies) and genetic (circulating tumor DNA, cell-free DNA and microRNA) markers are presented and discussed. The use of these markers would support the early detection of lung cancer and might be used for predicting disease progression, response of the disease to targeted therapies, monitoring the course of treatment, and developing individualized diagnostic and therapeutic strategies. Special attention was given to potential markers of nervous system involvement in the course of lung cancer, due to its prevalence and devastating impact. Limitations of the potential biomarkers are also outlined and future directions of investigations in this field highlighted, with the aim of improving the accuracy and practical utility of these biomarkers.

Key words: lung cancer, biomarkers, molecular, biochemical, immune

Cite as
Marschollek K, Brzecka A, Pokryszko-Dragan A. New biochemical, immune and molecular markers in lung cancer: Diagnostic and prognostic opportunities. *Adv Clin Exp Med*. 2022;31(12):1391–1411. doi:10.17219/acem/152349

DOI
10.17219/acem/152349

Introduction

According to the GLOBOCAN estimates,[1] lung cancer was the 2nd most common type of cancer in terms of incidence in 2020, accounting for 11.4% of all newly diagnosed cancer cases. It was also by far the leading cause of death due to malignancies, accounting for 18% of all cancer mortality, which is almost double that of the 2nd most common cause, colorectal cancer. Moreover, it is estimated that lung cancer will remain at the top of both of these categories by 2040, with an expected growth of 58.8% in the number of cases and 63.8% in mortality.[2] From a histological point of view, lung cancer is typically divided into subtypes: small cell lung cancer (SCLC), adenocarcinoma, squamous cell carcinoma (SCC), and large cell carcinoma, the latter 3 usually being jointly referred to as non-small cell lung cancer (NSCLC).[3] The main symptoms of lung cancer, that can occur separately or in combination, are cough, dyspnea, pain, hemoptysis, aphonia or hoarseness, weight loss or asthenia, and superior vena cava syndrome, although an asymptomatic course at the time of diagnosis is not unusual.[4] Moreover, distant metastases are frequent, especially to the central nervous system. In the early stages of NSCLC, brain metastases are present in 0.6–3% of patients[5] and this increases up to 50% in the course of the disease.[6] In SCLC, brain metastases occur in about 10% of patients at the time of diagnosis and in additional 40–50% at later stages.[7]

Another type of nervous system involvement, resulting from immune-mediated responses to the presence of lung cancer antigens, are paraneoplastic neurological syndromes (PNS). Lung cancer, predominantly SCLC, is considered to be the most common malignancy associated with PNS.[8,9] From a clinical perspective, PNS can involve both the central and peripheral nervous systems, with the most commonly reported syndromes being peripheral neuropathy, followed by limbic encephalitis, subacute cerebellar degeneration, Lambert–Eaton syndrome, myopathy, encephalomyelitis,[8–10] and neuromyelitis optica.[11,12] Paraneoplastic neurological syndromes may develop a few years before the detection of cancer,[13,14] which highlights the potential of using such syndromes for early diagnosis.[15,16]

Treatment options for lung cancer can be applied alone or in combination and include surgery (for early stage disease), chemotherapy, radiotherapy, targeted therapy, and immunotherapy.[17–21] Despite recent advances in the diagnosis and treatment of lung cancer, the prognosis is still unfavorable. According to the tumor-node-metastasis (TNM)-based staging of lung cancer, the 5-year survival rate for NSCLC varies between 50% in clinical stage IA and 2% in clinical stage IV.[22] Small cell lung cancer is associated with even worse outcomes, such as a 5-year survival of 10% in the early stage of disease, with only 4.6% of patients diagnosed in the extensive stage surviving 2 years.[23] As a consequence of high mortality rates and frequency of metastases present at diagnosis, much of the recent research has focused on early diagnosis and identification of potential markers of disease progression, local infiltration and metastatic activity, as well as treatment response. The early diagnosis of lung cancer is based mainly on computed tomography imaging, confirmed using cytological and histopathological examination of specimens obtained during bronchoscopy or other invasive procedures.[24] However, the diagnostic process and prognosis may be complemented by additional biomarkers.

By definition, biomarkers are molecules or abnormal parameters that distinguish an individual with a particular disease from the studied population. Biomarkers can be detected in bodily fluids such as blood, serum, urine, sputum, pleural effusion, or cerebrospinal fluid.[25,26] Recently, biochemical, immune and molecular biomarkers have been recognized as the most promising and clinically relevant with regard to lung cancer, and they are being extensively investigated to evaluate their sensitivity and specificity.[27] An early detection of the dissemination of neoplastic processes and the establishment of risk factors for its occurrence are particularly important in terms of prognosis and therapeutic possibilities. Given the significant impact of nervous system involvement on disease burden, morbidity and mortality, the identification of its presence and selection of patients at increased risk of this complication are of great importance.

Objectives

The aim of this study was to review the current data on the role of new biochemical, immune and molecular markers in the diagnosis of lung cancer, and to evaluate its progression, with a focus on the involvement of nervous system in the course of disease. Ongoing research and its future directions in this field have been reviewed in view of potential implications for early detection of cancer, tailoring treatment plans based on prognosis, and monitoring the course of disease.

Materials and methods

A literature search was performed using the PubMed and Embase databases, covering the period from the beginning of 2010 until February 28, 2022, with a combination of the search terms: "lung cancer", "NSCLC", "SCLC", "biomarker", "biochemical", and "molecular". After excluding papers written in a language other than English, conference abstracts and duplicates from further screening, a total of 2745 original studies and review articles were retrieved. Full texts of eligible papers were analyzed for their relevance to the topic, as well as several further potentially relevant papers that were identified in reference lists from the texts. Initially, the literature search was conducted by the lead author, with the results reviewed

and verified by the other authors. This led to the identification and inclusion of 217 published studies that were considered the most relevant to the topic. The preparation of the study was conducted by following the Enhancing Transparency in Reporting the Synthesis of Qualitative Research (ENTREQ) checklist,[28] selected according to the Enhancing the QUAlity and Transparency of Health Research (EQUATOR) Network guidelines (https://www.equator-network.org).

Biochemical markers of lung cancer

Several biochemical biomarkers have already been implemented into lung cancer diagnostics and management, including carcinoembryonic antigen (CEA), cytokeratin 19 fragment marker (CYFRA 21-1), neuron-specific enolase (NSE), and cancer antigen 125 (CA-125).[29,30] However, the sensitivity and specificity of these markers are disputable, as their levels can be elevated in other diseases. As such, new candidate biomarkers have been proposed that are thought to have better accessibility and clinical utility, such as soluble intercellular cell adhesion molecule-1 (sICAM-1), which plays an important role in adhesion between host cells and cancer cells in the promotion of tumor growth. The overexpression of sICAM-1 was reported in lung cancer patients with lymph node and distant metastases, and was linked to shorter overall survival (OS) and progression-free survival (PFS).[31] Similarly, high levels of angiopoietin-2, an important factor involved in angiogenesis, were associated with lymph node metastases and a poorer prognosis.[32] Transforming growth factor beta (TGF-β),[33] glucose transporter 1 (GLUT1), which enhances the supply of glucose to tumor cells,[34] and urinary GM2 activator protein (GM2AP), a molecule involved in the induction of cancer invasion,[35] are other recently proposed predictors of poor outcome. Podoplanin, a potential inhibitor of tumor cell growth and self-renewal, was identified as a marker of lower malignancy in SCC and better prognosis in patients with this type of lung cancer.[36] In another meta-analysis, high serum levels of amyloid A, a protein correlated with an acute inflammatory response, were suggested as a discriminative marker, especially for the detection of SCC.[37] Among other potential biomarkers, tumor necrosis factor receptor-associated protein 1 (TRAP1) was overexpressed in patients with higher pathological TNM stage and lymph node metastases, and was correlated with a shorter disease-free survival.[38]

Immune markers of lung cancer

The development of lung cancer is associated with a changing profile of immune system activity, with a shift from type 1 T helper cell-derived signaling to type 2 T helper cell pathways. Furthermore, dendritic cell, natural killer (NK) cell and T helper cell activity has been shown to decrease, whilst regulatory T cell (Treg) activity has been seen to increase. Additionally, programmed cell death protein 1 (PD-1) and cytotoxic T-lymphocyte-associated protein 4 (CTLA-4), which are markers of checkpoint inhibition, have also been shown to increase. Meanwhile, tumor-specific antigens and tumor-associated antigens (TAAs) are expressed by neoplastic cells and evoke an immune response, such as the induction of antibody production. Therefore, these immune-mediated processes might be used as markers for detection and monitoring of lung cancer, or for predicting its activity.[39,40]

A range of immunocompetent cells have been identified within lung tumors, with their type and distribution in the nest or stroma of the tumor found to have prognostic significance. The prevalence of Tregs, M2 macrophages and immature dendritic cells was associated with poor survival, while the presence of $CD8^+$ T cells, $CD4^+$ T cells, M1 macrophages, and NK cells was linked to better outcomes.[41] Some of these findings were specific for particular types of lung cancer, with high intratumoral neutrophil density being correlated with poor prognosis in patients with adenocarcinoma, contrary to the patients with SCC.[42] A similar analysis of bronchoalveolar lavage fluid demonstrated material obtained from the affected lung that contained an increased number of neutrophils and a predominance of $CD8^+$ T cells, Tregs and M2 macrophages.[43]

Measures of the systemic inflammatory response from peripheral blood, including monocyte count and neutrophil-to-lymphocyte ratio (NLR), might also serve as predictors of tumor development, especially its propensity to metastasize.[44] Indeed, a meta-analysis of 14 studies revealed that a high NLR was associated with shorter OS in NSCLC and SCLC patients.[45] Additionally, flow cytometry studies have demonstrated that $CD3^+$, $CD4^+$ and $CD4^+/CD8^+$ ratio, and NK cells were all decreased, and inversely correlated with the progression of clinical stage in NSCLC, while Tregs increased parallel to cancer progression.[46]

Emphasis has been put on measuring serum cytokine and chemokine levels, which reflect the inflammatory processes related to the development of the cancer, in both NSCLC[47] and SCLC.[48] Higher serum levels of interleukin (IL)-6 and IL-8 predicted a risk of lung cancer up to several years before the diagnosis,[49] whilst the expressions of IL-8 with IL-6 and IL-6 with IL-17 were shown to be negative prognostic factors for early-stage lung cancer.[50] In addition, elevated levels of IL-17 in the serum of SCLC patients correlated with a propensity to metastasize and a shorter OS.[51] Angiogenesis inhibitors IL-20, and IL-22, which promotes tumor growth, were also found to be prognostic factors of lung cancer outcomes. High serum levels of IL-20 adversely correlated with time to cancer progression, and lower levels of IL-22 in the bronchoalveolar lavage of NSCLC patients were associated with worse rates of survival.[52] Studies on the prognostic value

of chemokines have demonstrated that high levels of C-C motif chemokine ligand 2 (CCL2), CCL19 and C-X-C motif chemokine ligand 16 (CXCL16), and low levels of CCL5 were linked with better survival. In contrast, high levels of CXCL8 and C-X-C motif chemokine receptor 4 (CXCR4) were associated with worse survival rates.[53]

Autoantibodies to TAAs may be detectable in the asymptomatic stage of cancer and persist in high levels in serum, which indicates their potential use as biomarkers for early detection of lung cancer.[54] The Early CDT®-Lung is a panel test for the presence of 7 autoantibodies against TAAs (p53, NY-ESO-1, CAGE, GBU4–5, SOX2, HuD, and MAGE A4) that is currently used in patients with a high risk of lung cancer. The test was validated in large cohorts of NSCLC and SCLC patients and demonstrated high overall specificity, but a rather low sensitivity in SCLC, which was even lower in NSCLC.[40] The presence of relevant autoantibodies may also have a prognostic value in lung cancer, with 1 study reporting on patients with NSCLC who were positive for antineural and antinuclear antibodies, and showed better rates of survival.[55] Another study reported a panel of 4 antibodies (MAGEA1, PGP9.5, SOX2, and TP53) that were overexpressed in NSCLC and correlated negatively with OS.[56] In another report, levels of an antibody against human DNA-topoisomerase I were significantly higher in the NSCLC group than in the controls, though the prognosis was worse in the antibody-negative group.57

Studies on the tumor-related immune environment have identified antibodies against PD-1 and its ligand (PD-L1) as a potential therapeutic option in lung cancer. Thus, the value of PD-L1 was investigated as a predictive biomarker for the efectiveness of therapy with anti-PD1/PD-L1 agents. Higher levels of PD-L1 expression were shown to be associated with a more effective treatment and longer survival, although results have not been consistent across studies.[58] At the same time, a high expression of CTLA-4 predicted worse survival in NSCLC but was not validated as a predictive marker of the response to the anti-CTLA-4 treatment.[41] Other markers have been sought, with Zhou et al. constructing a panel of 5 tumor-associated autoantibodies (p53, BRCA2, HuD, TRIM21, and NY-ESO-1) designed to predict the response to immune checkpoint inhibitors.[59] Panel positivity was found to be indicative of a better response and longer PFS. In the previous work, the same association was established for NY-ESO-1 and XAGE1 serum antibodies,[60] anti-nuclear antigens, extractable nuclear antigens, and anti-smooth cell antigens.[61] In another study, SIX2 autoantibodies were consistently upregulated in the non-responder group.[62] A panel comprising 13 antibodies showed high accuracy in predicting poor outcome in pre-operative samples of NSCLC patients (stage I–IIIa).[63] Concordant prognostic utility was confirmed for an antibody against cyclin Y.[64] Moreover, autoantibody status was suggested to be helpful not only in predicting clinical outcome, but also in assessing the risk of immune-related adverse events during treatment.[65]

Different types of biomarkers can be combined to further improve their diagnostic and predictive value, with 1 report establishing a panel of markers that could identify patients at risk of lymph node metastases.[66] The panel included tumor necrosis factor alpha (TNF-α), tumor necrosis factor-receptor I (TNFR1) and macrophage inflammatory protein-1α (MIP-1α), along with 3 autoantibodies that target ubiquilin-1, hydroxysteroid-(17-β)-dehydrogenase and triosephosphate isomerase. Validation of the panel using a classification algorithm revealed a sensitivity of 94% and specificity of 97%. A meta-analysis on advanced lung cancer inflammation index, which is a prognostic score that considers body mass index (BMI), serum albumin and NLR, revealed a significant correlation between the score and OS and PFS.[67] The prediction of survival in SCC patients was proposed on the basis of 4 immunological markers, including monocyte ratio, NLR, PD-L1 immunostaining score, and PD-1-positive stained tumor-infiltrating lymphocyte counts.[44] A large study was performed comprising patients with NSCLC, treated with PD-1/PD-L1 inhibitors, in order to establish the potential efficacy of 2 combined biomarkers, defined as Lung Immune Prognostic Index (LIPI). This index measured derived neutrophil/(leukocyte minus neutrophil) ratio and lactate dehydrogenase levels in order to predict the resistance to immune checkpoint inhibitors.[68] Both of these factors were independently associated with worse OS and PFS in patients treated with immune checkpoint inhibitors, while no such correlation was observed in a group treated with chemotherapy only. Neutrophil-to-lymphocyte ratio was shown to correlate not only with shorter OS but also with the presence of Kirsten rat sarcoma viral oncogene homologue (*KRAS*) and epidermal growth factor receptor (*EGFR*) mutations.[69] Lung Immune Prognostic Index[70] and NLR[71] have also been investigated for their prognostic value in patients with SCLC. The aforementioned potential biochemical and immune biomarkers of lung cancer are summarized in Table 1.

Circulating tumor DNA and circulating tumor cells as lung cancer markers

Circulating tumor DNA

Circulating tumor DNA (ctDNA) enters the bloodstream predominantly as a result of necrosis and apoptosis of tumor cells, although there is also evidence that it can be actively released by viable cells and several other processes.[72] It usually constitutes a small fraction (0.1–1%) of cell-free DNA (cfDNA) in plasma[73]; however, its level reflects tumor activity and expansion and can be much higher in patients with a more advanced disease.[74] There is increasing interest in using ctDNA in the diagnosis of various types

Table 1. Biochemical and immune markers of lung cancer

Biomarker	Study	Type of study	Study group	Outcomes
sICAM-1 (serum)	Wu et al.[31]	meta-analysis	23 studies – out of them, 7 investigated prognostic value (915 LC patients)	LC detection, more advanced stage, lymph node metastases, distant metastases, shorter PFS and OS
Angiopoietin-2 (serum)	Xu et al.[32]	meta-analysis	20 studies – out of them, 7 investigated prognostic value (575 LC patients)	more advanced stage, lymph node metastases, shorter OS
Transforming growth factor beta (tissue and plasma)	Li et al.[33]	meta-analysis	8 studies – 579 LC patients	poor prognosis
Glucose transporter 1 (tissue)	Zhang et al.[34]	meta-analysis	26 studies – out of them, 10 investigated prognostic value (1731 LC patients)	differential diagnosis of SCC, more advanced stage, lymph node metastases, shorter OS, disease-specific and DFS
GM2 activator protein (serum, urine and lung tissue)	Potprommanee et al.[35]	observational	Serum and urine from 133 LC patients and 143 NSCLC lung tissue samples	LC detection, shorter OS and DFS
Podoplanin (tissue)	Hu et al.[36]	meta-analysis	8 studies – 725 SCC patients	better differentiation of SCC, longer OS and PFS
SAA (serum)	Biaoxue et al.[37]	meta-analysis	9 studies – 1392, including 960 LC patients	LC detection, especially SCC
TRAP1 (tissue)	Kuchitsu et al.[38]	observational	64 adenocarcinoma patients	more advanced stage, lymph node metastases, shorter DFS, worse response to platinum-based chemotherapy
Intratumoral $CD66b^+$ TANs density	Rakaee et al.[42]	observational	536 NSCLC patients (289 SCC, 201 adenocarcinoma, 46 large cell carninoma)	longer disease-specific survival in SCC, shorter disease-specific survival in adenocarcinoma
NLR, monocyte ratio, PD-L1 immunostaining score and, PD-1-positive stained tumor-infiltrating lymphocyte counts	Jiang et al.[44]	observational	156 SCC patients (104 in training, and 52 in validation group)	shorter OS
NLR	Yin et al.[45]	meta-analysis	2734 LC patients (2433 NSCLC, 301 SCLC)	shorter OS
$CD3^+$, $CD4^+$, $CD4^+/CD8^+$, and NK cells – downregulation Treg – upregulation (serum)	Wang et al.[46]	observational	153 NSCLC patients	NSCLC detection
IL-2, IL-4, IL-6, IL-8, TNF-α, MIP-1α (serum)	Hardy-Werbin et al.[48]	observational	84 SCLC patients	low IL-4, MIP-1α – more advanced stage IL-8 – shorter OS IL-2 – sensitivity to ipilimumab IL-6, TNF-α – resistance to ipilimumab
IL-6, IL-8 (serum)	Pine et al.[49]	observational	270 LC patients in the study group and 532 in the validation group	increased risk of LC development
IL-6, IL-8 and combined IL-6/IL-8 classifier (serum)	Ryan et al.[50]	observational	548 LC patients	shorter OS
IL-17, VEGF (serum)	Lin et al.[51]	observational	76 SCLC patients	both – LC detection, number of metastases IL-17 – more advanced stage, shorter OS
HGF, IL-20, IL-22 (serum and BALF)	Naumnik et al.[52]	observational	46 NSCLC patients (10 adenocarcinoma, 25 SCC, 11 large cell carcinoma)	HGF, IL-22 – NSCLC detection serum HGF, BALF IL-22 – shorter OS serum IL-20 – shorter PFS
Antineural and antinuclear antibodies (serum)	Blaes et al.[55]	observational	61 NSCLC patients (29 adenocarcinoma, 32 SCC)	longer OS
Panel of 4 antibodies: MAGEA1, PGP9.5, SOX2, and TP53 (serum)	Chen et al.[56]	observational	401 participants in training set, including 177 NSCLC patients and a validation set of 57 NSCLC patients	NSCLC detection, shorter OS
Human DNA-topoisomerase I antibody (serum)	Wu et al.[57]	observational	127 NSCLC patients (70 adenocarcinoma, 57 SCC)	NSCLC detection, longer OS
Panel of 5 autoantibodies: p53, BRCA2, HUD, TRIM21, and NY-ESO-1 (plasma)	Zhou et al.[59]	observational	166 NSCLC patients (37 in discovery cohort and 129 in validation cohort)	better response to immune checkpoint inhibitors: higher ORR, longer PFS

Table 1. Biochemical and immune markers of lung cancer – cont.

Biomarker	Study	Type of study	Study group	Outcomes
NY-ESO-1 and XAGE1 antibodies (serum)	Ohue et al.[60]	observational	88 NSCLC patients (13 in discovery and 75 in validation cohort)	good response to anti-PD-1 therapy: higher ORR, longer OS and PFS
ANA, ENA and ASMA antibodies	Giannicola et al.[61]	observational	92 NSCLC patients (55 adenocarcinoma, 31 SCC, 6 undefined)	good response to anti-PD-1 therapy: longer OS and PFS
SIX2 autoantibody (plasma)	Tan et al.[62]	observational	50 NSCLC patients (17 in discovery cohorts 1 and 2, 16 in verification and 17 in validation cohort)	worse response to anti-PD-1 therapy: higher plasma level in non-responders
Panel of 13 antibodies (serum)	Patel et al.[63]	observational	157 NSCLC patients (83 adenocarcinoma, 74 SCC; 111 in training and 46 in validation cohort)	shorter OS
Anti-CCNY antibody (serum)	Ma et al.[64]	observational	264 NSCLC patients (134 adenocarcinoma, 130 SCC)	shorter OS in postoperative patients
Rheumatoid factor, antinuclear, antithyroglobulin and antithyroid peroxidase antibodies (serum)	Toi et al.[65]	observational	137 NSCLC patients (86 non-squamous NSCLC, 51 SCC)	higher rate of immune-related adverse events, higher ORR, longer PFS
Biomarker panel: TNF-α, TNF-RI, MIP-1α, and autoantibodies against Ubiquilin-1, hydroxysteroid-(17-β)-dehydrogenase and triosephosphate isomerase (serum)	Patel et al.[66]	observational	127 NSCLC patients (81 adenocarcinoma, 32 SCC, 14 undefined; 20 in training and 107 in validation cohort)	lymph node metastases
Low ALI (serum)	Zhang and Chen[67]	meta-analysis	8 studies – 1587 LC patients	shorter OS and PFS
LIPI	Mezquita et al.[68]	observational	466 NSCLC patients treated with ICIs (270 adenocarcinoma, 159 SCC (remaining 37 patients were classified as 'NSCLC- other' in the original study); 161 in test and 305 in validation cohort)	worse response to immune checkpoint inhibitors: shorter OS and PFS
NLR	Seitlinger et al.[69]	observational	2027 NSCLC patients	shorter OS, detection of EGFR/*KRAS* mutations
LIPI	Sonehara et al.[70]	observational	171 SCLC patients	shorter OS and PFS
NLR	Lu et al.[71]	meta-analysis	20 studies – 5141 SCLC patients	more advanced stage, shorter OS and PFS
S100B and S100B autoantibody (serum)	Choi et al.[194]	observational	128 LC patients (61 adenocarcinoma, 40 SCC, 13 SCLC and 14 other), 150 NSCLC patients	detection of brain metastases
	Chen et al.[195]	observational	150 NSCLC patients	detection of brain metastases, shorter OS and PFS
ProApolipoprotein A1 (serum)	Marchi et al.[196]	observational	103 LC patients	detection of brain metastases
high NLR, platelet-to-lymphocyte radio and C-reactive protein	Sert et al.[197]	observational	208 NSCLC patients (41 adenocarcinoma, 124 SCC, 43 undefined)	development of brain metastases
NLR	Koh et al.[198]	observational	260 NSCLC patients (194 adenocarcinoma, 66 other)	detection and development of brain metastases
Lower mean platelet volume	Li et al.[199]	observational	476 NSCLC patients (113 adenocarcinoma, 119 other)	detection of brain metastases
Fibrinogen, platelet count	Zhu et al.[200]	observational	275 NSCLC patients	shorter OS and poor prognosis in patients with brain metastases
Purkinje cell cytoplasmic antibody type 2 (serum)	Gadoth et al.[212]	observational	96 patients (including lung cancer)	PNS detection
Anti-Hu (serum)	Graus et al.[213]	observational	196 SCLC patients	higher response rate, longer OS
	Gozzard et al.[214]	observational	238 SCLC patients	longer OS
	Monstad et al.[215]	observational	200 SCLC patients	not associated with survival

SAA – serum amyloid A; TRAP1 – tumor necrosis factor receptor-associated protein 1; NLR – neutrophil-to-lymphocyte ratio; PD – programmed cell death protein; NK – natural killer; TNF-α – tumor necrosis factor alpha; IL – interleukin; VEGF – vascular endothelial growth factor; BALF – bronchoalveolar lavage fluid; TNF-R1 – tumor necrosis factor receptor 1; MIP-1α – macrophage inflammatory protein-1α; LIPI – Lung Immune Prognostic Index; LC – lung cancer; NSCLC – non-small cell lung cancer; SCC – squamous cell carcinoma; ICIs – immune checkpoint inhibitors; PFS – progression-free survival; OS – overall survival; ORR – objective response rate; EGFR – epidermal growth factor receptor; KRAS – Kirsten rat sarcoma viral oncogene; DFS – disease-free survival; TAN – tumor-associated neutrophil; HGF – hepatocyte growth factor; ANA – anti-nuclear antigen, ENA – extractable nuclear antygen; ASMA – anti-smooth cell antygen; ALI – advanced lung cancer inflammation index.

of neoplasms, including lung cancer, and for monitoring the course of disease.[75] The method of obtaining ctDNA from plasma, known as liquid biopsy,[76] is considered a promising alternative to standard tissue biopsy. This noninvasive and safe technique may be easily implemented in all patients, even those for whom a traditional biopsy is not possible, and it enables avoiding complications such as pneumothorax, hemorrhage and air leaks.[77,78]

Rapid advances in molecular techniques that used to detect cancer-specific mutations in cfDNA, such as polymerase chain reaction (PCR) or next-generation sequencing, have offered new perspectives of on implementing liquid biopsies into clinical practice.[79] In a large analysis of data from over 8000 lung cancer patients, ctDNA profiling revealed somatic alterations in 86%, and identified driver oncogene mutations in 48.4% of them.[80] Furthermore, ctDNA profiling has been used to distinguish between benign and malignant lung tumors, and to detect lung cancer at an early stage. Indeed, the assay based on deep sequencing detected 63% of stage I and 83% of stage II lung cancers, respectively.[81]

In a study by Liang et al., the analysis of DNA methylation patterns was performed using tissue samples from patients with lung nodules in order to distinguish between malignant and benign tumors.[82] A predictive model based on 9 methylation markers for ctDNA was then applied to plasma samples, with a sensitivity of 79.5% and specificity of 85.2% for detecting lung cancer. Regarding its subtypes, the sensitivity was 73.9% for adenocarcinoma and 100% for SCC. This difference may be explained by higher intensity of necrotic processes observed in SCC tissue, which results in a greater release of ctDNA into the bloodstream, therefore being eligible for analysis. Existing data support the utility of ctDNA methylation analysis in detecting early-stage lung cancer,[83] and a subsequent study on a large group of lung cancer patients is being conducted to develop a ctDNA methylation classifier for incidental lung nodules.[84] Longitudinal methylation profiling along with somatic mutation analysis in patients with NSCLC have also shown prognostic potential in assessing the risk of recurrence.[85]

With regard to its prognostic value, the level of ctDNA was found indicative of lymph node involvement in resectable NSCLC.[86] Other investigators collected tissue and plasma samples from NSCLC patients before and after surgery in order to identify driver mutations in genes, including *EGFR*, *KRAS*, *TP53*, *BRAF*, *PIK3CA*, and *ERBB2*.[87] Out of 46.3% of plasma samples which were positive for ctDNA before tumor resection, a significant decrease in mutation frequency was noticed, from 8.88% before surgery to 0.28% after the procedure. Furthermore, ctDNA was more prominent in stage Ia and Ib cancers than in more advanced stages. In a follow-up study of surgically treated lung cancer patients, targeted mutations were present in 93% of patients before surgery and in 54% at some point after surgical resection. Interestingly, all of the patients with ctDNA still detectable after surgery experienced progression of the disease, while those without ctDNA remained disease-free.[88]

Use of ctDNA in detecting minimal residual disease was demonstrated in a study where multiplex-PCR assay panels were used to screen for ctDNA in plasma samples of early-NSCLC patients, pre- and postoperatively.[89] A sample was considered ctDNA-positive if at least 2 pre-established single nucleotide variants were detected. Circulating tumor DNA was found in 48% of pre-operative samples, and the detection rate was substantially higher for SCC (97%) than for adenocarcinoma (19%). Again, this discrepancy may be due to less extensive necrotic processes in the latter. Moreover, significant correlations were observed between the results of postoperative ctDNA profiling and the occurrence of clinical relapse or resistance to chemotherapy.[90–94] The use of ctDNA profiling has also been researched in SCLC, although to a lesser extent. In a Chinese study, SCLC patients with higher ctDNA levels had significantly shorter PFS and OS.[95] This relationship between ctDNA detection and poor prognosis has been also been observed in other research.[96] The potential role of ctDNA in SCLC detection and progression monitoring was further strengthened by a large ctDNA analysis in over 10,000 cancer patients. In this group, the highest detectability of ctDNA in all cancer types was in SCLC, reaching 91.1%.[97]

The role of ctDNA profiling is also gaining attention in tailoring and monitoring of lung cancer treatment, and several liquid biopsy tests have been developed for this purpose.[98–100] This method can be used before applying adjuvant chemotherapy, which is considered an option in NSCLC, to identify eligible patients.[101] Based on recent understanding of the mechanisms of resistance to tyrosine kinase inhibitors (TKIs),[102] ctDNA analysis may be a promising tool in this area. Circulating tumor DNA analysis has also been used to investigate resistance mechanisms in patients with NSCLC treated with rociletinib, a 3rd generation EGFR inhibitor.[103] Multiple resistance mechanisms to the drug were present in 46% of patients, while at least 1 such mechanism was found in 65% of them, with *MET* copy number gain being the most common, as it was found in 26% of the patients. In another experiment, researchers were able to identify driver and resistance mutations through next generation sequencing of ctDNA, even when tissue sequencing was not successful.[104] Furthermore, there is also some evidence for the detection of *T790M* mutation in ctDNA profiling in patients with *T970M*-negative tissue.[105] These observations support the potential of ctDNA not only as a supplementary method, but also as an independent screening tool that could be applied in the planning of individualized treatment strategies.

Detectable *EGFR* mutations in cfDNA were associated with a longer PFS in response to treatment with erlotinib, a TKI, while its persistence in a follow-up plasma analysis resulted in shorter PFS and OS.[106] In another study comprising patients treated with erlotinib, *EGFR T790M* mutations linked to TKI treatment resistance were detectable

in cfDNA even before disease progression.[107] Several other studies have also underlined the potential role of ctDNA profiling in the detection of resistance mutations as a part of disease monitoring.[108–113] Changes in ctDNA profile demonstrated a good predictive value in a study by Nabet et al., where plasma samples were analyzed in patients with advanced lung cancer treated with immune checkpoint inhibitors.[114] A significant (at least 50%) drop in detectable ctDNA levels at 4 weeks after the initial treatment was considered a molecular response and helped identify patients with durable clinical benefit, defined as PFS of at least 6 months. Similar results were found by other authors, underlining the association between ctDNA decrease and better PFS and OS.[115–118] Accordingly, baseline and post-treatment ctDNA indicated worse clinical outcomes.[119–122] Circulating tumor DNA has also been investigated in the evaluation of tumor mutation burden (TMB), a novel predictive marker reflecting the total number of existing mutations, which is thought to be predictive of the response to PD-1 and PD-L1 inhibitors. It was hypothesized that patients with a higher burden of somatic mutations would benefit from immune checkpoint inhibitors due to a better recognition of neoantigens. This beneficial effect was confirmed with tumor tissue analyses of NSCLC patients treated with pembrolizumab,[123] nivolumab or ipilimumab.[124] The evaluation of blood-based TMB, assessed with ctDNA genetic profiling, revealed complementary findings. Non-small cell lung cancer patients with high blood-based TMB treated with atezolizumab showed a better response to the therapy in 1 study,[125] while in another report,[126] higher TMB was found to correlate with shorter PFS and OS in NSCLC. These diverse results point to potential limitations of ctDNA analysis, such as a small possible range of mutations that can be detected using liquid biopsy. Future improvements to the method should include establishing validated sequencing panels and cut points.[127]

As a potential marker of lung cancer diagnosis and progression, ctDNA was also compared to previously known biomarkers and showed a higher detection rate and positive predictive value than CYFRA21-1, CEA, NSE, SCC, CA-125, and CA19-9.[87] Concordant results were obtained in a similar study, where plasma samples were taken before, during and after surgery.[128] In this study, the sensitivity of ctDNA detection was higher than for protein tumor markers (63.2% compared to 49.3%), and a significant drop in the average ctDNA mutation frequency after surgery was also reported.

Circulating tumor cells

Apart from ctDNA, the so-called "liquid biopsy" techniques may also reveal circulating tumor cells (CTCs) that originate from primary or metastatic tumors.[129] As CTC numbers in plasma are very low, they may be detected by means of various methods, including immunomagnetic separation with EpCAM- or CD45-based assays, PCR or telomerase-based assays, as well as cellular isolation with size-dependent filters.[130] A recently published meta-analysis, including 21 studies with almost 4000 participants, demonstrated high pooled sensitivity and specificity of CTCs in lung cancer detection.[131] There is also some evidence of CTC role as a potential marker of lung cancer progression and dissemination, as a higher abundance of detectable CTCs before the commencement of treatment resulted in shorter OS and PFS in NSCLC patients.[132] In another meta-analysis,[133] the presence of CTCs was shown to be associated with response to chemotherapy and prognosis. Patients who were CTC-positive at baseline or who converted to CTC-positive during treatment, presented with lower rates of disease control, as well as worse OS and PFS. Irrespective of their correlation with survival rates, CTCs were also associated with lymph node metastasis.[134]

The analysis of CTC number at baseline and at different time points in the course of SCLC was referred to for the prediction and monitoring of the response to chemotherapy.[135] Circulating tumor cells obtained from plasma samples may be also used for the detection of specific mutations related to lung cancer, such as EGFR[136] and KRAS,[137] with a higher sensitivity than ctDNA. Moreover, specific gene rearrangements can be detected in CTCs with promising acurracy. In patients with lung adenocarcinoma, anaplastic large-cell lymphoma (*ALK*) gene rearrangement and ALK protein expression in CTCs were concordant with findings from tumor tissue,[138] which has been confirmed by other researchers.[139,140] A rearrangement of repressor of silencing 1 (*ROS1*) is another example of chromosomal aberrations detectable in CTCs, with biopsy-confirmed gene fusion in NSCLC patients.[141] Dynamic changes in the number of CTCs with aberrant ALK-fluorescence in situ hybridization patterns, such as *ALK* copy number gain, might serve as predictive markers of the response to treatment, as these aberrations are considered to be one of the mechanisms underlying acquired resistance to crizotinib (an ALK and ROS1 inhibitor). A decrease in CTCs with *ALK* copy number gain during treatment with crizotinib was linked to a longer PFS.[142]

Apart from the lack of standardized methods of analysis, CTCs appear to have other limitations similar to ctDNA evaluation. These include low detection rate, especially in patients with an early stage of the disease, and an unclear influence of tumor heterogeneity and its localization on liquid biopsy findings. Table 2 and Table 3 summarize the results of studies concerning ctDNA and CTCs in lung cancer, respectively.

MicroRNA as a lung cancer marker

MicroRNAs (miRNAs) are noncoding small molecules, comprising approx. 21 nucleotides. They are considered post-transcriptional regulators of gene expression. They

achieve this by binding to the 3′-UTR of target messenger RNA, which results in repressing translation or promoting messenger RNA deadenylation and degradation.[143] Due to their biological role, miRNAs are thought to be important in cancer initiation and progression, as they can influence both oncogenes and tumor suppressor genes.[144] Furthermore, a potential role of miRNA in the diagnostics and treatment of lung cancer has been recently highlighted.[145] Considering the availability of miRNA expression in cancer tissue and bodily fluids, especially in serum, it can be easily measured using liquid biopsy.[145] A growing popularity of miRNA research has led to the development of diagnostic panels which may be used complementarily in the early detection of malignant lung lesions and are constantly being improved.[146,147]

A signature panel of 15 miRNAs was able to differentiate between patients with lung cancer and those with non-tumor lung disease, other systemic diseases, and healthy controls, with a sensitivity of 82.8% and a specificity of 93.5%.[148] Other authors used a panel of 2 miRNAs (miRs-31-5p and 210-3p) detected in sputum and 1 miRNA (miR-21-5p) from plasma, that reached sensitivity and specificity in the detection of lung cancer of 85.5% and 91.7%, respectively.[149] Even greater sensitivity and specificity (99% for both) was achieved by a combination of miR-1268b and miR-6075, and was validated in a group of over 3000 participants and maintained its performance regardless of TNM stage or histological type of tumor.[150] A number of specific miRNAs have also proven to be valuable in the early diagnosis of NSCLC,[151] distinguishing NSCLC from SCLC[152] and specific types of NSCLC.[153]

Numerous miRNAs are efficient in the prognosis of disease progression and resistance to treatment. The analysis of miRNA expression in advanced NSCLC cases revealed 17 miRNAs significantly associated with 2-year survival rate.[154] At the same time, the downregulation of miR-590-5p was linked to lower median survival rates in a cohort of NSCLC patients,[155] while the upregulation of miR-25 was higher in NSCLC patients compared to the control group, but also correlated negatively with OS and relapse-free survival.[156] In a separate analysis, patients with adenocarcinoma and SCC with high expression of miR-25-3p had shorter OS, regardless of tumor histology.[157] A meta-analysis on the prognostic value of the downregulation of miR-126 highlighted its relationship to unfavorable outcomes of NSCLC.[158] Others reported an association between miR-153,[159] miR-494,[160] miR-519d[161] and more advanced clinical stage, presence of lymph node metastases, and worse OS in NSCLC patients. Similar results regarding a poor prognosis in NSCLC patients were reported for the downregulation of miR-184,[162] miR-185,[163] miR-770,[164] and miR-30a-5p,[165], and the upregulation of miR-23b-3p, miR-10b-5p and miR-21-5p,[166] miR-31,[167] miR-378,[168] miR-942, and miR-601.[169] On the contrary, a high expression of miR-3195 resulted in longer OS,[170] while miR-21 and miR-4257 were established as predictors of NSCLC recurrence.[171] In patients with SCLC, the upregulation of miR-92b and miR-375 was related to chemotherapy resistance and shorter PFS.[172] At the same time, miR-422a and miR-135a showed a strong association with metastases to lymph nodes in lung cancer patients,[173,174] lower expression of miR-139-5p was found in NSCLC patients with bone metastases,[175] and miR-375-3p was also proposed to be a possible biomarker of SCLC metastatic activity.[176]

Expression profiles of miRNA may also serve as markers for treatment response,[170] with higher expression of miR-1249-3p observed in individuals who responded well to chemotherapy. Changes in serum levels of various miRNA panels have been used to predict worse sensitivity to chemotherapy.[177,178] Additionally, in a cohort of early-stage NSCLC patients, the expression of miR-216b was significantly increased after a successful tumor resection.[179] Profiling of miRNA may also be indicative of the response to radiotherapy[180,181] or immunotherapy, with patients who significantly overexpressed miR-320b-d before the treatment with PD-1/PD-L1 inhibitors not responding well to the therapy. In the same group, a decrease in miR-125b-5p was observed in those who presented with only a partial response.[182] In NSCLC patients, miR-504 expression differed significantly depending on *EGFR* mutation status.[183] An experimental miRNA panel was also tested for discrimination between *ALK*-positive and *ALK*-negative lung cancers,[184] which is relevant to immunotherapy treatment options. The miRNAs were also proposed as markers of resistance to EGFR-TKI therapy,[185] as shorter OS was reported in patients with high serum levels of miR-30b and miR-30c treated with erlotinib.[186] Furthermore, miR-30c expression patterns showed utility in predicting cardiotoxicity in patients treated with bevacizumab,[187] which indicates the potential of this method for stratifying the risk of adverse events for particular therapies. Further attempts to improve diagnostic and prognostic accuracy of miRNA in lung cancer patients include combining this method with other commonly used biomarkers, such as CEA and CYFRA21-1.[188,189]

Although miRNA profiling has gained much interest in recent years, its application in clinical practice still has some limitations. Methodological discrepancies within study design and technological details of tools applied can be seen throughout the studies on miRNA in lung cancer, which prevents consistent conclusions.[190] Another issue to be addressed is a lack of specificity of candidate miRNAs, as there is a large number of these being examined in various types of cancer, and these miRNAs are involved in the regulation of multiple biological pathways. Furthermore, miRNA expression can be affected by disease stage and the treatment used,[191,192] which has to be considered in the clinical interpretation of research findings. Therefore, there is a need for further studies on representative groups of patients with the use of consistent methodology,

Table 2. Circulating tumor DNA (ctDNA) in lung cancer

Biomarker	Study	Type of study	Study group	Outcomes
ctDNA profiling	Mack et al.[80]	observational	8388 NSCLC patients (4142 adenocarcinoma, 4246 not specified)	detection of driver and resistance mutations
ctDNA profiling	Peng et al.[81]	observational (clinical trial No. NCT03081741)	136 LC patients (100 adenocarcinoma, 28 SCC, 1 SCLC, 7 other)	LC detection
ctDNA methylation patterns	Liang et al.[82]	observational	132 LC patients in validation cohort	LC detection
ctDNA methylation profiling	Yang et al.[83]	observational	39 LC patients	LC detection
ctDNA methylation profiling	Li et al.[85]	obervational	65 NSCLC patients (49 adenocarcinoma, 11 SCC, 5 other)	higher risk of relapse
VAF level of ctDNA	Zhang et al.[86]	observational (cohort from TRACERx clinical trial No. NCT01888601)	95 NSCLC patients (55 adenocarcinoma, 32 SCC, 8 other; 58 in training, and 37 in validation cohort)	lymph node metastases
ctDNA profiling before and after surgery	Guo et al.[87]	observational	41 NSCLC patients (33 adenocarcinoma, 6 SCC, 1 neuroendocrine tumor and 1 large cell carcinoma)	response to treatment
ctDNA profiling	Chaudhuri et al.[88]	observational	40 LC patients (37 NSCLC, 3 SCLC)	detection of minimal residual disease, shorter OS and PFS
ctDNA profiling	Abbosh et al.[89]	observational (cohort from TRACERx clinical trial No. NCT01888601)	100 LC patients	higher risk of relapse
ctDNA profiling	Waldeck et al.[90]	observational	21 NSCLC patients	higher risk of relapse
ctDNA profiling	Kuang et al.[91]	observational (cohort from GASTO 1035 clinical trial No. NCT03465241)	38 NSCLC patients (23 adenocarcinoma, 6 SCC, 9 other)	shorter RFS, chemotherapy resistance
ctDNA profiling	Xia et al.[92]	observational	330 NSCLC patients	shorter RFS, increased RFS in patients who recieved adjuvant therapies
ctDNA profiling	Qiu et al.[93]	observational	103 NSCLC patients (60 adenocarcinoma, 38 SCC, 1 adenosquamous carcinoma, 1 atypical carcinoid, 3 large cell neuroendocrine carcinoma)	shorter RFS, increased RFS in patients who recieved adjuvant chemotherapy
ctDNA profiling	Zhang et al.[94]	observational	14 LC patients (7 adenocarcinoma, 2 SCC, 5 SCLC)	higher risk of relapse, chemotherapy resistance
ctDNA profiling	Nong et al.[95]	observational	22 SCLC patients	shorter OS and PFS
ctDNA profiling	Herbreteau et al.[96]	observational (cohort from IFCT-1603 clinical trial No. NCT03059667)	68 SCLC patients	shorter OS and PFS, longer OS in patients with low ctDNA abundance treated with atezolizumab
ctDNA profiling	Chabon et al.[103]	observational (cohort from clinical trials No. NCT01526928 and No. NCT02147990)	43 NSCLC patients	detection of resistance mutations to rociletinib (EGFR inhibitor)
ctDNA profiling	Thompson et al.[104]	observational	102 NSCLC patients	detection of driver and resistance mutations
ctDNA profiling	O'Kane et al.[105]	observational	72 NSCLC patients	detection of resistance mutations, shorter PFS
ctDNA profiling	Mok et al.[106]	observational (cohort from FASTACT-2 clinical trial No. NCT00883779)	305 NSCLC patients	*EGFR* mutations detection, longer PFS in EGFR-positive patients treated with erlotinib
ctDNA profiling	Oxnard et al.[107]	observational	13 NSCLC patients	resistance mutations detection, treatment response to erlotinib
ctDNA profiling	Kim et al.[108]	observational	81 adenocarcinoma patients	detection of *EGFR* mutations, higher number of metastases, shorter PFS, shorter duration of disease control by EGFR-TKIs

Table 2. Circulating tumor DNA (ctDNA) in lung cancer – cont.

Biomarker	Study	Type of study	Study group	Outcomes
ctDNA profiling	Dono et al.[109]	observational	42 adenocarcinoma patients	detection of *T790M* mutation
ctDNA profiling	Beagan et al.[110]	observational	20 adenocarcinoma patients with *EGFR T790M* mutation	response to osimertinib (TKI) – higher ctDNA level in nonresponders
ctDNA profiling	Boysen Fynboe Ebert et al.[111]	observational (clinical trial No. NCT02284633)	225 NSCLC patients with *EGFR* mutations: 82 treated with osimertinib (80 adenocarcinoma, 2 SCC)	response to osimertinib (TKI) – longer PFS, higher ORR and disease control rates in patients with clearing of ctDNA after treatment initiation
ctDNA profiling	Lei et al.[112]	observational	98 NSCLC patients with *EGFR* uncommon mutation	detection of resistance mutations to icotinib (TKI)
ctDNA profiling	Provencio et al.[113]	observational	228 NSCLC patients with *EGFR* mutation (210 adenocarcinoma, 18 other)	response to TKI – longer OS and PFS in patients with clearing of ctDNA after treatment initiation
ctDNA profiling	Nabet et al.[114]	observational	99 NSCLC patients (85 non-squamous LC, 14 SCC)	response to ICI – longer PFS in patients with significant drop of ctDNA after single ICI cycle
ctDNA profiling	Goldberg et al.[115]	observational	28 NSCLC patients (27 non-squamous LC, 1 SCC)	response to ICI – longer OS and PFS in patients with a significant drop of ctDNA after treatment
ctDNA profiling	Ricciuti et al.[116]	observational	62 NSCLC patients (56 non-squamous LC, 6 SCC)	response to pembrolizumab – higher ORR, longer OS and PFS in patients with significant drop of ctDNA after treatment
ctDNA profiling	Hellmann et al.[117]	observational	31 NSCLC patients (28 non-squamous, 3 SCC)	response to ICI – longer PFS in patients with undetectable ctDNA after treatment
ctDNA profiling	Guo et al.[118]	observational	64 NSCLC patients (28 non-squamous LC, 36 SCC)	response to treatment (surgery+chemotherapy) – longer OS in patients with decreasing ctDNA and methylated DNA
ctDNA profiling before and after surgery	Peng et al.[119]	observational	77 NSCLC patients (40 adenocarcinoma, 30 SCC, 7 other)	response to treatment – shorter OS and RFS in ctDNA-positive pre- and postoperative patients
ctDNA profiling	Giroux Leprieur et al.[120]	observational	23 NSCLC patients, 15 included in analysis (10 non-squamous LC, 5 SCC)	response to nivolumab – longer PFS in patients with significant drop of ctDNA after treatment
ctDNA profiling	Lee et al.[121]	observational	57 adenocarcinoma patients	bone metastases detection, response to TKI – shorter PFS
ctDNA profiling	Roosan et al.[122]	observational	370 NSCLC patients (345 adenocarcinoma, 13 SCC, 12 other)	detection of somatic mutations, longer PFS in patients with low ctDNA level
ctDNA tumor mutational burden	Gandara et al.[125]	observational (samples from POPLAR trial No. NCT01903993 and OAK trial No. NCT02008227)	211 samples from NSCLC patients (POPLAR study) and 583 samples from NSCLC patients (OAK study)	response to atezolizumab – longer OS and PFS
ctDNA tumor mutational burden	Chae et al.[126]	observational	136 NSCLC patients (99 adenocarcinoma, 27 SCC, 10 other)	response to ICIs – shorter OS and PFS
ctDNA profiling	Chen et al.[128]	observational	76 NSCLC patients (59 adenocarcinoma, 17 SCC)	detection of cancer-specific mutations
ctDNA profiling	Ma et al.[205]	observational	21 NSCLC patients	detection of cancer-specific mutations in CSF
ctDNA profiling	Huang et al.[206]	observational	35 adenocarcinoma patients	detection of *EGFR* mutations in patients with CNS metastases
ctDNA profiling	Belloum et al.[207]	observational	56 NSCLC patients (49 adenocarcinoma, 5 SCC, 2 other)	detection of cancer-specific mutations in patients with metastases
ctDNA profiling	Aldea et al.[208]	observational (clinical trial No. NCT02666612)	247 LC patients (230 adenocarcinoma, 5 SCC, 12 other)	detection of cancer-specific mutations in patients with metastases

VAF – variant allele frequency; RFS – relapse-free survival; LC – lung cancer; NSCLC – non-small cell lung cancer; SCC – squamous cell carcinoma; SCLC – small cell lung cancer; EGFR – epidermal growth factor receptor; OS – overall survival; PFS – progression-free survival; TKI – tyrosine kinase inhibitor; ORR – objective response rate; ICIs – immune checkpoint inhibitors; CSF – cerebrospinal fluid.

Table 3. Circulating tumor cells (CTCs) in lung cancer

Biomarker	Study	Type of study	Study group	Outcomes
CTCs	Zhao et al.[131]	meta-analysis	21 studies – 3997 participants, including 2714 LC patients	LC detection
CTCs	Jiang et al.[132]	meta-analysis	10 studies – 1002 NSCLC patients	high abundance of CTCs – shorter OS and PFS
CTCs	Wu et al.[133]	meta-analysis	8 studies – 453 LC patients	lower disease control rate, shorter OS and PFS in CTC-positive patients at baseline and during chemotherapy
CTCs	Wang et al.[134]	meta-analysis	20 studies – 1576 NSCLC patients	lymph node metastases, more advanced stage, shorter OS and PFS
CTCs	Jiang et al.[135]	meta-analysis	16 studies – 1103 SCLC patients	shorter OS and PFS in patients with high pre-treatment CTC level, shorter OS in patients with high CTCs level after treatment
CTCs	Liu et al.[136]	meta-analysis	8 studies – 170 NSCLC patients	*EGFR* mutations detection
CTCs	Shen et al.[137]	meta-analysis	12 studies – 1131 LC patients	*KRAS* mutation detection
CTCs	Ilie et al.[138]	observational	87 adenocarcinoma patients	*ALK* gene rearrangement detection
CTCs	Pailler et al.[139]	observational	32 NSCLC patients	*ALK* gene rearrangement detection
CTCs	Tan et al.[140]	observational	26 NSCLC patients	*ALK* gene rearrangement detection
CTCs	Pailler et al.[141]	observational	8 NSCLC patients	*ROS1* gene rearrangement detection
CTCs	Pailler et al.[142]	observational	39 NSCLC patients	response to crizotinib – longer PFS in patients with decrease in CTC number with *ALK*-CNG

LC – lung cancer; NSCLC – non-small cell lung cancer; PFS – progression-free survival; OS – overall survival; ORR – objective response rate; EGFR – epidermal growth factor receptor; KRAS – Kirsten rat sarcoma viral oncogene; SCLC – small cell lung cancer; ALK – anaplastic lymphoma kinase; ROS1 – repressor of silencing 1; CNG – copy number gain.

in order to ensure reproducibility and generalizability of results. Studies investigating miRNA in lung cancer are presented in Table 4.

Markers of nervous system involvement in the course of lung cancer

Markers of brain metastases

Calcium binding protein B (S100B), synthesized in astrocytic terminal processes,[193] is an established marker of blood–brain barrier disruption. The detection of S100B protein along with anti-S100B autoantibody allows to distinguish between lung cancer patients with or without brain metastases, with a sensitivity of 89% and a specificity of 58%.[194] Furthermore, the evidence of an association between serum S100B level and brain metastases with subsequently worse prognosis has been shown by other researchers.[195] However, low specificity for S100B is a main barrier to its implementation, as its abnormal expression has also been reported in patients with cerebrovascular disease. Nonetheless, pro-apolipoprotein A-1 levels, measured using proteomic techniques, appear to be a more specific marker as it was increased in lung cancer patients with brain metastases, regardless of cerebrovascular disease.[196]

Among other potential markers, high NLR, platelet-to-lymphocyte ratio and C-reactive protein (CRP) levels were suggested to indicate the development of brain metastases in lung cancer patients after definitive radiotherapy or radiotherapy combined with chemotherapy.[197] High NLR ($\geq$4.95) and lower mean platelet volume were associated with an increased risk of brain metastases in patients with NSCLC.[198,199] At the same time, high plasma fibrinogen concentration and platelet count correlated with shorter OS in NSCLC patients already diagnosed with brain metastases.[200]

The miRNA has also emerged as a relevant marker of brain metastases in lung cancer, with the overexpression of miR-330-3p noted in the serum of NSCLC patients with brain metastases, when compared to those without dissemination to the central nervous system.[201] Significantly lower expression of miR-330 was found in lung cancer patients who had undergone whole-brain radiation therapy, and these patients proved to be radiation-sensitive.[202] Furthermore, serum levels of miR-21 before and after radiotherapy in lung cancer patients with brain metastases were significantly correlated with OS.[203] The expression of miR-483-5p and miR-342-5p in serum and cerebrospinal fluid differed between patients with leptomeningeal and brain parenchymal metastases.[204]

The detection of ctDNA in the cerebrospinal fluid of patients with lung cancer brain metastases displayed higher mutation detection rates than peripheral blood samples.[205] Sensitivity of detecting *EGFR* mutations in ctDNA from plasma or cerebrospinal fluid was comparable, while *T790M* mutations were more prevalent in plasma samples.[206] With regard to the location of metastases, *EGFR*,

Table 4. MicroRNAs (miRNAs) in lung cancer

Biomarker	Study	Type of study	Study group	Outcomes
the miR-Test (13 miRNAs; serum)	Montani et al.[146]	observational (cohort from COSMOS clinical trial No. NCT01248806)	calibration set: 24 patients (12 with LC); validation set: 1008 patients (36 with LC); clinical set: 74 LC patients	LC detection
miRNA panel (24 miRNAs; plasma)	Sozzi et al.[147]	observational (cohort from MILD clinical trial No. NCT02837809)	939 participants, including 69 LC patients	LC detection
miRNA panel (15 miRNAs; whole blood)	Fehlmann et al.[148]	observational	3102 participants, including 606 LC patients	LC detection
miRNA panel (miR-31-5p and miR-210-3p in sputum and miR-21-5p in plasma)	Liao et al.[149]	observational	132 NSCLC patients (74 adenocarcinoma, 58 SCC; 76 in training and 56 in testing cohort)	NSCLC detection
miR-1268b and miR-6075 (serum)	Asakura et al.[150]	observational	1566 LC patients (1217 adenocarcinoma, 221 SCC, 23 SCLC, 105 other; 208 in discovery cohort and 1358 in validation cohort)	LC detection
miR-145 (serum and plasma)	Tao et al.[151]	meta-analysis	9 studies – 1394 NSCLC patients	NSCLC detection
serum miRNA panel (miR-9-5p, miR-21-5p, miR-223-3p, CEA, CYFRA21-1, and SCC)	Yang et al.[189]	observational	104 NSCLC patients (59 adenocarcinoma, 40 SCC, 5 other)	NSCLC detection
panel of 3 miRNAs: miR-17, miR-190b and miR-375 (plasma)	Lu et al.[152]	observational	1132 participants (456 high-risk individuals, 315 adenocarcinoma, 224 SCC, 137 SCLC; 106 in discovery cohort, 565 in training cohort and 461 in validation cohort)	discrimination between SCLC and NSCLC
6 miRNAs: miR-211-3p, miR-3679-3p, miR-4787-5p, miR-3613-3p, miR-3675-3p, and miR-5571-5p (tissue and plasma)	Pu et al.[153]	observational	40 NSCLC patients (27 adenocarcinoma, 13 SCC)	discrimination between NSCLC subtypes
panel of 17 miRNAs (serum)	Wang et al.[154]	observational	391 NSCLC patients (214 adenocarcinoma, 87 SCC, 90 other; 8 in screening, 192 in training and 191 in testing set)	higher risk of death, shorter median survival time
miR-590-5p (plasma; downregulation)	Khandelwal et al.[155]	observational	80 NSCLC patients (18 adenocarcinoma, 41 SCC, 21 mixed)	NSCLC detection, shorter OS
miR-25 (serum)	Li et al.[156]	observational	128 NSCLC patients (102 adenocarcinoma, 26 SCC)	NSCLC detection, more advanced stage, lymph node metastases, shorter OS and RFS
miR-126 (tissue and plasma; downregulation)	Sun et al.[158]	meta-analysis	8 studies investigated prognostic value (1102 NSCLC patients)	shorter OS
miR-494 (tissue and serum)	Zhang et al.[160]	observational	90 NSCLC patients (55 adenocarcinoma, 35 SCC)	more advanced stage, lymph node metastases, shorter OS and disease-free survival
miR-519d (tissue and serum; downregulation)	Wang et al.[161]	observational	130 NSCLC patients (40 adenocarcinoma, 90 SCC)	NSCLC detection, more advanced stage, lymph node and distant metastases, shorter OS
miR-184 (downregulation), miR-191 (both in serum)	Ding et al.[162]	observational	100 NSCLC patients (82 adenocarcinoma, 13 SCC, 5 large cell carcinoma)	NSCLC detection, shorter OS
miR-185 (serum; downregulation)	Liu et al.[163]	observational	146 NSCLC patients (88 adenocarcinoma, 58 SCC)	LC detection, more advanced stage, lymph node metastases, shorter OS

Table 4. MicroRNAs (miRNAs) in lung cancer – cont.

Biomarker	Study	Type of study	Study group	Outcomes
miR-770 (serum; downregulation)	Sun et al.[164]	observational	196 NSCLC patients	more advanced stage, lymph node metastases, shorter OS
miR-23b-3p, miR-10b-5p, miR-21-5p (plasma exosomal)	Liu et al.[166]	observational	10 adenocarcinoma patients in discovery cohort and 196 NSCLC patients in validation cohort (115 adenocarcinoma, 73 SCC, 8 other)	shorter OS
miR-378 (serum exosomal)	Zhang and Xu[168]	observational	103 NSCLC patients (53 adenocarcinoma, 46 SCC, 4 other)	more advanced stage, lymph node metastases, shorter OS, higher rate of radiotherapeutic response
miR-942 and miR-601 (serum)	Zhou et al.[169]	observational	125 NSCLC patients in validation cohort	NSCLC detection, more advanced stage, lymph node metastases, shorter OS and RFS
miR-3195, miR-1249-3p (both in serum)	Kumar et al.[170]	observational	75 NSCLC patients (42 adenocarcinoma, 33 SCC)	miR-1249-3p – adenocarcinoma detection, higher rate of complete and partial response to chemotherapy miR-3195 – longer OS
miR-21 and miR-4257 (plasma exosomal)	Dejima et al.[171]	observational	201 NSCLC patients (138 adenocarcinoma, 55 SCC, 8 other; 6 in discovery and 195 in validation cohort)	shorter RFS in surgically treated patients
miR-92b and miR-375 (plasma)	Li et al.[172]	observational	63 SCLC patients (including discovery and validation cohorts)	shorter PFS, a significant decrease in patients who responded to chemotherapy
miR-422a (lymph node tissue, plasma)	Wu et al.[173]	observational	77 LC patients (26 in training and 51 in validation cohort; 35 adenocarcinoma, 36 SCC, 6 SCLC)	lymph node metastases
miR-135a (serum)	Zou et al.[174]	observational	117 NSCLC patients (59 adenocarcinoma, 58 SCC)	lymph node metastases
miR-375-3p (plasma exosomal)	Mao et al.[176]	observational	126 SCLC patients (2 validation cohorts of 57 and 69 patients, respectively)	lymph node and distant metastases
miR-216b (serum exosomal; downregulation)	Liu et al.[179]	observational	105 NSCLC patients (45 adenocarcinoma, 60 SCC)	LC detection, more advanced stage, lymph node metastases, shorter OS and DFS
miR-96 (plasma exosomal)	Zheng et al.[180]	observational	52 NSCLC patients	shorter OS, higher levels in patients with radiotherapy-resistant NSCLC
panel of 11 miRNAs (serum)	Sun et al.[181]	observational (cohort from 4 clinical trials)	80 NSCLC patients	radiotherapy resistance – shorter OS
miR-320b-d, miR-125b-5p (plasma exosomal)	Peng et al.[182]	observational	30 NSCLC patients	worse response to PD-1/PD-L1 inhibitors – lower rate of complete and partial response
miR-504 (plasma)	Szpechcinski et al.[183]	observational	66 NSCLC patients (56 adenocarcinoma, 10 other)	detection of *EGFR* mutations
miR-28-5p, miR-362-5p, miR-660-5p (plasma; downregulation)	Li et al.[184]	observational	6 NSCLC patients in screening cohort and 73 NSCLC patients in validation cohort	detection of *ALK* mutations miR-660-5p – increased level after crizotinib treatment in responders miR-362-5p – shorter PFS
miR-21 (plasma)	Li et al.[185]	observational	25 non-squamous NSCLC patients	resistance to immunotherapy – miR-21 level higher at the time of acquired resistance to TKI than at baseline
miR-30b and miR-30c (plasma)	Hojbjerg et al.[186]	observational	29 adenocarcinoma patients with *EGFR* mutations	shorter PFS and OS in patients treated with erlotinib
miR-30c (serum)	Zhou et al.[187]	observational	80 NSCLC patients (47 adenocarcinoma, 23 SCC, 10 adenosquamous NSCLC)	cardiotoxicity during bevacizumab therapy
miR-762 (serum)	Chen et al.[188]	observational	148 NSCLC patients (84 adenocarcinoma, 64 SCC)	more advanced stage, lymph node metastases, shorter OS and RFS in patients treated with gefitinib

Table 4. MicroRNAs (miRNAs) in lung cancer – cont.

Biomarker	Study	Type of study	Study group	Outcomes
miR-330-3p (serum)	Wei et al.[201]	observational	122 NSCLC patients (95 adenocarcinoma, 18 SCC, 9 other)	detection of brain metastases
	Jiang et al.[202]	observational	258 LC patients with brain metastases (149 adenocarcinoma, 61 SCC, 48 other)	radiation sensitivity – lower survival rate and median survival time
miR-21 (serum)	Zhu et al.[203]	observational	200 LC patients with brain metastases (97 adenocarcinoma, 55 SCC, 48 large cell carcinoma)	radiation sensitivity – shorter OS
miR-483-5p and miR-342-5p (serum exosomal and CSF exosomal)	Xu et al.[204]	observational	38 LC patients (25 adenocarcinoma, 13 other)	detection of leptomeningeal metastases

CEA – carcinoembryonic antigen; CSF – cerebrospinal fluid; LC – lung cancer; NSCLC – non-small cell lung cancer; SCC – squamous cell carcinoma; SCLC – small cell lung cancer; EGFR – epidermal growth factor receptor; OS – overall survival; PFS – progression-free survival; RFS – relapse-free survival; DFS – disease-free survival; PD – programmed cell death protein; ALK – anaplastic lymphoma kinase; TKI – tyrosine kinase inhibitors.

KRAS, *BRAF*, or *ERBB2* mutations in plasma ctDNA could be detected in half of the patients with isolated brain metastases,[207,208] and ctDNA positivity was associated with a higher risk of extra central nervous system dissemination.

Markers of paraneoplastic neurological syndromes

Specific autoantibodies related to the development of PNS can be regarded as markers of the involvement of nervous system in the course of lung cancer.[14] Onconeural antibodies, directed against intracellular antigens, are already well recognized and commonly used in practice. Most prevalent among these antibodies are anti-Hu, anti-Yo, anti-Ri, anti-CV2, anti-Tr, anti-amphiphysin, and anti-Ma/Ta,[8] with anti-Hu, anti-Ri, anti-CV2, and anti-amphiphysin being closely linked to lung cancer.[209] Recent years have also seen advances in establishing the role of antibodies against cell-surface or synaptic antigens, such as antibodies against N-methyl-D-aspartate receptors, the α-amino-3-hydroxy-5-methyl-4-isoxazolepropionic acid receptor, the γ-aminobutyric acid receptor-B, leucine-rich glioma-inactivated protein 1, and contactin-associated protein-like 2.[210]

Several other autoreactive antibodies and related antigens were investigated for their use in the detection of PNS in lung cancer patients, including phosphodiesterase 10A and Purkinje cell cytoplasmic antibody type 2 antibodies.[211,212] Apart from early detection of lung cancer, some of these antibodies were investigated in terms of their prognostic value. Indeed, some reports have indicated that the presence of anti-Hu antibodies in patients with SCLC was associated with limited stage of the disease and satisfactory response to therapy[213] or longer median survival,[214] although this correlation was not clear.[215] Despite their clinical utility, onconeural and cell-surface antibodies have limited sensitivity and specificity, they are not detectable in every patient with PNS,[216] and may be associated with different kinds of neoplasms.[217] Thus, further exploration in this field seems warranted.

Conclusions

In this review, we outlined the recent development in the research on of potential biochemical, immunological and molecular markers of lung cancer that have shown promising sensitivity and/or specificity. Molecular markers are associated with improved understanding of complex tumor genetics, while immunological markers have provided a more thorough insight into the tumor-related immune environment, thus opening new perspectives in diagnosis and effective management of lung cancer. Diagnostic markers that enable an early detection of the disease may be valuable in supporting existing screening methods, while markers with predictive potential could contribute to the identification of patients at high risk of recurrence or with the propensity for metastases, with scope for the development of individualized monitoring and treatment strategies. With the advent of new treatment options such as immune checkpoint and kinase inhibitors, the recognition of mechanisms of resistance to targeted therapy and emerging decisions about personalized treatment strategies appear as key elements of lung cancer management, with the use of relevant biomarkers being indispensable. Further investigation should be aimed at improving the accuracy and specificity of these markers, perhaps by combining them into panels.

Circulating biomarkers seem particularly promising for practical use as their detection is non-invasive, safe and easily repeatable. However, the majority of molecules

investigated still need thorough validation, with standardization of techniques and assays used, and established cut-off values. Furthermore, a systematic comparative analysis of efficacy should be performed for findings from liquid biopsy and from tumor tissue studies. Finally, the implementation of markers into clinical practice needs more supportive evidence, preferably from clinical trials.

ORCID iDs

Karol Marschollek https://orcid.org/0000-0001-9093-180X
Anna Brzecka https://orcid.org/0000-0002-2721-5111
Anna Pokryszko-Dragan https://orcid.org/0000-0002-5203-112X

References

1. Sung H, Ferlay J, Siegel RL, et al. Global Cancer Statistics 2020: GLOBOCAN estimates of incidence and mortality worldwide for 36 cancers in 185 countries. *CA Cancer J Clin*. 2021;71(3):209–249. doi:10.3322/caac.21660
2. Ferlay J, Laversanne M, Ervik M, et al. *Global Cancer Observatory: Cancer Tomorrow*. Lyon, France: International Agency for Research on Cancer; 2020. https://gco.iarc.fr/tomorrow. Accessed October 18, 2021.
3. Travis W, Brambilla E, Burke A, Marx A, Nicholson A, eds. *WHO Classification of Tumours of the Lung, Pleura, Thymus and Heart*. 4th ed. Lyon, France: International Agency for Research on Cancer; 2015.
4. Ruano-Ravina A, Provencio M, Calvo de Juan V, et al. Are there differences by sex in lung cancer characteristics at diagnosis? A nationwide study. *Transl Lung Cancer Res*. 2021;10(10):3902–3911. doi:10.21037/tlcr-21-559
5. Saito G, Kono M, Koyanagi Y, et al. Significance of brain imaging for staging in patients with clinical stage T1-2 N0 non-small-cell lung cancer on positron emission tomography/computed tomography. *Clin Lung Cancer*. 2021;22(6):562–569. doi:10.1016/j.cllc.2021.06.004
6. Lombardi G, Di Stefano AL, Farina P, Zagonel V, Tabouret E. Systemic treatments for brain metastases from breast cancer, non-small cell lung cancer, melanoma and renal cell carcinoma: An overview of the literature. *Cancer Treat Rev*. 2014;40(8):951–959. doi:10.1016/j.ctrv.2014.05.007
7. Quan AL, Videtic GMM, Suh JH. Brain metastases in small cell lung cancer. *Oncology (Williston Park)*. 2004;18(8):961–972. PMID:15328892.
8. Giometto B, Grisold W, Vitaliani R, Graus F, Honnorat J, Bertolini G. Paraneoplastic neurologic syndrome in the PNS Euronetwork Database: A European study from 20 centers. *Arch Neurol*. 2010;67(3):330–335. doi:10.1001/archneurol.2009.341
9. Ma J, Wang A, Jiang W, Ma L, Lin Y. Clinical characteristics of paraneoplastic neurological syndrome related to different pathological lung cancers. *Thorac Cancer*. 2021;12(16):2265–2270. doi:10.1111/1759-7714.14070
10. Feldheim J, Deuschl C, Glas M, Kleinschnitz C, Hagenacker T. Simultaneous paraneoplastic cerebellar degeneration, Lambert–Eaton syndrome and neuropathy associated with AGNA/anti-SOX1 and VGCC antibodies. *Neurol Res Pract*. 2021;3(1):30. doi:10.1186/s42466-021-00129-w
11. Ding M, Lang Y, Cui L. AQP4-IgG positive paraneoplastic NMOSD: A case report and review. *Brain Behav*. 2021;11(10):e2282. doi:10.1002/brb3.2282
12. Eba S, Nishiyama S, Notsuda H, et al. Development of paraneoplastic neuromyelitis optica after lung resection in a patient with squamous cell carcinoma [published ahead of print October 23, 2021]. *Ann Thorac Cardiovasc Surg*. 2021. doi:10.5761/atcs.cr.21-00144
13. Kanaji N, Watanabe N, Kita N, et al. Paraneoplastic syndromes associated with lung cancer. *World J Clin Oncol*. 2014;5(3):197–223. doi:10.5306/wjco.v5.i3.197
14. Gozzard P, Maddison P. Which antibody and which cancer in which paraneoplastic syndromes? *Pract Neurol*. 2010;10(5):260–270. doi:10.1136/jnnp.2010.224105
15. Nakashima K, Fujii Y, Sato M, Igarashi K, Kobayashi M, Ishizuka T. A case of non-small cell lung cancer presenting anti-amphiphysin antibody-positive paraneoplastic neurological syndrome. *Respir Med Case Rep*. 2021;34:101525. doi:10.1016/j.rmcr.2021.101525
16. Morimoto T, Orihashi T, Yamasaki K, Tahara M, Kato K, Yatera K. Paraneoplastic sensory polyneuropathy related to anti-PD-L1-including anticancer treatment in a patient with lung cancer. *Intern Med*. 2021;60(10):1577–1581. doi:10.2169/internalmedicine.5629-20
17. Catania C, Muthusamy B, Spitaleri G, del Signore E, Pennell NA. The new era of immune checkpoint inhibition and target therapy in early-stage non-small cell lung cancer. A review of the literature. *Clin Lung Cancer*. 2022;23(2):108–115. doi:10.1016/j.cllc.2021.11.003
18. Luna J, Zafra J, Manrique MCA, et al. New challenges in the combination of radiotherapy and immunotherapy in non-small cell lung cancer. *World J Clin Oncol*. 2021;12(11):983–999. doi:10.5306/wjco.v12.i11.983
19. Marjanski T, Dziedzic R, Kowalczyk A, Rzyman W. Safety of surgery after neoadjuvant targeted therapies in non-small cell lung cancer: A narrative review. *Int J Mol Sci*. 2021;22(22):12244. doi:10.3390/ijms222212244
20. Ning X, Yu Y, Shao S, et al. The prospect of immunotherapy combined with chemotherapy in patients with advanced non-small cell lung cancer: A narrative review. *Ann Transl Med*. 2021;9(22):1703. doi:10.21037/atm-21-4878
21. Xiong A, Wang J, Zhou C. Immunotherapy in the first-line treatment of NSCLC: Current status and future directions in China. *Front Oncol*. 2021;11:757993. doi:10.3389/fonc.2021.757993
22. Goldstraw P, Crowley J, Chansky K, et al. The IASLC Lung Cancer Staging Project: Proposals for the revision of the TNM stage groupings in the forthcoming (seventh) edition of the TNM Classification of Malignant Tumours. *J Thorac Oncol*. 2007;2(8):706–714. doi:10.1097/JTO.0b013e31812f3c1a
23. Govindan R, Page N, Morgensztern D, et al. Changing epidemiology of small-cell lung cancer in the United States over the last 30 years: Analysis of the surveillance, epidemiologic, and end results database. *J Clin Oncol*. 2006;24(28):4539–4544. doi:10.1200/JCO.2005.04.4859
24. Duma N, Santana-Davila R, Molina JR. Non-small cell lung cancer: Epidemiology, screening, diagnosis, and treatment. *Mayo Clin Proc*. 2019;94(8):1623–1640. doi:10.1016/j.mayocp.2019.01.013
25. Durin L, Pradines A, Basset C, et al. Liquid biopsy of non-plasma body fluids in non-small cell lung cancer: Look closer to the tumor! *Cells*. 2020;9(11):2486. doi:10.3390/cells9112486
26. Henry NL, Hayes DF. Cancer biomarkers. *Mol Oncol*. 2012;6(2):140–146. doi:10.1016/j.molonc.2012.01.010
27. Voorzanger-Rousselot N, Garnero P. Biochemical markers in oncology. Part I: Molecular basis. Part II: Clinical uses. *Cancer Treat Rev*. 2007;33(3):230–283. doi:10.1016/j.ctrv.2007.01.008
28. Tong A, Flemming K, McInnes E, Oliver S, Craig J. Enhancing transparency in reporting the synthesis of qualitative research: ENTREQ. *BMC Med Res Methodol*. 2012;12(1):181. doi:10.1186/1471-2288-12-181
29. Salgia R, Harpole D, Herndon JE, Pisick E, Elias A, Skarin AT. Role of serum tumor markers CA 125 and CEA in non-small cell lung cancer. *Anticancer Res*. 2001;21(2B):1241–1246. PMID:11396194.
30. Seemann MD, Beinert T, Fürst H, Fink U. An evaluation of the tumour markers, carcinoembryonic antigen (CEA), cytokeratin marker (CYFRA 21-1) and neuron-specific enolase (NSE) in the differentiation of malignant from benign solitary pulmonary lesions. *Lung Cancer*. 1999;26(3):149–155. doi:10.1016/S0169-5002(99)00084-7
31. Wu M, Tong X, Wang D, Wang L, Fan H. Soluble intercellular cell adhesion molecule-1 in lung cancer: A meta-analysis. *Pathol Res Pract*. 2020;216(10):153029. doi:10.1016/j.prp.2020.153029
32. Xu Y, Zhang Y, Wang Z, Chen N, Zhou J, Liu L. The role of serum angiopoietin-2 levels in progression and prognosis of lung cancer: A meta-analysis. *Medicine (Baltimore)*. 2017;96(37):e8063. doi:10.1097/MD.0000000000008063
33. Li J, Shen C, Wang X, et al. Prognostic value of TGF-β in lung cancer: Systematic review and meta-analysis. *BMC Cancer*. 2019;19(1):691. doi:10.1186/s12885-019-5917-5
34. Zhang B, Xie Z, Li B. The clinicopathologic impacts and prognostic significance of GLUT1 expression in patients with lung cancer: A meta-analysis. *Gene*. 2019;689:76–83. doi:10.1016/j.gene.2018.12.006
35. Potprommanee L, Ma HT, Shank L, et al. GM2-activator protein: A new biomarker for lung cancer. *J Thorac Oncol*. 2015;10(1):102–109. doi:10.1097/JTO.0000000000000357
36. Hu L, Zhang P, Mei Q, Sun W, Zhou L, Yin T. Podoplanin is a useful prognostic marker and indicates better differentiation in lung squamous cell cancer patients? A systematic review and meta-analysis. *BMC Cancer*. 2020;20(1):424. doi:10.1186/s12885-020-06936-9

37. Biaoxue R, Hua L, Wenlong G, Shuanying Y. Increased serum amyloid A as potential diagnostic marker for lung cancer: A meta-analysis based on nine studies. *BMC Cancer*. 2016;16(1):836. doi:10.1186/s12885-016-2882-0
38. Kuchitsu Y, Nagashio R, Igawa S, et al. TRAP1 is a predictive biomarker of platinum-based adjuvant chemotherapy benefits in patients with resected lung adenocarcinoma. *Biomed Res*. 2020;41(1):53–65. doi:10.2220/biomedres.41.53
39. Lim RJ, Liu B, Krysan K, Dubinett SM. Lung cancer and immunity markers. *Cancer Epidemiol Biomarkers Prev*. 2020;29(12):2423–2430. doi:10.1158/1055-9965.EPI-20-0716
40. Broodman I, Lindemans J, van Sten J, Bischoff R, Luider T. Serum protein markers for the early detection of lung cancer: A focus on autoantibodies. *J Proteome Res*. 2017;16(1):3–13. doi:10.1021/acs.jproteome.6b00559
41. Catacchio I, Scattone A, Silvestris N, Mangia A. Immune prophets of lung cancer: The prognostic and predictive landscape of cellular and molecular immune markers. *Transl Oncol*. 2018;11(3):825–835. doi:10.1016/j.tranon.2018.04.006
42. Rakaee M, Busund LT, Paulsen EE, et al. Prognostic effect of intratumoral neutrophils across histological subtypes of non-small cell lung cancer. *Oncotarget*. 2016;7(44):72184–72196. doi:10.18632/oncotarget.12360
43. Osińska I, Stelmaszczyk-Emmel A, Polubiec-Kownacka M, Dziedzic D, Domagała-Kulawik J. $CD4^+/CD25$ high/$FoxP3^+/CD127^-$ regulatory T cells in bronchoalveolar lavage fluid of lung cancer patients. *Hum Immunol*. 2016;77(10):912–915. doi:10.1016/j.humimm.2016.07.235
44. Jiang L, Zhao Z, Jiang S, et al. Immunological markers predict the prognosis of patients with squamous non-small cell lung cancer. *Immunol Res*. 2015;62(3):316–324. doi:10.1007/s12026-015-8662-0
45. Yin Y, Wang J, Wang X, et al. Prognostic value of the neutrophil to lymphocyte ratio in lung cancer: A meta-analysis. *Clinics (Sao Paulo)*. 2015;70(7):524–530. doi:10.6061/clinics/2015(07)10
46. Wang WJ, Tao Z, Gu W, Sun LH. Variation of blood T lymphocyte subgroups in patients with non-small cell lung cancer. *Asian Pac J Cancer Prev*. 2013;14(8):4671–4673. doi:10.7314/APJCP.2013.14.8.4671
47. Lim JU, Yoon HK. Potential predictive value of change in inflammatory cytokines levels subsequent to initiation of immune checkpoint inhibitor in patients with advanced non-small cell lung cancer. *Cytokine*. 2021;138:155363. doi:10.1016/j.cyto.2020.155363
48. Hardy-Werbin M, Rocha P, Arpi O, et al. Serum cytokine levels as predictive biomarkers of benefit from ipilimumab in small cell lung cancer. *Oncoimmunology*. 2019;8(6):e1593810. doi:10.1080/2162402X.2019.1593810
49. Pine SR, Mechanic LE, Enewold L, et al. Increased levels of circulating interleukin 6, interleukin 8, C-reactive protein, and risk of lung cancer. *J Natl Cancer Inst*. 2011;103(14):1112–1122. doi:10.1093/jnci/djr216
50. Ryan BM, Pine SR, Chaturvedi AK, Caporaso N, Harris CC. A combined prognostic serum interleukin-8 and interleukin-6 classifier for stage 1 lung cancer in the prostate, lung, colorectal, and ovarian cancer screening trial. *J Thorac Oncol*. 2014;9(10):1494–1503. doi:10.1097/JTO.0000000000000278
51. Lin Q, Xue L, Tian T, et al. Prognostic value of serum IL-17 and VEGF levels in small cell lung cancer. *Int J Biol Markers*. 2015;30(4):e359–e363. doi:10.5301/jbm.5000148
52. Naumnik W, Naumnik B, Niklińska W, Ossolińska M, Chyczewska E. Clinical implications of hepatocyte growth factor, interleukin-20, and interleukin-22 in serum and bronchoalveolar fluid of patients with non-small cell lung cancer. In: Pokorski M, ed. *Advancements in Clinical Research*. Cham, Switzerland: Springer International Publishing; 2016:41–49. doi:10.1007/5584_2016_66
53. Rivas-Fuentes S, Salgado-Aguayo A, Pertuz Belloso S, Gorocica Rosete P, Alvarado-Vásquez N, Aquino-Jarquin G. Role of chemokines in non-small cell lung cancer: Angiogenesis and inflammation. *J Cancer*. 2015;6(10):938–952. doi:10.7150/jca.12286
54. Tan HT, Low J, Lim SG, Chung MCM. Serum autoantibodies as biomarkers for early cancer detection: Serum autoantibodies as diagnostic biomarkers. *FEBS J*. 2009;276(23):6880–6904. doi:10.1111/j.1742-4658.2009.07396.x
55. Blaes F, Klotz M, Huwer H, et al. Antineural and antinuclear autoantibodies are of prognostic relevance in non-small cell lung cancer. *Ann Thorac Surg*. 2000;69(1):254–258. doi:10.1016/S0003-4975(99)01198-4
56. Chen SS, Li K, Wu J, et al. Stem signatures associated antibodies yield early diagnosis and precise prognosis predication of patients with non-small cell lung cancer. *J Cancer Res Clin Oncol*. 2021;147(1):223–233. doi:10.1007/s00432-020-03325-4
57. Wu WB, Yie SM, Ye SR, et al. An autoantibody against human DNA-topoisomerase I is a novel biomarker for non-small cell lung cancer. *Ann Thorac Surg*. 2018;105(6):1664–1670. doi:10.1016/j.athoracsur.2018.01.036
58. Brody R, Zhang Y, Ballas M, et al. PD-L1 expression in advanced NSCLC: Insights into risk stratification and treatment selection from a systematic literature review. *Lung Cancer*. 2017;112:200–215. doi:10.1016/j.lungcan.2017.08.005
59. Zhou J, Zhao J, Jia Q, et al. Peripheral blood autoantibodies against tumor-associated antigen predict clinical outcome to immune checkpoint inhibitor-based treatment in advanced non-small cell lung cancer. *Front Oncol*. 2021;11:625578. doi:10.3389/fonc.2021.625578
60. Ohue Y, Kurose K, Karasaki T, et al. Serum antibody against NY-ESO-1 and XAGE1 antigens potentially predicts clinical responses to anti–programmed cell death-1 therapy in NSCLC. *J Thorac Oncol*. 2019;14(12):2071–2083. doi:10.1016/j.jtho.2019.08.008
61. Giannicola R, D'Arrigo G, Botta C, et al. Early blood rise in auto-antibodies to nuclear and smooth muscle antigens is predictive of prolonged survival and autoimmunity in metastatic-non-small cell lung cancer patients treated with PD-1 immune-check point blockade by nivolumab. *Mol Clin Oncol*. 2019;11(1):81–90. doi:10.3892/mco.2019.1859
62. Tan Q, Wang D, Yang J, et al. Autoantibody profiling identifies predictive biomarkers of response to anti-PD1 therapy in cancer patients. *Theranostics*. 2020;10(14):6399–6410. doi:10.7150/thno.45816
63. Patel AJ, Tan TM, Richter AG, Naidu B, Blackburn JM, Middleton GW. A highly predictive autoantibody-based biomarker panel for prognosis in early-stage NSCLC with potential therapeutic implications. *Br J Cancer*. 2022;126(2):238–246. doi:10.1038/s41416-021-01572-x
64. Ma L, Yue W, Teng Y, Zhang L, Gu M, Wang Y. Serum anti-CCNY autoantibody is an independent prognosis indicator for postoperative patients with early-stage nonsmall-cell lung carcinoma. *Dis Markers*. 2013;35(5):317–325. doi:10.1155/2013/935943
65. Toi Y, Sugawara S, Sugisaka J, et al. Profiling preexisting antibodies in patients treated with anti–PD-1 therapy for advanced non-small cell lung cancer. *JAMA Oncol*. 2019;5(3):376–383. doi:10.1001/jamaoncol.2018.5860
66. Patel K, Farlow EC, Kim AW, et al. Enhancement of a multianalyte serum biomarker panel to identify lymph node metastases in non-small cell lung cancer with circulating autoantibody biomarkers. *Int J Cancer*. 2011;129(1):133–142. doi:10.1002/ijc.25644
67. Zhang Y, Chen B. Prognostic value of the advanced lung cancer inflammation index in patients with lung cancer: A meta-analysis. *Dis Markers*. 2019;2019:2513026. doi:10.1155/2019/2513026
68. Mezquita L, Auclin E, Ferrara R, et al. Association of the lung immune prognostic index with immune checkpoint inhibitor outcomes in patients with advanced non-small cell lung cancer. *JAMA Oncol*. 2018;4(3):351–357. doi:10.1001/jamaoncol.2017.4771
69. Seitlinger J, Prieto M, Guerrera F, et al. Neutrophil-to-lymphocyte ratio is correlated to driver gene mutations in surgically-resected non-small cell lung cancer and its post-operative evolution impacts outcomes. *Clin Lung Cancer*. 2022;23(1):e29–e42. doi:10.1016/j.cllc.2021.08.001
70. Sonehara K, Tateishi K, Komatsu M, Yamamoto H, Hanaoka M. Lung immune prognostic index as a prognostic factor in patients with small cell lung cancer. *Thorac Cancer*. 2020;11(6):1578–1586. doi:10.1111/1759-7714.13432
71. Lu Y, Jiang J, Ren C. The clinicopathological and prognostic value of the pretreatment neutrophil-to-lymphocyte ratio in small cell lung cancer: A meta-analysis. *PLoS One*. 2020;15(4):e0230979. doi:10.1371/journal.pone.0230979
72. Stroun M, Lyautey J, Lederrey C, Mulcahy HE, Anker P. Alu repeat sequences are present in increased proportions compared to a unique gene in plasma/serum DNA: Evidence for a preferential release from viable cells? *Ann N Y Acad Sci*. 2001;945(1):258–264. doi:10.1111/j.1749-6632.2001.tb03894.x
73. Diehl F, Schmidt K, Choti MA, et al. Circulating mutant DNA to assess tumor dynamics. *Nat Med*. 2008;14(9):985–990. doi:10.1038/nm.1789

74. Ignatiadis M, Dawson SJ. Circulating tumor cells and circulating tumor DNA for precision medicine: Dream or reality? *Ann Oncol*. 2014; 25(12):2304–2313. doi:10.1093/annonc/mdu480
75. Keller L, Belloum Y, Wikman H, Pantel K. Clinical relevance of blood-based ctDNA analysis: Mutation detection and beyond. *Br J Cancer*. 2021;124(2):345–358. doi:10.1038/s41416-020-01047-5
76. Pisapia P, Malapelle U, Troncone G. Liquid biopsy and lung cancer. *Acta Cytol*. 2019;63(6):489–496. doi:10.1159/000492710
77. Neumann MHD, Bender S, Krahn T, Schlange T. ctDNA and CTCs in liquid biopsy: Current status and where we need to progress. *Comput Struct Biotechnol J*. 2018;16:190–195. doi:10.1016/j.csbj.2018.05.002
78. Zhang Y, Shi L, Simoff MJ, Wagner OJ, Lavin J. Biopsy frequency and complications among lung cancer patients in the United States. *Lung Cancer Manag*. 2020;9(4):LMT40. doi:10.2217/lmt-2020-0022
79. Wan JCM, Massie C, Garcia-Corbacho J, et al. Liquid biopsies come of age: Towards implementation of circulating tumour DNA. *Nat Rev Cancer*. 2017;17(4):223–238. doi:10.1038/nrc.2017.7
80. Mack PC, Banks KC, Espenschied CR, et al. Spectrum of driver mutations and clinical impact of circulating tumor DNA analysis in non-small cell lung cancer: Analysis of over 8000 cases. *Cancer*. 2020; 126(14):3219–3228. doi:10.1002/cncr.32876
81. Peng M, Xie Y, Li X, et al. Resectable lung lesions malignancy assessment and cancer detection by ultra-deep sequencing of targeted gene mutations in plasma cell-free DNA. *J Med Genet*. 2019;56(10): 647–653. doi:10.1136/jmedgenet-2018-105825
82. Liang W, Zhao Y, Huang W, et al. Non-invasive diagnosis of early-stage lung cancer using high-throughput targeted DNA methylation sequencing of circulating tumor DNA (ctDNA). *Theranostics*. 2019; 9(7):2056–2070. doi:10.7150/thno.28119
83. Yang Z, Qi W, Sun L, Zhou H, Zhou B, Hu Y. DNA methylation analysis of selected genes for the detection of early-stage lung cancer using circulating cell-free DNA. *Adv Clin Exp Med*. 2019;28(3):355–360. doi:10.17219/acem/84935
84. Liang W, Liu D, Li M, et al. Evaluating the diagnostic accuracy of a ctDNA methylation classifier for incidental lung nodules: Protocol for a prospective, observational, and multicenter clinical trial of 10,560 cases. *Transl Lung Cancer Res*. 2020;9(5):2016–2026. doi:10.21037/tlcr-20-701
85. Li H, Ma Z, Li B, et al. Potential utility of longitudinal somatic mutation and methylation profiling for predicting molecular residual disease in postoperative non-small cell lung cancer patients. *Cancer Med*. 2021;10(23):8377–8386. doi:10.1002/cam4.4339
86. Zhang R, Zhang X, Huang Z, et al. Development and validation of a preoperative noninvasive predictive model based on circular tumor DNA for lymph node metastasis in resectable non-small cell lung cancer. *Transl Lung Cancer Res*. 2020;9(3):722–730. doi:10.21037/tlcr-20-593
87. Guo N, Lou F, Ma Y, et al. Circulating tumor DNA detection in lung cancer patients before and after surgery. *Sci Rep*. 2016;6(1):33519. doi:10.1038/srep33519
88. Chaudhuri AA, Chabon JJ, Lovejoy AF, et al. Early detection of molecular residual disease in localized lung cancer by circulating tumor DNA profiling. *Cancer Discov*. 2017;7(12):1394–1403. doi:10.1158/2159-8290.CD-17-0716
89. Abbosh C, Birkbak NJ, Wilson GA, et al. Phylogenetic ctDNA analysis depicts early-stage lung cancer evolution. *Nature*. 2017;545(7655): 446–451. doi:10.1038/nature22364
90. Waldeck S, Mitschke J, Wiesemann S, et al. Early assessment of circulating tumor DNA after curative-intent resection predicts tumor recurrence in early-stage and locally advanced non-small-cell lung cancer. *Mol Oncol*. 2022;16(2):527–537. doi:10.1002/1878-0261.13116
91. Kuang PP, Li N, Liu Z, et al. Circulating tumor DNA analyses as a potential marker of recurrence and effectiveness of adjuvant chemotherapy for resected non-small-cell lung cancer. *Front Oncol*. 2021; 10:595650. doi:10.3389/fonc.2020.595650
92. Xia L, Mei J, Kang R, et al. Perioperative ctDNA-based molecular residual disease detection for non-small cell lung cancer: A prospective multicenter cohort study (LUNGCA-1). *Clin Cancer Res*. 2022;28(15): 3308–3317. doi:10.1158/1078-0432.CCR-21-3044
93. Qiu B, Guo W, Zhang F, et al. Dynamic recurrence risk and adjuvant chemotherapy benefit prediction by ctDNA in resected NSCLC. *Nat Commun*. 2021;12(1):6770. doi:10.1038/s41467-021-27022-z
94. Zhang M, Huang C, Zhou H, et al. Circulating tumor DNA predicts the outcome of chemotherapy in patients with lung cancer. *Thorac Cancer*. 2022;13(1):95–106. doi:10.1111/1759-7714.14230
95. Nong J, Gong Y, Guan Y, et al. Circulating tumor DNA analysis depicts subclonal architecture and genomic evolution of small cell lung cancer. *Nat Commun*. 2018;9(1):3114. doi:10.1038/s41467-018-05327-w
96. Herbreteau G, Langlais A, Greillier L, et al. Circulating tumor DNA as a prognostic determinant in small cell lung cancer patients receiving atezolizumab. *J Clin Med*. 2020;9(12):3861. doi:10.3390/jcm9123861
97. Zhang Y, Yao Y, Xu Y, et al. Pan-cancer circulating tumor DNA detection in over 10,000 Chinese patients. *Nat Commun*. 2021;12(1):11. doi:10.1038/s41467-020-20162-8
98. US Food & Drug Administration. *Cobas® EGFR Mutation Test v2. PMA P120019/S007: FDA Summary of Safety and Effectiveness Data*. https://www.accessdata.fda.gov/cdrh_docs/pdf12/p120019s007b.pdf. Accessed January 13, 2022.
99. Vallée A, Le Loupp AG, Denis MG. Efficiency of the Therascreen® RGQ PCR kit for the detection of EGFR mutations in non-small cell lung carcinomas. *Clin Chim Acta*. 2014;429:8–11. doi:10.1016/j.cca.2013.11.014
100. Odegaard JI, Vincent JJ, Mortimer S, et al. Validation of a plasma-based comprehensive cancer genotyping assay utilizing orthogonal tissue and plasma-based methodologies. *Clin Cancer Res*. 2018; 24(15):3539–3549. doi:10.1158/1078-0432.CCR-17-3831
101. Zhang Y, Chen H. Neoadjuvant or adjuvant chemotherapy for non-small-cell lung cancer: Does the timing matter? *J Thorac Cardiovasc Surg*. 2019;157(2):756–757. doi:10.1016/j.jtcvs.2018.10.006
102. Passaro A, Jänne PA, Mok T, Peters S. Overcoming therapy resistance in EGFR-mutant lung cancer. *Nat Cancer*. 2021;2(4):377–391. doi:10.1038/s43018-021-00195-8
103. Chabon JJ, Simmons AD, Lovejoy AF, et al. Circulating tumour DNA profiling reveals heterogeneity of EGFR inhibitor resistance mechanisms in lung cancer patients. *Nat Commun*. 2016;7(1):11815. doi:10.1038/ncomms11815
104. Thompson JC, Yee SS, Troxel AB, et al. Detection of therapeutically targetable driver and resistance mutations in lung cancer patients by next-generation sequencing of cell-free circulating tumor DNA. *Clin Cancer Res*. 2016;22(23):5772–5782. doi:10.1158/1078-0432.CCR-16-1231
105. O'Kane GM, Liu G, Stockley TL, et al. The presence and variant allele fraction of EGFR mutations in ctDNA and development of resistance. *Lung Cancer*. 2019;131:86–89. doi:10.1016/j.lungcan.2019.03.019
106. Mok T, Wu YL, Lee JS, et al. Detection and dynamic changes of EGFR mutations from circulating tumor DNA as a predictor of survival outcomes in NSCLC patients treated with first-line intercalated erlotinib and chemotherapy. *Clin Cancer Res*. 2015;21(14):3196–3203. doi:10.1158/1078-0432.CCR-14-2594
107. Oxnard GR, Paweletz CP, Kuang Y, et al. Noninvasive detection of response and resistance in EGFR-mutant lung cancer using quantitative next-generation genotyping of cell-free plasma DNA. *Clin Cancer Res*. 2014;20(6):1698–1705. doi:10.1158/1078-0432.CCR-13-2482
108. Kim T, Kim EY, Lee SH, Kwon DS, Kim A, Chang YS. Presence of mEGFR ctDNA predicts a poor clinical outcome in lung adenocarcinoma. *Thorac Cancer*. 2019;10(12):2267–2273. doi:10.1111/1759-7714.13219
109. Dono M, De Luca G, Lastraioli S, et al. Tag-based next generation sequencing: A feasible and reliable assay for EGFR T790M mutation detection in circulating tumor DNA of non small cell lung cancer patients. *Mol Med*. 2019;25(1):15. doi:10.1186/s10020-019-0082-5
110. Beagan JJ, Bach S, van Boerdonk RA, et al. Circulating tumor DNA analysis of EGFR-mutant non-small cell lung cancer patients receiving osimertinib following previous tyrosine kinase inhibitor treatment. *Lung Cancer*. 2020;145:173–180. doi:10.1016/j.lungcan.2020.04.039
111. Boysen Fynboe Ebert E, McCulloch T, Holmskov Hansen K, Linnet H, Sorensen B, Meldgaard P. Clearing of circulating tumour DNA predicts clinical response to osimertinib in EGFR mutated lung cancer patients. *Lung Cancer*. 2020;143:67–72. doi:10.1016/j.lungcan.2020.03.020

112. Lei L, Wang W, Zhu Y, et al. Potential mechanism of primary resistance to icotinib in patients with advanced non-small cell lung cancer harboring uncommon mutant epidermal growth factor receptor: A multi-center study. *Cancer Sci*. 2020;111(2):679–686. doi:10.1111/cas.14277
113. Provencio M, Serna-Blasco R, Franco F, et al. Analysis of circulating tumour DNA to identify patients with epidermal growth factor receptor–positive non-small cell lung cancer who might benefit from sequential tyrosine kinase inhibitor treatment. *Eur J Cancer*. 2021;149:61–72. doi:10.1016/j.ejca.2021.02.031
114. Nabet BY, Esfahani MS, Moding EJ, et al. Noninvasive early identification of therapeutic benefit from immune checkpoint inhibition. *Cell*. 2020;183(2):363–376.e13. doi:10.1016/j.cell.2020.09.001
115. Goldberg SB, Narayan A, Kole AJ, et al. Early assessment of lung cancer immunotherapy response via circulating tumor DNA. *Clin Cancer Res*. 2018;24(8):1872–1880. doi:10.1158/1078-0432.CCR-17-1341
116. Ricciuti B, Jones G, Severgnini M, et al. Early plasma circulating tumor DNA (ctDNA) changes predict response to first-line pembrolizumab-based therapy in non-small cell lung cancer (NSCLC). *J Immunother Cancer*. 2021;9(3):e001504. doi:10.1136/jitc-2020-001504
117. Hellmann MD, Nabet BY, Rizvi H, et al. Circulating tumor DNA analysis to assess risk of progression after long-term response to PD-(L)1 blockade in NSCLC. *Clin Cancer Res*. 2020;26(12):2849–2858. doi:10.1158/1078-0432.CCR-19-3418
118. Guo D, Yang L, Yang J, Shi K. Plasma cell-free DNA methylation combined with tumor mutation detection in prognostic prediction of patients with non-small cell lung cancer (NSCLC). *Medicine (Baltimore)*. 2020;99(26):e20431. doi:10.1097/MD.0000000000020431
119. Peng M, Huang Q, Yin W, et al. Circulating tumor DNA as a prognostic biomarker in localized non-small cell lung cancer. *Front Oncol*. 2020;10:561598. doi:10.3389/fonc.2020.561598
120. Giroux Leprieur E, Herbretau G, Dumenil C, et al. Circulating tumor DNA evaluated by Next-Generation Sequencing is predictive of tumor response and prolonged clinical benefit with nivolumab in advanced non-small cell lung cancer. *Oncoimmunology*. 2018;7(5):e1424675. doi:10.1080/2162402X.2018.1424675
121. Lee Y, Park S, Kim WS, et al. Correlation between progression-free survival, tumor burden, and circulating tumor DNA in the initial diagnosis of advanced-stage EGFR-mutated non-small cell lung cancer: Quantitative analysis of ctDNA. *Thorac Cancer*. 2018;9(9):1104–1110. doi:10.1111/1759-7714.12793
122. Roosan MR, Mambetsariev I, Pharaon R, et al. Usefulness of circulating tumor DNA in identifying somatic mutations and tracking tumor evolution in patients with non-small cell lung cancer. *Chest*. 2021;160(3):1095–1107. doi:10.1016/j.chest.2021.04.016
123. Rizvi NA, Hellmann MD, Snyder A, et al. Cancer immunology: Mutational landscape determines sensitivity to PD-1 blockade in non-small cell lung cancer. *Science*. 2015;348(6230):124–128. doi:10.1126/science.aaa1348
124. Hellmann MD, Ciuleanu TE, Pluzanski A, et al. Nivolumab plus Ipilimumab in lung cancer with a high tumor mutational burden. *N Engl J Med*. 2018;378(22):2093–2104. doi:10.1056/NEJMoa1801946
125. Gandara DR, Paul SM, Kowanetz M, et al. Blood-based tumor mutational burden as a predictor of clinical benefit in non-small-cell lung cancer patients treated with atezolizumab. *Nat Med*. 2018;24(9):1441–1448. doi:10.1038/s41591-018-0134-3
126. Chae YK, Davis AA, Agte S, et al. Clinical implications of circulating tumor DNA tumor mutational burden (ctDNA TMB) in non-small cell lung cancer. *Oncologist*. 2019;24(6):820–828. doi:10.1634/theoncologist.2018-0433
127. Sholl LM, Hirsch FR, Hwang D, et al. The promises and challenges of tumor mutation burden as an immunotherapy biomarker: A perspective from the International Association for the Study of Lung Cancer Pathology Committee. *J Thorac Oncol*. 2020;15(9):1409–1424. doi:10.1016/j.jtho.2020.05.019
128. Chen K, Zhang J, Guan T, et al. Comparison of plasma to tissue DNA mutations in surgical patients with non-small cell lung cancer. *J Thorac Cardiovasc Surg*. 2017;154(3):1123–1131.e2. doi:10.1016/j.jtcvs.2017.04.073
129. O'Flaherty JD, Gray S, Richard D, et al. Circulating tumour cells, their role in metastasis and their clinical utility in lung cancer. *Lung Cancer*. 2012;76(1):19–25. doi:10.1016/j.lungcan.2011.10.018
130. Tong B, Wang M. Circulating tumor cells in patients with lung cancer: Developments and applications for precision medicine. *Future Oncol*. 2019;15(21):2531–2542. doi:10.2217/fon-2018-0548
131. Zhao Q, Yuan Z, Wang H, Zhang H, Duan G, Zhang X. Role of circulating tumor cells in diagnosis of lung cancer: A systematic review and meta-analysis. *J Int Med Res*. 2021;49(3):030006052199492. doi:10.1177/0300060521994926
132. Jiang SS, Deng B, Feng YG, Qian K, Tan QY, Wang RW. Circulating tumor cells prior to initial treatment is an important prognostic factor of survival in non-small cell lung cancer: A meta-analysis and system review. *BMC Pulm Med*. 2019;19(1):262. doi:10.1186/s12890-019-1029-x
133. Wu ZX, Liu Z, Jiang HL, Pan HM, Han WD. Circulating tumor cells predict survival benefit from chemotherapy in patients with lung cancer. *Oncotarget*. 2016;7(41):67586–67596. doi:10.18632/oncotarget.11707
134. Huang J, Wang K, Xu J, Huang J, Zhang T. Prognostic significance of circulating tumor cells in non-small-cell lung cancer patients: A meta-analysis. *PLoS One*. 2013;8(11):e78070. doi:10.1371/journal.pone.0078070
135. Jiang AM, Zheng HR, Liu N, et al. Assessment of the clinical utility of circulating tumor cells at different time points in predicting prognosis of patients with small cell lung cancer: A meta-analysis. *Cancer Control*. 2021;28:107327482110505. doi:10.1177/10732748211050581
136. Liu Y, Xing Z, Zhan P, et al. Is it feasible to detect epidermal growth factor receptor mutations in circulating tumor cells in nonsmall cell lung cancer? A meta-analysis. *Medicine (Baltimore)*. 2016;95(47):e5115. doi:10.1097/MD.0000000000005115
137. Shen H, Che K, Cong L, et al. Diagnostic and prognostic value of blood samples for KRAS mutation identification in lung cancer: A meta-analysis. *Oncotarget*. 2017;8(22):36812–36823. doi:10.18632/oncotarget.15972
138. Ilie M, Long E, Butori C, et al. ALK-gene rearrangement: A comparative analysis on circulating tumour cells and tumour tissue from patients with lung adenocarcinoma. *Ann Oncol*. 2012;23(11):2907–2913. doi:10.1093/annonc/mds137
139. Pailler E, Adam J, Barthélémy A, et al. Detection of circulating tumor cells harboring a unique *ALK* rearrangement in *ALK*-positive non-small-cell lung cancer. *J Clin Oncol*. 2013;31(18):2273–2281. doi:10.1200/JCO.2012.44.5932
140. Tan CL, Lim TH, Lim TK, et al. Concordance of anaplastic lymphoma kinase (*ALK*) gene rearrangements between circulating tumor cells and tumor in non-small cell lung cancer. *Oncotarget*. 2016;7(17):23251–23262. doi:10.18632/oncotarget.8136
141. Pailler E, Auger N, Lindsay CR, et al. High level of chromosomal instability in circulating tumor cells of ROS1-rearranged non-small-cell lung cancer. *Ann Oncol*. 2015;26(7):1408–1415. doi:10.1093/annonc/mdv165
142. Pailler E, Oulhen M, Borget I, et al. Circulating tumor cells with aberrant *ALK* copy number predict progression-free survival during crizotinib treatment in *ALK*-rearranged non-small cell lung cancer patients. *Cancer Res*. 2017;77(9):2222–2230. doi:10.1158/0008-5472.CAN-16-3072
143. Krol J, Loedige I, Filipowicz W. The widespread regulation of microRNA biogenesis, function and decay. *Nat Rev Genet*. 2010;11(9):597–610. doi:10.1038/nrg2843
144. Calin GA, Croce CM. MicroRNA signatures in human cancers. *Nat Rev Cancer*. 2006;6(11):857–866. doi:10.1038/nrc1997
145. Wu KL, Tsai YM, Lien CT, Kuo PL, Hung JY. The roles of microRNA in lung cancer. *Int J Mol Sci*. 2019;20(7):1611. doi:10.3390/ijms20071611
146. Montani F, Marzi MJ, Dezi F, et al. miR-Test: A blood test for lung cancer early detection. *J Natl Cancer Inst*. 2015;107(6):djv063. doi:10.1093/jnci/djv063
147. Sozzi G, Boeri M, Rossi M, et al. Clinical utility of a plasma-based miRNA signature classifier within computed tomography lung cancer screening: A correlative MILD trial study. *J Clin Oncol*. 2014;32(8):768–773. doi:10.1200/JCO.2013.50.4357
148. Fehlmann T, Kahraman M, Ludwig N, et al. Evaluating the use of circulating microRNA profiles for lung cancer detection in symptomatic patients. *JAMA Oncol*. 2020;6(5):714–723. doi:10.1001/jamaoncol.2020.0001

149. Liao J, Shen J, Leng Q, Qin M, Zhan M, Jiang F. MicroRNA-based biomarkers for diagnosis of non-small cell lung cancer (NSCLC). *Thorac Cancer*. 2020;11(3):762–768. doi:10.1111/1759-7714.13337
150. Asakura K, Kadota T, Matsuzaki J, et al. A miRNA-based diagnostic model predicts resectable lung cancer in humans with high accuracy. *Commun Biol*. 2020;3(1):134. doi:10.1038/s42003-020-0863-y
151. Tao S, Ju X, Zhou H, Zeng Q. Circulating microRNA-145 as a diagnostic biomarker for non-small-cell lung cancer: A systemic review and meta-analysis. *Int J Biol Markers*. 2020;35(4):51–60. doi:10.1177/1724600820967124
152. Lu S, Kong H, Hou Y, et al. Two plasma microRNA panels for diagnosis and subtype discrimination of lung cancer. *Lung Cancer*. 2018;123:44–51. doi:10.1016/j.lungcan.2018.06.027
153. Pu Q, Huang Y, Lu Y, et al. Tissue-specific and plasma microRNA profiles could be promising biomarkers of histological classification and TNM stage in non-small cell lung cancer. *Thorac Cancer*. 2016;7(3):348–354. doi:10.1111/1759-7714.12317
154. Wang Y, Gu J, Roth JA, et al. Pathway-based serum microRNA profiling and survival in patients with advanced stage non-small cell lung cancer. *Cancer Res*. 2013;73(15):4801–4809. doi:10.1158/0008-5472.CAN-12-3273
155. Khandelwal A, Seam RK, Gupta M, et al. Circulating microRNA-590-5p functions as a liquid biopsy marker in non-small cell lung cancer. *Cancer Sci*. 2020;111(3):826–839. doi:10.1111/cas.14199
156. Li J, Yu M, Liu Z, Liu B. Clinical significance of serum miR-25 in non-small-cell lung cancer. *Br J Biomed Sci*. 2019;76(3):111–116. doi:10.1080/09674845.2019.1592915
157. Souza CP, Cinegaglia NC, Felix TF, et al. Deregulated microRNAs are associated with patient survival and predicted to target genes that modulate lung cancer signaling pathways. *Cancers (Basel)*. 2020;12(9):2711. doi:10.3390/cancers12092711
158. Sun L, Zhou H, Yang Y, et al. Meta-analysis of diagnostic and prognostic value of miR-126 in non-small cell lung cancer. *Biosci Rep*. 2020;40(5):BSR20200349. doi:10.1042/BSR20200349
159. Chen WJ, Zhang EN, Zhong ZK, et al. MicroRNA-153 expression and prognosis in non-small cell lung cancer. *Int J Clin Exp Pathol*. 2015;8(7):8671–8675.
160. Zhang J, Wang T, Zhang Y, et al. Upregulation of serum miR-494 predicts poor prognosis in non-small cell lung cancer patients. *Cancer Biomark*. 2018;21(4):763–768. doi:10.3233/CBM-170337
161. Wang A, Zhang H, Wang J, Zhang S, Xu Z. MiR-519d targets HER3 and can be used as a potential serum biomarker for non-small cell lung cancer. *Aging (Albany NY)*. 2020;12(6):4866–4878. doi:10.18632/aging.102908
162. Ding H, Wen W, Ding Q, Zhao X. Diagnostic valuation of serum miR-184 and miR-191 in patients with non-small-cell lung cancer. *Cancer Control*. 2020;27(1):107327482096478. doi:10.1177/1073274820964783
163. Liu J, Han Y, Liu X, Wei S. Serum miR-185 is a diagnostic and prognostic biomarker for non-small cell lung cancer. *Technol Cancer Res Treat*. 2020;19:153303382097327. doi:10.1177/1533033820973276
164. Sun B, Liu HF, Ding Y, Li Z. Evaluating the diagnostic and prognostic value of serum miR-770 in non-small cell lung cancer. *Eur Rev Med Pharmacol Sci*. 2018;22(10):3061–3066. doi:10.26355/eurrev_201805_15064
165. Jiang X, Yuan Y, Tang L, et al. Identification and validation prognostic impact of MiRNA-30a-5p in lung adenocarcinoma. *Front Oncol*. 2022;12:831997. doi:10.3389/fonc.2022.831997
166. Liu Q, Yu Z, Yuan S, et al. Circulating exosomal microRNAs as prognostic biomarkers for non-small-cell lung cancer. *Oncotarget*. 2017;8(8):13048–13058. doi:10.18632/oncotarget.14369
167. Gu W. Expression and significance of circulating microRNA-31 in lung cancer patients. *Med Sci Monit*. 2015;21:722–726. doi:10.12659/MSM.893213
168. Zhang Y, Xu H. Serum exosomal miR-378 upregulation is associated with poor prognosis in non-small-cell lung cancer patients. *J Clin Lab Anal*. 2020;34(6):e23237. doi:10.1002/jcla.23237
169. Zhou C, Chen Z, Zhao L, et al. A novel circulating miRNA-based signature for the early diagnosis and prognosis prediction of non-small-cell lung cancer. *J Clin Lab Anal*. 2020;34(11):e23505. doi:10.1002/jcla.23505
170. Kumar S, Sharawat SK, Ali A, et al. Differential expression of circulating serum miR-1249-3p, miR-3195, and miR-3692-3p in non-small cell lung cancer. *Hum Cell*. 2020;33(3):839–849. doi:10.1007/s13577-020-00351-9
171. Dejima H, Iinuma H, Kanaoka R, Matsutani N, Kawamura M. Exosomal microRNA in plasma as a non-invasive biomarker for the recurrence of non-small cell lung cancer. *Oncol Lett*. 2017;13(3):1256–1263. doi:10.3892/ol.2017.5569
172. Li M, Shan W, Hong B, et al. Circulating miR-92b and miR-375 for monitoring the chemoresistance and prognosis of small cell lung cancer. *Sci Rep*. 2020;10(1):12705. doi:10.1038/s41598-020-69615-6
173. Wu L, Hu B, Zhao B, et al. Circulating microRNA-422a is associated with lymphatic metastasis in lung cancer. *Oncotarget*. 2017;8(26):42173–42188. doi:10.18632/oncotarget.15025
174. Zou Y, Jing C, Liu L, Wang T. Serum microRNA-135a as a diagnostic biomarker in non-small cell lung cancer. *Medicine*. 2019;98(50):e17814. doi:10.1097/MD.0000000000017814
175. Xu S, Yang F, Liu R, et al. Serum microRNA-139-5p is downregulated in lung cancer patients with lytic bone metastasis. *Oncol Rep*. 2018;39(5):2376–2384. doi:10.3892/or.2018.6316
176. Mao S, Zheng S, Lu Z, et al. Exosomal miR-375-3p breaks vascular barrier and promotes small cell lung cancer metastasis by targeting claudin-1. *Transl Lung Cancer Res*. 2021;10(7):3155–3172. doi:10.21037/tlcr-21-356
177. Shi GL, Zhang XY, Chen Y, Ma S, Bai WQ, Yin YJ. Prognostic significance of serum miR-22, miR-125b, and miR-15b in non-small cell lung cancer patients. *Clin Lab*. 2020;66(6). doi:10.7754/Clin.Lab.2019.191129
178. Ponomaryova AA, Morozkin ES, Rykova EY, et al. Dynamic changes in circulating miRNA levels in response to antitumor therapy of lung cancer. *Exp Lung Res*. 2016;42(2):95–102. doi:10.3109/01902148.2016.1155245
179. Liu W, Liu J, Zhang Q, Wei L. Downregulation of serum exosomal miR-216b predicts unfavorable prognosis in patients with non-small cell lung cancer. *Cancer Biomark*. 2020;27(1):113–120. doi:10.3233/CBM-190914
180. Zheng Q, Ding H, Wang L, et al. Circulating exosomal miR-96 as a novel biomarker for radioresistant non-small-cell lung cancer. *J Oncol*. 2021;2021:5893981. doi:10.1155/2021/5893981
181. Sun Y, Hawkins PG, Bi N, et al. Serum microRNA signature predicts response to high-dose radiation therapy in locally advanced non-small cell lung cancer. *Int J Radiat Oncol Biol Phys*. 2018;100(1):107–114. doi:10.1016/j.ijrobp.2017.08.039
182. Peng XX, Yu R, Wu X, et al. Correlation of plasma exosomal microRNAs with the efficacy of immunotherapy in *EGFR/ALK* wild-type advanced non-small cell lung cancer. *J Immunother Cancer*. 2020;8(1):e000376. doi:10.1136/jitc-2019-000376
183. Szpechcinski A, Florczuk M, Duk K, et al. The expression of circulating miR-504 in plasma is associated with EGFR mutation status in non-small-cell lung carcinoma patients. *Cell Mol Life Sci*. 2019;76(18):3641–3656. doi:10.1007/s00018-019-03089-2
184. Li LL, Qu LL, Fu HJ, et al. Circulating microRNAs as novel biomarkers of ALK-positive non-small cell lung cancer and predictors of response to crizotinib therapy. *Oncotarget*. 2017;8(28):45399–45414. doi:10.18632/oncotarget.17535
185. Li B, Ren S, Li X, et al. MiR-21 overexpression is associated with acquired resistance of EGFR-TKI in non-small cell lung cancer. *Lung Cancer*. 2014;83(2):146–153. doi:10.1016/j.lungcan.2013.11.003
186. Hojbjerg JA, Ebert EBF, Clement MS, Winther-Larsen A, Meldgaard P, Sorensen B. Circulating miR-30b and miR-30c predict erlotinib response in EGFR-mutated non-small cell lung cancer patients. *Lung Cancer*. 2019;135:92–96. doi:10.1016/j.lungcan.2019.07.005
187. Zhou F, Lu X, Zhang X. Serum miR-30c level predicted cardiotoxicity in non-small cell lung cancer patients treated with bevacizumab. *Cardiovasc Toxicol*. 2018;18(3):284–289. doi:10.1007/s12012-018-9457-z
188. Chen L, Li Y, Lu J. Identification of circulating miR-762 as a novel diagnostic and prognostic biomarker for non-small cell lung cancer. *Technol Cancer Res Treat*. 2020;19:153303382096422. doi:10.1177/1533033820964222
189. Yang Y, Chen K, Zhou Y, Hu Z, Chen S, Huang Y. Application of serum microRNA-9-5p, 21-5p, and 223-3p combined with tumor markers in the diagnosis of non-small-cell lung cancer in Yunnan in southwestern China. *Onco Targets Ther*. 2018;11:587–597. doi:10.2147/OTT.S152957
190. Wu KL, Tsai YM, Lien CT, Kuo PL, Hung JY. The roles of microRNA in lung cancer. *Int J Mol Sci*. 2019;20(7):1611. doi:10.3390/ijms20071611

191. Zhao C, Lu F, Chen H, et al. Clinical significance of circulating miRNA detection in lung cancer. *Med Oncol*. 2016;33(5):41. doi:10.1007/s12032-016-0757-5
192. Du X, Zhang J, Wang J, Lin X, Ding F. Role of miRNA in lung cancer: Potential biomarkers and therapies. *Curr Pharm Des*. 2018;23(39):5997–6010. doi:10.2174/1381612823666170714150118
193. Marchi N, Cavaglia M, Fazio V, Bhudia S, Hallene K, Janigro D. Peripheral markers of blood–brain barrier damage. *Clin Chim Acta*. 2004;342(1–2):1–12. doi:10.1016/j.cccn.2003.12.008
194. Choi H, Puvenna V, Brennan C, et al. S100B and S100B autoantibody as biomarkers for early detection of brain metastases in lung cancer. *Transl Lung Cancer Res*. 2016;5(4):413–419. doi:10.21037/tlcr.2016.07.08
195. Chen L, Hu X, Wu H, et al. Over-expression of S100B protein as a serum marker of brain metastasis in non-small cell lung cancer and its prognostic value. *Pathol Res Pract*. 2019;215(3):427–432. doi:10.1016/j.prp.2018.11.011
196. Marchi N, Mazzone P, Fazio V, Mekhail T, Masaryk T, Janigro D. ProApolipoprotein A1: A serum marker of brain metastases in lung cancer patients. *Cancer*. 2008;112(6):1313–1324. doi:10.1002/cncr.23314
197. Sert F, Cosgun G, Yalman D, Ozkok S. Can we define any marker associated with brain failure in patients with locally advanced non-small cell lung cancer? *Cancer Radiother*. 2021;25(4):316–322. doi:10.1016/j.canrad.2020.11.002
198. Koh YW, Choi JH, Ahn MS, Choi YW, Lee HW. Baseline neutrophil–lymphocyte ratio is associated with baseline and subsequent presence of brain metastases in advanced non-small-cell lung cancer. *Sci Rep*. 2016;6(1):38585. doi:10.1038/srep38585
199. Li MM, Wang X, Yun ZY, Wang RT, Yu KJ. Platelet indices in non-small cell lung cancer patients with brain metastases. *Cancer Biomark*. 2019;24(4):515–519. doi:10.3233/CBM-192393
200. Zhu JF, Cai L, Zhang XW, et al. High plasma fibrinogen concentration and platelet count unfavorably impact survival in non-small cell lung cancer patients with brain metastases. *Chin J Cancer*. 2014;33(2):96–104. doi:10.5732/cjc.012.10307
201. Wei C, Zhang R, Cai Q, et al. MicroRNA-330-3p promotes brain metastasis and epithelial-mesenchymal transition via GRIA3 in non-small cell lung cancer. *Aging (Albany NY)*. 2019;11(17):6734–6761. doi:10.18632/aging.102201
202. Jiang LP, Zhu ZT, Zhang Y, He CY. Downregulation of microRNA-330 correlates with the radiation sensitivity and prognosis of patients with brain metastasis from lung cancer. *Cell Physiol Biochem*. 2017;42(6):2220–2229. doi:10.1159/000479996
203. Zhu Z, Li Q, Xu M, Qi Z. Effect of whole-brain and intensity-modulated radiotherapy on serum levels of miR-21 and prognosis for lung cancer metastatic to the brain. *Med Sci Monit*. 2020;26:e924640. doi:10.12659/MSM.924640
204. Xu Q, Ye L, Huang L, et al. Serum exosomal miRNA might be a novel liquid biopsy to identify leptomeningeal metastasis in non-small cell lung cancer. *Onco Targets Ther*. 2021;14:2327–2335. doi:10.2147/OTT.S291611
205. Ma C, Yang X, Xing W, Yu H, Si T, Guo Z. Detection of circulating tumor DNA from non-small cell lung cancer brain metastasis in cerebrospinal fluid samples. *Thorac Cancer*. 2020;11(3):588–593. doi:10.1111/1759-7714.13300
206. Huang R, Xu X, Li D, et al. Digital PCR-based detection of EGFR mutations in paired plasma and CSF samples of lung adenocarcinoma patients with central nervous system metastases. *Target Oncol*. 2019;14(3):343–350. doi:10.1007/s11523-019-00645-5
207. Belloum Y, Janning M, Mohme M, et al. Discovery of targetable genetic alterations in NSCLC patients with different metastatic patterns using a MassARRAY-based circulating tumor DNA assay. *Cells*. 2020;9(11):2337. doi:10.3390/cells9112337
208. Aldea M, Hendriks L, Mezquita L, et al. Circulating tumor DNA analysis for patients with oncogene-addicted NSCLC with isolated central nervous system progression. *J Thorac Oncol*. 2020;15(3):383–391. doi:10.1016/j.jtho.2019.11.024
209. Graus F, Dalmau J. Paraneoplastic neurological syndromes: *Curr Opin Neurol*. 2012;25(6):795–801. doi:10.1097/WCO.0b013e328359da15
210. Grativvol RS, Cavalcante WCP, Castro LHM, Nitrini R, Simabukuro MM. Updates in the diagnosis and treatment of paraneoplastic neurologic syndromes. *Curr Oncol Rep*. 2018;20(11):92. doi:10.1007/s11912-018-0721-y
211. Zekeridou A, Kryzer T, Guo Y, et al. Phosphodiesterase 10A IgG: A novel biomarker of paraneoplastic neurologic autoimmunity. *Neurology*. 2019;93(8):e815–e822. doi:10.1212/WNL.0000000000007971
212. Gadoth A, Kryzer TJ, Fryer J, McKeon A, Lennon VA, Pittock SJ. Microtubule-associated protein 1B: Novel paraneoplastic biomarker. *Ann Neurol*. 2017;81(2):266–277. doi:10.1002/ana.24872
213. Graus F, Dalmou J, Reñé R, et al. Anti-Hu antibodies in patients with small-cell lung cancer: Association with complete response to therapy and improved survival. *J Clin Oncol*. 1997;15(8):2866–2872. doi:10.1200/JCO.1997.15.8.2866
214. Gozzard P, Chapman C, Vincent A, Lang B, Maddison P. Novel humoral prognostic markers in small-cell lung carcinoma: A prospective study. *PLoS One*. 2015;10(11):e0143558. doi:10.1371/journal.pone.0143558
215. Monstad SE, Drivsholm L, Storstein A, et al. Hu and voltage-gated calcium channel (VGCC) antibodies related to the prognosis of small-cell lung cancer. *J Clin Oncol*. 2004;22(5):795–800. doi:10.1200/JCO.2004.01.028
216. Raspotnig M, Vedeler C, Storstein A. Paraneoplastic neurological syndromes in lung cancer patients with or without onconeural antibodies. *J Neurol Sci*. 2015;348(1–2):41–45. doi:10.1016/j.jns.2014.10.040
217. Vogrig A, Gigli GL, Segatti S, et al. Epidemiology of paraneoplastic neurological syndromes: A population-based study. *J Neurol*. 2020;267(1):26–35. doi:10.1007/s00415-019-09544-1

Correlation between osmolarity measurements using the TearLab™ and I-Pen® systems in subjects with a high body mass index

Mana A. Alanazi[A,C–F], Gamal A. El-Hiti[A,C–F], Naif Alhafy[B], Essam S. Almutleb[A,C–F], Raied Fagehi[A,C–F], Saud A. Alanazi[A,D–F], Ali M. Masmali[A,D–F]

Optometry Department, College of Applied Medical Sciences, King Saud University, Riyadh, Saudi Arabia

A – research concept and design; B – collection and/or assembly of data; C – data analysis and interpretation; D – writing the article; E – critical revision of the article; F – final approval of the article

Advances in Clinical and Experimental Medicine, ISSN 1899–5276 (print), ISSN 2451–2680 (online) *Adv Clin Exp Med*. 2022;31(12):1413–1418

Address for correspondence
Mana A. Alanazi
E-mail: amana@ksu.edu.sa

Funding sources
Researchers Supporting Project (No RSP-2021/404), King Saud University, Riyadh, Saudi Arabia.

Conflict of interest
None declared

Received on April 27, 2022
Reviewed on September 18, 2022
Accepted on November 17, 2022

Published online on December 8, 2022

Abstract

Background. Osmolarity is used to detect symptoms of dry eye disease (DED) and can be measured using TearLab™ and I-Pen® systems.

Objectives. To investigate the correlation between osmolarity measurements using the TearLab™ and I-Pen® systems in subjects with a high body mass index (BMI).

Materials and methods. Thirty male subjects with a high BMI (27–48 kg/m^2; 23.3 ±2.1 years old) participated in this study. The control group consisting of 30 healthy males (24.9 kg/m^2; 22.9 ±2.1 years old) was also enrolled. Osmolarity measurements were recorded from the right eye using the TearLab™ and I-Pen® systems, and interviews were conducted to determine ocular surface disease index (OSDI) scores.

Results. The OSDI ($p = 0.042$), TearLab™ ($p < 0.001$) and I-Pen® ($p < 0.001$) scores were significantly higher in the study group than in the control group. In the study group, OSDI scores ranged from 2 to 16 (median 8.0, interquartile range (IQR) 6.8), while it was from 0 to 10 (median 6.3, IQR 4.1) in the control group. The TearLab™ osmolarity scores were in the range of 278–309 mOsm/L in the study group, whereas the I-Pen® osmolarity measurements were in the range of 294–336 mOsm/L in the study group, compared with 263–304 mOsm/L and 278–317 mOsm/L in the control group, respectively. In the study group, there was a strong correlation between the TearLab™ and I-Pen® osmolarity scores ($r = 0.934$; $p = 0.001$). In addition, strong correlations were found between the BMI and both TearLab™ ($r = 0.736$; $p = 0.001$) and I-Pen® ($r = 0.707$; $p = 0.001$) scores, as well as between the OSDI scores and both TearLab™ ($r = 0.731$; $p = 0.001$) and I-Pen® measurements ($r = 0.666$; $p = 0.001$).

Conclusions. Osmolarity measurements using the I-Pen® system were significantly higher than those recorded using the TearLab™ system in subjects with a high BMI. The I-Pen® measurements showed large variations in osmolarity scores and were highly unreliable in correctly identifying normal eyes compared to the TearLab™ system. Also, a strong correlation was found between the osmolarity scores obtained from the TearLab™ and I-Pen® systems.

Key words: tear film, dry eye, tear osmolarity, high body mass index, TearLab™ system, I-Pen® system

Cite as
Alanazi MA, El-Hiti GA, Alhafy N, et al. Correlation between osmolarity measurements using the TearLab™ and I-Pen® systems in subjects with a high body mass index. *Adv Clin Exp Med*. 2022;31(12):1413–1418. doi:10.17219/acem/156645

DOI
10.17219/acem/156645

Background

The prevalence of obesity has been increasing in recent years and has become a challenge for society and a major public health concern globally.[1,2] The simplest measurement of obesity uses body mass index (BMI), and high BMI is a risk factor for many health problems and diseases.[3] For example, high BMI is associated with heart disease,[4] stroke,[5] hypertension,[6] diabetes,[7] and cancer.[8] In addition, it is a risk factor for glaucoma,[9] cataracts[10] and diabetic retinopathy.[11]

Dry eye disease (DED) is a common visual disorder that affects many people worldwide.[12] The prevalence of DED is increasing, and it has a negative effect on activities of daily life, quality of life, productivity, and on the economy.[13] This disease leads to discomfort, damage to the ocular surface, visual impairment, irritation, inflammation, light sensitivity, and increased osmolarity.[14] Dry eye disease occurs due to the loss of ocular surface homeostasis. It leads to tear film instability[15] and a decrease in wettability of the eye surface due dysfunction of goblet and epithelial cells.[16] Furthermore, the symptoms of DED can result from hyperosmolarity, lack of lubrication, and irregularities on the ocular surface.[16] Risk factors for DED include old age and female sex. They also include contact lenses wearing, cosmetics, medications, and systemic diseases such as diabetes, thyroid gland disorders and β thalassemia.[17] In addition, DED is associated with several environmental factors, including high temperature and humidity, sun exposure and wind.[17]

Diagnosis of DED should be based on quantifiable objective and subjective evaluations.[18] Multiple tools are available for such diagnosis, including the ocular surface disease index (OSDI), tear osmolarity, tear break-up time, and Schirmer tests, among others. The OSDI evaluates ocular symptoms, vision-related functions and environmental triggers, and has good validity, consistency and reliability.[18] Osmolarity testing provides useful information on the hyperosmolarity of the tear film,[19] and the in vivo tear osmolarity test has been commonly used since the introduction of new osmometers such as the TearLab™ system.[20] Tear osmolarity measurements using TearLab™ are accurate, precise and fast, and the system is easy to use to diagnose and classify DED based on severity.[21,22] However, other reports have raised questions over the ability of TearLab™ to diagnose DED.[23,24] The I-Pen® osmolarity system has also been used in recent years to measure tear osmolarity.[25] However, correlations between osmolarity scores based on the I-Pen® and other objective and subjective parameters of DED are poor.[25]

The prevalence of obesity in Saudi Arabia is high (24.7%).[26] Therefore, this comparative, nonrandomized, prospective study investigated the correlation between osmolarity scores in male subjects with a high BMI using 2 different devices. Data from these devices were then compared to scores obtained from the OSDI. In addition, OSDI and osmolarity scores were compared with the scores recorded for a healthy control group.

Objectives

To investigate the correlation between osmolarity measurements using the TearLab™ and I-Pen® systems in subjects with high BMI.

Materials and methods

Subjects

Thirty male subjects with a high BMI (27–48 kg/m^2; mean ± standard deviation (M ±SD) = 35.5 ±6.5 kg/m^2), aged 19–27 years (mean ±SD = 23.3 ±2.1 years), participated in the study. The benchmark for high BMI used in the study was 25 kg/m^2.[27] In addition, a control group of 30 healthy males (BMI < 24.9 kg/m^2; age range 20–28 years; mean age 22.9 ±2.1 years) was included in the study. The subjects were predominantly Saudi Arabians recruited from the population of Riyadh, the capital city of this country. Exclusion criteria included smoking, refractive errors, visual acuity less than 20/20, diabetes, anemia, wearing contact lenses, and a history of ocular surgery. In addition, subjects with high blood cholesterol (above 4 mmol/L), thyroid gland disorders, hypertension, and vitamin A or D deficiencies were excluded. Written informed consent was obtained from all participants. The study was conducted according to the guidelines of the Declaration of Helsinki and approved by the Institutional Review Board of King Saud University (approval No. E-22-6803).

Participants were asked to complete the OSDI questionnaire, after which osmolarity measurements were performed. The TearLab™ system was used first; then, after a 5-minute rest period, the I-Pen® system was applied. Tests were performed once on the right eye of each participant by the same examiner in the same session, and all tests were conducted at the Department of Optometry, College of Applied Medical Sciences, Riyadh, Saudi Arabia. The measurements took place on the morning over several days. We previously demonstrated TearLab™ measurements to have a low average coefficient of variation (CV) of 0.80%.[20] Therefore, to minimize inaccuracies due to variable environmental conditions, the temperature, humidity and airflow were controlled in the room where the measurements were made.

Ocular surface disease index

The OSDI questionnaire was conducted in English in an interview format. All 12 questions included in the OSDI were answered by all subjects in the study and control groups. A score was assigned to each participant, with a score greater than 13 used to confirm the diagnosis.[28]

Table 1. Median (IQR) for the ocular surface disease index (OSDI) and osmolarity scores

Parameter	Study group (n = 30)	Control group (n = 30)	p-value
OSDI	8.0 (6.8)	6.3 (4.1)	0.042
TearLab™ [mOsm/L]	295.5 (13.3)	287.0 (12.5)	<0.001
I-Pen® [mOsm/L]	318.5 (18.8)	298.5 (12.3)	<0.001

TearLab™ osmolarity

The TearLab™ osmolarity system was obtained from the TearLab Corporation (San Diego, USA). Electronic cards were used to test the osmolarity system (the value of 334 ±4 mOsm/L means that the system is functioning well) at the beginning of each day to ensure its proper function. The system uses a very small volume of tear sample (50 nL), which was collected from the lateral lower tear meniscus without touching the lid margin or the globe. The countertop unit of the system analyzed the tear sample and displayed the osmolarity score on a digital screen. Based on the osmolarity measurements, the subject's eyes were classified as normal (<308 mOsm/L) or dry (>308 mOsm/L).[29]

I-Pen® osmolarity

The I-Pen® osmolarity system was obtained from I-MED Pharma (Dollard-des-Ormeaux, Canada) and was used in a distance of at least 2 m from any electronic devices to reduce the risk of interference leading to inaccurate readings. A single-use sensor was utilized for each participant; it was placed against the conjunctiva in the lower fornix to determine tear osmolarity. Dry eye disease was defined as a score of more than 308 mOsm/L.[29]

Statistical analyses

Microsoft Excel 2016 (Microsoft Corp., Redmond, USA) was used to record the data, which were then analyzed with IBM SPSS v. 22 (IBM Corp., Armonk, USA). The data were determined to be non-normally distributed using the Kolmogorov–Smirnov test ($p < 0.05$). Therefore, the Mann–Whitney U test was employed to analyze the data in both groups. Spearman's correlation coefficient (r) was used to test the association between different parameters.[30] Meanwhile, the Wilcoxon signed-rank test was employed to investigate the significance of any differences between the 2 osmolarity measurements within the same group. The mean scores were represented as the median and interquartile range (IQR).

Results

Tear osmolarity measurements were significantly different between the TearLab™ and I-Pen® systems, in both the study and control groups ($p < 0.001$). Also, median scores for the OSDI and osmolarity measurements were significantly higher in the study group than in the control group (Table 1). Indeed, OSDI scores ranged from 2 to 16 in the study group and from 0 to 10 in the control group. Six subjects (20%) in the study group had symptoms of DED according to the OSDI scores, whilst no DED symptoms were found in the control group. The same 6 subjects were also diagnosed with dry eyes using both the TearLab™ and I-Pen® osmolarity systems. Osmolarity scores in the study group using TearLab™ (278–309 mOsm/L) indicated that 33% (n = 10) of the participants had symptoms of DED, whilst the control group showed no symptoms (263–304 mOsm/L). Meanwhile, I-Pen® osmolarity measurements in the study group (294–336 mOsm/L) indicated that 70% (n = 21) of studied people had DED, while 30% (n = 9) of members of the control group (278–317 mOsm/L) has this disease.

Subjects in the study group were stratified into 4 categories based on their BMI: overweight (27–28 kg/m^2; n = 7); class 1 obesity (30–32 kg/m^2; n = 8); class 2 obesity (35–39 kg/m^2; n = 9); and class 3 obesity (40–48 kg/m^2; n = 6). In the class 1 obesity group, there was a strong correlation ($r = 0.976$; $p = 0.001$) between the TearLab™ and I-Pen® measurements. Also, there were strong correlations between the OSDI scores and the TearLab™ ($r = 0.892$; $p = 0.017$) and I-Pen® ($r = 0.926$; $p = 0.0081$) measurements in this group. There was also a strong correlation between the TearLab™ and I-Pen® measurements in the class 2 obesity group ($r = 0.962$; $p = 0.009$) and in the class 3 obesity group ($r = 0.965$; $p = 0.035$). No correlations were found among the OSDI or osmolarity systems in the overweight subjects.

Correlations between age, BMI, OSDI, TearLab™, and I-Pen® scores for the whole study group were investigated. Strong correlations were found between the scores obtained from the TearLab™ and I-Pen® osmolarity systems ($r = 0.934$; $p= 0.001$). The BMI strongly correlated with both the TearLab™ ($r = 0.736$; $p = 0.001$) and I-Pen® ($r = 0.707$; $p = 0.001$) scores. In addition, the OSDI had strong correlations with TearLab™ ($r = 0.731$; $p = 0.001$) and I-Pen® ($r = 0.666$; $p = 0.001$).

Bland–Altman plots (Fig. 1) show the mean differences in osmolarity for TearLab and I-Pen® measurements in the study and control groups. There was a strong correlation ($r = 0.697$; $p < 0.01$) between the TearLab™ and I-Pen® measurements in the study group, while a weak correlation ($r = 0.358$; $p < 0.01$) was found between the 2 measurements in the control group. The correlation between the TearLab™ and I-Pen® osmolarity scores

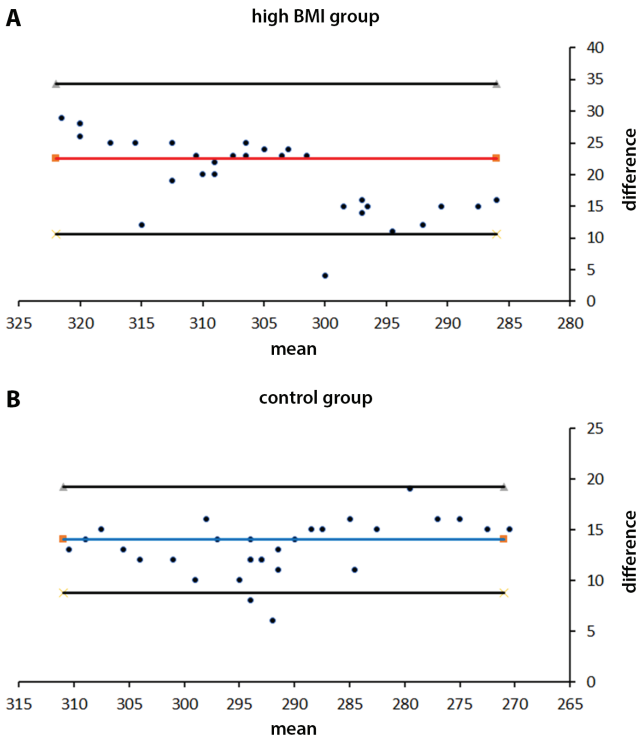

FIG. 1. Bland–Altman plots of the osmolarity mean differences for TearLab™ and I-Pen® measurements in (A) the study group (high body mass index) and (B) the control group

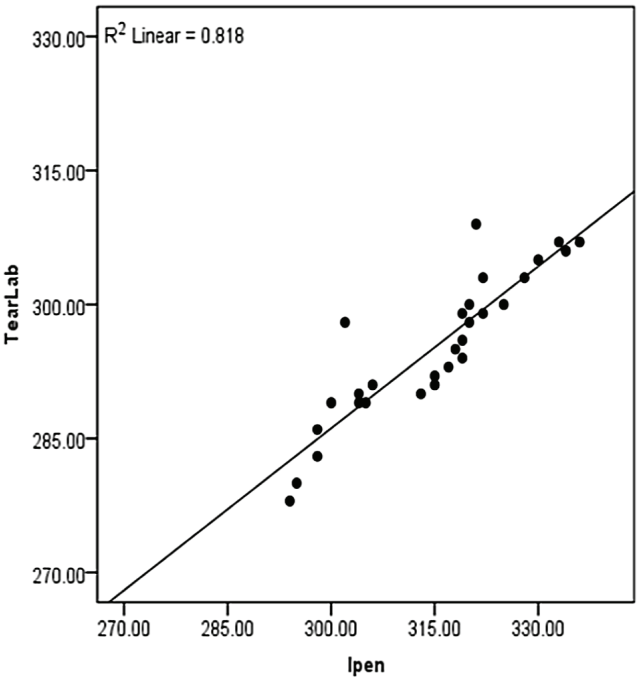

FIG. 2. Correlation between the TearLab™ and I-Pen® osmolarity scores in the study group

in the study group is shown in Fig. 2. Based on Spearman's correlation coefficient, a strong correlation was found between the TearLab™ and I-Pen® scores in both the study ($r = 0.904$; $p < 0.001$) and control ($r = 0.972$; $p < 0.001$) group.

Discussion

Obesity is associated with many disorders, such as neurological, behavioral and mental diseases.[31,32] Moreover, it is associated with high rates of mortality, bacterial infections, influenza, pneumonia, and many other illnesses.[33,34] An association between DED and body fat has been established.[35–37] As such, high BMI is a risk factor for DED and significantly affects tear film stability and the quality of tears.[35] Furthermore, an association between BMI and floppy eyelid syndrome has been reported.[38]

Osmolarity measurements using both I-Pen® and TearLab™ systems indicated that high BMI could induce DED. It should be noted that the median OSDI score for the control group (median 6.3 (IQR 4.1)) in the current study was comparable to those reported recently for healthy subjects by Fegahi et al. (median 8.3, IQR 8.8), Abusharha et al. (median 5.6, IQR 7.0) and Fagehi et al. (median 5.0, IQR 5.6).[39–41] For the study group, the median OSDI score (median 8.0 (IQR 6.8)) was comparable to smokers (median 8.3 (IQR 16.2))[39] and lower than for subjects with high BMI (median 10.2 (IQR 16.4)),[39] diabetes (median 12.0 (IQR 8.3)),[40] myopia (median 11.0 (IQR 7.5)),[41] and hyperopia (median 10.0 (IQR 33.5)).[41]

As reported in a study by Alanazi et al., in subjects with high BMI, there were strong correlations between age and OSDI scores ($r = 0.522$; $p = 0.018$), tear meniscus height (TMH) measurements ($r = -0.503$; $p = 0.024$) and tear fern-ing (TF) grades ($r = 0.579$; $p = 0.007$).[35] The noninvasive tear break-up time had strong negative correlations with the TMH ($r = -0.520$; $p = 0.008$) and phenol red thread (PRT) scores ($r = -0.498$; $p = 0.029$). In addition, the TF grades had strong negative correlations with the TMH ($r = -0.575$; $p = 0.008$) and PRT ($r = -0.773$; $p = 0.001$) scores.[35]

The hyperosmolarity of tears can be used as a marker of DED, as subjects with DED tend to have significantly greater hyperosmolarity than healthy subjects.[21] Hyperosmolarity is responsible for many DED symptoms, such as irritation, inflammation and ocular surface damage.[42] Also, osmolarity testing provides useful information on the tear film.[25] However, the correlations between osmolarity scores and those obtained from other DED tests are poor.[19] The current study suggests that osmolarity measurements using both the TearLab™ and I-Pen® systems are strongly correlated to each other in subjects with high BMI. However, the I-Pen® scores were significantly higher than the TearLab™ scores. Similar results were obtained in healthy subjects.[43] In addition, a correlation between tear film stability (tear break-up time) and tear volume (TMH and PRT) was reported.[44]

Rocha et al. measured osmolarity of 3 tear solutions of known osmolarity values (297 mOsm/L, 342 mOsm/L and 383 mOsm/L), containing mono- and divalent electrolytes along with albumin, were measured using the TearLab™, I-Pen® and Wescor 5520 osmometers. Mean osmolarity scores for the 3 tear solutions were 300.6 ±3.7 mOsm/L,

341.4 ±4.7 mOsm/L and 376.8 ±5.1 mOsm/L using TearLab™, 336.4 ±21.5 mOsm/L, 342.0 ±20.7 mOsm/L and 345.7 ±22.0 mOsm/L using I-Pen®, and 305.6 ±4.0 mOsm/L, 352.2 ±5.5 mOsm/L and 389.8 ±4.0 mOsm/L using the Wescor 5520 osmometer.[45] Meanwhile, the CV was in the range of 1.2–2.3%, 1.0–1.6% and 6.1–6.4% for TearLab™, I-Pen® and the Wescor 5520 osmometer, respectively.[45] Clearly, the TearLab™ and Wescor 5520 osmometers provided more accurate and precise measurements than the I-Pen® system.[45] Indeed, both the osmolarity scores and CV were high when using the I-Pen® system.

In a study by Nolfi et al., osmolarity was measured in 20 subjects (mean age: 27 ±8 years) with normal eyes (16 females and 4 males) using both the TearLab™ and I-Pen® systems. The mean osmolarity recorded was significantly ($p < 0.001$) lower for TearLab™ (295.4 ±8.6 mOsm/L) than for I-Pen® (319.4 ±20.3 mOsm/L).[46] In terms of diagnostic accuracy, I-Pen® identified normal eyes in only 15% of the subjects ($n = 3$), whereas TearLab™ indicated normal eyes in all subjects ($n = 20$).[47] The CV for the TearLab™ measurements was 1.3%, which agrees with that reported by the manufacturer (1.5%).[47] Clearly, I-Pen® showed large variations among osmolarity measurements and was highly unreliable in identifying normal eyes correctly. Calles et al. showed that I-Pen® is very sensitive to temperature and the measurements can vary by 2% for a 1°C change in temperature.[48] Motion is another factor that can affect the osmolarity measurements using the I-Pen® system. However, such a factor is not an issue with a highly skilled researcher.

Another study conducted among healthy subjects showed that the average osmolarity scores were 299.2 ±10.3 mOsm/L and 298.4 ±10.0 mOsm/L using the TearLab™ and Wescor 5520 osmometers, respectively, with a moderate correlation ($r = 0.500$, $p < 0.05$) between both scores.[49] The correlation ($r = 0.650$, $p < 0.05$) between TearLab™ and Wescor 5520 was better when using samples of collected tears (3 µL). Recently, the repeatability of the I-Pen® measurements has been tested in normal-eye subjects.[50] The main score was 308 ±4.8 mOsm/L, with a CV of 4.6%, which is much higher than that for the TearLab™ system.[50]

Limitations

Limitations of the study include the recruitment of a small sample size, only young males participating, a single osmolarity measurement, and single location (Riyadh). In addition, the effect of the order of use of the osmolarity systems was not tested.

Conclusions

Osmolarity measurements using the I-Pen® system were significantly higher than those using the TearLab™ system in subjects with a high BMI. The I-Pen® measurements showed large variations in osmolarity scores and were highly unreliable in identifying normal eyes correctly compared with the TearLab™ system. A strong correlation was found between the osmolarity scores obtained using TearLab™ and I-Pen®.

ORCID iDs

Mana A. Alanazi https://orcid.org/0000-0003-3599-6242
Gamal A. El-Hiti https://orcid.org/0000-0001-6675-3126
Raied Fagehi https://orcid.org/0000-0002-6255-4549
Ali M. Masmali https://orcid.org/0000-0001-5992-6332

References

1. Stenholm S, Head J, Aalto V, et al. Body mass index as a predictor of healthy and disease-free life expectancy between ages 50 and 75: A multicohort study. *Int J Obes*. 2017;41(5):769–775. doi:10.1038/ijo.2017.29
2. Ng M, Fleming T, Robinson M, et al. Global, regional, and national prevalence of overweight and obesity in children and adults during 1980–2013: A systematic analysis for the Global Burden of Disease Study 2013. *Lancet*. 2014;384(9945):766–781. doi:10.1016/S0140-6736(14)60460-8
3. Hwang IC, Bae JH, Kim JM, Lee JM, Nguyen QD. Adult body height and age-related macular degeneration in healthy individuals: A nationwide population-based survey from Korea. *PLoS One*. 2020;15(5):e0232593. doi:10.1371/journal.pone.0232593
4. Bibbins-Domingo K, Coxson P, Pletcher MJ, Lightwood J, Goldman L. Adolescent overweight and future adult coronary heart disease. *N Engl J Med*. 2007;357(23):2371–2379. doi:10.1056/NEJMsa073166
5. Kurth T, Gaziano JM, Berger K, et al. Body mass index and the risk of stroke in men. *Arch Intern Med*. 2002;162(22):2557–2562. doi:10.1001/archinte.162.22.2557
6. Nissinen A, Kastarinen M, Tuomilehto J. Community control of hypertension: Experiences from Finland. *J Hum Hypertens*. 2004;18(8):553–556. doi:10.1038/sj.jhh.1001696
7. National Institutes of Health. Clinical Guidelines on the Identification, Evaluation, and Treatment of Overweight and Obesity in Adults: The evidence report. *Obes Res*. 1998;6(Suppl 2):51S–209S. PMID:9813653.
8. Renehan AG, Tyson M, Egger M, Heller RF, Zwahlen M. Body mass index and incidence of cancer: A systematic review and meta-analysis of prospective observational studies. *Lancet*. 2008;371(9612):569–578. doi:10.1016/S0140-6736(08)60269-X
9. Cheung N, Wong TY. Obesity and eye diseases. *Surv Ophthalmol*. 2007;52(2):180–195. doi:10.1016/j.survophthal.2006.12.003
10. Kuang TM. Body mass index and age-related cataract: The Shihpai Eye Study. *Arch Ophthalmol*. 2005;123(8):1109–1114. doi:10.1001/archopht.123.8.1109
11. van Leiden HA, Dekker JM, Moll AC, et al. Blood pressure, lipids, and obesity are associated with retinopathy. *Diabetes Care*. 2002;25(8):1320–1325. doi:10.2337/diacare.25.8.1320
12. Stapleton F, Alves M, Bunya VY, et al. TFOS DEWS II Epidemiology Report. *Ocul Surf*. 2017;15(3):334–365. doi:10.1016/j.jtos.2017.05.003
13. O'Neil EC, Henderson M, Massaro-Giordano M, Bunya VY. Advances in dry eye disease treatment. *Curr Opin Ophthalmol*. 2019;30(3):166–178. doi:10.1097/ICU.0000000000000569
14. Miljanović B, Dana R, Sullivan DA, Schaumberg DA. Impact of dry eye syndrome on vision-related quality of life. *Am J Ophthalmol*. 2007;143(3):409–415.e2. doi:10.1016/j.ajo.2006.11.060
15. Benítez-del-Castillo J, Labetoulle M, Baudouin C, et al. Visual acuity and quality of life in dry eye disease: Proceedings of the OCEAN Group meeting. *Ocul Surf*. 2017;15(2):169–178. doi:10.1016/j.jtos.2016.11.003
16. Bron AJ, de Paiva CS, Chauhan SK, et al. TFOS DEWS II pathophysiology report. *Ocul Surf*. 2017;15(3):438–510. doi:10.1016/j.jtos.2017.05.011
17. Aragona P, Giannaccare G, Mencucci R, Rubino P, Cantera E, Rolando M. Modern approach to the treatment of dry eye, a complex multifactorial disease: A P.I.C.A.S.S.O. board review. *Br J Ophthalmol*. 2021;105(4):446–453. doi:10.1136/bjophthalmol-2019-315747
18. Okumura Y, Inomata T, Iwata N, et al. A review of dry eye questionnaires: Measuring patient-reported outcomes and health-related quality of life. *Diagnostics*. 2020;10(8):559. doi:10.3390/diagnostics10080559

19. Tashbayev B, Utheim TP, Utheim ØA, et al. Utility of tear osmolarity measurement in diagnosis of dry eye disease. *Sci Rep*. 2020;10(1):5542. doi:10.1038/s41598-020-62583-x
20. Masmali A, Alrabiah S, Alharbi A, El-Hiti GA, Almubrad T. Investigation of tear osmolarity using the TearLab Osmolarity System in normal adults in Saudi Arabia. *Eye Contact Lens*. 2014;40(2):74–78. doi:10.1097/ICL.0000000000000002
21. Lemp MA, Bron AJ, Baudouin C, et al. Tear osmolarity in the diagnosis and management of dry eye disease. *Am J Ophthalmol*. 2011;151(5):792–798.e1. doi:10.1016/j.ajo.2010.10.032
22. Yoon D, Gadaria-Rathod N, Oh C, Asbell PA. Precision and accuracy of TearLab osmometer in measuring osmolarity of salt solutions. *Curr Eye Res*. 2014;39(12):1247–1250. doi:10.3109/02713683.2014.906623
23. Baenninger PB, Voegeli S, Bachmann LM, et al. Variability of tear osmolarity measurements with a point-of-care system in healthy subjects: Systematic review. *Cornea*. 2018;37(7):938–945. doi:10.1097/ICO.0000000000001562
24. Bunya VY, Fuerst NM, Pistilli M, et al. Variability of tear osmolarity in patients with dry eye. *JAMA Ophthalmol*. 2015;133(6):662–667. doi:10.1001/jamaophthalmol.2015.0429
25. Shimazaki J, Sakata M, Den S, Iwasaki M, Toda I. Tear film osmolarity measurement in Japanese dry eye patients using a handheld osmolarity system. *Diagnostics*. 2020;10(10):789. doi:10.3390/diagnostics10100789
26. Althumiri NA, Basyouni MH, AlMousa N, et al. Obesity in Saudi Arabia in 2020: Prevalence, distribution, and its current association with various health conditions. *Healthcare*. 2021;9(3):311. doi:10.3390/healthcare9030311
27. Zierle-Ghosh A, Jan A. Physiology, body mass index. In: *StatPearls*. Treasure Island, USA: StatPearls Publishing; 2022. http://www.ncbi.nlm.nih.gov/books/NBK535456/. Accessed November 17, 2022.
28. Schiffman RM. Reliability and validity of the Ocular Surface Disease Index. *Arch Ophthalmol*. 2000;118(5):615–621. doi:10.1001/archopht.118.5.615
29. Willcox MDP, Argüeso P, Georgiev GA, et al. TFOS DEWS II Tear Film Report. *Ocul Surf*. 2017;15(3):366–403. doi:10.1016/j.jtos.2017.03.006
30. Cohen J. *Statistical Power Analysis for the Behavioral Sciences*. 2nd ed. Hillsdale, USA: L. Erlbaum Associates; 1988. ISBN:978-0-8058-0283-2.
31. Malik VS, Ravindra K, Attri SV, Bhadada SK, Singh M. Higher body mass index is an important risk factor in COVID-19 patients: A systematic review and meta-analysis. *Environ Sci Pollut Res*. 2020;27(33):42115–42123. doi:10.1007/s11356-020-10132-4
32. Bhaskaran K, dos-Santos-Silva I, Leon DA, Douglas IJ, Smeeth L. Association of BMI with overall and cause-specific mortality: A population-based cohort study of 3.6 million adults in the UK. *Lancet Diabetes Endocrinol*. 2018;6(12):944–953. doi:10.1016/S2213-8587(18)30288-2
33. Huttunen R, Karppelin M, Syrjänen J. Obesity and nosocomial infections. *J Hosp Infect*. 2013;85(1):8–16. doi:10.1016/j.jhin.2013.06.012
34. Kassir R. Risk of COVID-19 for patients with obesity. *Obes Rev*. 2020;21(6):e13034. doi:10.1111/obr.13034
35. Alanazi SA. Assessment of tear film in subjects with a high body mass index. *Clin Otom (Auckl)*. 2019;11:77–84. doi:10.2147/OPTO.S218109
36. Ho KC, Jalbert I, Watt K, Golebiowski B. A possible association between dry eye symptoms and body fat: A prospective, cross-sectional preliminary study. *Eye Contact Lens*. 2017;43(4):245–252. doi:10.1097/ICL.0000000000000275
37. Yamanishi R, Sawada N, Hanyuda A, et al. Relation between body mass index and dry eye disease: The Japan Public Health Center–Based Prospective Study for the Next Generation. *Eye Contact Lens*. 2021;47(8):449–455. doi:10.1097/ICL.0000000000000814
38. Beis PG, Brozou CG, Gourgoulianis KI, Pastaka C, Chatzoulis DZ, Tsironi EE. The floppy eyelid syndrome: Evaluating lid laxity and its correlation to sleep apnea syndrome and body mass index. *ISRN Ophthalmol*. 2012;2012:650892. doi:10.5402/2012/650892
39. Fagehi R, El-Hiti GA, Almojalli A, et al. Assessment of tear film parameters in smokers and subjects with a high body mass index. *Optom Vis Sci*. 2022;99(4):358–362. doi:10.1097/OPX.0000000000001891
40. Abusharha A, El-Hiti GA, Alsubaie MH, et al. Evaluation of tear evaporation rate in patients with diabetes using a hand-held evaporimeter. *Healthcare*. 2022;10(1):104. doi:10.3390/healthcare10010104
41. Fagehi R, El-Hiti GA, Alsubaie MH, et al. Measurements of tear evaporation rate in subjects with refractive errors using a portable evaporimeter. *Healthcare*. 2022;10(2):405. doi:10.3390/healthcare10020405
42. Craig JP, Nichols KK, Akpek EK, et al. TFOS DEWS II Definition and Classification Report. *Ocul Surf*. 2017;15(3):276–283. doi:10.1016/j.jtos.2017.05.008
43. Fagehi R, Alanazi MA, Abdualkarim W, et al. Correlation between tear osmolarity measurements using TearLab and I-Pen osmolarity systems in normal young Saudi subjects. *EC Ophthalmol*. 2021;12(2):40–46. https://www.ecronicon.com/ecop/pdf/ECOP-12-00737.pdf. Accessed January 15, 2022.
44. Glasson MJ, Stapleton F, Keay L, Sweeney D, Willcox MDP. Differences in clinical parameters and tear film of tolerant and intolerant contact lens wearers. *Invest Ophthalmol Vis Sci*. 2003;44(12):5116–5124. doi:10.1167/iovs.03-0685
45. Rocha G, Gulliver E, Borovik A, Chan C. Randomized, masked, in vitro comparison of three commercially available tear film osmometers. *Clin Ophthalmol*. 2017;11:243–248. doi:10.2147/OPTH.S127035
46. Nolfi J, Caffery B. Randomized comparison of in vivo performance of two point-of-care tear film osmometers. *Clin Ophthalmol*. 2017;11:945–950. doi:10.2147/OPTH.S135068
47. Food and Drug Administration (FDA). K083184, TearLab Osmolarity System. Silver Spring, USA: Food and Drug Administration (FDA); 2009. https://www.accessdata.fda.gov/cdrh_docs/pdf8/k083184.pdf.
48. Calles B, Calles UM. Temperature correction of electrical conductivity values. *Earth Surf Process Landforms*. 1990;15(7):673–678. doi:10.1002/esp.3290150708
49. Gokhale M, Stahl U, Jalbert I. In situ osmometry: Validation and effect of sample collection technique. *Optom Vis Sci*. 2013;90(4):359–365. doi:10.1097/OPX.0b013e31828aaf10
50. Fagehi R, Al-Bishry A, Alanazi M, Abusharha A, El-Hiti G, Masmali A. Investigation of the repeatability of tear osmolarity using an I-PEN osmolarity device. *Taiwan J Ophthalmol*. 2021;11(2):168–174. doi:10.4103/tjo.tjo_65_20

Annual Contents

No. 1 (January)

Editorials

Original papers

Reviews

No. 2 (February)

Editorials

Original papers

Reviews

Research letters

No. 3 (March)

Editorials

Original papers

Reviews

Research letters

No. 4 (April)

Editorials

Original papers

Reviews

Research letters

No. 5 (May)

Editorials

Original papers

Reviews

Research letters

No. 6 (June)

Meta-analyses

Original papers

Research letters

No. 7 (July)

Original papers

Research letters

No. 8 (August)

Editorials

Meta-analysis

Original papers

Reviews

No. 9 (September)

Editorials

Original papers

Research letters

No. 10 (October)

Editorials

Original papers

Reviews

No. 11 (November)

Editorials

Meta-analysis

Original papers

Reviews

No. 12 (December)

Editorials

Meta-analysis

Original papers

Reviews

Research letters

Index of Authors